

**PROCEEDINGS OF THE XIV SERBIAN-BULGARIAN  
ASTRONOMICAL CONFERENCE**

**Vrnjačka Banja, Serbia, September 23–27, 2024**

**Eds. Milan S. Dimitrijević, Evgeni Semkov, Zoran Simić,  
Goran Damljanović, Momchil Dechev**



BELGRADE, 2025



**PROCEEDINGS OF THE XIV SERBIAN-BULGARIAN  
ASTRONOMICAL CONFERENCE**

**Vrnjačka Banja, Serbia, September 23–27, 2024**

**Eds. Milan S. Dimitrijević, Evgeni Semkov, Zoran Simić,  
Goran Damljanović, Momchil Dechev**

Belgrade, 2025

## SCIENTIFIC ORGANIZING COMMITTEE

Zoran Simić (AOB) - co-chair	Vladimir A. Srećković (IPhB)
Goran Damljanović (AOB) - co-chair	Rumen Bachev (IANA0)
Momchil Dechev (IANA0) - co-chair	Svetlana Boeva (IANA0)
Milan S. Dimitrijević (AOB) - co-vice-chair	Lubomir Iliev (IANA0)
Evgeni Semkov (IANA0) - co-vice-chair	Rositsa Miteva (IANA0)
Bojan Arbutina (UB)	Nikola Petrov (IANA0)
Dejan Urošević (UB)	Kamen Kozarev (IANA0)
Milica Vučetić (UB)	Magdalena Christova (TUS)
Andjelka Kovačević (UB)	Kostadinka Koleva (SRTI)
Luka Č. Popović (AOB)	Ognyan Kounchev (IMI)
Jelena Kovačević (AOB)	Petko Nedialkov (SU)
Monika Jurković (AOB)	Gordana Apostolovska (US)
Oliver Vince (AOB)	Robert Beuc (IPhZ)
Sladjana Knežević (AOB)	Branko Predojević (FS)
Nenad Sakan (IPhB)	Sylvie Sahal-Bréchet (OP)

## LOCAL ORGANIZING COMMITTEE

Zoran Simić (AOB) - chair	Monika Jurković (AOB)
Goran Damljanović (AOB) - co-chair	Oliver Vince (AOB)
Sladjana Knežević (AOB) - sci. secretary	Vesna Mijatović (AOB)
Milan S. Dimitrijević (AOB)	Jasmina Horvat (UB)
Jelena Kovačević Dojčinović (AOB)	Nataša Pavlov (UB)
Nikola Knežević (AOB)	

### Legend:

AOB - Astronomical Observatory, Belgrade	IMI - Institute of Mathematics and Informatics, Bulgarian Academy of Sciences
IANA0 - Institute of Astronomy with National Astronomical Observatory, Bulgarian Academy of Sciences	SU - Sofia University
UB - University of Belgrade	US - Ss. Cyril and Methodius University in Skopje
IPhB - Institute of Physics, Belgrade	IPhZ - Institute of Physics, Zagreb
TUS - Technical University of Sofia	FS - Faculty of Sciences, Banja Luka
SRTI - Space Research and Technology Institute, Bulgarian Academy of Sciences	OP - Observatoire de Paris, Meudon

### Organizers:

Astronomical Observatory, Belgrade, Serbia  
Institute of Astronomy with National Astronomical Observatory, Bulgarian Academy of Sciences, Sofia, Bulgaria

### Co-organizer:

Faculty of Mathematics and Department of Astronomy, University of Belgrade

Published by: Astronomical Observatory Belgrade, Volgina 7, 11060 Belgrade 38, Serbia

Conference logo design: Zoran Simić  
Text arrangement by computer: Sladjana Knežević

ISBN 978-86-82296-15-7

---

Production: Vesna Vasić-Pavlović PR, Rakari bb, 14242 Mionica, in 100 copies.

# Table of Contents

R. Bachev	
<b>FAST VARIABILITY OF THE OPTICAL POLARIZATION IN BLAZARS: FIRST RESULTS FROM BELOGRADCHIK OBSERVATORY</b>	<b>.. 5</b>
S. Boeva, G. Latev, R. Miteva, Z. Cvetković	
<b>ARE THE DWARF NOVAE OUTBURSTS ABSENT IN VY SCL-TYPE STARS LOW STATES?</b>	<b>..... 13</b>
M. D. Christova, M. S. Dimitrijević	
<b>ASTROPHYSICAL APPLICATIONS OF STARK BROADENING OF SINGLY IONIZED PALADIUM SPECTRAL LINES</b>	<b>.....21</b>
R. Miteva, S. W. Samwel, M. Dechev	
<b>SOHO/ERNE PROTON FLUENCE IN SOLAR CYCLES 23 AND 24</b>	<b>. 29</b>
N. Petrov, Ts. Tsvetkov, A. Mishev, V. Yotov, G. Shirov	
<b>FIRST OBSERVATIONAL DATA FROM THE MINI-NEUTRON MONITORING STATION AT THE ROZHEN NATIONAL ASTRONOMICAL OBSERVATORY (MNMS-ROZH)</b>	<b>..... 37</b>
N. Arsenov, S. Frey, A. Kovács, K. É. Gabányi, K. Perger, J. Fogasy, L. Slavcheva-Mihova, Á. Bogdán	
<b>QUAIA × VLASS: A NEW SAMPLE OF COMPACT EXTRAGALACTIC RADIO SOURCES</b>	<b>..... 43</b>
V. Borka Jovanović, D. Borka, P. Jovanović	
<b>CONSTRAINTS ON GRAVITON MASS FROM S2-LIKE STAR ORBITS AROUND Sgr A*</b>	<b>..... 51</b>
G. Damjanović, M. Stojanović, M.D. Jovanović, R. Bachev, S. Boeva	
<b>SERBIAN-BULGARIAN COOPERATION ABOUT GAIA ALERTS DURING 2023</b>	<b>..... 57</b>
M. S. Dimitrijević, M. D. Christova, S. Sahal-Bréchet	
<b>STARK BROADENING DATA FOR N VI SPECTRAL LINES</b>	<b>..... 63</b>
L. Marinkova, T. V. Veltchev, S. Donkov	
<b>COLUMN DENSITY DISTRIBUTIONS FROM DECOMPOSED MAPS OF STAR-FORMING REGIONS</b>	<b>..... 69</b>
H. Mihaylov, O. Stanchev, T. V. Veltchev	
<b>GRAVITY-BASED STRUCTURAL ANALYSIS OF THE MOLECULAR CLOUDS PERSEUS AND ORION A</b>	<b>..... 75</b>
E. Mikhailov, T. Khasaeva, M. Frolova	
<b>MAGNETIC FIELD GROWTH IN GALACTIC DISCS OF VARIOUS THICKNESS</b>	<b>..... 81</b>
D. Boneva, K. Yankova	
<b>ACCRETION MECHANISMS AND SUPERHUMPS OF THE NOVA-LIKE SYSTEM V592 CAS</b>	<b>..... 87</b>

Ts. Georgiev, A. Valcheva, P. Nedialkov	
<b>PHOTOMETRIC PERIODS OF M31 LBV AF AND IDENTIFIED VIA STRUCTURE EMINENCE FUNCTION METHOD</b> .....	91
N. Janc	
<b>THE PATH OF MILUTIN MILANKOVIĆ'S BOOK MANUSCRIPT "MATHEMATICAL THEORY OF THERMAL PHENOMENA CAUSED BY SOLAR RADIATION"</b> .....	95
M. D. Jovanović, G. Damljanović	
<b>INTRA-NIGHT VARIABILITY OF 1722+119</b> .....	99
K. Koleva, M. Dechev, P. Duchlev	
<b>MULTI-INSTRUMENT OBSERVATION OF A FILAMENT ERUPTION AND ASSOCIATED CME DEFLECTION</b> .....	103
M. D. Lakićević, J. Kovačević-Dojčinović, L. Č. Popović	
<b>X-RAY HARDNESS RATIO AND MID-INFRARED PARAMETERS FOR AGNS</b> .....	109
D. Marchev, B. Borisov, S. Ibryamov, T. Atanasova, G. Yordanova, N. Pavlova, A. Georgiev	
<b>THE NEW 60-cm TELESCOPE OF THE SHUMEN UNIVERSITY ASTRONOMICAL CENTER</b> .....	113
B. M. Mihov, L. S. Slavcheva-Mihova	
<b>MULTI-BAND INTRA-NIGHT VARIABILITY OF THE BLAZAR CTA 102 DURING ITS 2016 DECEMBER OUTBURST</b> .....	117
R. Pavlović, Z. Cvetković, Z. Simić, G. Damljanović, S. Samurović, B. Rovčanin, D. Lukić, D. Bjelajac	
<b>URBAN OBSERVATORY OF BELGRADE (UrbObsBel)</b> .....	123
R. Pavlović, Z. Cvetković, D. Bjelajac, G. Damljanović, D. Lukić, B. Rovčanin, S. Samurović, Z. Simić	
<b>THE UrbObsBel PROJECT: INSTRUMENTS AND DETECTORS</b> ..	129
N. M. Sakan, Z. Simić, V. A. Srećković, M. Dechev	
<b>THE INFLUENCE OF THE COLLECTIVE EFFECTS IN PLASMA, BEHIND SIMPLE CUT-OFF</b> .....	135
K. Yankova	
<b>ZONES OF ACCRETION DISK ACTIVITY</b> .....	139
<b>IN MEMORY OF EVGENI SEMKOV</b> .....	145
<b>AUTHORS' INDEX</b> .....	147

## FAST VARIABILITY OF THE OPTICAL POLARIZATION IN BLAZARS: FIRST RESULTS FROM BELOGRADCHIK OBSERVATORY

R. BACHEV 

*Institute of Astronomy and NAO, Bulgarian Academy of Sciences, 1784 Sofia, Bulgaria  
E-mail: bachevr@astro.bas.bg*

**Abstract.** Blazars are relativistic jet-dominated active galactic nuclei, whose emission in the optical region is mostly synchrotron in nature and is consequently polarized. We monitored several objects on night-to-night and long-term time scales in order to study their flux and polarization variability. Our primary goal was to study the variability of the optical polarization of blazars and its relation to the X-ray polarization, which had been measured for a number of objects with the newly introduced *IXPE* orbital observatory. Among the objects we studied were BL Lacertae, S4 0954+65, S5 0716+714, PG 1553+115, 4C 29.45, OJ 287, Mkn 421, Mkn 501, B2 1308+32, 1ES 1959+65, etc. Our first results suggest the presence of rapid changes in both – polarization degree and position angle in practically all the objects we studied. Such and similar polarization studies can facilitate the detailed modeling of the relativistic jet emission mechanisms.

### 1. INTRODUCTION

Blazars are among the most powerful and the highest-energy persistent sources in the Universe. They are a subclass of Active Galactic Nuclei (AGN), where the emitted energy is generated via accretion onto a supermassive black hole, located in the center of the galactic nucleus (Lynden-Bell, 1969; Rees, 1984). For the case of blazars, however, the observed electromagnetic energy is produced primarily as a result of non-thermal processes in a relativistic jet (Blandford & Rees, 1978), even though the primary energy driver can still be accretion onto a supermassive black hole. These jet-related processes may include synchrotron radiation, Compton scattering, particle cascades, etc. As blazars are classified those jet-dominated objects, whose jet is pointed almost directly towards the observer (Urry & Padovani, 1995). There are several distinctive features, making blazars unique objects in the Universe due to their significant *Doppler* boosting and the specific processes, taking place in their relativistic jets. These features include extremely powerful emission (as detected by the observer), extremely broad spectral energy distribution (SED), rapid flux and polarization variability (examples in Bachev 2015; Bachev et al. 2011, 2017, 2023 and the references therein), among others.

The blazar SED is almost entirely non-thermal in nature and consists primarily of two peaks. Depending on the location of these peaks the objects are classified as low- (LSP), intermediate- (ISP) and high-spectrum peaked (HSP), creating a sequence

known as the "blazar sequence" (Fossati et al., 1998).

The low-energy peak (LEP), located in the optical-IR region, is most likely produced by relativistic charged particles (electrons) via synchrotron processes in a magnetic field. The synchrotron radiation is naturally linearly polarized up to 75% (Rybicki & Lightman, 1985) with a position angle (PA) perpendicular to the magnetic field of the corresponding emitting region. The overall polarization can be smaller if the magnetic field is too much disordered or if many independent emitting regions contribute to the total emission.

The energy production mechanisms for the high-energy peak (HEP), located in the X/gamma-ray region are less clear and can be broadly divided into *leptonic* and *hadronic* models (Bottcher et al., 2013).

The *leptonic* models include synchrotron-self Compton (SSC) processes, where the high energy (X/gamma-ray) photons are produced by inverse Compton scattering of the already produced IR/optical synchrotron photons off the same population of relativistic electrons that generates them (i.e. relativistic electrons generate both peaks via different processes). Since the seed photons are polarized, the SSC radiation will also be polarized after the scattering, yet at levels  $P_{\text{HEP}} \simeq 0.3 - 0.5 P_{\text{LEP}}$  or less (Zhang et al., 2024). Another possibility is that the seed photons come from an external source as the accretion disk, broad line region or dusty torus, being scattered off the relativistic electrons in the jet (External-Compton process, EC). Since the seed photons are unpolarized in this case, then they remain unpolarized after the Compton scattering and  $P_{\text{HEP}} \simeq 0$ .

The *hadronic* models include proton synchrotron mechanism and photo-meson processes/cascades (Bottcher et al., 2013). The proton synchrotron mechanism, however, requires much stronger magnetic field, than normally assumed (i.e 10–100G vs. 0.1–1G) and naturally produces polarized high-energy radiation, with a  $P_{\text{HEP}} \simeq P_{\text{LEP}}$ . The same is for photo-meson processes/cascades case, where  $P_{\text{HEP}}$  should again be high, as the cascades produce ultra-relativistic charged particles (pions, muons, electrons, positrons), moving in a magnetic field. The photo-meson cascade option is perhaps required for the neutrino production, as the first neutrino-emitting blazar, TXS 0506+056 (among other suspected) has been already identified in 2017 (IceCube collaboration, 2018a, b).

In short, while the leptonic processes can provide a wide range of HEP polarizations, for the hadronic models the polarization is always expected to be high. Therefore, studying the HEP polarization can help to constrain different mechanisms that are likely to produce the high energy emission. Recently a new window of opportunity in that respect was open with the introduction of the X-ray polarization explorer satellite (*IXPE*), making possible to probe the polarization of both SED peaks almost simultaneously, if combined with ground-based optical measurements.

The main objective of this work is to explore the optical polarization in a number of relatively bright blazars, trying to answer two questions:



(i) How variable is the optical polarization in terms of polarization degree and position angle for objects of different types?

(ii) How much is this optical polarization related to the X-ray polarization and what can we learn about the HEP energy production mechanisms?

## 2. OBSERVATIONS AND RESULTS

The optical polarization measurements of the objects we studied were performed with the 60-cm telescope of Belogradchik Observatory, Bulgaria, equipped with a CCD and standard UBVRI filters. Additional polarimetric filters were added in 2020 on a second wheel (Bachev et al., 2023; Bachev, 2024), allowing polarization measurements in any of the UBVRI bands. Some of the first results (as of 2024, August) are presented below and the most frequently observed objects are discussed individually.

**BL Lacertae.** This was the most frequently studied object, showing occasionally significant polarization variability, even on intra-night time scales (Bachev et al., 2023; Imazawa et al. 2023; Shablovinskaya et al., 2023). We obtained polarization measurements of this blazar during 98 nights, in 2% of which only upper limits of the polarization degree could be measured. The distributions of the polarization degrees and position angles are shown in Fig. 1. The average polarization was 9% (5% standard deviation) with a log-normal distribution, which cannot be rejected with more than 90% probability. The position angle was concentrated between 10 and 30 degrees (40% of all cases), which is close to the radio jet position angle (about 20 deg, Raiteri et al., 2023). The object was observed by *IXPE* (2022, November) and an X-ray polarization was detected with a high level of confidence ( $P_x \simeq 22\%$ ;  $PA \simeq 151$  deg; Peirson et al., 2023). The authors conclude that the SSC mechanism dominates over possible hadronic contribution. On the other hand, two other *IXPE* observations produced only upper limits of the polarization.

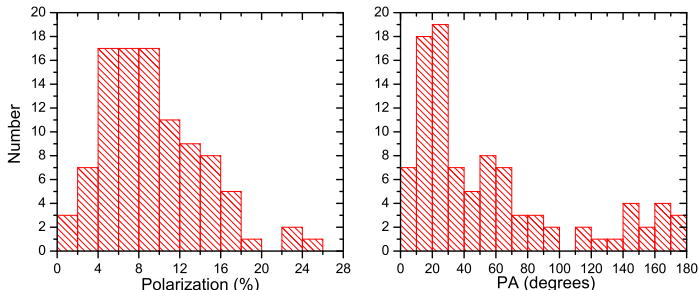


Figure 1: The distribution of polarization degrees (left panel) and position angles (right panel) of the R-band polarization of BL Lacertae (see the text).

**S5 0716+714.** This is another frequently observed blazar. During 54 nights (Fig. 2) we obtained average polarization  $P_{opt} \simeq 7 \pm 4\%$  with only upper limits in 4% of the nights. The PA was concentrated between 70 and 100 deg (in 60% of all cases). *IXPE* observations set very loose upper limits for the X-ray polarization (Marshall et

al., 2024).

**OJ 287.** This blazar was observed during 18 nights (Fig. 3) with  $P_{opt} \simeq 17 \pm 5\%$  (with 6% upper limits) and PA concentrated between 140 and 160 deg for 82% of all cases. The object has not been observed with *IXPE* but should be a proper target, being bright enough and with high optical polarization.

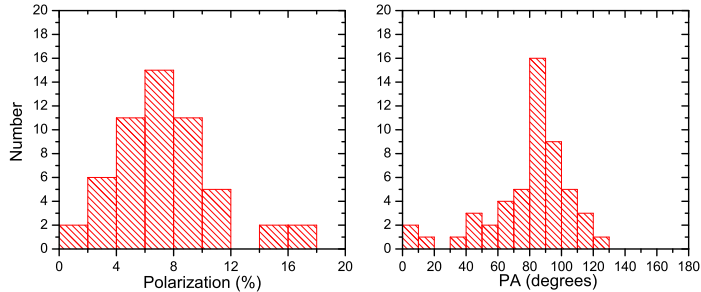


Figure 2: The same as Fig. 1 for S5 0716+714 (see also the text).

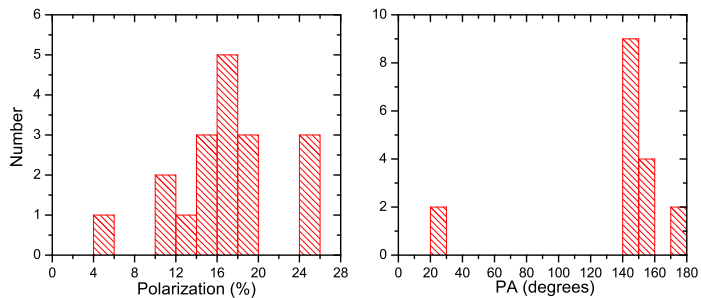


Figure 3: The same as Fig. 1 for OJ 287 (see also the text).

**S4 0954+65.** The object was observed during 59 nights with  $P_{opt} \simeq 15 \pm 8\%$  (with 7% upper limits) and no apparent PA concentration (Fig. 4). *IXPE* has not yet observed this blazar.

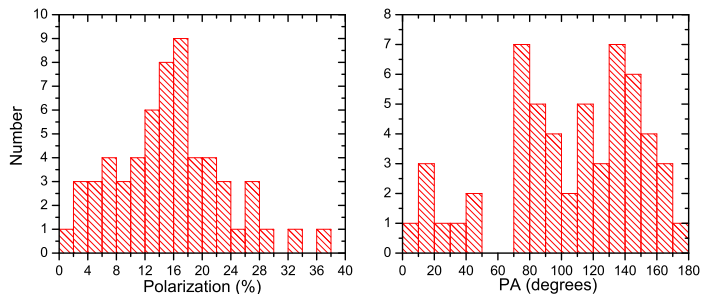


Figure 4: The same as Fig. 1 for S4 0954+65 (see also the text).

**4C 29.45.** This blazar was observed during 29 nights (Fig. 5) with  $P_{opt} \simeq 17 \pm 5\%$  (with 21% upper limits as it was rather weak during some epochs) and PA concentrated between 10 and 30 deg for 56% of all cases. The object has not been observed with *IXPE*.

**B2 1308+326.** The object was observed during 27 nights with  $P_{opt} \simeq 14 \pm 8\%$  (with 15% upper limits) and no apparent PA concentration (Fig. 6). *IXPE* has not yet observed this blazar.

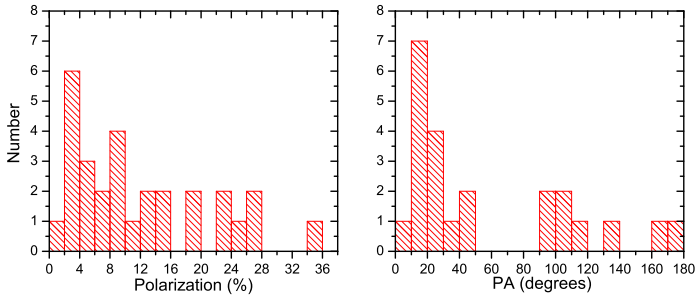


Figure 5: The same as Fig. 1 for 4C 29.45 (see also the text).

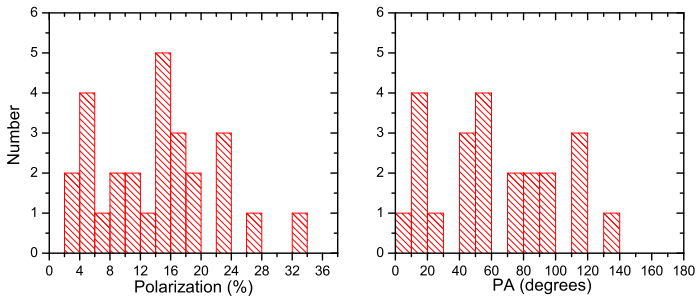


Figure 6: The same as Fig. 1 for B2 1308+326 (see also the text).

The blazars above are all classified as LSP/ISP. The blazars below, however, are all HSP with X-ray polarization measurements by *IXPE*. For these objects the X-ray polarization is typically much larger than the optical polarization.

**PG 1553+113.** We measured  $P_{opt} \simeq 3.4 \pm 2\%$  (with 37% upper limits) during 38 nights (Fig. 7). The PA was concentrated between 90 and 120 deg (for 54% of the nights). *IXPE* observations (2023, February) showed  $P_x \simeq 10 \pm 2\%$  and  $PA \simeq 86 \pm 8$  deg (Middei et al., 2023). The radio jet of this blazar is positioned at about 50 degrees and does not seem to coincide with both – optical and X-ray polarization PAs.

**Mkn 501.** For most nights (29 in total) we obtained only upper limits for the optical polarization of this blazar (54%). When measured,  $P_{opt} \simeq 1.8 \pm 0.7\%$  and PA was always between 120 and 160 deg (Fig. 8). *IXPE* observed this object on many occasions with  $P_x$  between 6 and 18% and PA between 100 and 140 deg. For this

blazar the position angles of the optical polarization, X-ray polarization and the radio jet appear to coincide within certain limits (Marscher et al., 2024).

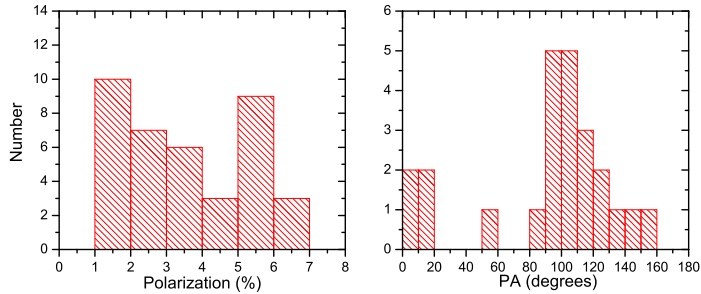


Figure 7: The same as Fig. 1 for PG 1553+113 (see also the text).

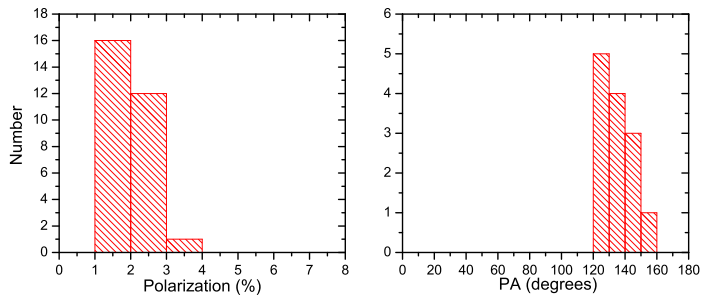


Figure 8: The same as Fig. 1 for Mkn 501 (see also the text).

**1ES 1959+650.** The object was observed during 7 nights with  $P_{opt} \simeq 4 \pm 2\%$  (no upper limits) and PA always between 100 and 170 deg (Fig. 9). *IXPE* results showed  $P_x \simeq 8 \pm 2\%$  and  $PA \simeq 123 \pm 8$  deg and only upper limits during a second run (Errando et al., 2024). For this object the position angles of the optical polarization, X-ray polarization and the radio jet again appear to coincide within certain limits (Marscher et al., 2024).

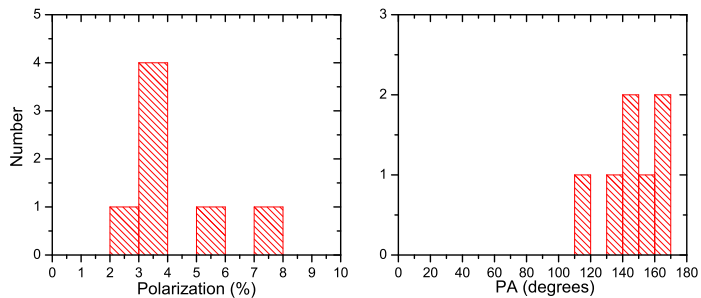


Figure 9: The same as Fig. 1 for 1ES 1959+650 (see also the text).

### 3. DISCUSSION AND CONCLUSION

The polarization results can be interpreted in terms of the processes, involved to produce the corresponding SED peak. The LEP polarization, which we measured in the optical region depends mostly on the level of disorder of the magnetic field and can reach typically up to 40 – 50%, but normally is about 10 – 20% for the most of the objects. What concerns the HEP polarization, however, the situation there is more complicated. The *IXPE* range, where the X-ray polarization is measured, can belong in principle to high-end of LEP (for HSP objects), low-end of HEP (for LSP objects) or be in the middle region (see Fig. 1 from Marscher et al., 2024). Therefore, the X-ray polarization, if present, should be interpreted with care as different processes might be involved in different (LSP/HSP) objects to produce the observed emission in these different peaks.

In addition, one should bear in mind that *IXPE* integration time is often in the realm of weeks, which reflects into detection as zero of any variable in position angle (but otherwise non-zero) linear polarization. Provided, of course, that the PA changes occur faster than the integration time.

Our preliminary results confirm the common understanding that the optical polarization can be moderate to significant for the LSP objects and is variable in both – polarization degree and position angle. The X-ray polarization for LSP objects (in the range of HEP for them) is usually not detected, perhaps suggesting the SSC/EC mechanism for the HEP emission generation. For the HSP objects we detected very low-level (if any) polarization in the optical. The X-ray polarization, however, which still covers the high-end of the LEP for these objects, appears to be significant, suggesting possible energy stratification caused by a standing or moving shock (Marscher et al., 2024). The shock orders the magnetic field and in the same time produces the highest energy photons close to the shock front, which causes only the high-energy X-rays to be polarized, while the low-energy optical photons, produced further out in a more disordered magnetic field – not that much. For the HSP blazars, X-ray polarization cannot help much to understand the HEP emission mechanisms, but hopefully the future gamma-ray polarization missions will.

To conclude, any high-energy polarization measurements should be supplemented by similar measurements in the low-energy (optical) range in order to successfully model the emission-production mechanisms. This is especially true when the optical polarization is highly variable in both – polarization degree and position angle, as our results suggest. Here, even small optical observatories, like Belogradchik observatory, if equipped with the proper instrumentation can contribute to further understand the highest energy phenomena in the Universe.

#### Acknowledgements

This research was partially supported by the Bulgarian National Science Fund of the Ministry of Education and Science under grant KP-06-PN68/4 (2022).

## References

- Bachev R., 2015, *MNRAS*, **451**, L21, doi: 10.1093/mnras/slv059
- Bachev R., 2024, *Bulgarian Astronomical Journal*, **40**, 78
- Bachev R., Popov V., Strigachev A., et al., 2017, *MNRAS*, **471**, 2216, doi: 10.1093/mnras/stx1818
- Bachev R., Semkov E., Strigachev A., et al., 2011, *A&A*, **528**, L10, doi: 10.1051/0004-6361/201116637
- Bachev R., Tripathi T., Gupta Alok C., et al., 2023, *MNRAS*, **522**, 3018, doi: 10.1093/mnras/stad1063
- Blandford R. D., Rees M. J., 1978, *Phys. Scr.*, **17**, 265, doi: 10.1088/0031-8949/17/3/020
- Bottcher M., Reimer A., Sweeney K., Prakash A., 2013, *ApJ*, **768**, 54, doi: 10.1088/0004-637X/768/1/54
- Errando M., Liodakis I., Marscher A.P., et al., 2024, *ApJ*, **963**, 5, doi: 10.3847/1538-4357/ad1ce4
- Fossati G., Maraschi L., Celotti A., Comastri A., Ghisellini G., 1998, *MNRAS*, **299**, 433, doi: 10.1046/j.1365-8711.1998.01828.x
- IceCube collaboration, 2018a, *Science*, **361**, 147, doi: 10.1126/science.aat2890
- IceCube collaboration, 2018b, *Science*, **361**, id. eaat1378, doi: 10.1126/science.aat1378
- Imazawa R. et al., 2023, *PASJ*, **75**, 1, doi: 10.1093/pasj/psac084
- Lynden-Bell, D. 1969, *Nature*, **223**, 690, doi: 10.1038/223690a0
- Marscher A. P., Di Gesu L., Jorstad S. G., et al., 2024, *Galaxies*, **12**, 50, doi: 10.3390/galaxies12040050
- Marshall H. L., Liodakis I., Marscher A.P., et al., 2024, *ApJ*, **972**, 74, doi: 10.3847/1538-4357/ad5671
- Middei R., Perri M., Puccetti S., Liodakis I., et al., 2023, *ApJL*, **953**, L28; doi: 10.3847/2041-8213/acec3e
- Raiteri C. M., Villata M., Jorstad S. G., et al., 2023, *MNRAS*, **522**, 102, doi: 10.1093/mnras/stad942
- Rees M. J., 1984, *ARA&A*, **22**, 471, doi: 10.1146/annurev.aa.22.090184.002351
- Rybicki G. B., Lightman A. P., "Radiative processes in astrophysics", John Wiley & Sons, 1985
- Peirson A. L., Negro M., Liodakis I., et al., 2023, *ApJL*, **948**, L25, doi: 10.3847/2041-8213/acd242
- Shablovinskaya E., Malygin E., Oparin D., 2023, *MNRAS*, **519**, 3798, doi: 10.1093/mnras/stac3775
- Urry C. M., Padovani P., 1995, *PASP*, **107**, 803, doi: 10.1086/133630
- Zhang H., Bottcher M., Liodakis I., 2024, *ApJ*, **967**, 93, doi: 10.3847/1538-4357/ad4112

## ARE THE DWARF NOVAE OUTBURSTS ABSENT IN VY SCL-TYPE STARS LOW STATES?

S. BOEVA<sup>1</sup> , G. LATEV<sup>1</sup> , R. MITEVA<sup>1</sup>  and Z. CVETKOVIĆ<sup>2</sup> 

<sup>1</sup>*Institute of Astronomy and National Astronomical Observatory  
(IANAO), Bulgarian Academy of Sciences, 1784 Sofia, Bulgaria*

*E-mail: sboeva@astro.bas.bg*

<sup>2</sup>*Astronomical Observatory, Volgina 7, 11060 Belgrade, Serbia*

**Abstract.** Low states light curves of VY Scl type systems show rises with amplitudes 35 mag. Despite the accepted belief that this type of star does not exhibit outbursts similar to the dwarf novae (DNe) one, their amplitudes, shapes and periods are similar to DNe with the same orbital periods. MV Lyr, TT Ari and KR Aur show periodicities in the range 200-400 d, but second maximum in power spectra also occurs around 850-1000 d.

The estimation of the change of mass loss via coronal mass ejections during the solar activity cycle can vary more than 5 times. The red dwarfs magnetic cycles with duration of years can explain the reduced mass transfer and long deep states in VY Scl variables.

### 1. INTRODUCTION

Cataclysmic variables (CVs) are evolved semi-contact close binary systems containing usually white dwarf and a donor of mass – a red dwarf. In rare cases, the donor may be a slightly evolved main sequence (MS) star, giant, or other white dwarf. Depending on the strength of the magnetic field of the white dwarf, systems can be magnetic or non-magnetic and the accreting matter falls through L1 via an accretion disk or accretion columns onto the primary star. According to the light curves, they are divided into different types and subtypes – novae (Ne), recurrent novae (RNe), dwarf novae (DNe) and novae-like (NLs) stars.

DNe are stars that show periodic bursts with an amplitude of 2–6 magnitudes at intervals from days to several years due to thermal-viscous instability of the disk. NLs, in contrast, are stars with a high accretion rate and a hot stable bright disk. VY Scl type stars (or anti-dwarf novae) are their subclass, which due to reduction or cessation of the accretion rate from the secondary star fall into low states with an amplitude of 2–6 mag, lasting several months to years. These low states are perceived to be occasional. Low states are also observed in other types of CVs – AM Her type (polars – systems without disk), intermediate polars (IP), DNe. It is accepted that due to magnetic properties of the secondary star mass transfer  $\dot{M}$  impedes or stops completely. These components are low mass, almost fully convective stars with powerful magnetic field and they could produce  $10^3$ – $10^4$  mass loss rate more than Sun via stellar wind, flares and coronal mass ejections (CMEs) (Mullan, 1996).

A possible physical mechanism of the mass transfer decrease was given by Livio and Pringle (1994) – magnetic spots on the surface of the secondary near L1 can

prevent Roche-lobe overflow. Bianchini (1990) proposed another explanation – solar-like cycles of the secondaries can cause radius variations  $\Delta R/R \sim 10^{-4}$  and the shrink can reduce mass transfer  $\dot{M}$  too. Other mechanisms like tidal instability, irradiation effects on the secondary star etc. can affect mass transfer in the binaries.

The typical  $\dot{M}$  in NLs is  $\sim 10^{-8}$ – $10^{-9}$   $M_{\odot}/\text{yr}$ . In DNe  $\dot{M}$  is smaller,  $\sim 10^{-11}$  (up to  $10^{-10}$ )  $M_{\odot}/\text{yr}$ . At low state of VY Scl type stars reduced mass transfer is estimated to be similar to the DNe ones and the theoretical calculations show that the mass in their disks is enough to start up and sustain dwarf nova eruptions. Although the low state brightness of stars shows rise and decline, it is assumed in the literature that such eruptions are not observed. Leach et al. (1999) and Hameury and Lasota (2002) assumed that the disc instability outbursts can be suppressed by hot white dwarf ( $T \sim 40\,000$  K) or by the magnetic field on the white dwarf with a strength comparable to the values in IPs.

In this study we compare some properties of the observed outbursts in low states in MV Lyr, TT Ari and KR Aur to the dwarf novae ones. The analogy with the solar activity at different phases of the Sun’s magnetic cycle could explain the existence of low states in cataclysmic variables and the observed mass accretion rate drop values.

## 2. DATA AND DATA ANALYSIS

The study of low states is difficult because of the low brightness of the objects. Only in the last 20–30 years, with the development of observation techniques they become available for observation by many amateur organizations such as the AAVSO<sup>1</sup>. We used AAVSO light curves in visual and Johnson’s V band for MV Lyr, TT Ari and KR Aur.

For data extracting, selecting and plotting we use the AAVSO multi-platform VStar (Benn, 2012). The periodogram analysis was performed by Date Compensated Discrete Fourier Transform (DC DFT) method implemented in VStar period analyser routine.

Data from SOHO/LASCO CDAW catalog<sup>2</sup> were used for the calculations of the occurrence rate and the mass lose due to the observed CMEs at different solar activity states in 1996 – 2020.

## 3. RESULTS

### 3. 1. OUTBURSTS DURING LONG LOW STATES IN VY SCL VARIABLES AND DWARF NOVAE ERUPTIONS

VY scl type stars in rare occasions show peculiar very long deep states up to  $\sim 10$  years. A few of them, e.g., MV Lyr, KR Aur and TT Ari, repeated several times such low states. Many authors noticed their erratic behavior with sudden drops and rises. For instance, Fig. 1 shows the long-term light curve of MV Lyr. Shugarov and Pavlenko (1998) revealed 3 types of outbursts in low state with amplitudes 1 to 4 mag and duration from few days to 200 days and always the brightness was fainter than the one in the high state. The upper rows of Figures 2 and 3 give more detailed picture of MV Lyr behavior at the minima in 1995–2003 (Min1) and 2007–2015 (Min2).

<sup>1</sup><https://www.aavso.org/>

<sup>2</sup><https://cdaw.gsfc.nasa.gov>



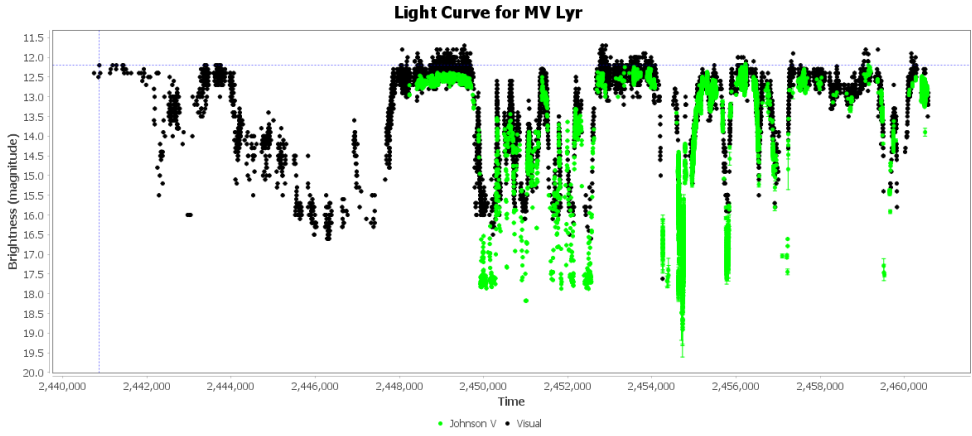


Figure 1: Long-term light curve of MV Lyr from 1971 to 2024 in Visual and V band.

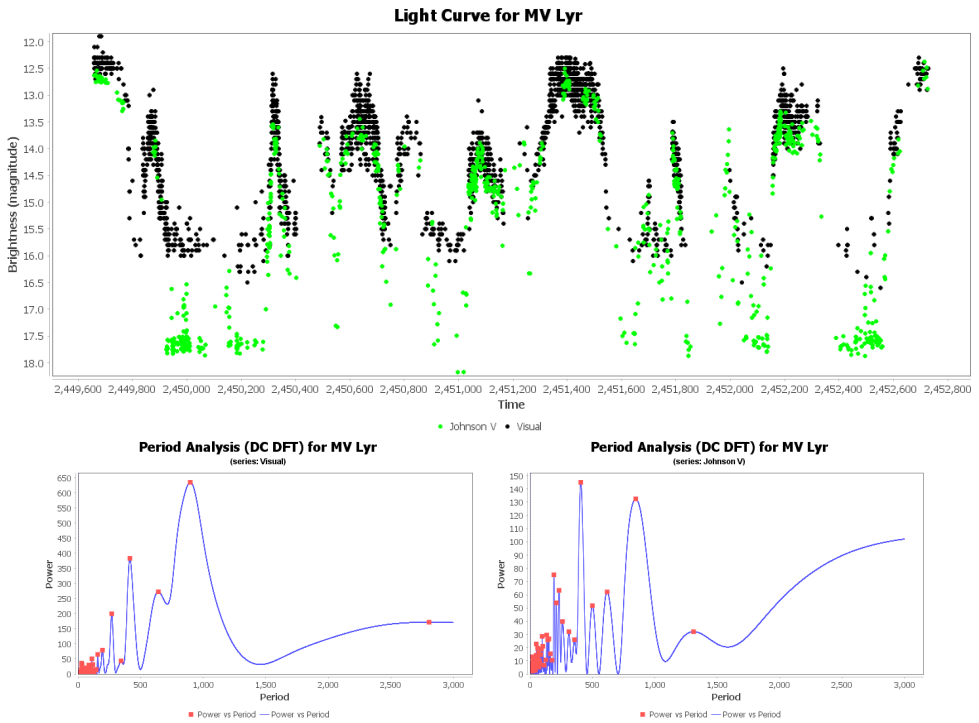


Figure 2: Upper plot: Low state of MV Lyr from 1995 to 2003. Lower plots: Power spectra in Visual (left) and V band (right).

Dwarf novae light curves are also not strictly periodic. They show different lengths and shapes of the outbursts. DNe outbursts can be with fast or slow rise, short or long, normal or superoutburst with larger amplitude and duration. Figure 4 represents the behavior of a typical DN variable SS Cyg. Despite the different time scale quite a few similarities can be seen between the shapes of the outbursts of SS Cyg and MV Lyr at the first minimum (Min1). The next low state of MV Lyr was quite different in occurrence rate and amplitudes of outbursts.

The period analysis was performed for 5 MV Lyr low states, 2 for TT Ari and 3 for KR Aur. Figures 2 and 3 (lower rows) show power spectra for visual and Johnsons V filter observations for Min1 and Min2 respectively. Similar power spectra gives analogical periods for all 3 variables in the range 200–400 d, but second maximum occurs around 850–1000 d.

Many statistical studies were carried out for DNe systems parameters and their outbursts, e.g. Coppejans et al. (2016) and Otulakowska-Hypka et al. (2016). The orbital periods ( $P_{orb}$ ) of VY Scl type variables ( $\sim 3.5\text{--}4$  h) are longer than DNe  $P_{orb}$  (usually  $< 2$  h). For such  $P_{orb}$  the lower-limit on the outburst amplitude is in the range 2.5–3 mag and the upper-limit of the recurrence time is from 20–30 d to 1000 d. Probably the duty cycle value  $\sim 0.6$  is larger, but values  $\sim 0.4$  also exist, usually for DNe with larger  $P_{orb}$ .

Several empirical relations for DNe are valid for VY Scl type stars too. For instance in Min1 MV Lyr shows two types of outbursts: short (with amplitudes  $\sim 4$  mag and a period  $\sim 250$  d) and long (with amplitudes  $\sim 5$  mag and a period  $\sim 800$  d). The first type can be interpreted as normal outbursts and the second one – as superoutbursts. In Min2, the system shows a different behavior that can be explained by entering in the superoutbursts regime without normal outbursts. That event may occur due to a higher mass accretion rate. These properties of low-state bursts led us to assume that their nature is similar to DNe eruptions.

### 3. 2. LOW STATES AND SOLAR MAGNETIC CYCLE

The Sun is our closest star and various parameters of its magnetic activity can be observed and measured easier than on other stars. Various space-borne instruments in the last 30 years improved the volume and accuracy of the collected solar data.

Prior to the space era, observations of the solar activity and sunspots have been carried out for about 400 years, while similar cycles were discovered for other stars about 40 years ago, including the late-type secondary components of various classes of cataclysmic stars, e.g., GK Per, TT Ari, SS Cyg, etc. (Bianchini, 1990). The sunspot cycle is nearly 11 years long while solar-like stellar cycles last usually 3–20 (30) years, with a maximum of the distribution  $\sim 6$  years.

The mass loss rate of the Sun via solar wind is  $\sim 2\text{--}3 \times 10^{-14}$   $M_{\odot}/\text{yr}$  and consists of almost constant component – thermal solar wind, and variable one – solar flares and CMEs. In the solar wind, CMEs component can contribute up to 15–20% of the mass loss rate. In the late type MS stars the magnetic activity is stronger and thermal winds can exceeded more than 1000 times the solar wind. CMEs in active dwarfs can contribute to larger part of the stellar mass loss.

The stellar activity on the secondary star can produce mass transfer bursts via CMEs or solar flares. In the light curves of the stars fast variations of the brightness were observed. In time-scales from seconds (minutes) to 1–2 hours such flare events

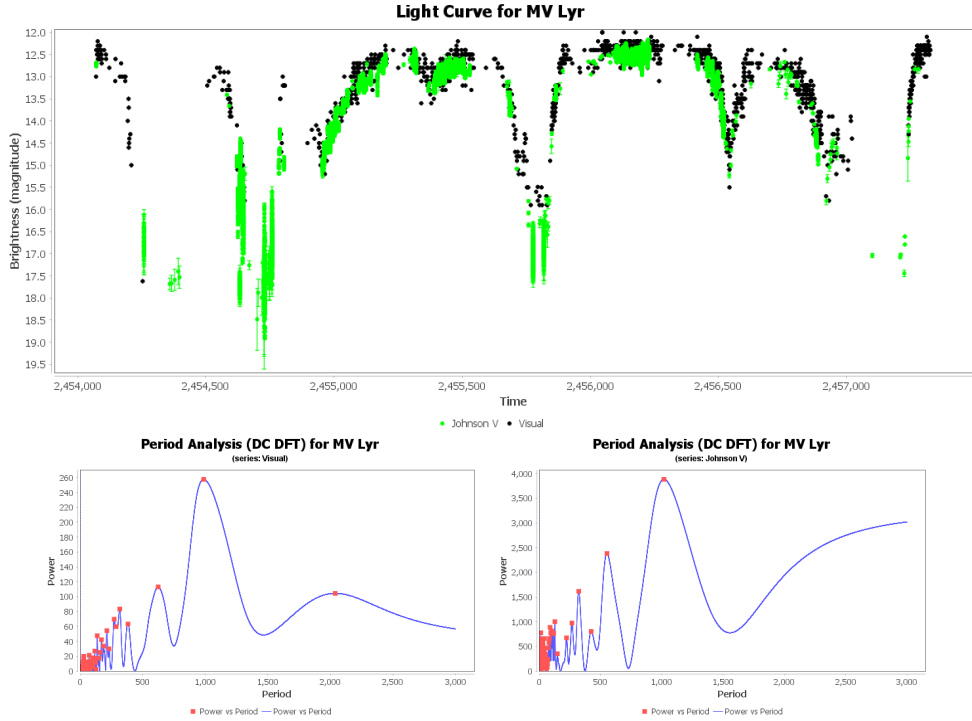


Figure 3: Upper plot: Low state of MV Lyr from 2007 to 2015. Lower plots: Power spectra in Visual (left) and V band (right).

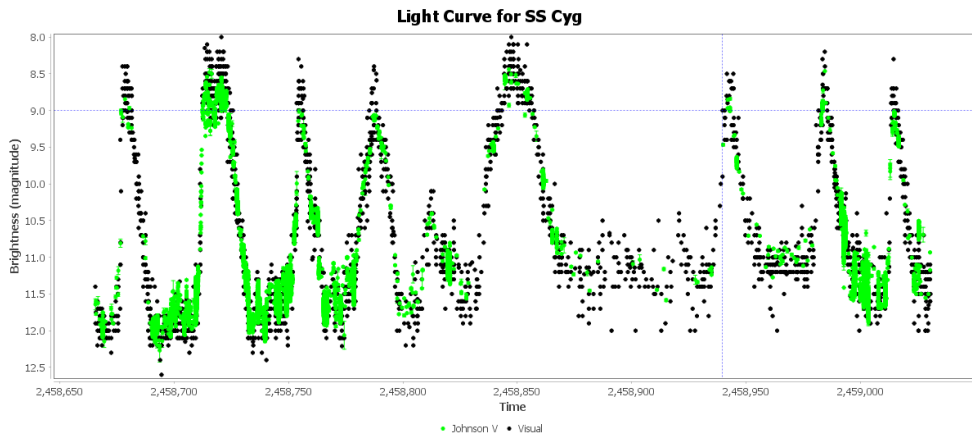


Figure 4: AAVSO light curve of SS Cyg (2019–2020).

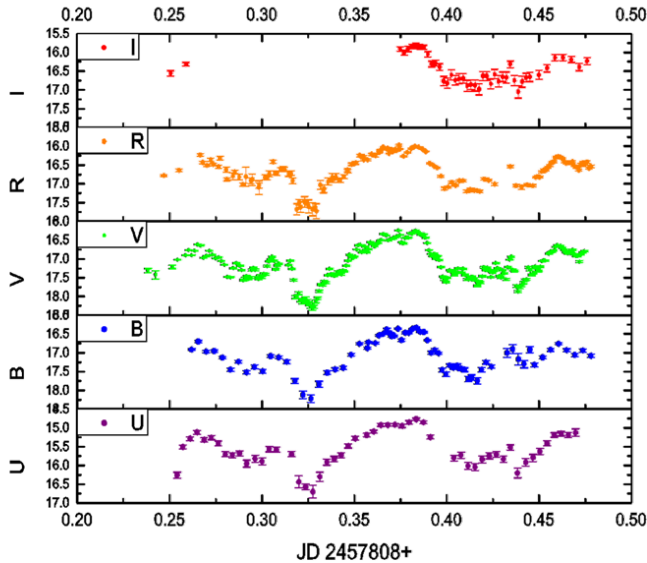


Figure 5: Multicolor simultaneous light curve of KR Aur received on 23.02.2017 using 4 telescopes in Bulgaria and Serbia (from Boeva et al, 2021a).

reach amplitudes 1–2 or more magnitudes and they are visible in the range from X-rays to radio wavelengths. The energy of the most powerful stellar flares is  $\sim 10^{36}$ – $10^{37}$  erg (Schmitt et al., 2019).

Figure 5 presents 5 color observations of flare in KR Aur, received on 23.02.2017. The total energy of this flare is calculated to be  $\sim 10^{36}$  erg, which value is close to the strongest observed flares (Boeva et al., 2021b). It is not clear if these bursts are flares on the secondary star or they represent sporadic accretion of blobs onto the white dwarf (Rodrguez-Gil et al., 2020).

There are many statistical studies of the occurrence rate of flares and CMEs with solar cycle phase. X-rays observations show  $\sim 100$  times increase of the number of flares during maximum of the solar activity compared to the minimum of the cycle (Aschwanden and Freeland, 2012). Lamy et al. (2019) reported 10–40 times more CMEs at solar maximum versus minimum. A correlation exists between occurrence rate of CMEs and total sunspot number however the total mass loss rate from the Sun through CMEs does not depend significantly on the strength of the cycle and the CMEs occurrence rate (Michalek et al., 2022). The fraction of mass loss due to CMEs vary from less than 1% at minimum to  $\sim 10\%$  at maximum.

The temporal evolution of mass loss rate of the secondaries in CVs during the solar-like cycle can affect mass transfer in the system. To study this we calculated the average CME number ( $N$ ) and their mass ( $m$ ) for three-month periods near maxima and minima of solar activity using CDAW catalog. The database contains 3 minima and 2 maxima from 1996 to 2020. Average mass ( $m$ ) of CMEs (those with reported mass) and the total mass ( $M$ ) are given in Table 1. We obtained 2.44 more events in maximum versus minimum, with 2.45 larger average mass, which provides 5 times more mass loss. The average total mass of CMEs varies slightly at maxima but at

Table 1: CMEs average number, average mass and overall mass at minimum and maximum of solar activity.

	N	m (g)	M (g)
Minima			
1996	120.33	5.79E+14	7.19E+16
2008/2009	61.00	8.37E+14	5.38E+16
2019/2020	44.67	2.59E+14	1.16E+16
average	75.33	5.58E+14	4.58E+16
Maxima			
2001	144.33	1.61E+15	2.09E+17
2014	224.00	1.13E+15	2.52E+17
average	184.17	1.37E+15	2.30E+17

minima it fluctuates around 6 times. The result can explain the decrease of mass transfer rate in the order of 1–2 magnitudes at VY Scl stars minima.

Solar cycles show long-term modulation too. The 11-year sunspot and 22-year magnetic cycles are well known but solar activity can vary significantly over the cycles length, shape and strength and also over longer periods. The amplitude of the solar cycle is modulated by the larger 100 ( $\pm 40$ ) years Gleissberg cycle, but longer periodicities exist too (Biswas et al., 2023). Such long cycles can explain the different VY Scl type variables behavior even between adjacent low states.

#### 4. CONCLUSIONS

The mass transfer never stops completely because of weak accretion rate due to the magnetic activity of the secondary. Long-term light curves of VY Scl type systems shows rises with amplitudes 3–5 mag, which durations and intervals between outbursts are similar to the dwarf novae eruptions. The detected periods for several systems are in agreement with empirical relations obtained for dwarf novae. The red dwarf magnetic cycles with duration of years can explain the reduced mass transfer and long deep states in VY Scl variables.

We estimated the increase in the mass loss via CMEs for the Sun by a factor of 5 (or more) during maximum versus minimum of the solar activity. Long-term modulations of solar-like cycles can cause different photometric behavior in the low states.

#### Acknowledgments

This work was supported by the Ministry of Science, Technological Development and Innovations of the Republic of Serbia through the Project contract No. 451-03-66/2024-03/200002.

The authors gratefully acknowledge the observing and financial grant support from the Institute of Astronomy with NAO – Bulgarian Academy of Sciences through the bilateral SANU-BAN joint research project *Astrometry and photometry of visual double and multiple stars*.

## References

- Aschwanden, M. J.; Freeland, S. L.: 2012, *ApJ*, **754**, 112, doi: 10.1088/0004-637X/754/2/112
- Benn, D.: 2012, *JAAVSO*, **40**, 852
- Bianchini, A.: 1990, *AJ*, **99**, 1941, doi: 10.1086/115476
- Biswas, A., Karak, B. B., Usoskin, I., Weisshaar, E.: 2023, *SSRv*, **219**, 19, doi: 10.1007/s11214-023-00968-w
- Boeva, S., Latev, G., Zamanov, R., Tsvetkova, S., Nikolov, P., Petrov, B., Spassov, B., Cvetković, Z., Stoyanov, K., Damljanović, G.: 2021, *The Golden Age of Cataclysmic Variables and Related Objects V, 2–7 September 2019, Palermo, Italy*, id.28, doi: 10.22323/1.368.0028
- Boeva, S., Zamanov, R., Koleva, K., Dechev, M.: 2021, *Proceedings of the Thirteenth Workshop "Solar Influences on the Magnetosphere, Ionosphere and Atmosphere", held in Primorsko, Bulgaria, 13–17 September 2021, edited by Katya Georgieva, Boian Kirov and Dimitar Danov, ISSN 2367-7570*, p. 4–7, doi: 10.31401/WS.2021.proc
- Coppejans, D. L.; Körding, E. G.; Knigge, C.; Pretorius, M. L.; Woudt, P. A.; Groot, P. J., Van Eck, C. L., Drake, A. J.: 2016, *MNRAS*, **456**, 4441, doi: 10.1093/mnras/stv2921
- Hameury, J.-M.; Lasota, J.-P.: 2002, *A&A*, **394**, 231, doi: 10.1051/0004-6361:20021136
- Lamy, P. L., Floyd, O., Boclet, B., Wojak, J., Gilardy, H., Barlyaeva, T.: 2019, *SSRv*, **215**, 39, doi: 10.1007/s11214-019-0605-y
- Leach, R., Hessman, F. V., King, A. R., Stehle, R., Mattei, J.: 1999, *MNRAS*, **305**, 225, doi: 10.1046/j.1365-8711.1999.02450.x
- Livio, M., Pringle, J. E.: 1994, *ApJ*, **427**, 956, doi: 10.1086/174202
- Michalek, G.; Gopalswamy, N.; Yashiro, S.: 2022, *ApJ*, **930**, 74, doi: 10.3847/1538-4357/ac4fcb
- Mullan, D. J.: 1996, *Cool stars; stellar systems; and the sun: 9; Proceedings of the 9th Cambridge workshop; held 3–6 October 1995 in Florence; Italy; San Francisco: Astronomical Society of the Pacific (ASP); edited by Roberto Pallavicini and Andrea K. Dupree*, **109**, 461
- Otulakowska-Hypka, M., Olech, A., Patterson, J.: 2016, *MNRAS*, **460**, 2526, doi: 10.1093/mnras/stw1120
- Rodríguez-Gil, P., Shahbaz, T., Torres, M. A. P., Gänsicke, B. T., Izquierdo, P., Toloza, O., Álvarez-Hernández, A., Steeghs, D., van Spaandonk, L., Koester, D., Rodríguez, D.: 2020, *MNRAS*, **494**, 425, doi: 10.1093/mnras/staa612
- Schmitt, J. H. M. M., Ioannidis, P., Robrade, J., Czesla, S., Schneider, P. C.: 2019, *A&A*, **628**, 79, doi: 10.1051/0004-6361/201935374
- Shugarov, S. Yu., Pavlenko, E. P.: 1998, *ARep*, **42**, 370

## ASTROPHYSICAL APPLICATIONS OF STARK BROADENING OF SINGLY IONIZED PALLADIUM SPECTRAL LINES

M. D. CHRISTOVA<sup>1</sup>  and M. S. DIMITRIJEVIĆ<sup>2,3</sup> 

<sup>1</sup> *Department of Applied Physics, Technical University of Sofia, 1000 Sofia, Bulgaria*

*E-mail: mchristo@tu-sofia.bg*

<sup>2</sup> *Astronomical Observatory, Volgina 7, 11060 Belgrade, Serbia*

<sup>3</sup> *LERMA, Observatoire de Paris, Université PSL,  
CNRS, Sorbonne Université, F-92190 Meudon, France*

**Abstract.** We review our recently published work on the Stark broadening of Pd II spectral lines, calculated by employing the Modified semiempirical theory, which includes the applications of obtained results for the investigation of the influence of Stark broadening in the atmospheres of A type stars, DB and DO white dwarfs. The influence of Stark broadening in stellar atmospheres is discussed including the previously published Stark width results (calculated with the help of the same method) for spectral lines of other chemical elements. Discussion on the astrophysical applications is included. As an application of obtained results, Stark width behaviour with temperature of Pd II spectral lines is also analyzed.

### 1. INTRODUCTION

According to the literature, palladium spectral lines are detected in spectra of different types of stars. Biémont *et al.* (1982) report the presence of neutral palladium in solar spectrum. In very metal poor red giants HD 107 752, HD110 184, HD85 773, HD23 798, and BD+6°648 are found Pd I spectral lines by Aoki *et al.* (2017). Adelman *et al.* (1979) present neutral palladium spectra for peculiar A star  $\gamma$  Equulei. Singly ionized palladium spectral lines are observed in the spectra of HgMn star  $\chi$  Lupi by Lundberg *et al.* (1996) and in a post-asymptotic giant branch star of spectral type B8 III in the globular cluster 47 Tucanae (NGC104) by Dixon *et al.* (2021). This is an indication that experimental and calculated spectroscopic results for palladium lines are of interest for reliable analysis and stellar atmosphere modeling of these objects. Particularly, for hot stars, for Hg-Mn stars, A and late B type stars, and white dwarfs, Stark broadening data are needed.

In this study, we inform shortly about our work on Stark broadening of Pd II spectral lines and the influence of this broadening mechanism in stellar atmospheres spectra (Dimitrijević and Christova, 2024). Additionally, temperature dependence of Stark widths of Pd II spectral lines is discussed. The studied lines belong to  $5s^2F - 5p^2G^\circ$ ,  $5s^4F - 5p^4D^\circ$ ,  $5s^4F - 5p^4G^\circ$  and  $5s^4F - 5p^4F^\circ$  multiplets. The table with calculated Stark widths could be found in Dimitrijević and Christova (2024). The temperature interval covers values from 5 000 K to 160 000 K and the perturber density is  $10^{17}$  cm<sup>-3</sup>. The modified semiempirical method (MSE) of Dimitrijević and Konjević (1980) is applied for 47 spectral lines of singly charged palladium ion.

Illustration of the importance of Stark broadening of spectral lines for the modelling of stellar atmospheres of DB and DO white dwarfs, as well as of A type star is also presented.

In the discussion of the influence of Stark broadening in stellar atmospheres, our previously published Stark width results (calculated with the help of the MSE method) for spectral lines of other chemical elements: Lu II (Dimitrijević and Christova, 2021), Si II (Dimitrijević *et al.*, 2023), Al IV (Dimitrijević and Christova, 2023), Zn III (Dimitrijević and Christova, 2022), *etc.* are also commented. For all these elements, including Pd II, we found in literature the need of Stark broadening data for the investigation, analysis and modeling of stellar plasma, which was our principal reason for investigations. These elements play a key role in nucleosynthesis mechanisms and could provide valuable interpretation of such processes. For example, for elements heavier than iron, nucleosynthesis is governed by two leading neutron-capture processes, s-process, and r-process. The difference is in time scale in comparison to the half-life of beta decay. The s-process is ongoing at a slower rate, while r-process occurs at a rapid rate. The r-elements formation is not well understood. An outstanding example of the information on the r-process signature is uranium-rich metal-poor star CS 31082-001 (Siqueira *et al.*, 2013), where Lu spectral lines are measured in the near-UV HST/STIS and optical UVES spectra. Since CS 31082-001 is an extremely metal poor star (EMP) with large r-element excesses, adequate abundance interpretation could help r-nucleosynthesis understanding. Lutetium belongs to rare earth elements (REE) and the main part of the line spectrum is in UV diapason. According to Roederer *et al.* (2012), the spectroscopic observations from Goddard High Resolution Spectrograph (GHRS) and Space Telescope Imaging Spectrograph (STIS) on board of the Hubble Space Telescope (HST) for spectral lines of heavy elements indicate that almost all stars contain traces, at least of chemical elements heavier than iron. Lu is one of these elements which determine a key role for understanding neutron-capture nucleosynthesis mechanisms and could be observed mainly in near ultraviolet. It is reported that rare earth elements, as lutetium, are detected in metal poor red giant stars as first ions. The reliable modeling of metal poor stars atmospheres requires huge atomic and molecular data and Stark broadening parameters, also. The lack of experimental and theoretical Lu II Stark broadening data in the literature, was the motivation for our investigation.

In contrast to lutetium, silicon and aluminum are one of the richly populated elements in the universe, the sixth and twelfth most common elements, respectively. Silicon ions are very important for investigations of stellar and solar plasmas. One of the earlier papers (Peytreman, 1972) presents various cosmic light sources that contain silicon atoms and ions as emitters. He observed many singly charged ion lines in the atmospheres of A, B and O type stars, and white dwarfs, also. Lanz *et al.* (1988) report that the spectrum of Si II is dominant for stars from A0 to B3 spectral type (effective temperatures from 10,000 to 20,000 K) where strong visible spectral lines are observed. At these plasma conditions, broadening due to collisions with electrons is the main pressure broadening mechanism. Solar photosphere study is performed by Shi *et al.* (2008) using ionized silicon lines. The widths of such lines enable the diversity determination of supernovae Ia by Arsenijević *et al.* (2008). Prominent Si II lines take part in the emission spectra of the first helium nova V445 Puppis (Iijima and Nakanishi, 2008).



As was mentioned above, aluminum has high cosmic abundance and astrophysical significance in the Universe. Its spectral lines are frequently present in stellar spectra (Smiljanic *et al.*, 2016, Carretta *et al.*, 2018, Smith, 1993). Aluminum abundances in giants and dwarfs were determined (Smiljanic *et al.*, 2016) and their implications on stellar and galactic chemical evolution were investigated. Aluminum abundances for red giant branch (RGB) stars in NGC 2808 were derived by Carretta *et al.* (2018). Smith (1993) reports atmospheric abundance of aluminum for a sample of normal, superficially normal and HgMn-type main-sequence late-B stars.

Similar as in the case of lutetium, the nucleosynthesis of zinc is not well understood (Barbuy *et al.*, 2015). To be investigated, abundances for various galactic stars are needed, as is underlined in Sneden *et al.* (1988). Zinc is also significant for: i) examination of star formation rate; ii) chemical enrichment of the Galactic bulge (Barbuy *et al.*, 2015, Da Silveira *et al.*, 2018 and references therein); iii) chemical evolution of the Universe at high redshifts, by studying abundances in damped Lyman- $\alpha$  systems (DLAs) (Pettini *et al.*, 1999, Rafelski *et al.*, 2012, 2014). For abundance determination, various atomic data for zinc, including Stark broadening parameters are of interest. Spectral lines of Zn III are observed in spectra of several O type stars, pulsators, etc. Lehmann *et al.* (2010) report observations of Zn III line in  $\theta$ 1 Ori C (O type star) from multiple stellar system Theta Orionis. Zinc abundance determination is published in Dorsch *et al.* (2019) for hot subdwarf stars of O type (sdO) HZ 44 and HD 127493 using spectral lines of Zn III and Zn IV. Zinc abundances were obtained for intermediate He-sdOB star: the pulsators Feige 46 and LS IV14 $^{\circ}$ 116 where strong Zn III spectral lines were applied. Abundance determination of zinc needs Stark broadening parameters (Sneden *et al.*, 1988, Barbuy *et al.*, 2015). There are no experimental Stark broadening results in the literature where calculations for a few spectral lines were available, only.

All these astrophysical goals need reliable Stark widths and shifts that was the reason for our Stark broadening calculations. These data enter chemical abundance determination, modelling of radiative transfer and stellar atmospheres, analysis and synthesis of stellar spectra.

## 2. METHOD

The modified semiempirical method (Dimitrijević and Konjević, 1980) is developed to calculate the full width at half intensity maximum (FWHM) of an isolated spectral line, emitted or absorbed by a non-hydrogenic ion perturbed by surrounding electrons. When important spectroscopic data for non-hydrogenic ions are missed in the literature, and there is no enough data for more sophisticated methods, the modified semiempirical method could be used, what is its major advantage. According to the MSE the Stark width is given by the expression:

$$W_{MSE} = N \frac{8\pi}{3} \frac{\hbar^2}{m^2} \left( \frac{2m}{\pi kT} \right)^{1/2} \frac{\pi}{\sqrt{3}} \frac{\lambda^2}{2\pi c} \times$$

$$\times \left\{ \sum_{\ell_i \pm 1} \sum_{L_i, J_i} \bar{R}^2 [n_i \ell_i L_i J_i, n_i (\ell_i \pm 1) L_i' J_i'] \tilde{g}(x_{\ell_i, \ell_i \pm 1}) + \right.$$

$$\begin{aligned}
& + \sum_{\ell_f \pm 1} \sum_{L_f, J_f} \vec{R}^2[n_f \ell_f L_f J_f, n_f(\ell_f \pm 1) L_f J_f] \tilde{g}(x_{\ell_f, \ell_f \pm 1}) + \\
& + \left( \sum_{i'} \vec{R}_{ii'}^2 \right)_{\Delta n \neq 0} g(x_{n_i, n_i+1}) + \left( \sum_{f'} \vec{R}_{ff'}^2 \right)_{\Delta n \neq 0} g(x_{n_f, n_f+1}) \}. \quad (1)
\end{aligned}$$

where  $i$  and  $f$  indicate initial and final energy level of the studied transition. The square of the matrix element is given by expression:

$$\begin{aligned}
& \vec{R}^2[n_k \ell_k L_k J_k, n_k(\ell_k \pm 1) L'_k J'_k] = \\
& \frac{\ell_{>}}{2J_k + 1} Q[\ell_k L_k, (\ell_k \pm 1) L'_k] Q(J_k, J'_k) [R_{n_k^* \ell_k}^{n_k^* \ell_k \pm 1}]^2. \quad (2)
\end{aligned}$$

The quantity  $x_{\ell_k, \ell_k'}$  in Eq. (1) denotes the ratio:

$$x_{\ell_k, \ell_k'} = \frac{E}{\Delta E_{\ell_k, \ell_k'}}, \quad k = i, f. \quad (3)$$

For  $\Delta n \neq 0$ , the energy difference between energy levels with  $n_k$  and  $n_k+1$ , is represented by the following equation:

$$\Delta E_{n_k, n_k+1} = 2Z^2 E_H / n_k^{*3}, \quad (4)$$

where  $n_k^* = [E_H Z^2 / (E_{ion} - E_k)]^{1/2}$  is the effective principal quantum number,  $N$  the electron density,  $T$  the temperature,  $Z$  the residual ionic charge,  $E_{ion}$  the appropriate spectral series limit,  $Q(\ell L, \ell' L')$ , multiplet factor and  $Q(J, J')$  line factor (Shore and Menzel, 1965). Gaunt factors are denoted as  $g(x)$  (Griem, 1968, 1974) and  $\tilde{g}(x)$  (Dimitrijević and Konjević, 1980). Radial integrals  $[R_{n_k^* \ell_k}^{n_k^* \ell_k \pm 1}]$  are calculated by applying the Coulomb approximation (Bates and Damgaard, 1949), tables in Oertel and Shomo (1968) and the method of Van Regemorter *et al.* (1979), in cases when for higher atomic energy levels the tables in Oertel and Shomo (1968) are not applicable.

### 3. RESULTS

In order to demonstrate the importance of Stark broadening in astrophysics, particularly in the modelling of stellar atmospheres, we examined in Dimitrijević *et al.* (2024), by using the obtained results, three cases of plasma and surface gravity conditions. Stark broadening (full width at half intensity maximum) of singly ionized palladium spectral line  $(^1G)5s^2G - (^1G)5p^2H^o$ ,  $\lambda = 2486.36 \text{ \AA}$  is calculated versus Rosseland optical depth. It is compared with Doppler broadening for models of stellar atmosphere of: an A type star ( $T_{eff} = 8500 \text{ K}$  and  $\log g = 4.5$ ); a DB white dwarf with an effective temperature of  $25,000 \text{ K}$  and  $\log g = 8$  and a DO white dwarf ( $T_{eff} = 60,000 \text{ K}$  and  $\log g = 8$ ). Model of Kurucz (1979) is applied for an A type star and model of Wesemael (1981) for atmospheres of hot and high-gravity stars. Our results for Stark and Doppler dependance on the Rosseland optical depth outline the significance of Stark broadening mechanism of Pd II spectral lines in the atmospheres of hotter stars, DB and DO white dwarfs. It is the major broadening mechanism in these environments for the corresponding plasma conditions. This is valid even

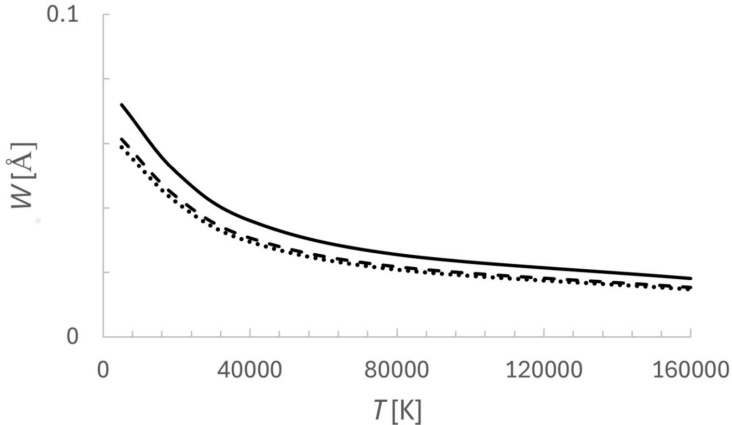


Figure 1: Temperature dependence of the Stark width for spectral lines from multiplet Pd II  $5s^4F - 5p^4D^o$  for an electron density of  $10^{17} \text{ cm}^{-3}$ :  $5s^4F_{5/2} - 5p^4D_{3/2}^o$  - dot line;  $5s^4F_{7/2} - 5p^4D_{7/2}^o$  - dash line;  $5s^4F_{5/2} - 5p^4D_{7/2}^o$  - solid line.

for DO dwarf atmosphere with  $T_{eff} = 60,000 \text{ K}$ , in spite of the increase of Doppler broadening with temperature. Stark widths are larger than Doppler ones, more than an order of magnitude for all examined optical depths, in this case. In the case of the considered A-type star atmosphere, Stark broadening is negligible within the whole range of examined optical depths. We found the same result in our recent studies of 19 spectral lines in the spectrum of singly charged lutetium ion (Dimitrijević *et al.*, 2021), 13 Si II multiplets (Dimitrijević *et al.*, 2023), 23 Al IV transitions (Dimitrijević and Christova, 2023), and 24 Zn III multiplets (Dimitrijević and Christova, 2022). However, in the case of A-type stars, there are spectral lines where Stark broadening is not negligible. An example are the Sn II lines, considered in Dimitrijević *et al.* (2024).

Additionally, we used the obtained results to show the Stark width dependence on the temperature. In Figure 1, results for three spectral lines from Pd II  $5s^4F - 5p^4D^o$  multiplet is shown. The results for three lines (nine lines belong to this multiplet) include the largest and the smallest width within the considered multiplet. We see that the difference is noticeable. For example, for  $T = 20,000 \text{ K}$ , the width of the highest curve is 22% larger than the width of the lowest one. If expressed in angular frequency units, the difference is 8.6%, which is much smaller. We note that Wise and Konjević (1982), on the basis of analysis of existing experimental Stark widths within multiplets, supermultiplets and transition arrays, concluded that the differences between linewidths within a multiplet, if expressed in angular frequency units, are a few per cent, within a supermultiplet about 30% and in transition array within a range of about 40%. In the considered case the difference is larger than predicted by Wiese and Konjević (1982). This is because the difference between the highest and lowest energy level in the term  $5p^4D^o$  is  $5931.341 \text{ cm}^{-1}$  and this value is not much smaller in comparison with the distance to the term  $5s^4F$ . The temperature dependence of the Stark width for spectral lines from Pd II multiplets  $5s^2F - 5p^2G^o$  and  $5s^4F - 5p^4G^o$  is similar.

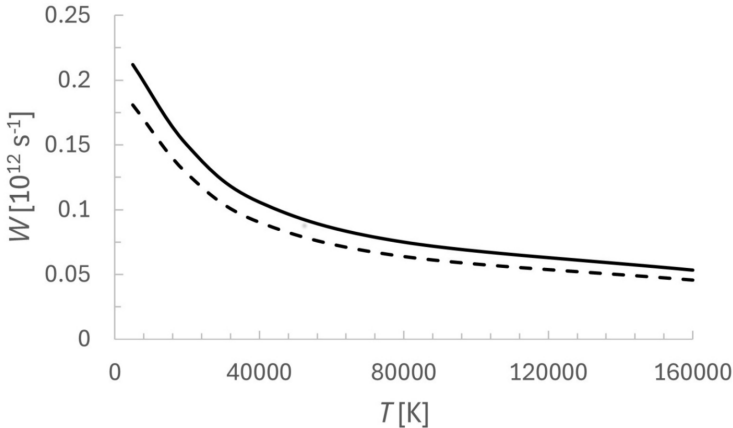


Figure 2: Variation of the Stark width in angular frequency units versus temperature for a supermultiplet Pd II  $5s^2F - 5p^2L^o$  ( $L = G, F$ ) for an electron density of  $10^{17} \text{ cm}^{-3}$ :  $5s^2F_{5/2} - 5p^2F_{7/2}^o$  - dash line;  $5s^2F_{3/2} - 5p^4D_{3/2}^o$  - solid line.

To illustrate the T-dependence of Stark broadening within a supermultiplet, we include such results in Figure 2 for the case of  $5s^2F - 5p^2L^o$  ( $L = G, F$ ) supermultiplet. The smallest and the largest width within this supermultiplet ( $5s^2F_{7/2} - 5p^2F_{7/2}^o$ ,  $\lambda = 2715.7 \text{ \AA}$  and  $5s^2F_{7/2} - 5p^2G_{9/2}^o$ ,  $\lambda = 2855.4 \text{ \AA}$ ) are given in angular frequency units. The largest width is 31% larger than the smallest one when it is expressed in Ångströms and 17% in angular frequency units, which is well within the limits predicted by Wiese and Konjević (1982).

#### 4. SUMMARY

Temperature dependence of calculated Stark widths belonging to Pd II spectral lines within a multiplet and supermultiplet is presented in this work. Possible applications of the results for astrophysical purposes are proposed. The significance of Stark broadening of Pd II spectral lines, in stellar atmospheres of hot stars from spectral type DB and DO white dwarfs is demonstrated. The modelling of their atmospheres according to Kurucz (1979) and Wesemael (1981) outlines that the principal broadening mechanism of singly charged palladium spectral lines for the corresponding conditions is Stark broadening. For A-type star atmospheres, the model of Kurucz (1979) indicates weak and negligible influence of Stark broadening on the considered Pd II spectral lines. Discussion of Stark/Doppler broadening ratio behavior as a function of the optical depth is performed for previously published results for Lu II, Al IV, Zn III and Sn II spectral lines. The conclusion is that Stark broadening is very important for DB and DO white dwarf atmospheres and that there are cases, as for example Sn II lines, where it is not negligible for A-type stars,

Stark broadening data of Pd II spectral lines could be applied for different goals in astrophysics, as abundance determination of palladium, analysis and synthesis of singly ionized palladium lines in stellar spectra, opacity calculations, spectroscopic diagnostics of laboratory and industrial plasmas, but also to investigate palladium

plasma created by generation of high-order harmonics of laser pulses.

### Acknowledgements

This work has been supported with a STSM visit grant E-COST-GRANT-CA18222-5308184a for M.S.D. within the framework of COST Action CA18222 Attosecond Chemistry - ATTOCHEM. We are kindly thankful to the Local organizing comity of the XIV Serbian Bulgarian Astronomical Conference to support our participation.

### References

- Adelman, S. J., Bidelman, W. P., Pyper, D. M.: 1979, *Astrophys. J. Suppl. Series*, **40**, 371, doi:10.1086/190592
- Aoki, M., Ishimaru, Y., Aoki, W., Wanajo, S.: 2017, *Astrophys. J.*, **837**, 837, doi:10.3847/1538-4357/aa5d08
- Arsenijević, V., Fabbro, S., Mourão, A. M., Rica da Silva, A. J.: 2008, *Astron. Astrophys.*, **492**, 535, doi:10.1051/0004-6361/200810675
- Barbuy, B., Friaça, A.C.S., da Silveira, C.R., Hill, V., Zoccali, M., Minniti, D., Renzini, A., Ortolani, S., Gómez, A.: 2015, *Astron. Astrophys.*, **580**, A40, doi:10.1051/0004-6361/201525694
- Bates, D. R., Damgaard, A.: 1949, *Philos. Trans. R. Soc. Lond. A*, **242**, 101, doi:10.1098/rsta.1949.0006
- Biémont, E., Grevesse, N., Kwiatkowski, M., Zimmermann, P.: 1982, *Astron. Astrophys.*, **108**, 127, doi:10.1051/0004-6361/201525694
- Carretta, E., Bragaglia, A., Lucatello, S., Gratton, R.G., D'Orazi, V., Sollima, A.: 2018, *Astron. Astrophys.*, **615**, A17, doi:10.1051/0004-6361/201732324
- Da Silveira, C. R., Barbuy, B., Friaça, A. C. S., Hill, V., Zoccali, M., Rafelski, M., Gonzalez, O. A., Minniti, D., Renzini, A., Ortolani, S.: 2018, *Astron. Astrophys.*, **614**, A149, doi:10.1051/0004-6361/201730562
- Dimitrijević, M. S., Christova, M.: 2021, *Eur. Phys. J. D*, **75**, 172, doi:10.1140/epjd/s10053-021-00179-4
- Dimitrijević, M. S., Christova, M. D.: 2022, *Universe*, **8**, 430, doi:10.3390/universe8080430
- Dimitrijević, M. S., Christova, M. D.: 2023, *Universe*, **9**, 126, doi:10.3390/universe9120511
- Dimitrijević, M. S., Christova, M. D.: 2024, *Physics Scripta*, **99**, 065613, doi:10.1088/1402-4896/ad4e13
- Dimitrijević, M. S., Christova, M. D., Yubero, C.: 2023, *Advances in Space Research*, **71**, 1275, doi:10.1016/j.asr.2022.05.048
- Dimitrijević, M. S., Christova, M. D., Yubero, C., Sahal-Bréchet, S.: 2024, *J. Quant. Spectrosc. Radiat. Transf.*, **330**, 109241, doi:10.1016/j.jqsrt.2024.109241
- Dimitrijević, M. S., Konjević, N.: 1980, *J. Quant. Spectrosc. Radiat. Transf.*, **24**, 451, doi:10.1016/0022-4073(80)90014-X
- Dixon, W. V., et al.: 2021, *Astron. J.*, **162**, 126, doi:10.3847/1538-3881/ac0dbb
- Dorsch, M., Latour, M., Heber, U.: 2019, *Astron. Astrophys.*, **630**, A130, doi:10.1051/0004-6361/201935724
- Dorsch, M., Latour, M., Heber, U., Irrgang, A., Charpinet, S., Jeffery, C. S.: 2020, *Astron. Astrophys.*, **643**, A22, doi:10.1051/0004-6361/202038859
- Griem, H. R.: 1968, *Phys. Rev.*, **165**, 258, doi:10.1103/PhysRev.165.258
- Griem, H. R.: 1974, *Spectral line Broadening by Plasmas* (Elsevier) <https://shop.elsevier.com/books/spectral-line-broadening-byplasmas/griem/978-0-12-302850-1>
- Iijima, T., Nakanishi, H.: 2008, *Astron. Astrophys.*, **482**, 865, doi:10.1051/0004-6361:20077502
- Kurucz, R. L.: 1979, *Astrophys. J. Suppl. Ser.*, **40**, 1, doi:10.1086/190589
- Lanz, T., Dimitrijević, M. S., Artru, M.-C.: 1988, *Astron. Astrophys.*, **192**, 249.
- Lehmann, H., Vitrichenko, E., Bychkov, V., Bychkova, L., Klochkova, V.: 2010, *Astron. Astrophys.*, **514**, A34, doi:10.1051/0004-6361/201013992
- Lundberg, H., et al.: 1996, *Astrophys. J.*, **469**, 388, doi:10.1086/177788
- Oertel, G. K., Shomo, L. P.: 1968, *Astrophys. J. Suppl. Ser.*, **16**, 175, doi:10.1086/190173

- Pettini, M., Ellison, S. L., Steidel, C. C., Bowen, D. V.: 1999, *Astrophys. J.*, **510**, 576, doi:10.1086/306635
- Peytremann, E.: 1972, *Astron. Astrophys.*, **17**, 76.
- Rafelski, M., Wolfe, A. M., Prochaska, J. X., Neeleman, M., Mendez, A. J.: 2012, *Astrophys. J.*, **755**, 89, doi:10.1088/0004-637X/755/2/89
- Rafelski, M., Neeleman, M., Fumagalli, M., Wolfe, A. M., Prochaska, J. X.: 2014, *Astrophys. J.*, **782**, L29, doi:10.1088/2041-8205/782/2/L29
- Roederer, I. U., Lawler, J. E., Sobeck, J. S., Beers, T. C., Cowan, J. J., Frebel, A., Ivans, I. I., Schatz, H., Sneden, C., Thompson, I. B.: 2012, *Astrophys. J. Suppl.*, **203**, 27, doi:10.1088/0067-0049/203/2/27
- Shi, J. R., Gehren, T., Butler, K., Mashonkina, L. I., Zhao, G.: 2008, *Astron. Astrophys.*, **486**, 303, doi:10.1051/0004-6361:200809452
- Shore, B. W., Menzel, D.: 1965, *Astrophys. J. Suppl. Ser.*, **12**, 187, doi:10.1086/190124
- Siqueira, M. C. et al.: 2013, *Astron. Astrophys.*, **550**, 122, doi:10.1051/0004-6361/201219949
- Smiljanic, R. et al.: 2016, *Astron. Astrophys.*, **589**, A115, doi:10.1051/0004-6361/201528014
- Smith, K.C.: 1993, *Astron. Astrophys.*, **276**, 393.
- Sneden, C., Crocker, D. A.: 1988, *Astrophys. J.*, **335**, 406, doi:10.1086/166935
- Van Regemorter, H., Dy, H. B., Prudhomme, M.: 1979, *J. Phys. B*, **12**, 1053, doi: 10.1088/0022-3700/12/7/009
- Wesemael, F.: 1981, *Astrophys. J. Suppl. Ser.*, **45**, 177, doi:10.1086/190712
- Wiese, W. L., Konjević, N.: 1982, *J. Quant. Spectrosc. Radiat. Transf.*, **28**, 185, doi:10.1016/0022-4073(82)90022-X

## SOHO/ERNE PROTON FLUENCE IN SOLAR CYCLES 23 AND 24

R. MITEVA<sup>1</sup> , S. W. SAMWEL<sup>2</sup> and M. DECHEV<sup>1</sup> 

<sup>1</sup>*Institute of Astronomy and National Astronomical Observatory (IANAO), Bulgarian Academy of Sciences, 1784 Sofia, Bulgaria*  
E-mail: [rmiteva@nao-rozhen.org](mailto:rmiteva@nao-rozhen.org)

<sup>2</sup>*National Research Institute of Astronomy and Geophysics (NRIAG), Helwan, Cairo 11421, Egypt*

**Abstract.** The focus of this study is on solar proton events detected by the SOHO/ERNE instrument during solar cycles (SC) 23 and 24. We select the output produced by the first channel of the high energy detector or at about 15 MeV. This report presents the distributions of the onset-to-peak proton fluences, in terms of their strength, location of their solar origin and mutual correlations, well as the SC trends.

## 1. INTRODUCTION

In the current phase of its evolution, our Sun emits nearly steady amounts of light, heat, and plasma (solar wind). In addition, there are episodes of less or more violent eruptions with variable occurrence. The manifestations of this activity is entirely driven by the changes in the solar magnetic field. The minute-to-month influence of the solar activity in the heliosphere, planetary magnetospheres and atmospheres, technological devices (both in space and on ground) and the health of humans is known as space weather (Temmer, 2021) and is currently a topic of multidisciplinary research.

Historically, the activity of our star is reflected in the rise and fall of the numbers of sunspots (Arlt and Vaquero 2020, <https://www.sidc.be/SILSO/home>), which are the darker than the surrounding photosphere when observed in white light and places of concentrations of magnetic flux. The roughly 11-year period from the first appearance, via a (double) maximum, to the disappearance of sunspots is known as a solar cycle (SC), Hathaway (2015), and currently the 25th SC is in its maximum phase. The variation of the sunspot number is followed closely by the other manifestations of solar activity, namely, active regions (ARs), solar flares (SFs), coronal mass ejections (CMEs), filament eruptions, solar energetic particles (SEPs), see, e.g., Miteva (2024). Concise definitions are given below:

- ARs: 'The totality of all observable phenomena preceding, accompanying and following the birth of sunspots including radio-, X-, EUV- and particle emission.' (by van Driel-Gesztelyi and Green 2015)
- SFs: can be regraded '...observationally as a brightening of any emission across the electromagnetic spectrum occurring at a time scale of minutes to hours.

Most manifestations seem to be secondary responses to the original energy release process, converting magnetic energy into particle energy, heat, waves, and motion.’ (by Benz, 2017)

- CMEs: ‘...consist of large structures containing plasma and magnetic fields that are expelled from the Sun into the heliosphere.’ (by Webb and Howard, 2012)
- Filaments/prominences: Arcade-like structures (i.e. long and thin clouds) suspended in the solar corona but about hundred times cooler and denser than the coronal material (e.g., Parenti, 2014). The former term is used when observing the structure against the bright solar disk, whereas the latter term is used when viewing the phenomena over the solar limb.
- SEPs: Protons, electrons and heavy ions accelerated near the Sun from ‘suprathermal (few keV) up to relativistic (few GeV) energies’ (Desai and Giacalone, 2016)

The majority of the key players of solar activity extend their (direct or indirect) influence into the heliosphere. The focus of this study, however, is on the solar protons, accelerated in the solar corona or/and interplanetary (IP) space (Klein and Dalla, 2017). The energetic protons are one of the main drivers of space weather effects, due to their risk of radiation exposure to astronauts (Semkova et al. 2018), and electronics onboard spacecraft (Samwel et al., 2019; Zheng et al., 2019). The remaining drivers, namely, the extreme ultraviolet emission during SFs causes disturbances in the terrestrial ionosphere (Buonsanto 1999) and can disrupt the radio signals. Tens of hours to several days later, upon reaching Earth, the IP counterparts of the CMEs, namely ICMEs, can cause geomagnetic disturbances (Lakhina and Tsurutani, 2016). Also, fast streams of the solar wind are nowadays recognized to have space weather consequences, though of lower intensity compared to the ICMEs.

The two main accelerators in the solar corona by the process of magnetic reconnection during SFs, and shocks formed due to ICMEs are nowadays widely recognized as SEP accelerators (Trottet et al., 2015; Klein and Dalla, 2017). Although some researchers tend to split their effects based on the SEP profile, others tend to regard the combined influence of SF with CME to the solar particles. In our analyses, we will assume either driver as plausible and will retain them in the analyses.

There is a large number of former studies that focus on various aspects of the SEP research: time coverage, energy, instrument, observations, modeling, forecasting (Whitman et al., 2023), and thus describing them goes beyond the scope of this report. Below we list several open-access proton catalogs:

- [http://sepem.eu/help/event\\_ref.html](http://sepem.eu/help/event_ref.html)
- <https://sepserver.eu/>
- <https://umbra.nascom.nasa.gov/SEP/>
- <http://www.stil.bas.bg/SEPcatalog/>
- <https://catalogs.astro.bas.bg/>

whereas the only catalog of solar electron events is available here:

- [https://www.nriag.sci.eg/ace\\_electron\\_catalog/](https://www.nriag.sci.eg/ace_electron_catalog/).



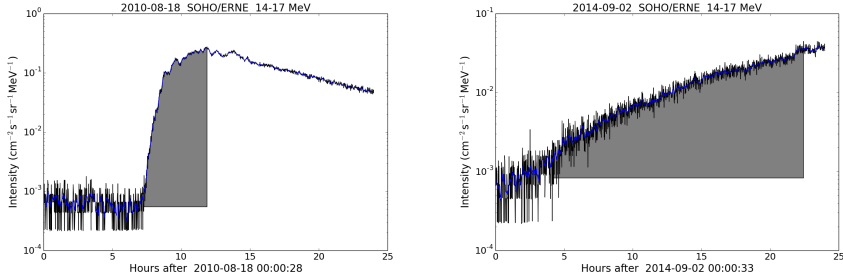


Figure 1: Examples of different time profiles (the fluence is calculated over the shaded area).

## 2. METHODS

### 2. 1. PROTON FLUENCE

For the study presented here we use proton data from SOHO/ERNE instrument (Torsti et al. 1995). The complete description on the procedure of proton identification in the SOHO/ERNE high energy detector (HED) data together with the association of their solar origin can be found in Miteva et al. (2024), noted henceforth as Paper I. For this study the proton data is taken from <https://export.srl.utu.fi/> over SCs 23 and 24 (1996–2019).

In contrast to Paper I, here we performed calculations of the onset-to-peak fluences by integration of the time profiles of the proton amplitude (or flux) based on one-day plots. The onset and peak times are identified based on the respective pre-event and peak-time intervals selected by an observer. For this report we use fluences in the first HED channel, namely over the energy range 14–17 (15.5) MeV. It is denoted as  $F_p$  and the fluence is measured in  $(\text{cm}^2 \text{sr MeV})^{-1}$ . The value of the proton fluences in all 10 HED energy channels will be made publicly available by us via <https://catalogs.astro.bas.bg/>.

The proton fluence is shown for two examples in Figure 1. Since the definition for the end of a proton event is less objective, we decided to use onset-to-peak proton fluences for the presented below analyses. Nevertheless, depending on whether the event has a fast or a slowly rising profile, the onset-to-peak fluence adopted here covers a different portion of the total event fluence. Based on these limitations, our results can be regarded as representative for the initial phase of the proton event development.

### 2. 2. SOLAR ERUPTIVE PHENOMENA

The solar origin of the SEP events are adopted from Paper I, based on the following catalogs, which are widely used in solar physics research:

- SFs: <ftp://ftp.swpc.noaa.gov/pub/warehouse/> and <https://solarmonitor.org/> We adopt the reported there SF class, helio-longitude and timing (onset, peak and end).
- CMEs: [https://cdaw.gsfc.nasa.gov/CME\\_list/](https://cdaw.gsfc.nasa.gov/CME_list/) (Gopalswamy et al. 2009). We use the linear (projected) CME speed and angular width (AW) as reported.

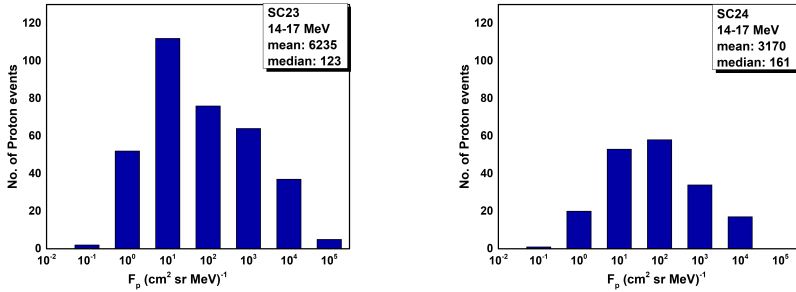


Figure 2: Histograms for the SEP fluence in SC23 (left) and in SC24 (right plot).

### 3. RESULTS

#### 3. 1. FLUENCE DISTRIBUTION

In total of 664 proton events were identified in HED01 channel in Paper I, however we could calculate the fluence for 475 cases (348 in SC23 and 179 in SC24), due to some data issues for the remaining ones. The distributions of the values for the proton fluences are shown in Figure 2, separately for SC23 (left) and SC24 (on the right).

Over SC23, the peak of the fluence distribution of the 15 MeV protons is at  $10 \text{ (cm}^2 \text{ sr MeV)}^{-1}$  (median value of 123), whereas in SC24 the peak is slightly shifted at  $100 \text{ (cm}^2 \text{ sr MeV)}^{-1}$  (median of 161), with large contribution at the lower bin as well. The mean value for the proton fluence in SC23 is about twice as larger compared to the value in SC24.

#### 3. 2. FLUENCE VS. PEAK INTENSITY

For comparative purpose, we also show the scatter plots between the proton fluence (this study) vs. peak proton intensity (Paper I), see Figure 3. The (double  $\log_{10}$ ) Pearson correlation coefficient  $F_p - J_p$  in SC23 (top plot) is  $0.89 \pm 0.02$  based on 348 pairs, whereas for SC24 (bottom plot) we obtain nearly the same value for the correlation,  $0.87 \pm 0.03$ , over a much smaller number of pairs, 179.

In order to evaluate the statistical uncertainty on a correlation between two sets of data, we use the bootstrapping method (Wall, J.V. and Jenkins, 2003), where out of the original sample are drawn events (with repetitions allowed), by means of a random selection. The 'replica' distribution has the same number of proton events as the original one and its Pearson correlation coefficient is calculated. The procedure is repeated 1000 times and the standard deviation over all (1000) Pearson correlations is adopted as the uncertainty on the correlation of the original sample.

Using this method were obtained the uncertainties on the  $F_p - J_p$  calculations above, as well as on the correlations between the proton fluence and the solar origin.

#### 3. 3. SOLAR ORIGIN DISTRIBUTIONS

In SC23 the proton-associated SFs range from X28 to B2.3 with mean/median values M9.2/M1.5, whereas in SC24 we obtain a much narrow range in SF class, from

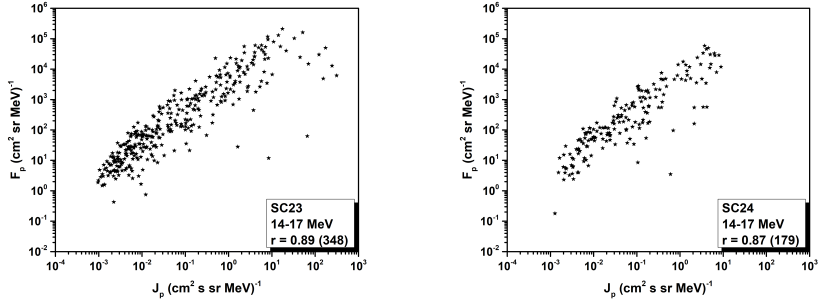


Figure 3: Scatter plots between the SEP fluence and peak intensity in SC23 (left) and in SC24 (on the right).

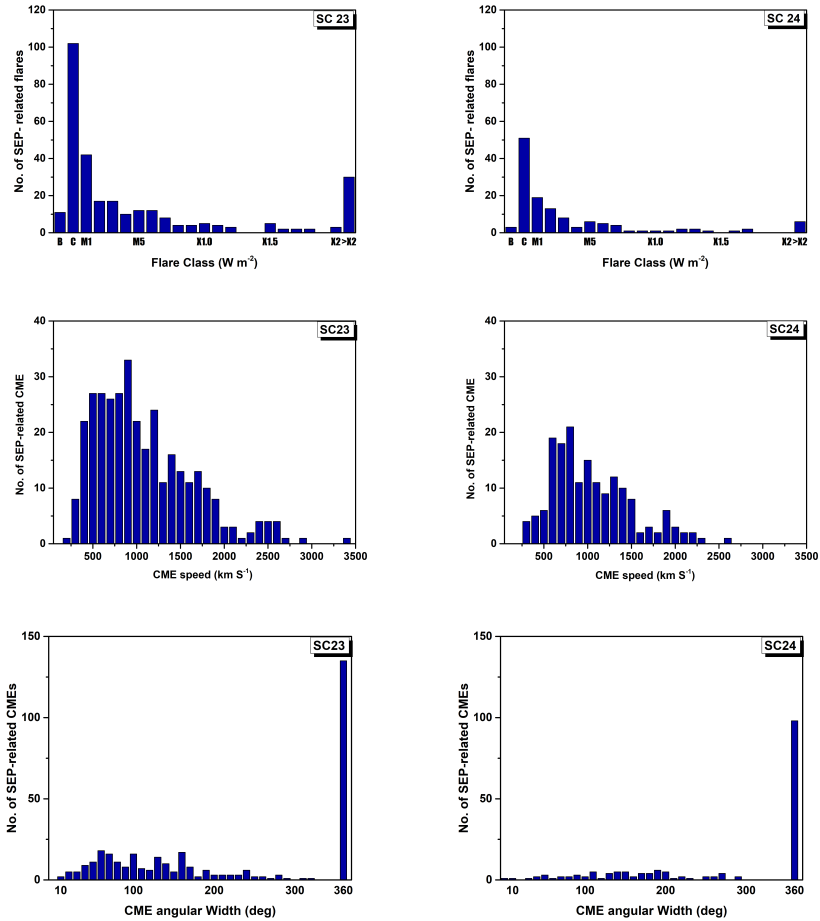


Figure 4: Histograms of the SF class (top) and CME speed (middle) and AW (bottom) for SC23 (left) and SC24 (on the right).

Table 1: Table of the Pearson correlation coefficients in SC23 and SC24 between the proton fluence with the SF class and CME speed, respectively. The event size is given in parentheses.

correlations	SC23	SC24
$F_p - I_{\text{SXR}}$		
all events	$0.50 \pm 0.05$ (241)	$0.40 \pm 0.09$ (110)
Eastern	$0.44 \pm 0.09$ (56)	$0.42 \pm 0.17$ (31)
Western	$0.52 \pm 0.06$ (180)	$0.44 \pm 0.10$ (79)
strong	$0.43 \pm 0.07$ (134)	$0.38 \pm 0.04$ (61)
weak	$0.13 \pm 0.11$ (107)	$0.10 \pm 0.15$ (49)
$F_p - V_{\text{CME}}$		
all events	$0.51 \pm 0.05$ (275)	$0.48 \pm 0.06$ (154)
Eastern	$0.48 \pm 0.11$ (59)	$0.35 \pm 0.15$ (42)
Western	$0.53 \pm 0.05$ (216)	$0.55 \pm 0.07$ (112)
strong	$0.44 \pm 0.07$ (148)	$0.38 \pm 0.09$ (80)
weak	$0.11 \pm 0.08$ (127)	$0.26 \pm 0.10$ (74)

X9.3 to B6.2 and weaker mean values compared to SC23, namely M5.4, but slightly stronger in median values, M1.8. The SF class distribution is shown in the top row of Figure 4.

With respect to the SF impulsiveness, in SC23 the SFs are more impulsive, with mean/median rise times (onset-to-peak duration) of 27/17 minutes, whereas in SC24 the SFs show a more gradual rise time, with values 36/23 minutes, correspondingly. With respect to their helio-longitude, we have 56 SFs with Eastern helio-longitudes in SC23 and 31 in SC24. At Western helio-longitudes are located 180 SFs in SC23 and 79 in SC24.

The mean/median values for the CME speeds and AWs are:

- SC23:  $\sim 1020/900$  km s<sup>-1</sup>; 218/190 degrees
- SC24:  $\sim 980/860$  km s<sup>-1</sup>; 277/360 degrees

indicating faster but narrower proton-associated CMEs in SC23 comparing to SC24. The CME speed distribution is shown in the middle row of Figure 4 with slightly more pronounced tail towards large values. Despite the pronounced peak for halo CMEs (with AW of 360 degrees) both for SC23 and SC24 (bottom row), there is a larger number of narrow CMEs (AW < 200) in SC23 leading to the lower mean/median values.

### 3. 4. PEARSON CORRELATIONS

An important evaluation of the influence of the solar origin (SF vs. CME) to the proton intensity or/and fluence is the calculation of Pearson correlations between the values. Here, the correlations are performed between the ( $\log_{10}$ ) proton fluence with the ( $\log_{10}$ ) SF class ( $I_{\text{SXR}}$ ) or/and with CME speed ( $V_{\text{CME}}$ ), respectively. The results are summarized in Table 1 for different sub-samples of the proton events and separately for SC23 and SC24.

For the entire sample (denoted as 'all events'), we obtain stronger correlations in SC23 compared to SC24, both with the SFs and with the CMEs. Considering the uncertainty ranges, however, the differences are not statistically significant.

Furthermore, the proton sample is divided into Eastern and Western, according to the longitude of their associated SFs or measurement position angle of the associated CMEs. A prevalence of the correlations with protons at Western-origin is obtained, both with SFs and CMEs, and in either SCs. However, due to the lower number of events in the respective samples, the uncertainty ranges are larger and thus there is no statistical significance.

The last division of the proton sample is done according to the median value of the proton fluence (see Figure 2), namely into strong vs. weak. A statistically different correlations with the SFs are obtained between the strong and weak proton events in either SC. Similarly, the correlations between the strong proton fluences and the CMEs have larger values compared to the correlations with the weaker protons, however the difference in SC24 are not statistically significant.

#### 4. SUMMARY

This report presents the first results on the analyses of the 14–17 MeV proton fluences from SOHO/ERNE data in terms of their distribution, cross-correlation with the respective proton peak intensity values and Pearson correlations with the SF class and CME speed. The proton sample is subsequently split into Eastern vs. Western (based on the solar origin helio-location) and strong vs. weak events (based on the median values of the entire fluence sample). Finally, the results are outlined separately for SC23 and SC24 in order to investigate the SC trends. The notable trends are summarized below, both for the SF class and CME speed, though mostly not statistically significant differences are found:

- SC: Overall, the Pearson correlations in SC24 are weaker compared to those in SC23.
- Helio-longitude: The Pearson correlations for the Western sub-sample shows larger values compared to the Eastern sub-sample.
- Fluence-strength: The proton events with stronger (than the median) fluences show higher Pearson correlations compared to the weaker events.

The above trends will be explored for the remaining HED channels and the results will be presented elsewhere. The values of the SOHO/ERNE HED fluences will be released via an open-access database: <https://catalogs.astro.bas.bg/>.

#### Acknowledgments

This research was supported by SCOSTEP/PRESTO project 'On the relationship between major space weather phenomena in solar cycles 23 and 24'; by the Bulgarian-Egyptian inter-academy project 'On space effects at near Earth environment - from remote observations and in situ forecasting to impacts on satellites' (2022-2024), Bulgarian Academy of Sciences IC-EG/08/2022-2024 and Egyptian Academy of Scientific Research and Technology (ASRT)/NRIAG (ASRT/BAS/2022-2023/10116) and by the Bulgarian-Serbian inter-academy project 'Active Events on The Sun. Catalogs of

Proton Events and Electron Signatures in X-Ray, UV and Radio Diapason. Influence of Collisions on Optical Properties of Dense Hydrogen Plasma.' (2023-2025).

## References

- Arlt, R., Vaquero, J. M.: 2020, *Living Reviews in Solar Physics*, **17**, article id.1, doi: 10.1007/s41116-020-0023-y
- Benz, A. O.: 2017, *Living Reviews in Solar Physics*, **14**, article id. 2, 59 pp., doi: 10.1007/s41116-016-0004-3
- Buonsanto, M. J.: 1999, *Space Science Reviews*, **88 (3/4)** 563–601, doi: 10.1023/A:1005107532631
- Desai, M. and Giacalone, J.: 2016, *Living Reviews in Solar Physics*, **13**, article id. 3, 132 pp., doi: 10.1007/s41116-016-0002-5
- Hathaway, D. H.: 2015, *Living Reviews in Solar Physics*, **12**, article id. 4, 87 pp., doi: 10.1007/lrsp-2015-4
- Gopalswamy, N., Yashiro, S., Michalek, G., Stenborg, G., Vourlidas, A., Freeland, S., Howard, R.: 2009, *Earth Moon and Planets*, **104**, 295–313, doi: 10.1007/s11038-008-9282-7
- Klein, K.-L.; Dalla, S.: 2017, *Space Science Reviews*, **212 (3–4)**, 1107–1136, doi: 10.1007/s11214-017-0382-4
- Lakhina, G. S. and Tsurutani, B. T.: 2016, *Geoscience Letters*, **3**, article number 5, doi: 10.1186/s40562-016-0037-4
- Miteva, R.: 2024, *Journal of Physics: Conference Series*, **2794 (1)**, id.012004, 8 pp., doi: 10.1088/1742-6596/2794/1/012004
- Miteva, R., Samwel, S. W., Dechev, M.: 2024, *Atmosphere*, **15 (8)**, id.1016, doi: 10.3390/atmos15081016
- Parenti, S.: 2014, *Living Reviews in Solar Physics*, **11**, article id. 1, 88 pp., doi: 10.12942/lrsp-2014-1
- Samwel, S. W., Abd El-Aziz, E., Garrett, H. B., Hady, A. A., Ibrahim, M., Amin, M. Y.,: 2019, *Advances in Space Research*, **64**, 239–251, doi: 10.1016/j.asr.2019.03.025
- Semkova, J., Koleva, R., Benghin, V., Dachev, T., Matviichuk, Y., Tomov, B., Krastev, K., Maltchev, S., Dimitrov, P., Mitrofanov, I., Malahov, A., Golovin, D., Mokrousov, M., Sanin, A., Litvak, M., Kozyrev, A., Tretyakov, V., Nikiforov, S., Vostrukhin, A., Fedosov, F., Grebennikova, N., Zelenyi, L., Shurshakov, V., Drobishev, S.: 2018, *Icarus*, **303**, 53–66, doi: 10.1016/j.icarus.2017.12.034
- Temmer, M.: 2021, *Living Reviews in Solar Physics*, **18 (1)**, article id.4, doi: 10.1007/s41116-021-00030-3
- Torsti, J., Valtonen, E., Lumme, M., Peltonen, P., Eronen, T., Louhola, M., Riihonen, E., Schultz, G., Teittinen, M., Ahola, K., Holmlund, C., Kelh , V., Lepp l , K., Ruuska, P., Str mmer, E.: 1995, *Solar Physics*, **162 (1-2)**, 505–531, doi: 10.1007/BF00733438
- Trottet, G., Samwel, S., Klein, K.-L. Dudok de Wit, T. and Miteva, R.: 2015, *Solar physics*, **290**, 819–839, doi: 10.1007/s11207-014-0628-1
- van Driel-Gesztelyi, L., Green, L. M.: 2015, *Living Reviews in Solar Physics*, **12**, article id. 1, 98 pp., doi: 10.1007/lrsp-2015-1
- Wall, J. V., Jenkins, C. R.: 2003, *Practical Statistics for Astronomers*, **3**
- Webb, D. F., Howard, T. A.: 2012, *Living Reviews in Solar Physics*, **9**, article id. 3, 83 pp., doi: 10.12942/lrsp-2012-3
- Whitman, K., Egeland, R., Richardson, I. G. et al.: 2023, *Advances in Space Research (review)*, **72, (12)**, 5161–5242, doi: 10.1016/j.asr.2022.08.006
- Zheng, Y., Ganushkina, N. Y., Jiggins, P., Jun, I., Meier, M., Minow, J. I., O'Brien, T. P., Pitchford, D., Shprits, Y., Tobiska, W. K., Xapsos, M. A., Guild, T. B., Mazur, J. E., Kuznetsova, M. M.: 2019, *Space Weather*, **17**, 1384–1403, doi: 10.1029/2018SW002042

## FIRST OBSERVATIONAL DATA FROM THE MINI-NEUTRON MONITORING STATION AT THE ROZHEN NATIONAL ASTRONOMICAL OBSERVATORY (MNMS-ROZH)

N. PETROV<sup>1</sup> , TS. TSVETKOV<sup>1</sup>, A. MISHEV<sup>2</sup>, V. YOTOV<sup>1</sup>

and G. SHIROV<sup>1</sup>

<sup>1</sup>*Institute of Astronomy and National Astronomical Observatory, Bulgarian Academy of Sciences, 72 Tsarigradsko shose blvd., 1784 Sofia, Bulgaria*  
*E-mail: nick@astro.bas.bg*

<sup>2</sup>*University of Oulu, 90570 Oulu, Finland*

**Abstract.** We demonstrate the first observational data from the newly built mini-neutron monitoring station at the Rozhen National Astronomical Observatory. The data is freely accessible with search option in the up-to-date archive. Provided are the main parameters of the station and equipment. The station is equipped with sensors for measuring and storing in accessible online data base of meteorological parameters, which are also provided.

### 1. INTRODUCTION

The study of cosmic rays began after their discovery in 1912 by Victor Hess. Observations and reports of cosmic radiation affecting the Earth's environment began in the early 1930s with ionization chambers, and in the early 1950s the construction and use of neutron monitors began. Records of the state of the Earth's ionosphere date back to 1942, and ozone data to about 1957.

Cosmic rays (CRs) are high-energy particles traveling at close to the speed of light. There are two types of CRs according to their origin – Galactic cosmic rays (GCRs) and Solar cosmic rays (SCRs). GCRs generally originate in supernova explosions and/or stellar fusion processes. The energy of protons and helium nuclei of GCRs mostly lies in the range 100 – 3000 MeV, yet extreme energies as 1000 of EeV are observed. SCRs or solar energetic particles (SEPs) arise mainly from solar flares (large eruptions of electromagnetic radiation; a burst of radiation) and coronal mass ejections (solar material of charged particles (plasma)) and the energy of protons and helium nuclei is between 5 and 100 MeV. SEPs (and secondary particles) are produced through eruptive and non-thermal processes. About 85 – 90% of CRs are protons (nuclei of hydrogen atoms) and about 9 – 13% consisting of alpha particles (helium nuclei). The remaining 1 – 2% are electrons and nuclei of heavier atoms (HZE ions).

Direct observations and registration of high-energy particles from outer space ("primary" CRs) are impossible from the Earth's surface. But their interaction with the molecules in the Earth's atmosphere leads to the reproduction of new particles called "secondary" CRs, which are able to reach the ground so we can register and

study them. A significant leap in scientific research in this area was made by J. A. Simpson (Simpson 1948), who established the possibility of studying temporal variations of primary CRs at lower energies with ionisation chambers or muon counters by establishing the first network of ground-based detectors. He established the strong variability of the intensity of CRs (200-400%) by latitude and altitude, by the change in the intensity of the geomagnetic field, but also by the systematic changes in the intensity of cosmic radiation with respect to the 11-year solar cycle (Meyer and Simpson 1955; Simpson 2000). These and similar studies (Forbush 1954) are fundamental to develop a new type of detector that measures secondary CRs (neutrons) in the Earth's atmosphere in the GeV range (the energy of primary CRs is from 500 MeV to 30 GeV). The neutron monitor designed by Simpson (Simpson 1957) was adopted as the standard detector during the International Geophysical Year (IGY) 1957/58 and was called the IGY neutron monitor (Btikofer 2018). This is the beginning of the systematic investigations of the effects of the Earth's magnetic field on the CRs as observed on the ground. Lately the IGY detectors were considerably improved, leading to development of NM-64, as a standard device. The secondary CR (neutron) flux detectors created more than 7 decades ago by Simpson are still in use today, of course, improved over time.

Almost half a century of intense observation, research and significant modeling of CR and heliosphere physics was summarized in two notable works at the end of the last century (Fisk *et al.* 1998; Balogh *et al.* 1999).

## **2. THE NEW MINI-NEUTRON MONITORING STATION AT ROZHEN OBSERVATORY**

In our modern world of rapidly developing technologies, CRs and especially the sporadic manifestation of the influence of SEPs on the Earth's magnetosphere, ionosphere and our surrounding environment are an increasingly significant and determining factor. Their impact on our environment is a key factor in understanding short-term (up to a few tens of years) and long-term (more than hundreds or thousands of years) changes in our climate. Their influence on communications and generally electrical devices and appliances is essential to the tense rhythm of our existence. The greater the need for knowledge in this area, the more relevant is the issue of presenting better opportunities for CRs research. There is increased interest in the scientific community to build a denser ground-based network of CR detectors to cover observations from different latitudes and altitudes. We present our new mini-neutron detector (MNM-ROZH), based on gas-filled proportional counters type LND2043 BF3 (Figure 1). This type of NMs are effective detectors of CRs, by detecting a raid of the secondary flux of cosmic rays (neutrons).

Each of our three detectors has a cylindrical design with an outer diameter of 350 mm, a length of 750 mm, and a weight of almost 300 kg. The outermost cylinder of the detector is a polyethylene reflector. This reflector (75 mm thick) shielding the instrument from external thermal neutrons, while containing neutrons produced within the NM. Under the external reflector there is a 206-mm lead cylinder producing additional low energy neutrons via nuclear interactions to increase the monitors detection efficiency. The next layer is again made of polyethylene – an internal moderator of thickness 15 mm thermalizing the newly produced neutrons. The gas-filled



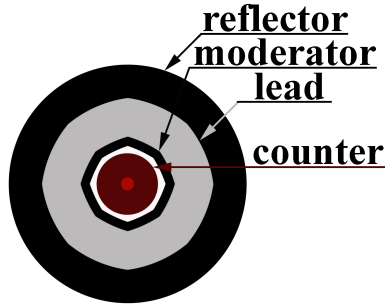


Figure 1: Cross-sectional sketch of the mini-NM-ROZH. The outer part of the detector (black) is a polyethylene reflector, then the lead sheath (gray), again a polyethylene moderator (black), which houses the proportional counter (red).

proportional counters type LND2043 BF3 are located in the middle of the cylinder. The pressure in a mini-NM detector is 930 mbar. The completed mini-NM set-up, while undergoing testing, is shown on Figure 2.



Figure 2: Completed and installed system of 3 mini-neutron counters on the territory of the National Astronomical Observatory. MNM-Rozh is currently still running in calibration mode.

Neutrons in the energy range of tens to thousands of MeV are produced and moderated to thermal energy before reaching the interior of the counter, which is filled with BF<sub>3</sub> and operates as a proportional gas counter. At this low energy level, neutrons are adsorbed by boron, which splits into <sup>7</sup>Li and alpha-particle (Knoll 2010). The kinetic energy of these two ions is dissipated by ionizing the gas. The charge momentum induced by these ions is counted.

Gas-filled proportional counters type LND2043 are cylindrical BF<sub>3</sub> neutron detectors produced by LND Inc., USA. The detector control electronics were completely designed and assembled to the detectors by the Center for Space Research, North West University, the Republic of South Africa (RSA). A Raspberry Pi 3 B, a fully-functional single-board computer is used to interface with the system components. The on-board computing power enables data processing and data validation in real-time. This allows functionality like digital filters and enables units to alert or automatically reset

if an error occurs. The built-in network interface allows remote monitoring, administration, and data synchronization. The USB (universal serial bus) interface allows for a local data backup when network connectivity is interrupted or unavailable.

Our neutron monitor (NM) station is located at  $41^{\circ}41'43.4''\text{N}$ ,  $24^{\circ}44'22.3''\text{E}$  at altitude 1730 m (Figure 3). The trajectories of charged particles are influenced by the magnetic field generated by the Earth’s core. We use the new open-source tool for magnetospheric computations and modelling of CR propagation in the geomagnetosphere, named OuluOpen-source geomagneToSphereprOpagation tool (OTS0), available on GitHub (<https://github.com/NLarsen15/OTS0>) and Zenodo (<https://doi.org/10.5281/zenodo.7516233>) (Larsen et al. 2023).

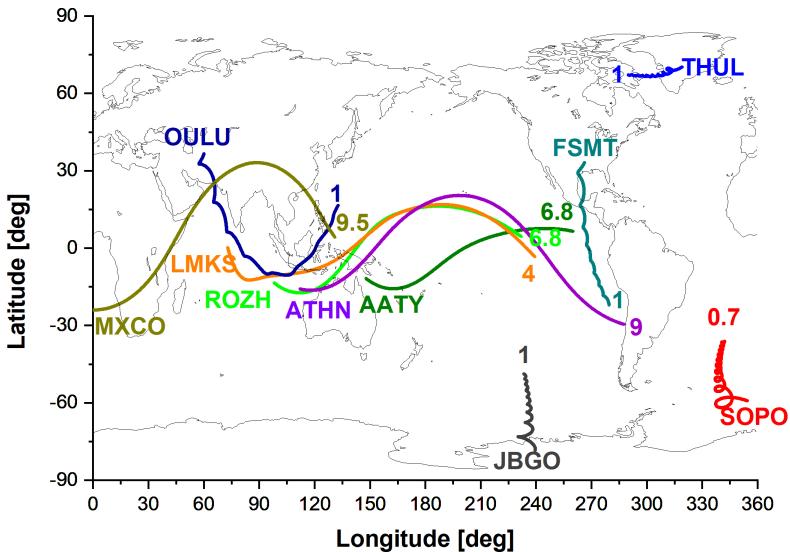


Figure 3: Computed asymptotic cones over various rigidity ranges for several selected neutron monitors stations including ours (ROZH).

Figure 4 shows the first test results for our three detectors individually – a binned 2D histogram of the pulse width and pulse histogram. The data is the sum of three consecutive days for the period 19-21 September 2024. The distributions are projected onto each plane. From the 2D histogram, we can clearly identify low amplitude noise below 0.5 V, consisting of short and longer pulses. Calculating and monitoring these distributions (e.g. on an hourly basis) allows us to determine and track the accuracy of the detector. Any external noise (e.g., mechanical vibrations or high-voltage ripple currents) will change the shape of the distributions. Visualizing the pulses in such a 2D plane also permits performing a detailed separation of the pulses into noise and/or data (counts) by applying an appropriate cut through the pulse amplitude/width plane (Strauss et al. 2020).

In addition to our equipment for observing and recording cosmic rays, we have been able to add detectors for various meteorological components of the Earth’s atmosphere. Neutron flux data are related to atmospheric pressure, humidity and tem-

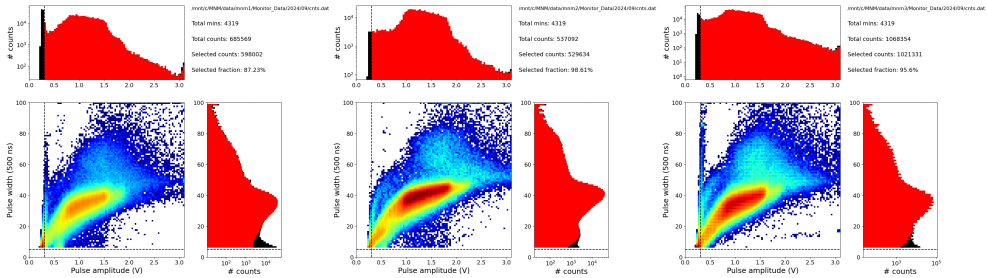


Figure 4: A 2D pulse width-amplitude histogram as registered MNM-RZH (for each individual detector). The distribution is projected onto each plane. The dashed lines show the cut applied to the pulses in order to discriminate between measurements and noise. On the projected histograms, all the pulses are indicated by a black histogram, while the red histogram indicated pulses assumed to be measurements free from noise.

perature. For this purpose, a meteorological tower was built in close proximity to the neutron monitoring station to reliably measure multiple meteorological parameters (Figure 5).

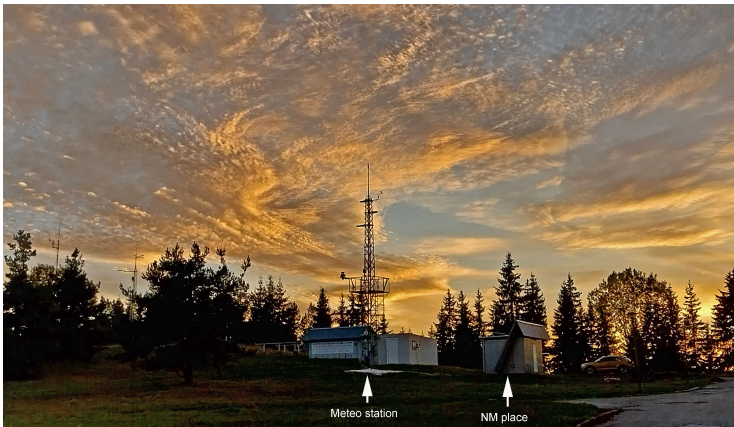


Figure 5: Part of the infrastructure of NAO Rozhen, including a tower with installed detectors for various meteorological parameters and a pavilion that houses the newly built MNM.

The data we currently monitor are the total solar radiation, UVA, temperature, humidity, pressure, etc. The open-access database is still under construction, but will be fully accessible soon on <https://helio.astro.bas.bg/livecam/>. The data is partially available on: <https://meter.ac/gs/meteo/M16/history.html> (solar radiation) and <https://meter.ac/gs/meteo/M161/history.html> (temperature/humidity).

### 3. SUMMARY

The construction of cosmic ray detectors is important scientific task for solving current issues related to near-Earth space. Determining the problems of space weather are of prior importance for our new and modern world. These problems are related both to the study of purely scientific phenomena as well as their influence on our environment, which is beginning to become an increasingly broad concept as it includes various parameters of space weather in our solar system as a whole.

NM stations located at different locations are an important step in networked research, which enables better scientific activities between different international teams. Currently MNM-ROZH is working and accumulating data, which after additional calibrations and tests will be presented online with open access through an active database. We believe that the results will find their significance in future scientific research in several directions such as the importance and influence of space factors on global climate changes on Earth (both short-term and long-term), finding new solutions for the prevention and protection of the population from the influence of space factors time, including protection and prevention of all activities related to electricity/electrical engineering and communications.









### Acknowledgements

This work is supported by the National Science Fund of Bulgaria with contracts No. KP-06-N64/3 and KP-06-M78/1. Part of this work was supported by the Academy of Finland (project 330063 QUASARE and 354280 GERACLIS) and we acknowledge the support of the International Space Science Institute (Bern, Switzerland) team No. 585 (REASSESS). NP acknowledges for support through the joint project of the Serbian Academy of Sciences and Arts and Bulgarian Academy of Sciences. NP is grateful to Prof. D.T. Strauss for his help on the realization of the project.

### References

- Balogh, A., Gosling, J. T., Jokipii, J. R., Kallenbach, R., Kunow, H. (eds.): 1999, Corotating Interaction Regions, Kluwer Academic Publishers, Dordrecht, doi: 10.1007/978-94-017-1179-1
- Larsen, N., Mishev, A., Usoskin, I.: 2023, , *Journal of Geophysical Research: Space Physics*, **128**, e2022JA031061, doi: 10.1029/2022JA031061
- Strauss, D. T., Poluianov, S., van der Merwe, C., Kruger, H., Diedericks, C., et al.: 2020. *J. Space Weather Space Clim.*, **10**, 39, doi: 10.1051/swsc/2020038
- Simpson, J.A.: 1948, *Phys. Rev.*, **73**, 13891391, doi: 10.1103/PhysRev.73.1389
- Simpson, J.A.: 1957, *Bulletin of the Atomic Scientists*, **13**, 351356, doi: 10.1080/00963402.1957.11457599
- Simpson, J.A.: 2000, *Space Sci. Rev.*, **10**, Edited by J. W. Bieber, E. Eroshenko (eds), Cosmic rays and earth, Proceedings of an ISS/ Workshop, pp.11-32, doi: 10.1023/A:1026567706183
- Btikofer, R.: 2018, *Astrophysics and Space Science Library*, **444**, doi: 10.1007/978-3-319-60051-2.6
- Fisk, L. A., Jokipii, J. R., Simnett, G. M., von Steiger, R., and Wenzel, K.-P. (eds.): 1998, *Cosmic Rays in the Heliosphere*, Kluwer Academic Publishers, Dordrecht, doi: 10.1007/978-94-017-1189-0
- Forbush, S. E.: 1954, *J. Geophys. Res.*, **59**, 525, doi: 10.1029/JZ059i004p00525
- Meyer, P., Simpson, J. A.: 1955, *Phys. Rev.*, **99**, 1517, doi: 10.1103/PhysRev.99.1517

**QUAIA × VLASS: A NEW SAMPLE OF COMPACT  
EXTRAGALACTIC RADIO SOURCES**

N. ARSENOV<sup>1,2</sup> , S. FREY<sup>3,4,5</sup> , A. KOVÁCS<sup>3,4,2</sup> , K. É. GABÁNYI<sup>6,7,3,4</sup> ,  
K. PERGER<sup>3,4</sup> , J. FOGASY<sup>3,4</sup> , L. SLAVCHEVA-MIHOVA<sup>1</sup>   
and Á. BOGDÁN<sup>2,6</sup> 

<sup>1</sup>*Institute of Astronomy and NAO,  
Tsarigradsko Chaussee Blvd. 72, 1784 Sofia, Bulgaria  
E-mail: nestorarsenov@gmail.com*

<sup>2</sup>*MTA–CSFK Lendlet “Momentum” Large-Scale Structure (LSS) Research Group,  
Konkoly Thege Miklós út 15-17, H-1121 Budapest, Hungary*

<sup>3</sup>*Konkoly Observatory, HUN-REN Research Centre for Astronomy and Earth Sciences,  
Konkoly Thege Miklós út 15-17, H-1121 Budapest, Hungary*

<sup>4</sup>*CSFK, MTA Centre of Excellence,  
Konkoly Thege Miklós út 15-17, H-1121 Budapest, Hungary*

<sup>5</sup>*Institute of Physics and Astronomy, ELTE Eötvös Loránd University,  
Pázmány Péter sétány 1/A, H-1117 Budapest, Hungary*

<sup>6</sup>*Department of Astronomy, Institute of Physics and Astronomy,  
ELTE Eötvös Loránd University, Pázmány Péter sétány 1/A, H-1117 Budapest, Hungary*

<sup>7</sup>*HUN-REN–ELTE Extragalactic Astrophysics Research Group,  
Eötvös Loránd University, Pázmány Péter sétány 1/A, H-1117 Budapest, Hungary*

**Abstract.** Compact radio sources, radio-emitting active galactic nuclei, are scarce objects, yet important as reference points for astrometric, astrophysical, and spacecraft navigation applications. We present over 3900 potential new compact radio sources derived from a cross-match between the Very Large Array Sky Survey (VLASS) radio catalogue and the recently published Quiaia quasar catalogue. The VLASS catalogue provides a list of individual radio sources identified at 3 GHz with flux densities  $\gtrsim 1$  mJy, while the Quiaia catalogue is derived from the *Gaia* optical astrometric catalogue by selecting sources with negligible proper motion and performing a *k*-means search method on colour–colour parameter spaces to extract quasars. We find more than 45 000 matched sources between the two catalogues with separations less than  $2''$  from which more than 3900 present themselves as high-fidelity compact radio source candidates by having radio flux density  $> 20$  mJy and a compactness ratio  $> 0.8$ . A proposal for observing 80 of these sources has been accepted by the European Very Long Baseline Interferometry Network which should validate the candidates and provide constraints on the parent sample. A follow-up analysis of the cosmologically important properties of the sources will be valuable, e.g. an analysis of the radio-loudness, its correlation to the spatial density in clusters and voids, and the correlation to colour–colour parameter spaces.

## 1. INTRODUCTION

Currently, the largest list of compact radio sources observed with very long baseline interferometry (VLBI), the 2024a edition of the Radio Fundamental Catalog (RFC, Petrov & Kovalev 2024), contains almost 22 000 objects targeted in absolute astrometric/geodetic programs since 1980. These include the  $\sim 4500$  extragalactic radio sources in the 3rd realization of the International Celestial Reference Frame (ICRF3, Charlot et al. 2020) at  $\sim 8$  GHz ( $X$  band). Apart from obvious astrophysical reasons of studying jet physics in more individual bright radio-loud active galactic nuclei (AGN), there is huge scientific potential in substantially increasing the number of VLBI-detected sources. The many fields that could benefit from such an increase include cosmology (finding much more objects for meaningful tests of cosmological models, e.g. Mosoni et al. 2006, and correlating radio-loudness of quasars with the large-scale structure that these objects are part of, e.g. Li et al. 2022), astrometry (improving the tie between the most accurate optical and radio reference frames, e.g. Bourda et al. 2010), astrophysics (availability of more nearby calibrators for high-resolution VLBI observations of various types of faint radio sources by means of traditional and in-beam phase-referencing, Beasley & Conway 1995), and navigation of interplanetary spacecraft using relative astrometric observations with respect to background AGN (e.g. Gurvits et al. 2023).

The small imaging fields of view inherent in the technique make all-sky VLBI surveys unfeasible. While deep wide-field observing projects (e.g. Njeri et al. 2023) are capable of investigating selected areas and characterising the faint (sub-mJy) AGN population, the sky is generally sparsely populated with compact radio sources having flux densities of tens of mJy or higher. However, these brighter sources would be essential phase-reference calibrators, because the smallest possible target-calibrator separation plays a crucial role in imaging and achieving the most accurate relative position measurements (Rioja & Dodson 2020). Therefore, an efficient method that could be applied to pre-select radio sources suitable for VLBI detection based on existing sky survey data found in the radio and other wavebands, but without wasting much of the precious VLBI observing resources, would be an important contribution to the VLBI community.

## 2. SAMPLE SELECTION

Most recently, a new all-sky quasar catalogue called Quaia (Storey-Fisher et al. 2024) was constructed based on *Gaia* DR3 (Gaia Collaboration 2023) quasar candidates, and using *Wide-field Infrared Survey Explorer* (*WISE*, Lang 2014) mid-infrared photometry to remove contaminants and improve the precision of photometric redshift estimates. While the primary purpose of Quaia containing  $\sim 1.3$  million objects with  $G < 20.5^m$  is facilitating cosmological studies, its high purity and completeness make this catalogue a potentially valuable asset for other applications as well. On the radio side, the ongoing 3-GHz Very Large Array Sky Survey (VLASS, Lacy et al. 2020) offers an excellent opportunity for cross-matching Quaia optical quasars with known radio sources that are compact on arcsec scale.

Among the  $\sim 1.1$  million Quaia quasars at declinations  $\delta > -40^\circ$ , i.e. the sky coverage of VLASS,  $\sim 47\,000$  have unique counterparts within  $2''$  search radius (Fig. 1) in the VLASS Epoch 2 catalogue. The estimated false-match probability is  $< 0.2\%$

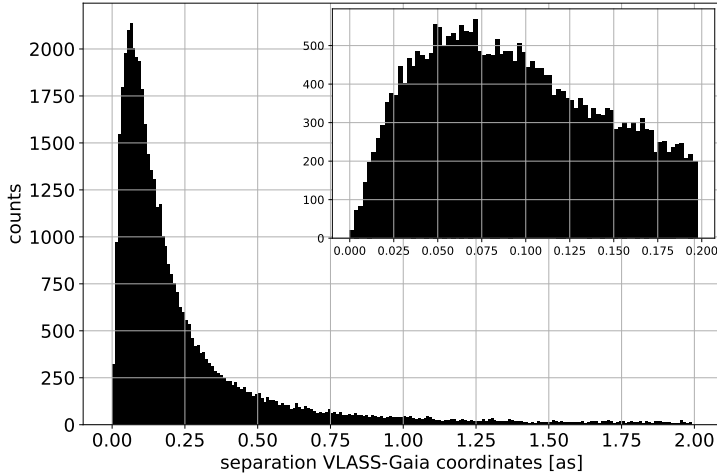


Figure 1: Histogram of the number of cross-matched sources as a function of the separation in VLASS–*Gaia* coordinates. We consider proper cross-matches objects with separations up to  $2''$ , yielding a high completeness. The inlet in the top right is a zoom-in on the range of radio–optical separations from 0 to  $0.2''$ .

(Fig. 2). In particular, 3956 of those satisfy the following radio selection criteria: *(i)* total flux density  $S_{3\text{ GHz}} > 20\text{ mJy}$ , *(ii)* compactness  $C > 0.8\text{ beam}^{-1}$  defined as the ratio of peak brightness and total flux density, and *(iii)* not contained in the most recent RFC (Petrov & Kovalev 2024) as an already known VLBI source. These 3956 objects are potential new VLBI targets, from which we got approved 80 sources for test observations by the European VLBI Network (EVN).

Optical classification plays an important role in enhancing the chance of VLBI detection of radio sources known at arcsec scale (Deller & Middelberg 2014). Indeed, earlier pilot studies on small samples, based on cross-matching Sloan Digital Sky Survey optical quasars with radio sources from the Faint Images of the Radio Sky at Twenty-Centimeters (FIRST, Becker, White & Helfand 1995) survey at 1.4 GHz (Garrington et al. 1999; Frey et al. 2008) indicated that the VLBI detection rate with phase-referenced observations can be as high as  $\sim 90\%$  using simple selection criteria similar to ours. The quality of the Quiaia catalogue, as well as the higher frequency and angular resolution of VLASS compared to FIRST, promise an even more favourable selection. However, we are now interested in quasars that are bright and compact enough to enable VLBI fringe-fitting (Schwab & Cotton 1983). A notable benefit of using Quiaia is that the accuracy of the *Gaia* quasar coordinates, that can be used as a-priori positions, is comparable to that of VLBI (Kovalev, Petrov & Plavin 2017).

The sizeable sample of 80 objects from the cross-matched Quiaia–VLASS list of quasars, that are not yet known as VLBI-detected sources and satisfy the above criteria for flux density *(i)* and compactness *(ii)*, will be subject to observations by the EVN at  $X$  band. The primary goals of the project are

- to check, for the first time at  $X$  band, how efficient these selection criteria are for pre-selecting potential future VLBI reference sources, without applying phase

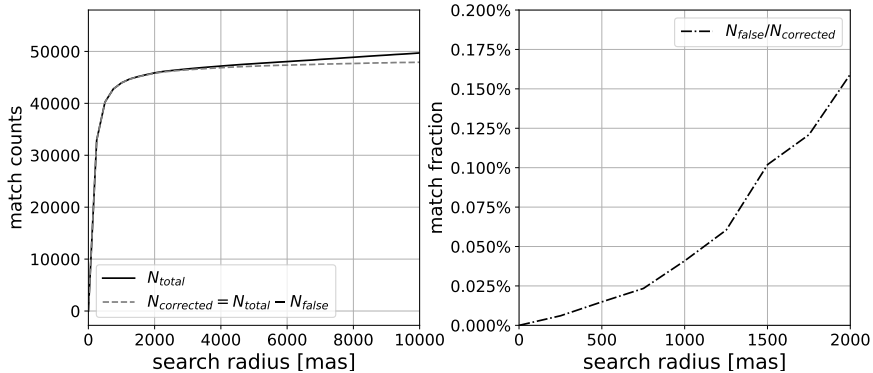


Figure 2: *Left:* The cumulative histogram to Fig. 1 is shown by the  $N_{total}$  curve. To estimate the false-match probability, we performed a random rotation of the Quiaia catalogue and then cross-matched it with the VLASS one. This gives us  $N_{false}$  matches, a proxy for the non-physical cross-matches between VLASS and Quiaia that just happen to overlap in the 2D right ascension–declination projection. By subtracting  $N_{false}$  from  $N_{total}$ , we get a corrected distribution of the true cross-matched sources (dashed curve). *Right:* The contamination  $N_{false}/N_{corrected}$  of the cross-matches as a function of the search radius. It shows that at the chosen threshold for the cross-matches of  $2''$  we expect to have  $< 0.2\%$  false matches, meaning a very high purity. The horizontal axes are scaled in milliarcseconds (mas).

referencing;

- to investigate, for further refinements, how the likelihood of VLBI detection depends on various factors like optical magnitude, total radio flux density, arcsec-scale compactness, etc.;
- to estimate how existing all-sky optical and radio catalogues could be utilised for a significant densification of the grid of compact VLBI reference sources for astrophysical and astrometric applications;
- as a by-product, to find additional potential phase-reference sources in a selected region around the Ecliptic, in support of spacecraft navigation;
- as another by-product, to find potential VLBI phase-reference sources in an *Euclid* deep field around the well-studied Northern Ecliptic Pole (NEP) region (Euclid Collaboration 2022).

Assuming that the full sample of nearly 4000 Quiaia–VLASS quasars with no existing information about their X-band VLBI structure contains 50% of detectable objects, the probability of determining their true ratio with an error within  $\pm 10\%$  by observing a sub-sample of just 80 sources is 63%. In turn, if the true detectability ratio is as large as 80%, our sample proposed here for observations will provide a result with  $\sim 91\%$  probability at that level of uncertainty.



For the upcoming EVN observations, we selected two different regions with 40–40 test sources in each (Fig. 3), to represent the whole Quaia–VLASS sample above  $\delta > -40^\circ$ . One of them is in the NEP region where the number of Quaia objects is not limited by extinction in the Galactic plane. A secondary benefit of choosing this particular test area is its overlap with one of the deep fields of the *Euclid* space telescope (Euclid Collaboration 2022) of the European Space Agency (ESA). Identifying suitable new VLBI phase-reference sources would help any future radio interferometric observing project here. The other selected region is located close to the northernmost section of the Ecliptic belt. This area of the sky is somewhat closer to the Galactic plane. While around the Ecliptic, it has reasonably good common visibility from the EVN antennas. Here the secondary benefit is the densification of the phase-reference source grid to aid spacecraft navigation. For example, ESA’s *JUICE* (Gurvits et al. 2023), en route to Jupiter, will pass this region in mid-Aug 2025, just weeks before its Venus flyby. In terms of VLASS flux density distribution (Fig. 4) as well as radio compactness (Fig. 5), these 80 sources are representative of the whole Quaia–VLASS sample, allowing us to draw more general statistical conclusions after analysing the observations.

The X-band EVN observations (project code: EF033, PI: S. Frey) will take place in the near future (early 2025) in two segments, using a global network of more than 10 radio telescopes in Europe, China, and South Africa. The data will be recorded at the telescope sites and shipped to the central correlator facility at the Joint Institute for VLBI European Research Infrastructure Consortium where the interference is achieved (Keimpema et al. 2015). Upon successful performance, the correlated data are expected to become available for analysis later in 2025.

We intend to make the calibrated visibility data and images of all the detected sources publicly available for the community. After completing the EVN observations and the analysis of the VLBI data, we will be able to statistically express our confidence in the larger catalogue of about 45 000 Quaia–VLASS matches and we will publish the full quasar list.

### 3. SUMMARY AND OUTLOOK

We selected a total of nearly 4000 radio-emitting AGN by cross-matching the recent Quaia optical and VLASS Epoch 2 radio catalogues with a search radius of  $2''$ . The selected quasars at declinations north of  $\delta = -40^\circ$  have accurate optical astrometric positions from *Gaia* DR3, as well as photometric redshift information. They have flux densities  $S_{3\text{GHz}} > 20$  mJy and compactness parameter  $C > 0.8 \text{ beam}^{-1}$  based on VLASS data. These objects are promising targets for VLBI observations that provide radio images with mas-scale angular resolution. A representative sub-sample of 80 quasars is being observed with the EVN at X-band (around 8 GHz frequency). The results of this pilot project will allow us to estimate the fraction of VLBI-detectable objects in the entire cross-matched Quaia–VLASS sample, leading to an estimate of potential new VLBI target sources, and providing a comprehensive list of them. This would facilitate follow-up observations in various celestial areas of interest. The availability of a large number of yet unknown new VLBI sources would be beneficial for a multitude of potential scientific applications in the fields of astrometry, astrophysics, cosmology, and interplanetary spacecraft navigation.

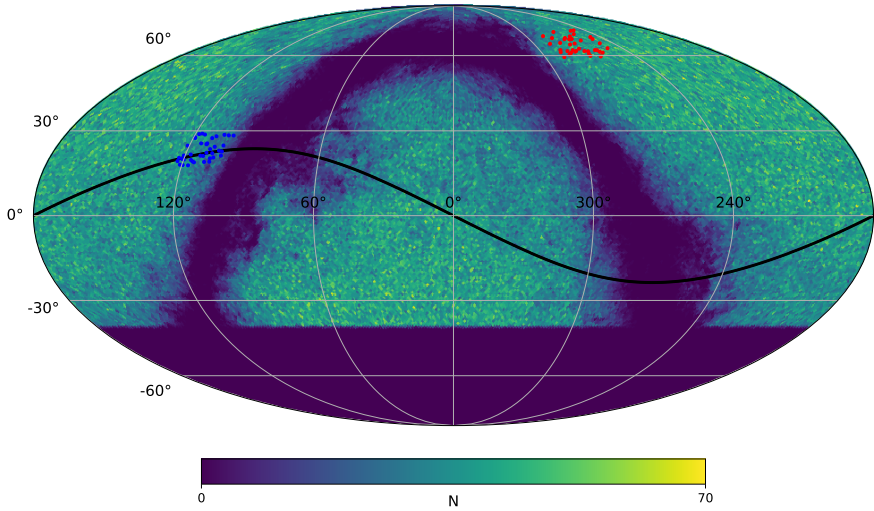


Figure 3: Sky map of the Quaia catalogue (Storey-Fisher et al. 2024) sources north of  $-40^\circ$  declination. The shades represent the density of objects, the darkest being the Galactic plane. The matching Quaia–VLASS sources in the two areas selected for test observations are indicated with 40 blue and 40 red dots in the Ecliptic and NEP regions, respectively. The black curve represents the Ecliptic plane.

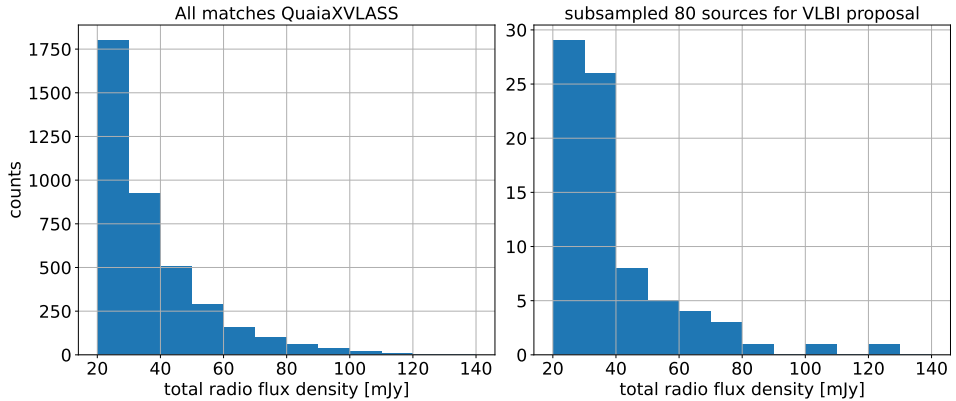


Figure 4: Total VLASS (Lacy et al. 2020) flux density ( $S_{3\text{GHz}} > 20$  mJy) distribution for the entire matching Quaia–VLASS sample (*left*) and for the representative sub-sample of 80 sources proposed for EVN observations (*right*).

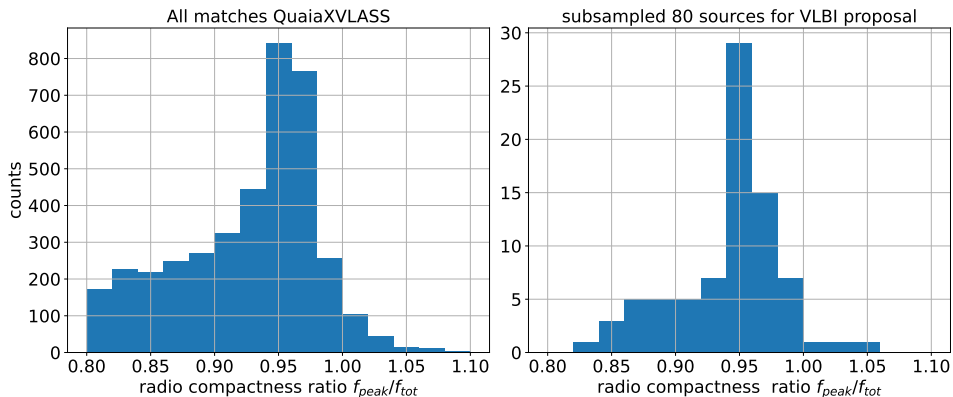


Figure 5: Distribution of arcsec-scale compactness of radio emission based on the ratio of the VLASS peak brightness to the flux density ( $C > 0.8 \text{ beam}^{-1}$ ), for the entire Quiaia–VLASS sample (*left*) and for the representative sub-sample of 80 sources proposed for EVN observations (*right*).

### Acknowledgements

S.F., G.K.É., J.F., and K.P. acknowledge the ESA PRODEX support (project PEA 4000136207). The Large-Scale Structure (LSS) research group at Konkoly Observatory has been supported by a *Lendület* excellence grant by the Hungarian Academy of Sciences (MTA). This project has received funding from: the European Unions Horizon Europe research and innovation programme under the Marie Skłodowska-Curie grant agreement number 101130774, the Hungarian Ministry of Innovation and Technology NRDI Office grant OTKA NN147550, the HUN-REN, and the NKFIH excellence grant TKP2021-NKTA-64.

### References

- Beasley A. J., Conway J. E., 1995, *ASPC*, **82**, 327, doi: 10.1007/978-94-011-0880-5\_13
- Becker R. H., White R. L., Helfand D. J., 1995, *ApJ*, **450**, 559, doi: 10.1086/176166
- Bourda G. et al., 2010, *A&A*, **520**, A113, doi: 10.1051/0004-6361/201014248
- Charlot P. et al., 2020, *A&A*, **644**, A159, doi: 10.1051/0004-6361/202038368
- Deller A.T., Middelberg E., 2014, *AJ*, **147**, 14, doi: 10.1088/0004-6256/147/1/14
- Euclid Collaboration, Moneti A. et al., 2022, *A&A*, **658**, A126, doi: 10.1051/0004-6361/202142361
- Frey S. et al., 2008, *A&A*, **477**, 781, doi: 10.1051/0004-6361:20078711
- Gaia Collaboration, Vallenari A. et al., 2023, *A&A*, **674**, A1, doi: 10.1051/0004-6361/202243940
- Garrington S.T. et al., 1999, *New Astron. Rev.*, **43**, 629, doi: 10.1016/S1387-6473(99)00067-6
- Gurvits L.I. et al., 2023, *Space Sci. Rev.*, **219**, 79, doi: 10.1007/s11214-023-01026-1
- Keimpema A. et al., 2015, *Exp. Astron.*, **39**, 259, doi: 10.1007/s10686-015-9446-1
- Kovalev Y.Y., Petrov L., Plavin A.V., 2017, *A&A*, **598**, L1, doi: 10.1051/0004-6361/201630031
- Lacy M. et al., 2020, *PASP*, **132**, 035001, doi: 10.1088/1538-3873/ab63eb
- Lang D., 2014, *AJ*, **147**, 108, doi: 10.1088/0004-6256/147/5/108

- Li Z. et al., 2022, *JCAP*, **8**, 029, doi: 10.1088/1475-7516/2022/08/029  
Mosoni L. et al., 2006, *A&A*, **445**, 413, doi: 10.1051/0004-6361:20053473  
Njeri A. et al., 2023, *MNRAS*, **519**, 1732, doi: 10.1093/mnras/stac3569  
Petrov L., Kovalev Y., 2024, *arXiv:2410.11794*, doi: 10.48550/arXiv.2410.11794  
Rioja M.J., Dodson R., 2020, *A&AR*, **28**, 6, doi: 10.1007/s00159-020-00126-z  
Schwab F.R., Cotton W.D., 1983, *AJ*, **88**, 688, doi: 10.1086/113360  
Storey-Fisher K. et al., 2024, *ApJ*, **964**, 69, doi: 10.3847/1538-4357/ad1328

## CONSTRAINTS ON GRAVITON MASS FROM S2-LIKE STAR ORBITS AROUND Sgr A\*

V. BORKA JOVANOVIĆ<sup>1</sup> , D. BORKA<sup>1</sup>  and P. JOVANOVIĆ<sup>2</sup> 

<sup>1</sup>*Department of Theoretical Physics and Condensed Matter Physics (020), Vinča  
Institute of Nuclear Sciences - National Institute of the Republic of  
Serbia, University of Belgrade, P.O. Box 522, 11001 Belgrade, Serbia  
E-mail: vborka@vinca.rs*

<sup>2</sup>*Astronomical Observatory, Volgina 7, P.O. Box 74, 11060 Belgrade, Serbia*

**Abstract.** Here we present our achieved results on the bounding graviton mass by the observed orbits of bright stars around Sgr A\*. We used available observations of the S-star orbits in our Galactic center. By comparison of these stellar orbits with their simulated orbits in Yukawa gravitational potential, we estimated the constraints on the parameters of this modified theory of massive gravity. Then, we connected one of these parameters with the Compton wavelength of the graviton and used it for estimation of the graviton mass. In that way we obtained a new method of determining the upper limit of graviton mass, completely independent from other methods published until now. The constraints on the Compton wavelength of the graviton and its mass, obtained using this method, were in a good agreement with the corresponding LIGO results.

### 1. INTRODUCTION

Our researches connected with graviton mass, which were initiated as one of the topics of the successfully finished national project 176003 "Gravitation and the large scale structure of the Universe", are further developing in the scope of new national projects "Gravitation and cosmology" and "Gravitation and astroparticle physics", funded by Ministry of Science, Technological Development and Innovations of the Republic of Serbia. This scientific research has been done at the Astronomical Observatory Belgrade, in cooperation with VINA Institute of Nuclear Sciences.

The results of our researches regarding bounds on graviton mass are presented at more national and international conferences (poster session, short talks, invited talks, seminars), and the papers are published in proceedings and refereed journals, as well. At the end of this paper we give the bibliography of the papers published on this topic.

### 2. GRAVITON AND ITS MASS

Elementary particles of the Standard Model consist of leptons and quarks (there are 24 of them in total: six leptons and six quarks, as well as the same number of their antiparticles). Elementary particles interact in the way they are exchanging quanta

of interaction field, i.e. the calibration or gauge bosons. Graviton is a gauge boson of the gravitation interaction which acts on massive particles. Here we give some of its characteristics:

- intrinsic spin (in units of reduced Planck constant  $\hbar$ ):  $\sigma = 2$  (tensor boson),
- charge (in units of elementary charge  $e$ ):  $Q = 0$ , i.e. it is electrically neutral,
- mass: if it has a mass, then it is very small (we calculate its upper limit).

Graviton, a spin-2 (tensor) and electrically uncharged gauge boson of the gravitational interaction, according to General Relativity travels along null geodesics at the speed of light  $c$  (like photon). However, according to some alternative theories, gravity is propagated by a massive field, i.e. by a graviton with some small, nonzero mass  $m_g$ . Let us mention here that the existence of massive graviton plays a fundamental role in modern physics, and its non-zero mass leads to modifications of the speed of gravitational waves depending on their frequencies.

### 3. MASSIVE GRAVITY THEORIES

Theories of massive gravity, which are first proposed by Fierz & Pauli (1939), make the following two important predictions (Will, 1998):

1. the effective Newtonian potential has a Yukawa form:  $\Phi(r) \propto r^{-1} \exp(-r/\lambda_g)$ , where  $\lambda_g = \hbar/(m_g c)$  is the Compton wavelength of graviton, and
2. massive graviton propagates at an energy (or frequency) dependent speed  $v_g$ :  $v_g^2/c^2 = 1 - m_g^2 c^4/E^2 = 1 - \hbar^2 c^2/(\lambda_g^2 E^2) = 1 - c^2/(f\lambda_g)^2$ .

Gravitational potential with a Yukawa correction can be obtained in the Newtonian limit of any analytic  $f(R)$  gravity model given by the following action (Capozziello et al. 2014):

$$\mathcal{S} = \int d^4x \sqrt{-g} [f(R) + \mathcal{X} \mathcal{L}_m], \quad \mathcal{X} = \frac{16\pi G}{c^4}. \quad (1)$$

In such a case, the gravitational potential in the weak field limit is given by:

$$\Phi(r) = -\frac{GM}{(1+\delta)r} \left( 1 + \delta e^{-\frac{r}{\Lambda}} \right), \quad (2)$$

where  $\Lambda$  is the range of Yukawa interaction and  $\delta$  is a universal constant.

The limits on graviton mass can be obtained through different methods in modified gravity theories. The experimental limits to  $m_g$ <sup>1</sup> have been set based on a Yukawa potential, dispersion relation, or other modified gravity theories (Particle Data Group 2024). The massive gravity theories are tested at different astrophysical and cosmological scales. Thus, in addition to the ground and space-based gravitational wave detectors such as LIGO/Virgo or LISA, the graviton mass can be also determined from observations in electromagnetic band of gravitational systems such as: Solar System planetary astrometric data, orbits of S-stars around Sgr A\*, binary pulsars, galactic clusters, black holes and their mergers, and weak gravitational lensing. See, for instance,  $m_g$  from constrains to the range of Yukawa gravity interaction from S-star orbits around black hole at Galactic Center obtained by Zakharov et al. (2016a); Jovanović et al. (2023). Or, for example, Jovanović et al. (2024a,b) analyzed the Schwarzschild precession of S2 in the framework of Yukawa gravity theory, and set an

<sup>1</sup>Particle Data Group, 2024: <https://pdg.lbl.gov/2024/listings/rpp2024-list-graviton.pdf>

upper limit to the mass of the graviton, which is compatible with limits from aLIGO gravitational-wave data.

#### 4. RECENT RESULTS ON GRAVITON MASS CONSTRAINTS

With aim of obtaining the constraints on the parameters of the Yukawa-like gravitational potentials, as well as on the graviton mass  $m_g$ , in our recent investigations we studied the trajectories of bright S-stars around Sgr A\* at Galactic Center (GC), representing the central supermassive black hole (SMBH) of our Galaxy, in the frame of Yukawa gravity (see e.g. Borka et al. 2013, 2023; Capozziello et al. 2014; Jovanović et al. 2021, 2023, 2024a,b; Zakharov et al. 2016a,b, 2017a,b,c, 2018a,b,c,d, 2020). For that purpose we used combined astrometric observations of the S-star orbits by both Very Large Telescope (VLT) and Keck telescope available in Gillessen et al. (2017), as well as the recent results by the GRAVITY Collaboration about their detection of the Schwarzschild precession in the orbit of S2 star (GRAVITY Collaboration 2020, 2022).

In these investigations we assumed that the parameter  $\Lambda$  of the Yukawa-like gravitational potential, representing the range of interaction, corresponds to the graviton Compton wavelength  $\lambda_g$ . Besides, we also assumed that the orbital precession in Yukawa gravity should be close to the prediction of General Relativity (GR) for Schwarzschild precession. This enabled us to obtain the constraints on the graviton mass  $m_g$  in two different ways:

1. by direct fitting of the simulated orbits in Yukawa gravity into the corresponding observed orbits of S-stars, and
2. from the factor  $f_{SP}$  under which the observed orbital precession deviates from the Schwarzschild precession in GR<sup>2</sup>, and which was recently measured by the GRAVITY Collaboration.

Regarding the first approach, direct orbital fitting in the frame of Yukawa gravity was performed by minimization of the reduced  $\chi^2$  statistics using the differential evolution optimization method, implemented as Python Scipy function `scipy.optimize.differential_evolution` (detailed description of the fitting procedure can be found in Jovanović et al. 2024b). An example of such orbital fitting in the case of S2 star and universal constant of  $\delta = 1$  is presented in Fig. 1, while the resulting best-fit values of the parameters, obtained for  $\chi_{\text{red}}^2 = 1.1084$ , are given in Table 1. The best-fit value for the graviton Compton wavelength of  $\lambda_g = 5.8 \pm 0.98 \times 10^4$  AU corresponds to the graviton mass of  $m_g = 142.9 \pm 24.1 \times 10^{-24}$  eV.

In the second approach, we first derived the following relation between the parameter  $\Lambda$  and  $f_{SP}$  when universal constant is  $\delta = 1$  (Jovanović et al. 2023, 2024a,b):

$$\Lambda(P, e; f_{SP}) \approx \frac{cP}{4\pi} \sqrt{\frac{(\sqrt{1-e^2})^3}{3(f_{SP}-1)}}, \quad (3)$$

for which Yukawa gravity results with practically the same orbital precession as GR in case of a star with orbital period  $P$  and eccentricity  $e$ . Taking that the graviton Compton wavelength  $\lambda_g = \Lambda$ , we then obtained the corresponding estimates for the graviton mass  $m_g$  in the case of different S-stars. Table 2 presents several such

<sup>2</sup>Factor  $f_{SP}$  in GR is equal to 1 and in Newtonian gravity to 0.

estimates in the case of S2 star which are obtained for the best-fit value of  $f_{SP}$  given in GRAVITY Collaboration (2020):  $f_{SP} = 1.10 \pm 0.19$ , as well as for the following three upper bounds which are  $1\sigma$  compatible with the GR value of  $f_{SP} = 1$ :

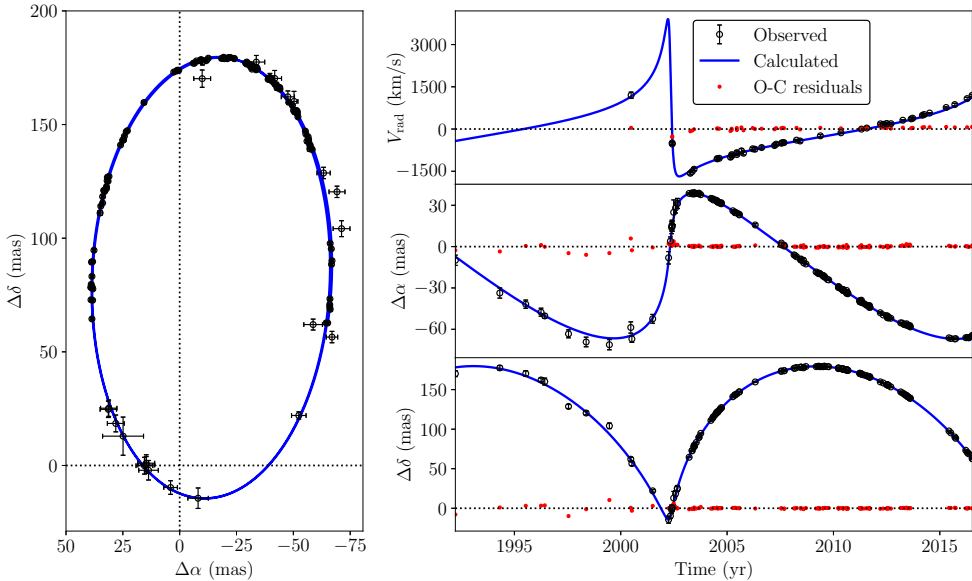


Figure 1: *Left*: Comparison between the best-fit simulated orbit of the S2 star in Yukawa gravity (blue solid line), and the corresponding astrometric observations from Gillessen et al. (2017) (black circles with error bars). *Right*: The same for the radial velocity of the S2 star (top), as well as for its  $\alpha$  (middle) and  $\delta$  (bottom) offset relative to the position of Sgr A\* at the coordinate origin. Red dots in the right panels denote the corresponding O-C residuals.

Table 1: Best-fit values of the graviton Compton wavelength  $\lambda_g$ , SMBH mass  $M$ , distance  $R$  to the GC and the osculating orbital elements  $a, e, i, \Omega, \omega, P, T$  of the S2 star orbit.

Parameter	Value	Fit error	Unit
$\lambda_g$	5.8	0.98	$10^4$ AU
$M$	4.10	0.579	$10^6 M_\odot$
$R$	8.30	0.246	kpc
$a$	0.1229	0.00527	arcsec
$e$	0.8787	0.01213	
$i$	134.90	2.049	$^\circ$
$\Omega$	224.51	6.840	$^\circ$
$\omega$	62.70	5.781	$^\circ$
$P$	16.05	0.541	yr
$T$	2018.29626	1.629346	yr



$f_{SP} = 1.19 \pm 0.19$ ,  $f_{SP} = 1.16 \pm 0.16$  and  $f_{SP} = 1.144 \pm 0.144$ . These  $1\sigma$  measurement errors are taken from GRAVITY Collaboration (2020, 2022).

Table 2: The Compton wavelength of the graviton  $\lambda_g$ , its mass  $m_g$ , as well as their relative and absolute errors, calculated for four different values of  $f_{SP}$  in the case of S2 star.

$f_{SP}$	$\Delta f_{SP}$	$\lambda_g \pm \Delta\lambda_g$ (AU)	$m_g \pm \Delta m_g$ ( $10^{-24}$ eV)	R.E. (%)
1.100	0.190	4.7e+04 $\pm$ 4.5e+04	176.6 $\pm$ 170.0	96.3
1.190	0.190	3.4e+04 $\pm$ 1.7e+04	243.5 $\pm$ 124.8	51.3
1.160	0.160	3.7e+04 $\pm$ 1.9e+04	223.4 $\pm$ 114.6	51.3
1.144	0.144	3.9e+04 $\pm$ 2.0e+04	211.9 $\pm$ 108.7	51.3

As it can be seen from the presented results, our constraints on the graviton mass obtained using the above two methods are independent, but consistent with the corresponding LIGO's result of  $m_g \leq 1.2 \times 10^{-22}$  eV estimated from the first gravitational wave signal GW150914 (LIGO/Virgo Collaboration, 2016).

In addition to the mentioned references, our graviton mass constraints are also presented and cited in the below Seminars and White Paper: **Seminar 1:** Vesna Borka Jovanović and Duško Borka, *Nobel prize for Physics for 2020 and our researches at this topic*, Seminar for geometry and applications, 22<sup>nd</sup> October 2020, Mathematical Faculty, University of Belgrade; **Seminar 2:** Predrag Jovanović, *Observational cosmology and cosmological tests*, Seminar for geometry and applications, 8<sup>th</sup> April 2021, Mathematical Faculty, University of Belgrade; **White Paper:** CosmoVerse White Paper - Addressing observational tensions in cosmology with systematics and fundamental physics (CA21136), Chapter "Modified gravity" (in preparation, 2024).

## 5. CONCLUSIONS

Here we presented a short overview of our recent results on the bounding graviton mass by analysis of the stellar orbits around Sgr A\* in the frame of Yukawa gravity. For that purpose we used two different approaches based on: (i) direct orbital fitting and (ii) recovering the recently detected Schwarzschild precession in the orbit of S2 star using the Yukawa-like gravitational potential. The both approaches resulted with the constraints on the graviton mass which are independent, but consistent with the corresponding LIGO's estimate. The obtained results also demonstrate that the existence of massive graviton plays a fundamental role in modern physics, and that it is important to further develop this topic.

**Acknowledgments.** This research was funded by the Ministry of Science, Technological Development and Innovations of the Republic of Serbia through the Project contracts No. 451-03-66/2024-03/200002 and 451-03-66/2024-03/200017.

## References

- Borka, D., Jovanović, P., Borka Jovanović, V., Zakharov, A. F.: 2013, *J. Cosmol. Astropart. P.*, **2013**, No. 11, 050, doi: 10.1088/1475-7516/2013/11/050  
 Borka, D., Borka Jovanović, V., Jovanović, P.: 2023, *Filomat*, **37**, 8591, doi: 10.2298/FIL2325591B

- Capozziello, S., Borka, D., Jovanović, P., Borka Jovanović, V.: 2014, *Phys. Rev. D*, **90**, 044052, doi: 10.1103/PhysRevD.90.044052
- Fierz, M., Pauli, W.: 1939, *Proc. R. Soc. London Ser. A*, **173**, 211, doi: 10.1098/rspa.1939.0140
- Gillessen, S., Plewa, P.M., Eisenhauer, F., Sari, R.E., Waisberg, I., Habibi, M., Pfuhl, O., George, E., Dexter, J., von Fellenberg, S., et al.: 2017, *Astrophys. J.*, **837**, 30, doi: 10.3847/1538-4357/aa5c41
- GRAVITY Collaboration, Abuter, R., Amorim, A., Baubck, M., Berger, J.P., Bonnet, H., Brandner, W., Cardoso, V., Clénet, Y., de Zeeuw, P.T. et al.: 2020, *Astron. Astrophys.*, **636**, L5, doi: 10.1051/0004-6361/202037813
- GRAVITY Collaboration, Abuter, R., Aymar, N., Amorim, A. et al.: 2022, *Astron. Astrophys.*, **657**, L12, doi: 10.1051/0004-6361/202142465
- Jovanović, P., Borka, D., Borka Jovanović, V., Zakharov, A. F.: 2021, *Eur. Phys. J. D*, **75**, 145, doi: 10.1140/epjd/s10053-021-00154-z
- Jovanović, P., Borka Jovanović, V., Borka, D., Zakharov, A. F.: 2023, *J. Cosmol. Astropart. P.*, **2023** No. 03, 056, doi: 10.1088/1475-7516/2023/03/056
- Jovanović, P., Borka Jovanović, V., Borka, D., Zakharov, A. F.: 2024a, *Phys. Rev. D*, **109**, 064046, doi: 10.1103/PhysRevD.109.064046
- Jovanović, P., Borka Jovanović, V., Borka, D., Zakharov, A. F.: 2024b, *Symmetry*, **16**, 397, doi: 10.3390/sym16040397
- LIGO Scientific Collaboration and Virgo Collaboration, Abbot, B. P. et al.: 2016, *Phys. Rev. Lett.*, **116**, 061102, doi: 10.1103/PhysRevLett.116.061102
- Particle Data Group Collaboration, Navas, S. et al.: 2024, *Phys. Rev. D*, **110**, 030001, doi: 10.1103/PhysRevD.110.030001
- Will, C. M.: 1998, *Phys. Rev. D*, **57**, 2061, doi: 10.1103/PhysRevD.57.2061
- Zakharov, A. F., Jovanović, P., Borka, D., Borka Jovanović, V.: 2016a, *J. Cosmol. Astropart. P.*, **2016**, No. 05, 045, doi: 10.1088/1475-7516/2016/05/045
- Zakharov, A. F., Jovanović, P., Borka, D., Borka Jovanović, V.: 2016b, *EPJ Web Conf.*, **125**, 01011, doi: 10.1051/epjconf/201612501011
- Zakharov, A. F., Jovanović, P., Borka, D., Borka Jovanović, V.: 2017a, *EPJ Web Conf.*, **138**, 01010, doi: 10.1051/epjconf/201713801010
- Zakharov, A. F., Jovanović, P., Borka, D., Borka Jovanović, V.: 2017b, *J. Phys.: Conf. Ser.*, **798**, 012081, doi: 10.1088/1742-6596/798/1/012081
- Zakharov, A. F., Jovanović, P., Borka, D., Borka Jovanović, V.: 2017c, *Proceedings of the 52nd Rencontres de Moriond (Gravitation Session), La Thuile, Italy, March 25 - April 1*, 247
- Zakharov, A. F., Jovanović, P., Borka, D., Borka Jovanović, V.: 2018a, *J. Cosmol. Astropart. P.*, **2018**, No. 04, 050, doi: 10.1088/1475-7516/2018/04/050
- Zakharov, A. F., Borka, D., Jovanović, P., Borka Jovanović, V.: 2018b, *Book of abstracts of the 42nd Committee on Space Research, Pasadena, USA, July 14-22*, H0.2-14-18
- Zakharov, A. F., Jovanović, P., Borka, D., Borka Jovanović, V.: 2018c, *Int. J. Mod. Phys. Conf. Ser.*, **47**, 1860096, doi: 10.1142/S2010194518600960
- Zakharov, A. F., Jovanović, P., Borka, D., Borka Jovanović, V.: 2018d, *Proceedings IAU Symposium 347: Early Science with ELTs (EASE)*
- Zakharov, A. F., Jovanović, P., Borka, D., Borka Jovanović, V.: 2020, *Contrib. Astron. Obs. Skalnaté Pleso*, **50**, 203, doi: 10.31577/caosp.2020.50.1.203

## SERBIAN-BULGARIAN COOPERATION ABOUT GAIA ALERTS DURING 2023

G. DAMLJANOVIĆ<sup>1</sup> , M. STOJANOVIĆ<sup>1</sup> , M.D. JOVANOVIĆ<sup>1</sup> ,

R. BACHEV<sup>2</sup>  and S. BOEVA<sup>2</sup> 

<sup>1</sup>*Astronomical Observatory, Volgina 7, 11060 Belgrade, Serbia*

*E-mail: gdamljanovic@aob.rs*

<sup>2</sup>*Institute of Astronomy and National Astronomical Observatory, Bulgarian Academy of Sciences, 72 Tsarigradsko Shosse, 1784 Sofia, Bulgaria*

**Abstract.** From October 2014 until now (about 10 years) we have done astronomical observations of the Gaia Alerts or Gaia Follow Up Network for Transients Objects (Gaia-FUN-TO). In 2013 we organized our local cooperation *Serbian-Bulgarian mini-network telescopes* to get better results. Also, the mentioned observations and investigations are in line with actual joint research SANU-BAN project *Gaia astrometry and fast variable astronomical objects* from 2023 to 2025; SANU-BAN are Serbian and Bulgarian Academies of Sciences. Now, there are 8 astronomical instruments at two sites in Bulgaria (at Belogradchik and Rozhen) and one site in Serbia (Astronomical Station Vidojevica - ASV). Usually, we have done  $\approx 15$  Gaia Alerts per year. Because of the COVID-problem, in 2021 we observed just 5 Gaia Alerts: Gaia19dke (11 times), Gaia21awo (1), Gaia21azb (13), Gaia21efs (1), and Gaia21ehu (1);  $\approx 300$  CCD images were done. At 2022 we did 7 Gaia Alerts: Gaia21cgt (1 time), Gaia22aeu (1), Gaia22atp (1), Gaia22btj (1), Gaia22btc (1), Gaia22dym (1), and Gaia21brx (1);  $\approx 70$  images. During 2023, we did 12 Gaia Alerts: Gaia22ang (5 times), Gaia22dze (1), Gaia23bay (6), Gaia19dmj (2), Gaia21cgt (2), Gaia22eem (2), Gaia23afy (1), Gaia23cer (2), Gaia23cri (3), Gaia20cwd (1), Gaia23bbk (1), and Gaia23cvq (1);  $\approx 300$  images were done using the 60 cm and 1.4 m ASV telescopes. We present some results here.

### 1. INTRODUCTION

The predecessor of the Gaia space mission was the Hipparcos one (High Precision PARallax Collecting Satellite) of the European Space Agency (ESA). The Hipparcos mission changes astronomy, with nearly 118000 stars and position standard deviation about 1 milliarcsec astrometry (ESA 1997, van Leeuwen 2007), at the end of the last century. At the beginning, the plan of Gaia was nearly 1 billion stars and nearly 500000 extragalactic sources (Prusti 2012) with position standard deviation about 1 microarcsec astrometry. Both ESA missions are a revolution in astronomy.

The Gaia astronomical spacecraft was launched at the end of 2013, with scientific operations commencing in July 2014 and useful data from August 2014. The Gaia observational period was 5 years, and now it is much longer than the predicted operation phase. The Gaia satellite is surveying the full sky, and the obtained results (astrometrically, photometrically, and spectroscopically) are useful for all the relevant scientific communities: our understanding of the Milky Way galaxy, for the stellar physics, the Solar System bodies, astrometry, etc. The main goal of Gaia mission is a catalogue

(for the objects from  $G = 3$  mag to 21 mag) of the high-precision astrometric data: the positions, proper motions and parallaxes. That catalogue is an important step in the realization of the Gaia Celestial Reference Frame (Gaia CRF). The last Gaia solution (the third one) or data release (Gaia DR3) was made publicly available on 13th June 2022. There are about 1.806 billion sources with  $G$  magnitude in it (nearly two times more than the plan of Gaia).

Because of the Gaia scanning process and data (it is observing the sky multiple times and provides near-real-time photometric data), it is possible to detect some changes in brightness from all over the sky and appearance of new objects. As a result, the Gaia Science Alerts (GSA) system produces alerts on these interesting objects, and after that we continue astronomical observations of the mentioned objects using the ground-based telescopes (as the *Serbian-Bulgarian mini-network telescopes*). The GSA system made its first discovery of a transient event (it was the object Gaia14aaa) in September 2014 (shortly after mid-2014), and the GSA was among the leading transient surveys in the world a few years after that. There are more than 3000 transients which were discovered during three years (from September 2014 to September 2017), and about 4000 transients were discovered during 2022. Over the past decade, GSA announced over 20000 transients of various types. It is a really impressive result. The transients are: supernovae, novae, young stellar objects, cataclysmic variables, microlensing events, R Coronae Borealis (RCrB) dimming stars, flaring quasars, and many other rare phenomena. It is evident that the Gaia Alerts have significantly contributed to time-domain and transient astronomy from September 2014 to September 2024. The numerous targets were extensively studied and the data were widely used in multiple publications using the Global Telescope Network and Black Hole Target Observation Manager (BHTOM). The long-term follow-up and monitoring of alerts from Gaia are in accordance with the establishment of a global telescope network (initiated in 2010, now with about 100 telescopes) and the programme of GSA. Recently it was supported by the European Commission's OPTICON-Radionet Pilot grant. From some time ago, that network operates through a BHTOM web service. The BHTOM provides thousands of CCD images (of hundreds of astronomical objects) per week. In 2024, there are 10 years of the GSA and 15 years of the mentioned telescope network. The last workshop about the Gaia Science Alerts and its follow-up programme was held in Heraklion (Crete, 2024) with about 80 registered participants.

## 2. SERBIAN-BULGARIAN COOPERATION ABOUT GAIA ALERTS

The plan of Gaia astronomical observations was to observe each object in the sky nearly 70 times over the mission lifetime (5 years), and there are a lot of alerts because of that kind of observations. As a result, for each object the number of alerts increases with number of observations. Over the past decade, it was reported over 20000 transients (Gaia Alerts) from all over the sky. On the other hand, the Astronomical Station Vidojevica (ASV) of Astronomical Observatory in Belgrade (AOB, Serbia) was established in 2011. It was the Serbian new astronomical site. At the beginning we used a new  $D=60$  cm telescope *Nedeljković*. At mid-2016 there was another new telescope ( $D=1.4$  m) *Milanković* via the Belissima project. At Belogradchik and Rozhen sites (in Bulgaria), we used 4 instruments in accordance with our regional collaboration *Serbian-Bulgarian mini-network telescopes* from 2013. At that time, that cooperation was in line with the SANU-BAN joint research project *Observations*

Table 1: The main information about the telescopes and CCD cameras of Serbian – Bulgarian cooperation.

Telescope D/F [m]	Camera	Chip size [pixel]	Pixel size [ $\mu\text{m}$ ]	Scale [ $''/p$ ]	Field of view FoV[arcmin]
ASV					
1.4/11.42	ApogeeAltaU42	2048x2048	13.5x13.5	0.243	8.3x8.3
	Andor iKon-L	2048x2048	13.5x13.5	0.24	8.3x8.3
ASV					
0.6/6	ApogeeAltaU42	2048x2048	13.5x13.5	0.465	15.8x15.8
	FLI PL230	2048x2064	15x15	0.517	17.7x17.8
Rozhen					
2/15.774	VersArray1300B	1340x1300	20x20	0.261	5.6x5.6
	Andor iKon-L	2048x2048	13.5x13.5	0.176	6.0x6.0
Rozhen					
0.6/7.5	FLI PL09000	3056x3056	12x12	0.33	16.8x16.8
Belogradchik					
0.6/7.5	FLI PL09000	3056x3056	12x12	0.33	16.8x16.8
Rozhen					
0.5/0.7/1.72	FLI PL16803	4096x4096	9x9	1.08	73.7x73.7

of *ICRF radio-sources visible in optical domain* for three years period (2014-2016); the Serbian Academy of Sciences and Arts (SANU) and Bulgarian Academy of Sciences (BAN) supported mentioned project. The next two ones were: *Study of ICRF radio-sources and fast variable astronomical objects* (2017-2019), and *Gaia Celestial Reference Frame (CRF) and fast variable astronomical objects* (2020-2022). The last one is *Gaia astrometry and fast variable astronomical objects* (2023-2025), and the leaders are G.Damljanović (Serbia) and R.Bachev (Bulgaria). The main information about the telescopes and CCD cameras is in Table 1, and it has been published in a few papers (Damljanović et al. 2014, Taris et al. 2018, Damljanović et al. 2020), also. The first column in Table 1 is telescope (with diameter - D and focal length - F in meters), and site (ASV, Rozhen or Belogradchik). The other columns are: CCD camera, chip size (in pixels), pixel size (in micrometers), scale (in arcseconds per pixel), and field of view - FoV (in arcminutes).

Three Bulgarian telescopes are at National Astronomical Observatory (NAO) BAN Rozhen (D=2 m, D=60 cm, and Schmidt-camera 50/70 cm), and one is at Belogradchik AO site (D=60 cm). At the end of 2023, there is a new D=1.5 m one at NAO Rozhen, but not used until now (it is going to be a robotic instrument, soon). From the end of 2023, we have used the Meade D=40 cm at ASV.

### 3. RESULTS

Our investigations about Gaia Alerts (over the past decade) are in accordance with *Serbian-Bulgarian mini network telescopes* and mentioned SANU-BAN joint research projects. Also, we can use D=1.31 m telescope of the Aryabhata Research Institute of observational sciencES (ARIES, Manora Peak, Nainital, India). It is in line with our useful cooperation with some colleagues from India (A.C. Gupta and others). Here,

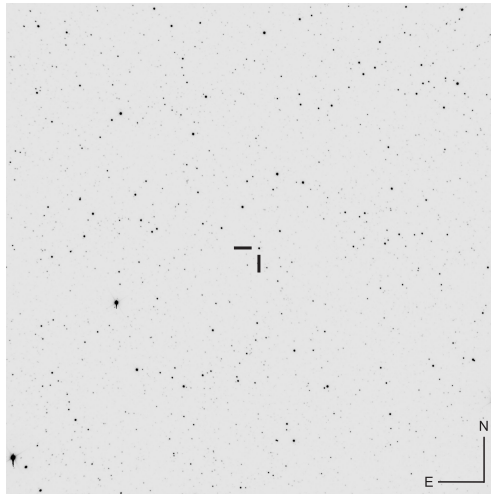


Figure 1: Original image of the object Gaia23bay (R-band,  $Exp. = 60^s$ ) on October 7<sup>th</sup> 2023 using the  $D = 1.4$  m ASV telescope with CCD camera Andor iKon-L.

we present a few published papers (Damljanovic et al. 2014, Campbell et al. 2015, Wyrzykowski et al. 2020, Szegedi-Elek et al. 2020, Damljanovic et al. 2020, Hodgkin et al. 2021, etc.) using our data. Usually, we have done 3 CCD images per filter during observations of some Gaia Alerts and Johnson-Cousins BVRcIc filters. The standard bias, dark and flat-fielded corrections are done (also, hot/dead pixels are removed), and the Astrometry.Net and Source Extractor are used. For further calibration, the output is supposed to be submitted to the Cambridge Photometric Calibration Server (CPCS), but some time ago to the BHTOM. Over the past decade, we collected about 4000 CCDs for 130 Gaia Alerts or Gaia-Follow-Up Network for Transients Objects (Gaia-FUN-TO), and it was 460 images per year (near 15 objects per year) before the problem with COVID virus. Because of the COVID problems, in 2020 we did 11 objects, just 5 objects in 2021, 7 objects in 2022. During 2023 we did 12 Gaia Alerts: Gaia22ang (5 times), Gaia22dze (1), Gaia23bay (6), Gaia19dmj (2), Gaia21cgt (2), Gaia22eem (2), Gaia23afy (1), Gaia23cer (2), Gaia23cri (3), Gaia20cwd (1), Gaia23bbk (1), and Gaia23cvq (1); about 300 CCD images were done.

Here, we present the object Gaia23bay ( $\alpha = 19^h 49^m 43.^s 00$ ,  $\delta = 10^\circ 43' 41.'' 45$ , see Table 2 and Fig. 1 with seeing= $1.'' 1$ ): alerting date is March 7<sup>th</sup> 2023, class is unknown, candidate is unknown, but the photometric class is Red Giant (98.2%). We did it using two ASV instruments (60 cm and 1.4 m). The Gaia23bay was observed 6 times during 2023 (see Table 2): on June 19<sup>th</sup> using D=1.4 m ASV telescope with CCD Andor iKon-L ( $0.'' 391$  per pixel), on July 24<sup>th</sup> using D=60 cm ASV with FLI PL230 ( $0.'' 517$  per pixel), on August 17<sup>th</sup> using D=1.4 m ASV, on September 18<sup>th</sup> using D=60 cm ASV, on October 6<sup>th</sup> using D=1.4 m ASV, and on October 7<sup>th</sup> using D=1.4 m ASV; Modified Julian Day or  $MJD = JD - 240000.5$  where JD is Julian Day. The first line in Table 2 is the date of observation (after that it is suitable MJD), and other 5 lines are BVRI and g magnitudes (with suitable standard deviation) after photometry. The standard deviation of our magnitudes is on the level 0.01 mag (for 60 cm ASV) and 0.001 (for 1.4 m ASV).

Table 2: Our photometry results (BVRI and g magnitudes with their standard deviations and MJD time) of Gaia23bay during 2023.

Date	June 19 <sup>th</sup>	July 24 <sup>th</sup>	Aug. 17 <sup>th</sup>	Sept. 18 <sup>th</sup>	Oct. 6 <sup>th</sup>	Oct. 7 <sup>th</sup>
MJD	60114.9	60149.9	60174.0	60205.8	60223.8	60224.8
I [mag]	12.716 ±0.005	12.772 ±0.002	12.778 ±0.003	12.801 ±0.004	12.805 ±0.002	12.790 ±0.005
R [mag]	13.423 ±0.004	13.501 ±0.002	13.503 ±0.002	13.519 ±0.004	13.524 ±0.002	13.509 ±0.004
V [mag]	14.188 ±0.004	14.239 ±0.003	14.262 ±0.002	14.256 ±0.004	14.278 ±0.002	14.263 ±0.004
g [mag]	- -	15.013 ±0.007	- -	15.030 ±0.009	- -	- -
B [mag]	15.548 ±0.005	15.588 ±0.008	15.610 ±0.004	15.605 ±0.011	15.630 ±0.005	15.642 ±0.004

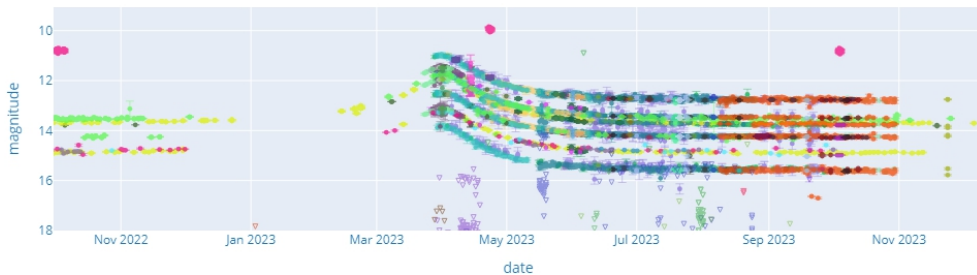


Figure 2: Light curve of the Gaia23bay using all BHTOM data.

Our original CCD image of the Gaia23bay is shown in Fig. 1 after the standard reduction (bias/dark/flat, hot/dead pixels, etc.) and the object is marked with lines. The east (E) is left and north (N) is up,  $FoV = 8.3 \times 8.3$  arcmin, binning=1x1,  $scale = 0.391$  arcsec per pixel. The light curve of all BHTOM data is in Fig. 2 (it is from BHTOM site): x-axis is date, and y-axis is suitable magnitude. Our results are in good accordance with: the ground-based relative photometry, results obtained from other telescopes (at BHTOM site), possibilities of our instruments, etc. The values of some of our magnitudes are transferred from our set of filters (Johnson BV and Cousins RcIc) into another one (see g magnitudes in Table 2) via BHTOM. We hope, there are enough relevant Gaia23bay data for our next paper in the future.

#### 4. CONCLUSIONS

In mid-2014 the first observations of the ESA Gaia satellite were done, and since September 2014 the Gaia Photometric Science Alerts started to publish alerts. Over the past decade, GSA announced over 20000 transients. They were issued by the GSA group: supernovae, novae, cataclysmic variables, young stellar objects, microlensing events, R Coronae Borealis (RCrB) dimming stars, flaring quasars, etc. As a part of that job, we established our regional cooperation the *Serbian-Bulgarian mini-network*

telescopes and our activities were in line with a few SANU-BAN projects. We have used 6 Serbian-Bulgarian telescopes for these investigations. Using D=2 m Rozhen and D=1.4 m ASV telescopes with  $Exp. = 300^s$ , we can observe the objects down to 21 mag in the R-band, and down to 19 mag using smaller telescopes. From September 2014 to September 2024, we observed about 130 Gaia Alerts (usually, nearly 15 objects per year). There are  $\approx 4000$  CCD images ( $\approx 460$  images per year). We did these observations (usually, three CCD images per band) in Johnson BV and Cousins RcIc filters. A lot of papers were published with our results. Three papers were published during 2020 and 2021: about Gaia16aye or Ayers Rock (Wyrzykowski et al. 2020), about Gaia18dvy (Szegedi-Elek et al. 2020), and about the main results of Gaia Alerts (Hodgkin et al. 2021). Some of our results were presented at a few conferences. As an example, we present our results of the object Gaia23bay here. We hope, the Gaia23bay will be the subject of our next paper, soon.

### Acknowledgements

We gratefully acknowledge support by the Astronomical Station Vidojevica and the Ministry of Science, Technological Development and Innovation of the Republic of Serbia (MSTDIRS) through contract no. 451-03-66/2024-03/200002 made with Astronomical Observatory (Belgrade), by the EC through project BELISSIMA (call FP7-REGPOT-2010-5, No. 256772), the observing and financial grant support from the Institute of Astronomy and Rozhen NAO BAS through the bilateral SANU-BAN joint research project *GAIA astrometry and fast variable astronomical objects*, and support by the SANU project F-187. This research was supported by the Science Fund of the Republic of Serbia, grant no. 6775, Urban Observatory of Belgrade - UrbObsBel. Also, we acknowledge ESA Gaia DPAC and Photometric Science Alerts Team (<http://gsaweb.ast.cam.ac.uk/alerts>).

### References

- Campbell, H.C., Marsh, T.R., Fraser, M., ... , Damljanović, G., ... , Vince, O., et al.: 2015, *Monthly Notices of the Royal Astronomical Society*, **452**, 1060, doi: 10.1093/mnras/stv1224
- Damljanović, G., Vince, O., Boeva, S.: 2014, *Serbian Astronomical Journal*, **188**, 85, doi: 10.2298/SAJ1488085D
- Damljanović, G., Boeva, S., Latev, G., Bachev, R., Vince, O., Jovanović, M.D., Cvetković, Z., Pavlović, R.: 2020, *Bulgarian Astronomical Journal*, **32**, 108
- ESA: 1997, in ESA Special Publication, Vol. SP-1200 (Nordwijk: ESA Publ. Division)
- Hodgkin, S.T., Harrison, D.L., Breedt, E., ... , Damljanović, G., et al.: 2021, *Astronomy and Astrophysics*, **652**, A76, doi: 10.1051/0004-6361/202140735
- Szegedi-Elek, E., Abraham, P., Wyrzykowski, L., ... , Damljanović, G., et al.: 2020, *The Astrophysical Journal*, **899:130**, (8pp), doi: 10.3847/1538-4357/aba129
- Prusti, T.: 2012, *Astronomische Nachrichten*, **333**, 453, doi: 10.1002/asna.201211688
- Taris, F., Damljanović, G., Andrei, A., et al.: 2018, *Astronomy and Astrophysics*, **611**, A52, doi: 10.1051/0004-6361/201731362
- van Leeuwen, F.: 2007, *Hipparcos, the New Reduction of the Raw Data* (Dordrecht: Springer), doi: 10.1007/978-1-4020-6342-8
- Wyrzykowski, L., Mroz, P., Rybicki, K.A., ... , Boeva, S., ... , Damljanović, G., ... , Gupta, A.C., ... , Jovanović, M.D., ... , Latev, G., ... , Vince, O., et al.: 2020, *Astronomy and Astrophysics*, **633**, A98, doi: 10.1051/0004-6361/201935097



## STARK BROADENING DATA FOR N VI SPECTRAL LINES

M. S. DIMITRIJEVIĆ<sup>1,2</sup> , M. D. CHRISTOVA<sup>3</sup> and S. SAHAL-BRÉCHOT<sup>2</sup> <sup>1</sup> *Astronomical Observatory, Volgina 7, 11060 Belgrade, Serbia**E-mail: mdimitrijevic@aob.rs*<sup>2</sup> *LERMA, Observatoire de Paris, Université PSL,  
CNRS, Sorbonne Université, F-92190 Meudon, France*<sup>3</sup> *Department of Applied Physics, Technical University of Sofia, 1000 Sofia, Bulgaria*

**Abstract.** The results of semiclassical perturbation calculations of Stark widths and shifts, for N VI spectral lines broadened by collisions with electrons, protons, alpha particles (He III) and B III, B IV, B V and B VI ions, are presented and discussed.

## 1. INTRODUCTION

Data for Stark broadening of spectral lines are useful for a number of topics in astronomy as e.g. for stellar spectroscopy, radiative transfer calculations, abundance determination, stellar atmosphere modelling etc.

Spectral lines of N VI are observed in stellar plasma (see e.g. Fleig et al. (2008), Newman et al. (2021), Ness et al. (2023)), so that the corresponding Stark broadening data are useful for their investigation and interpretation, particularly in the case of hot and dense stars such as e.g. white dwarfs.

Another topic where N VI Stark broadening data are of interest is the proton-boron fusion (Batani, 2023), which is aneutronic and without radioactive species. In some of such experiments, boron nitride target is used (Schollmeier, 2022). Since plasma diagnostic is needed here to optimize the fusion yield (Hegelich et al., 2023), Stark broadening data for N VI are needed for such purpose. Also, data on broadening by collisions with B IV, B V and B VI ions are useful since their presence has been confirmed (Kong et al., 2022).

Recently, we have calculated Stark line widths and shifts, for 15 multiplets of N VI, which spectral lines are broadened by collisions with electrons, protons, alpha particles (He III) and B III, B IV, B V and B VI ions. They have been calculated by employing the semiclassical perturbation method (Sahal-Bréchet, 1969ab, Sahal-Bréchet et al., 2014), for temperatures from 50,000 K to 2,000,000 K, and perturber densities from  $10^{16}$  cm<sup>-3</sup> up to  $10^{24}$  cm<sup>-3</sup>. Here we present a short review of obtained results.

Table 1: Stark full widths and shifts at half intensity maximum for N VI multiplets due to interactions with electrons, and protons. The perturber density is  $10^{19} \text{ cm}^{-3}$ .

TRANSITION	T(K)	ELECTRONS		PROTONS	
		WIDTH(Å)	SHIFT(Å)	WIDTH(Å)	SHIFT(Å)
SINGLETs					
N VI $1s^2$ -2p	50000.	0.142E-03	-0.300E-04	0.183E-06	-0.382E-06
28.8 Å	100000.	0.933E-04	-0.304E-05	0.546E-06	-0.907E-06
C=0.29E+19	300000.	0.543E-04	-0.640E-06	0.243E-05	-0.262E-05
	500000.	0.431E-04	-0.448E-06	0.401E-05	-0.370E-05
	1000000.	0.322E-04	-0.337E-06	0.650E-05	-0.514E-05
	2000000.	0.247E-04	-0.116E-06	0.914E-05	-0.631E-05
N VI $1s^2$ -3p	50000.	0.487E-03	-0.315E-04	0.177E-04	-0.297E-04
24.9 Å	100000.	0.361E-03	-0.154E-04	0.413E-04	-0.513E-04
C=0.16E+18	300000.	0.238E-03	-0.179E-04	0.967E-04	-0.869E-04
	500000.	0.199E-03	-0.175E-04	0.122E-03	-0.101E-03
	1000000.	0.158E-03	-0.137E-04	0.170E-03	-0.120E-03
	2000000.	0.126E-03	-0.105E-04	0.223E-03	-0.139E-03
N VI $2s$ -2p	50000.	1.89E+00	-0.823E-01	0.261E-02	-0.172E-01
2897.2 Å	100000.	1.36E+00	-0.436E-01	0.113E-01	-0.396E-01
C=0.29E+23	300000.	0.838E+00	-0.488E-01	0.635E-01	-0.948E-01
	500000.	0.681E+00	-0.480E-01	0.954E-01	-0.122E+00
	1000000.	0.525E+00	-0.452E-01	0.156E+00	-0.152E+00
	2000000.	0.414E+00	-0.382E-01	0.215E+00	-0.183E+00
N VI $2s$ -3p	50000.	0.253E-01	-0.759E-03	0.880E-03	-0.147E-02
173.3 Å	100000.	0.190E-01	-0.792E-03	0.204E-02	-0.254E-02
C=0.79E+19	300000.	0.126E-01	-0.102E-02	0.477E-02	-0.427E-02
	500000.	0.105E-01	-0.100E-02	0.600E-02	-0.497E-02
	1000000.	0.836E-02	-0.814E-03	0.840E-02	-0.589E-02
	2000000.	0.671E-02	-0.640E-03	0.110E-01	-0.678E-02
N VI $3s$ -3p	50000.	1.12E+02	-3.84E+00	*4.15E+00	*-6.29E+00
9624.6 Å	100000.	8.48E+01	-5.63E+00	*8.93E+00	*-1.06E+01
C=0.24E+23	300000.	5.72E+01	-6.45E+00	*1.89E+01	*-1.73E+01
	500000.	4.83E+01	-6.48E+00	2.37E+01	-2.00E+01
	1000000.	3.87E+01	-5.36E+00	3.33E+01	-2.40E+01
	2000000.	3.10E+01	-4.24E+00	4.19E+01	-2.59E+01
N VI $2p$ -3s	50000.	0.208E-01	0.917E-03	0.385E-03	0.984E-03
187.9 Å	100000.	0.157E-01	0.140E-02	0.118E-02	0.181E-02
C=0.37E+20	300000.	0.105E-01	0.146E-02	0.292E-02	0.312E-02
	500000.	0.890E-02	0.149E-02	0.365E-02	0.366E-02
	1000000.	0.712E-02	0.128E-02	0.495E-02	0.438E-02
	2000000.	0.569E-02	0.102E-02	0.652E-02	0.499E-02

Table 1: Cont.

TRANSITION	T(K)	ELECTRONS		PROTONS	
		WIDTH(Å)	SHIFT(Å)	WIDTH(Å)	SHIFT(Å)
TRIPLETS					
N VI 2s-2p	50000.	0.742E+00	0.979E-02	0.787E-03	-0.444E-02
1901.5 Å	100000.	0.530E+00	-0.137E-01	0.297E-02	-0.104E-01
C=0.19E+23	300000.	0.321E+00	-0.172E-01	0.171E-01	-0.270E-01
	500000.	0.259E+00	-0.164E-01	0.268E-01	-0.349E-01
	1000000.	0.198E+00	-0.155E-01	0.461E-01	-0.455E-01
	2000000.	0.155E+00	-0.140E-01	0.634E-01	-0.544E-01
N VI 2s-3p	50000.	0.199E-01	-0.569E-04	0.204E-03	0.270E-03
161.2 Å	100000.	0.147E-01	0.115E-03	0.499E-03	0.549E-03
C=0.19E+20	300000.	0.959E-02	0.132E-03	0.124E-02	0.107E-02
	500000.	0.800E-02	0.153E-03	0.160E-02	0.126E-02
	1000000.	0.634E-02	0.108E-03	0.218E-02	0.151E-02
	2000000.	0.511E-02	0.892E-04	0.303E-02	0.179E-02
N VI 2s-4p	50000.	0.335E-01	0.143E-03	*0.135E-02	*0.126E-02
122.4 Å	100000.	0.257E-01	0.397E-03	*0.233E-02	*0.209E-02
C=0.48E+19	300000.	0.176E-01	0.657E-03	*0.414E-02	*0.339E-02
	500000.	0.149E-01	0.657E-03	*0.505E-02	*0.394E-02
	1000000.	0.120E-01	0.524E-03	*0.661E-02	*0.463E-02
	2000000.	0.977E-02	0.443E-03	*0.822E-02	*0.531E-02
N VI 3s-3p	50000.	5.32E+01	0.829E+00	0.373E+00	-0.466E+00
6993.0 Å	100000.	3.99E+01	-1.20E+00	0.906E+00	-0.956E+00
C=0.36E+23	300000.	2.65E+01	-1.29E+00	2.27E+00	-1.89E+00
	500000.	2.23E+01	-1.26E+00	3.00E+00	-2.22E+00
	1000000.	1.79E+01	-1.18E+00	4.29E+00	-2.67E+00
	2000000.	1.44E+01	-0.937E+00	6.14E+00	-3.15E+00
N VI 3s-4p	50000.	0.576E+00	-0.121E-02	*0.182E-01	*0.164E-01
474.5 Å	100000.	0.441E+00	-0.555E-03	*0.316E-01	*0.275E-01
C=0.72E+20	300000.	0.303E+00	0.280E-02	*0.569E-01	*0.448E-01
	500000.	0.257E+00	0.273E-02	*0.698E-01	*0.529E-01
	1000000.	0.208E+00	0.149E-02	*0.956E-01	*0.602E-01
	2000000.	0.169E+00	0.157E-02	*0.120E+00	*0.692E-01
N VI 2p-3s	50000.	0.175E-01	0.412E-03	0.203E-03	0.654E-03
180.7 Å	100000.	0.130E-01	0.107E-02	0.703E-03	0.126E-02
C=0.47E+20	300000.	0.857E-02	0.118E-02	0.199E-02	0.224E-02
	500000.	0.721E-02	0.118E-02	0.254E-02	0.261E-02
	1000000.	0.576E-02	0.107E-02	0.333E-02	0.310E-02
	2000000.	0.462E-02	0.865E-03	0.434E-02	0.360E-02
N VI 2p-4s	50000.	0.269E-01	0.150E-02	*0.161E-02	*0.192E-02
131.9 Å	100000.	0.207E-01	0.216E-02	*0.297E-02	*0.322E-02
C=0.10E+20	300000.	0.144E-01	0.259E-02	*0.542E-02	*0.515E-02
	500000.	0.122E-01	0.255E-02	*0.658E-02	*0.606E-02
	1000000.	0.985E-02	0.206E-02	*0.842E-02	*0.692E-02
	2000000.	0.785E-02	0.169E-02	*0.110E-01	*0.780E-02

Table 1: Cont.

TRANSITION	T(K)	ELECTRONS		PROTONS	
		WIDTH(Å)	SHIFT(Å)	WIDTH(Å)	SHIFT(Å)
TRIPLETS					
N VI 3p-4s	50000.	0.575E+00	0.246E-01	*0.242E-01	*0.290E-01
524.5 Å	100000.	0.441E+00	0.319E-01	*0.446E-01	*0.487E-01
C=0.16E+21	300000.	0.303E+00	0.382E-01	*0.802E-01	*0.778E-01
	500000.	0.258E+00	0.375E-01	*0.101E+00	*0.918E-01
	1000000.	0.208E+00	0.303E-01	*0.131E+00	*0.104E+00
	2000000.	0.166E+00	0.247E-01	*0.170E+00	*0.122E+00

## 2. RESULTS AND DISCUSSION

For the calculation of Stark broadening parameters, full widths at half intensity maximum (FWHM - W) and shifts - d for 15 N VI multiplets, the semiclassical perturbation approach (Sahal–Bréchet, 1969ab, Sahal–Bréchet et al., 2014) has been used. The theoretical method and all details of calculations are described in Dimitrijević et al. (2023a). Also, the obtained results for N VI Stark widths and shifts due to collisions with electrons, protons, alpha particles (He III) and B III, B IV, B V and B VI ions, for temperatures from 50,000 K to 2,000,000 K, and a perturber density of  $10^{16}$  cm $^{-3}$ , have been presented and discussed. The obtained results have been used to investigate and demonstrate the influence and significance of Stark broadening of N VI spectral lines in atmospheres of white dwarfs. In Dimitrijević et al. (2023b), the behavior of N VI Stark widths and shifts within a spectral series has been investigated and the influence of collisions with different charged particles (e, p, He III, B III, B IV, B V and B VI) on N VI linewidths and shifts due to different perturbers have been compared and discussed in detail. In Dimitrijević et al. (2023b), all above mentioned data for perturber densities from  $10^{16}$  cm $^{-3}$  up to  $10^{24}$  cm $^{-3}$  have been presented as an online data set in computer readable form.

As an example of obtained results, in Table 1 are presented Stark full widths at half intensity maximum and shifts for 15 N VI multiplets due to interactions with electrons, and protons, for a perturber density of  $10^{19}$  cm $^{-3}$  and temperatures from 50,000 K to 2,000,000 K. In the Table is given and the quantity C (Dimitrijević and Sahal–Bréchet, 1984). When it is divided by the corresponding FWHM, one obtains the maximal perturber density for the validity of the isolated line approximation. We checked for all values presented in the Table the validity of impact approximation calculating the value of  $NV$ , where V is the collision volume and N the perturber density. If  $NV < 0.1$ , the impact approximation is valid. We excluded the cases when  $NV > 0.5$  from the tables, while for  $0.1 < NV \leq 0.5$ , we put an asterisk before the corresponding Stark broadening parameter in order to draw attention that this value is on the limit of validity of impact approximation. In Table 2, the same data as in Table 1, but for B V and B VI ions as perturbers are presented,

The obtained results for N VI Stark broadening parameters, obtained in this investigation, will also enter in STARK-B database (<http://stark-b.obspm.fr/> - Sahal–Bréchet et al., 2015ab), a part of european Virtual Atomic and Molecular Data Center VAMDC (<http://www.vamdc.org/> - Dubernet et al., 2010, 2016, Albert et al., 2020).

Table 2: Stark full widths at half intensity maximum and shifts of N VI multiplets due to interactions with B V and B VI ions. The perturber density is  $10^{19} \text{ cm}^{-3}$ .

TRANSITION	T(K)	B V		B VI	
		WIDTH(Å)	SHIFT(Å)	WIDTH(Å)	SHIFT(Å)
SINGLETs					
N VI $1s^2-2p$	50000.	0.332E-06	-0.644E-06	0.254E-06	-0.547E-06
28.8 Å	100000.	0.135E-05	-0.270E-05	0.131E-05	-0.302E-05
C=0.29E+19	300000.	0.765E-05	-0.103E-04	0.827E-05	-0.128E-04
	500000.	0.137E-04	-0.155E-04	0.155E-04	-0.197E-04
	1000000.	0.230E-04	-0.224E-04	0.278E-04	-0.293E-04
	2000000.	0.324E-04	-0.284E-04	0.419E-04	-0.382E-04
N VI $2s-2p$	50000.	0.524E-02	-0.290E-01	0.434E-02	-0.247E-01
2897.2 Å	100000.	0.313E-01	-0.119E+00	0.320E-01	-0.134E+00
C=0.29E+23	300000.	0.230E+00	-0.381E+00	0.266E+00	-0.483E+00
	500000.	0.371E+00	-0.512E+00	0.464E+00	-0.658E+00
	1000000.	0.640E+00	-0.683E+00	0.828E+00	-0.912E+00
	2000000.	0.842E+00	-0.833E+00	1.10E+00	-1.11E+00
TRIPLETs					
N VI $2s-2p$	50000.	0.150E-02	-0.748E-02	0.119E-02	-0.636E-02
1901.5 Å	100000.	0.777E-02	-0.311E-01	0.774E-02	-0.348E-01
C=0.19E+23	300000.	0.574E-01	-0.106E+00	0.672E-01	-0.133E+00
	500000.	0.107E+00	-0.146E+00	0.134E+00	-0.191E+00
	1000000.	0.185E+00	-0.206E+00	0.232E+00	-0.273E+00
	2000000.	0.251E+00	-0.250E+00	0.328E+00	-0.333E+00
N VI $2s-3p$	50000.	*0.423E-03	*0.449E-03		
161.2 Å	100000.	*0.156E-02	*0.165E-02		
C=0.19E+20	300000.	*0.450E-02	*0.422E-02		
	500000.	*0.619E-02	*0.535E-02		
	1000000.	*0.781E-02	*0.672E-02	*0.101E-01	*0.893E-02
	2000000.	*0.923E-02	*0.816E-02	*0.127E-01	*0.110E-01
N VI $3s-3p$	50000.	*0.763E+00	*-0.778E+00	*0.628E+00	*-0.659E+00
6993.0 Å	100000.	*2.81E+00	*-2.88E+00	*3.05E+00	*-3.28E+00
C=0.36E+23	300000.	*8.01E+00	*-7.39E+00	*9.85E+00	*-9.45E+00
	500000.	*1.11E+01	*-9.50E+00	*1.41E+01	*-1.26E+01
	1000000.	*1.40E+01	*-1.20E+01	*1.80E+01	*-1.58E+01
	2000000.	*1.71E+01	*-1.43E+01	*2.23E+01	*-1.95E+01

The obtained results are of interest for astrophysical applications as for example for abundance determination, analysis and synthesis of stellar spectra, stellar atmosphere modelling, radiative transfer calculations..., particularly for white dwarfs. They are also useful for proton-boron fusion research, since the boron nitride BN, as a target for laser radiation, is important in such experiments, and N VI spectral lines may be used for diagnostic and modelling of created plasma.

### Acknowledgements

This article/publication is based upon work from COST Action CA21128- PROBONO PROton BORon Nuclear fusion: from energy production to medical applicatiOns, supported by COST (European Cooperation in Science and Technology - [www.cost.eu](http://www.cost.eu)). Thanks also to Technical University of Sofia for the provided help.

Sylvie Sahal-Béchet acknowledges the French Research Laboratory LERMA (Paris Observatory and the CNRS UMR 8112) and the Programme National de Physique Stellaire (PNPS) of CNRS/INSU, CEA and CNES, France for their support.

### References

- Albert, D., Antony, B. K., Ba, Y. A., Babikov, Y. L., Bollard, P., Boudon, V., Delahaye, F., Del Zanna, G., et al.: 2020, *Atoms*, **8**, 76, doi:10.3390/atoms8040076
- Batani, K.: 2023, *J. Instrum.*, **18**, C09012, doi:10.1088/1748-0221/18/09/C09012
- Dimitrijević, M. S., Christova, M. D., Sahal-Bréchet, S.: 2023a, *Universe*, **9**, 511, doi:10.3390/universe9120511
- Dimitrijević, M. S., Christova, M. D., Sahal-Bréchet, S.: 2023b, *Contrib. Astron. Obs. Skalnat Pleso*, **53(3)**, 84, doi:10.31577/caosp.2023.53.3.84
- Dimitrijević, M. S., Christova, M. D., Sahal-Bréchet, S.: 2024, *Data*, **9**, 77, doi:10.3390/data9060077 -
- Dimitrijević, M. S., Sahal-Bréchet, S.: 1984, *J. Quant. Spectrosc. Radiat. Transf.*, **31**, 301, doi:10.1016/0022-4073(84)90092-X
- Dubernet, M. L., Antony, B. K., Ba, Y. A., Babikov, Y. L., Bartschat, K., Boudon, V., Braams, B. J., Chung, H. K., Daniel, F., Delahaye, F., et al.: 2016, *J. Phys. B*, **49**, 074003, doi:10.1088/0953-4075/49/7/074003
- Dubernet, M., Boudon, L. V., Culhane, J. L., Dimitrijević, M. S., et al.: 2010, *J. Quant. Spectrosc. Radiat. Transfer*, **111**, 2151, doi:10.1016/j.jqsrt.2010.05.004
- Fleig, J., Rauch, T., Werner, K., Kruk, J. W.: 2008, *Astron. Astrophys.*, **492**, 565, doi:10.1051/0004-6361/200810738
- Heglich, B. M., Labun, L. O., Labun, Z., Mehlhorn, T. A.: 2023, *Laser Part. Beams*, **2023**, e7, doi:10.1155/2023/6924841
- Kong, D., Xu, S., Shou, Y., Gao, Y., Mei, Z., Pan, Z., Liu, Z., Cao, Z., Liang, Y., Peng, Z., et al.: 2022, *Laser Part. Beams*, **2022**, e7, doi:10.1155/2022/5733475
- Ness, J.-U., Beardmore, A. P., Bode, M. F., Darnley, M. J., Dobrotka, A., Drake, J. J., Magdolen, J., Munari, U., Osborne, J. P., Orio, M., Page, K. L., Starrfield, S.: 2023, *Astron. Astrophys.*, **670**, A131, doi:10.1051/0004-6361/202245269
- Newman, J., Tsuruta, S., Liebmann, A. C., Kunieda, H., Haba, Y.: 2021, *Astrophys. J.*, **907**, 45, doi:10.3847/1538-4357/abd1da
- Sahal-Bréchet, S.: 1969a, *Astron. Astrophys.*, **1**, 91.
- Sahal-Bréchet, S.: 1969b, *Astron. Astrophys.*, **2**, 322.
- Sahal-Bréchet, S.; Dimitrijević, M. S., Ben Nessib, N.: 2014, *Atoms*, **2**, 225, doi:10.3390/atoms2020225
- Sahal-Bréchet, S., Dimitrijević, M. S., Moreau, N., Ben Nessib, N.: 2015, *Phys. Scr.*, **90**, 054008, doi:10.1088/0031-8949/90/5/054008
- Sahal-Bréchet, S., Dimitrijević, M. S., Moreau, N.: 2024, STARK-B Database, Available online: <http://stark-B.obspm.fr> (accessed on 30 October 2024).
- Schollmeier, M. S., Shirvanyan, V., Capper, C., et al.: 2022, *Laser Part. Beams*, **2022**, e4, doi:10.1155/2022/2404263

## COLUMN DENSITY DISTRIBUTIONS FROM DECOMPOSED MAPS OF STAR-FORMING REGIONS

L. MARINKOVA<sup>1</sup>, T. V. VELTCHEV<sup>2</sup> , S. DONKOV<sup>3</sup>

<sup>1</sup> *Department of Applied Physics, Faculty of Applied Mathematics, Technical University-Sofia, 8 Kliment Ohridski Blvd., Sofia 1000, Bulgaria*

*E-mail: ln@phys.uni-sofia.bg*

<sup>2</sup> *University of Sofia, Faculty of Physics, 5 James Bourchier Blvd., 1164 Sofia, Bulgaria*

<sup>3</sup> *Institute of Astronomy and NAO, Bulgarian Academy of Sciences, 72 Tsarigradsko Chausee Blvd., 1784 Sofia, Bulgaria*

**Abstract.** Probability distribution functions of mass- ( $\rho$ -PDF) and column density ( $N$ -PDF) in star-forming regions often display one or multiple power-law tails (PLT) in the high-density range. The correct PLT extraction is of key significance for understanding morphological and dynamical structure of star-forming regions since the PDF properties can be directly linked to the role of different factors in the star formation process: gravity, turbulence, magnetic fields, etc. Many observations indicate that the PLT regime in the  $N$ -PDF corresponds to highly fragmented, filamentary regions in a star-forming cloud - thus, it is interesting to compare  $N$ -PDFs of small-scale structures extracted in those areas with the  $N$ -PDF of the whole cloud. We present analyses of the  $N$ -PDFs in Galactic regions of various star-forming activity obtained from Herschel data, by use of a novel method (Li 2022) for decomposition of a map into multiple components containing structures of different sizes.

### 1. INTRODUCTION

Molecular clouds and/or their fragments associated with some star formation activity are usually labeled star-forming regions (SFRs). They exhibit highly complex structure: clumps of various density, hub-filament systems hosting pre-/protostellar cores (Kumar et al. 2020, Zhou et al. 2022), H II regions around newborn massive stars and dust lanes. Contraction and collapse in SFRs on multiple physical scales and take place in the context of interplay of gravity, turbulence and magnetic fields (Chevance et al. 2020) as gravity governs the formation and growth of dense gas structures.

An increasingly popular tool to assess the physical conditions and processes in SFRs is the analysis of the probability distribution functions of mass- ( $\rho$ -PDF) and column density ( $N$ -PDF). Isothermal, non-gravitating medium dominated by supersonic turbulence is characterized by a lognormal  $\rho$ -PDF (i.e. normal distribution of logdensity; e.g., Federrath, Klessen & Schmidt 2008) while the development of high-density power-law tail (PLT) of the distribution is typically due to the increasing role of self-gravity in contracting clouds (Kritsuk, Norman & Wagner 2011, Federrath & Klessen 2012, 2013). At later evolutionary times, at the stage of local collapses, the PLT slope becomes shallower and tends toward a constant value as substantiated theoretically (Girichidis et al. 2014) and confirmed by numerical simulations (e.g.,

Veltchev et al. 2019).  $N$ -PDFs obtained from high-resolution observations of SFRs display similar shapes like the  $\rho$ -PDFs. The main part is (quasi-)lognormal or a combination of two lognormals while a single (Kainulainen et al. 2009) or even double PLT (Schneider et al. 2015, 2022) appear at the high-density end.

In view of the multi-scale nature of the star-forming process and of the cloud evolution in general, it is critically important to quantify the contribution of different spatial scales to the PDF shape. In analytical or numerical analysis of the  $\rho$ -PDF, this can be done, for instance, attributing effective sizes by some density cutoff (see Donkov, Veltchev & Klessen 2012). However, the  $N$ -PDF of an observed SFRs is a result of various projection effects of complex structures and straightforward approaches are not applicable. A method to decompose  $N$ -PDFs to contributions of different abstract spatial scales in the cloud have been suggested by Stanchev et al. (2015); it starts by extracting the PLT and then fitting the main part of the distribution by combination of lognormals. Their approach is based on specific assumptions about cloud physics: the PLT range is attributed to gravoturbulent regime while the main PDF part is attributed to predominantly turbulent regime.

In this report we present some preliminary results from another, essentially different approach of decomposition of  $N$ -PDFs in several Galactic SFRs of various activity. It makes use of a method for multiscale decomposition of astronomical maps recently suggested by G.-X. Li (2022) which allows to disentangle the physical scales accounting for the observed PLTs.

## 2. DECOMPOSITION OF MAPS AND N-PDFs

Typical maps of SFRs obtained from high-resolution observations reveal a bunch of structures with different characteristic sizes. Robust decomposition of such maps into components of multiple scales enables new approaches to data analysis – for example, study of the relative importance of filaments and cores.

The method of G.-X. Li (2022) produces a set of smoothed images  $I_k(x, y)$  from an input map  $I_0(x, y)$  through a modified version of wavelet transformation. (For more information, we refer the reader to the original paper and the references therein.) The wavelet kernel defines the spatial scale in pixels  $l = 2^k$ , where  $k = 1, 2, \dots, k_{\max}$  and  $2^{k_{\max}}$  is the larger side of the input rectangular map. As the scale increases with  $k$ , the intensity  $I_k(x, y)$  decreases monotonically with  $k$ . Now one can construct decomposed maps  $C_k = I_{k-1} - I_k$  which contain structures with size between  $2^{k-1}$  and  $2^k$  pixels. Correspondingly, the input map can be recovered through summation over the decomposed ones:

$$I_0(x, y) = \sum_k C_k(x, y) + I_{k_{\max}}(x, y) \quad , \quad (1)$$

where the residual  $I_{k_{\max}}(x, y)$  is significant only in regions of very low intensities (column densities).

This technique can be used to assess the contribution of structures with some typical size to a studied part of the  $N$ -PDF. Let us consider a pixel from the input map. Its column density is equal to the sum of column densities from the decomposed maps (eq. 1). The total number of all pixels from the input map  $I_0(x, y)$  with column densities  $\log N \leq \log N' < \log N + \Delta \log N$  yields the value of the  $N$ -PDF  $P(\log N)$



in the considered bin. Accordingly, the relative contribution  $f_k$  of structures with sizes between  $2^{k-1}$  and  $2^k$  pixels to  $P(\log N)$  is obtained through summation over all pixels from  $C_k$  corresponding to the pixels with  $\log N'$  from  $I_0(x, y)$ :

$$f_k(\log N) = \frac{\sum_{N' \in [\log N, \log N + \Delta \log N]} C_k(x, y)}{\sum_{N' \in [\log N, \log N + \Delta \log N]} I_0(x, y)} . \quad (2)$$

### 3. DATA USED

We extract and analyze high-density  $N$ -PDFs from *Herschel* maps constructed from convolved SPIRE maps (at 500, 350 and 250  $\mu\text{m}$ ) of 8 SFRs initially studied by Schneider et al. (2022). The high angular resolution ( $18''$ ) allows for resolve the high-density part of the  $N$ -PDF which is accounted for mostly by clumps and cores on parsec and subparsec scales. The emission of the dust has been converted to  $A_V$  assuming a power-law for dust opacity in the far infrared and a gas-to-dust ratio of 100 (for details, see Veltchev et al. 2018, Sect. 2.2.) The PLTs are defined through:

$$P_{\text{PLT}}(\log N) = C(N/N_0)^n , \quad (3)$$

where  $N_0$  is some normalizing value (typically, the mean column density in the SFR) and  $C$  is a constant. The slopes  $n < 0$  were extracted by the technique adapted BPLFIT (Veltchev et al. 2019, 2024) which provides the best fit of the presumed power-law part of the distribution without any presuppositions about its main part.

Table 1: Studied star-forming regions: some characteristics. Column 4 gives the lowest resolved scale (LRS)

SFR	Distance [kpc]	Eff. size ( $A_V > 1$ ) [pc]	LRS [pc]	PLT slopes (from BPLFIT)
<b>High-mass</b>				
M16	2.00	18.3	0.18	$n = -2.54$
M17	2.20	28.1	0.18	$n_1 = -2.87, n_2 = -1.97$
<b>Intermediate-mass</b>				
Mon R2	0.86	5.1	0.10	$n_1 = -1.66, n_2 = -1.42$
Mon OB1	0.80	4.3	0.10	$n_1 = -1.89, n_2 = -3.62$
<b>Low-mass</b>				
Lupus III	0.16	1.3	0.02	$n = -2.21$
Lupus VI	0.20	1.5	0.02	$n_1 = -2.63, n_2 = -3.38$
<b>Quiescent</b>				
Musca	0.15	1.0	0.02	$n_1 = -2.17, n_2 = -5.75$
Polaris	0.49	1.9	0.06	$n = -4.32$

We studied SRFs with different activity and size (Table 1). The low-mass ones are clouds with masses  $10^3 - 10^4 M_\odot$  that typically give birth to low-mass stars while the high-mass regions are giant molecular clouds ( $10^5 - 10^6 M_\odot$ ) and observational signatures of high-mass star formation; they often contain gravitationally unstable

filamentary structures of high column density. In between these categories are SFRs with masses  $10^4 - 10^5 M_\odot$  where mainly low- and intermediate-mass stars emerge. Quiescent clouds are those with no or very little SF activity (up to a few protostars or prestellar cores) containing mostly atomic gas.

#### 4. RESULTS

Figure 1 (top) displays the  $N$ -PDFs of the selected high- and intermediate-mass SFRs together with the column-density distributions from the decomposed maps  $C_k$ . The dynamic range of  $N$  (proportional to  $A_V$ ) is large but the extracted PLTs correspond, in general, to  $A_V \gtrsim 10$  (see the deviation points in dashed). Most of the  $N$ -PDFs from the decomposed maps have PLTs as well; typically of similar slope (plotted with solid black line). Comparison with the functions  $f_k(A_V)$  reveals that a few dominating scales (DS) contribute to the PLT from the input map. This is evident in case of a single PLT (M16) or for the *second* PLT when a double PLT is detected (M17, Mon R2, Mon OB1). In the latter case, the first PLT is a result of various scales and probably cannot be associated with self-gravitating gas in dense compact clumps.

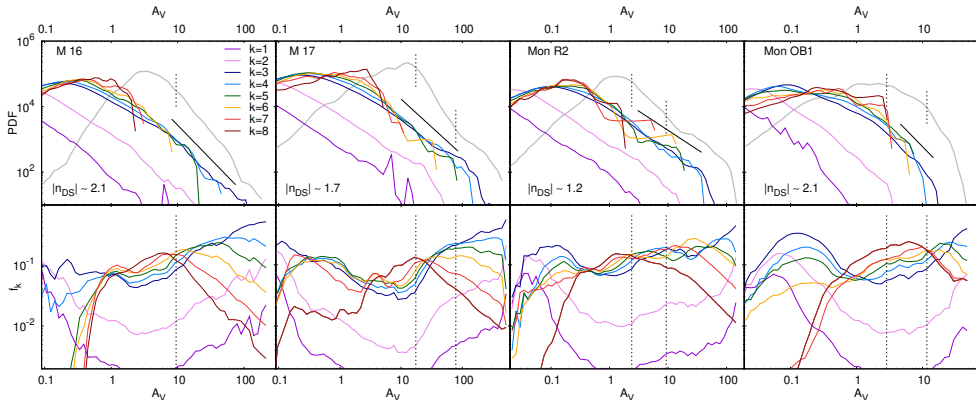


Figure 1: Decomposition of  $N$ -PDFs in the studied high- and intermediate-mass SFRs (See Table 1). The  $N$ -PDFs from the input map (thick grey line) and from  $C_k$  (color lines) are plotted in the top panel. The bottom panel displays the contributions  $f_k$  of structures with different size (eq. 2). The deviation points of the detected PLTs are shown (vertical dashed). The typical slope of the PLTs from the dominating scales ( $n_{DS}$ ) is given and drawn (black solid line in the top panels).

The picture in low-mass and quiescent SFRs seems to be more complicated (Fig. 2).  $N$ -PDFs from  $C_k$  do not have smooth PLTs. Various scales contribute to the single (Lupus III, Polaris) or the first PLT from the input map (Lupus VI, Musca). There are no clear dominating scales for the second PLT as well. In view of its high slope, one can argue that it is not real but can be rather interpreted as a resolution cutoff in zones of high extinction or other incompleteness effects.

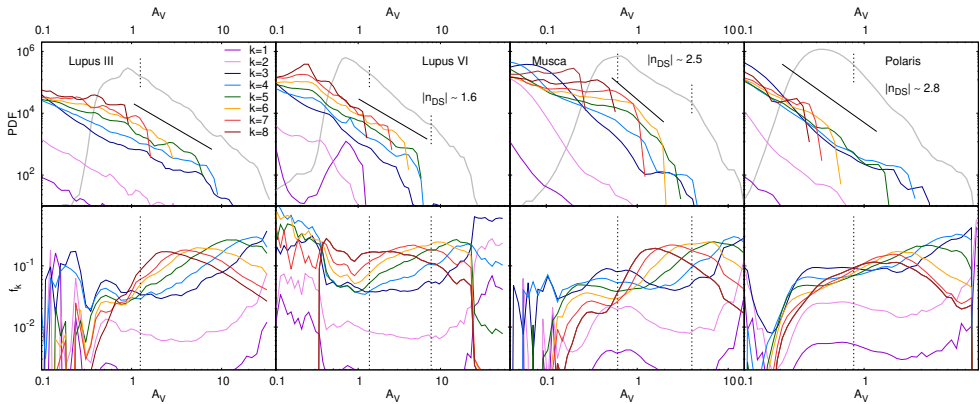


Figure 2: The same like Fig. 1 but for low-mass and quiescent SFRs.

## 5. SUMMARY

The novel method of map decomposition (G.-X. Li 2022) allows for distinguishing the contribution of different spacial scales to the morphology of  $N$ -PDF in observed Galactic star-forming regions (SFRs). Preliminary analysis from a sample of *Herschel* maps of SFRs (Table 1) shows that:

- In high- and intermediate-mass SFRs the detected single PLTs result from contribution of a few dominating scales corresponding to structures with sizes  $0.1 - 0.5$  pc. The same is true about the regime of a second detected PLT, while the first PLT results from contributions of wide range of scales and may be is not associated with self-gravitating structures.
- The typical slopes of PLTs  $1.2 \leq |n| \leq 2.1$  from the maps  $C_k$  corresponding to the dominating scales ( $k = 3 - 5$ ) are in general agreement with the theoretical expectations from density profiles of envelopes of collapsing protostellar cores (Larson 1969, Penston 1969, Donkov, Veltchev & Klessen 2017).
- Multiple scales of various size contribute to the detected PLTs in the studied low-mass and quiescent nearby SFRs. This hinders any clear physical interpretation.

Applying the method for map decomposition to G-Virial maps of SFRs by use of CO emission data (see the contribution of Mihaylov et al. in this volume) would allow to assess the gravitational boundedness of the structures at different scales and thus shed light at the physical picture behind the PLT phenomenon.

## Acknowledgements

We acknowledge support by the Deutsche Forschungsgemeinschaft (DFG) under grant number KL 1358/20-3 and additional funding from the Ministry of Education and Science of the Republic of Bulgaria, National RI Roadmap Project DO1-326/4.12.2023.

## References

- Chevance, M., Kruijssen, J. M. D., Vazquez-Semadeni, E., Nakamura, F. et al. (2020). *Space Science Reviews*, **216**, Issue 4, article id. 50, doi: 10.1007/s11214-020-00674-x
- Donkov, S., Veltchev, T. V., Klessen, R. S. (2017). *Monthly Notices of the Royal Astronomical Society*, **466**, 914., doi: 10.1093/mnras/stw3147
- Federrath, C., Klessen, R. S. (2012). *Astrophysical Journal*, **761**, L156, doi: 10.1088/0004-637X/761/2/156
- Federrath, C., Klessen, R. S. (2013). *Astrophysical Journal*, **763**, L51, doi: 10.1088/0004-637X/763/1/51
- Federrath, C., Klessen, R. S., Schmidt, W. (2008). *Astrophysical Journal*, **688**, L79, doi: 10.1086/595280
- Girichidis, P., Konstandin, L., Whitworth, A. P., Klessen, R. S. (2014). *Astrophysical Journal*, **781**, L91, doi: 10.1088/0004-637X/781/2/91
- Kainulainen, J., Beuther, H., Henning, T., Plume, R. (2009). *Astronomy & Astrophysics*, **508**, 35, doi: 10.1051/0004-6361/200913605
- Kritsuk, A., Norman, M., Wagner, R. (2011). *Astrophysical Journal*, **727**, L20, doi: 10.1088/2041-8205/727/1/L20
- Kumar, M., Palmeirim, P., Arzoumanian, D., Inutsuka, S. I. (2020). *Astronomy & Astrophysics*, **642**, 87, doi: 10.1051/0004-6361/202038232
- Larson, R. (1969). *Monthly Notices of the Royal Astronomical Society*, **145**, 271, doi: 10.1093/mnras/145.3.271
- Li, G.-X., (2022). *Astrophysical Journal Supplement Series*, **259**, 59, doi: 10.3847/1538-4365/ac4bc4
- Mihaylov, H., Stanchev, O., Veltchev, T. V. (2025). *Publ. Astron. Obs. Belgrade*, **107**, 75, doi: 10.69646/14sbac11p
- Penston, M. V. (1969). *Monthly Notices of the Royal Astronomical Society*, **144**, 425., doi: 10.1093/mnras/144.4.425
- Schneider, N., Bontemps, S., Girichidis, P., Rayner, T., Motte, F. et al. (2015). *Monthly Notices of the Royal Astronomical Society*, **453**, 41, doi: 10.1093/mnrasl/slv101
- Schneider, N., Ossenkopf-Okada, V., Clarke, S., Klessen, R. S., Kabanovic, S., Veltchev, T. et al. (2022). *Astronomy & Astrophysics*, **666**, 165, doi: 10.1051/0004-6361/202039610
- Stanchev, O., Veltchev, T. V., Kauffmann, J., Donkov, S., et al. (2015). *Monthly Notices of the Royal Astronomical Society*, **451**, 5575, doi: 10.1093/mnras/stv998
- Veltchev, T., Girichidis, P., Donkov, S., Schneider, N. et al. (2019). *Monthly Notices of the Royal Astronomical Society*, **489**, 788, doi: 10.1093/mnras/stz2151
- Veltchev, T., Girichidis, P., Marinkova, M., Donkov S. et al. (2024). *Monthly Notices of the Royal Astronomical Society*, **528**, 432., doi: 10.1093/mnras/stae031
- Veltchev, T., Ossenkopf-Okada, V., Stanchev, O., Schneider, N., et al. (2018). *Monthly Notices of the Royal Astronomical Society*, **475**, 2215, doi: 10.1093/mnras/stx3267
- Zhou, J.-W., Liu, T., Evans, N. J. et al. (2022). *Monthly Notices of the Royal Astronomical Society*, **514**, 603, doi: 10.1093/mnras/stac1735

## GRAVITY-BASED STRUCTURAL ANALYSIS OF THE MOLECULAR CLOUDS PERSEUS AND ORION A

H. MIHAYLOV<sup>1</sup> , O. STANCHEV<sup>1</sup>  and T. V. VELTCHEV<sup>1</sup> 

<sup>1</sup>*University of Sofia, Faculty of Physics, 5 James Bourchier Blvd., 1164 Sofia, Bulgaria*  
*E-mail: mihaylov@phys.uni-sofia.bg*

**Abstract.** This paper presents an analysis of the structural characteristics of the giant molecular clouds Perseus and Orion A using the gravity-based method G-virial applied to <sup>13</sup>CO(1-0) data cubes. The method utilizes a physical quantity called gravitational boundedness and through it defines gravitationally coherent regions. To define the gravitationally coherent regions we used the Dendrogram method. The results from our analysis reveal four things: the studied gravitationally coherent regions follow Larson-type relations, the gravitational boundedness rises towards the centers of these structures, cluster-forming regions generally have higher values of gravitational boundedness, and Orion A is characterized with higher values of gravitational boundedness than Perseus.

### 1. INTRODUCTION

Molecular clouds (MCs) represent the densest components of the interstellar medium where star formation takes place. Observations and simulations reveal that MCs exhibit highly complex, filamentary structures driven by the interplay of gravity, turbulence, and magnetic fields (Schneider & Elmegreen 1979; Menshchikov et al. 2010). Gravity plays an important role in MC evolution on multiple physical scales (Heyer et al. 2009; Kauffmann et al. 2013) and is particularly significant, as it governs the formation and growth of dense gas structures. However, quantifying its influence is not straight forward, as is also the case for the rest of the factors that contribute to the dynamics and kinematics of MCs. Observational data alone isn't enough to provide a clear picture of the role of gravity. Observational constraints, projection effects, and theoretical obstacles call for the development of better methods for analysis of the data (Beaumont et al. 2013).

In this paper we use the G-Virial method (Guang-Xing Li et al., 2015) to analyze the structures of two prominent MCs: Perseus and Orion A. Our goal is to reproduce the results of Guang-Xing Li et al. (2015) for some of the regions in Perseus and apply the method to a set of entirely new regions for which the method has not been tested. We aim to quantify the gravitational boundedness of said regions and to establish whether these gravitationally coherent structures follow Larson's relations.

The structure of the paper is as follows: Section 2 details the G-Virial method, Section 3 describes the data we have used, Section 4 discusses the results, and Section 5 provides a summary.

## 2. THE METHOD G-VIRIAL

Up until now the analysis of gravity in MCs has been done via the virial parameter ( $\alpha_{vir}$ ) as defined by Bertoldi & McKee (1992). It is derived from the Virial Theorem and is a measure of the balance between gravitational potential energy and kinetic energy for a given region. The most common form of the equation is:

$$\alpha_{vir} = \frac{Gm}{5\sigma_v^2 r}$$

where  $G$  gravitational constant;  $m$  mass of the system of particles;  $\sigma_v$  the velocity dispersion;  $r$  size of the system.

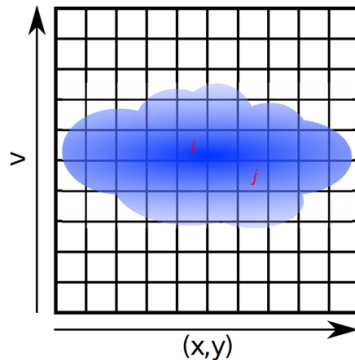


Figure 1:  $(x,y)$  represents the spatial dimensions and  $v$  represents the velocity dimension. The mass distribution is represented in blue. For each voxel  $i$  its total gravitational boundedness can be determined by adding up the gravitational boundedness to all the voxels  $j$  (not excluding  $i$ ). Source: Guang-Xing Li et al. (2015)

There are two main issues with this approach: (1) the virial parameter is defined locally, so it provides no information on the effect the surrounding medium has on the region; (2) it requires geometric assumptions about the size and shape of the region which then inform how we determine its mass and velocity dispersion.

The G-Virial method provides an approach to overcome these and other challenges by calculating the gravitational boundedness between voxels in a 3D Position-Position-Velocity (PPV) data cube (Figure 1), resulting in a 3D map of the gravitational boundedness which allows one to define gravitationally coherent regions (GCRs). In essence, it aims to redefine what a region is, based on the gravitational interaction.

The gravitational boundedness of voxel  $i$  with respect to voxel  $j$  is defined as:

$$I_{j \rightarrow i} = \frac{Gm_j}{\delta r_{ij} \delta v_{ij}^2}$$

where  $G$  gravitational constant;  $m_j$  mass of the  $j$ -th voxel in the PPV space;  $\delta v_{ij}$  the velocity difference between voxels  $i$  and  $j$ ;  $\delta r_{ij}$  distance between voxels  $i$  and  $j$ .

The G-Virial parameter is the total gravitational boundedness. For a discrete density distribution it is defined as:

$$\alpha_{G-virial}^i = \sum_j I_{j \rightarrow i} = G \sum_j \frac{m_j}{\sqrt{(x_i - x_j)^2 + (y_i - y_j)^2 + (v_i - v_j)^2 + c_0^2}}.$$

This sets up the G-Virial parameter as a generalized version of the the virial parameter.

The method has three main aims: (1) to provide a new way of selecting regions within MCs; (2) to provide a quantitative analysis of the global gravitational boundedness of MCs within a PPV space without assuming any geometry; (3) to provide a quantitative analysis of the properties of GCRs within MCs.

For more information we refer the reader to the original paper (Guang-Xing Li et al., 2015).

### 3. DATA USED

For this study, we utilized  $^{13}\text{CO}$  maps from the COMPLETE survey (Ridge et al., 2006) and Bell Laboratories (Bally et al., 1987) for two MCs: Perseus and Orion A. These regions were selected due to their well-studied properties. Additionally, Perseus was selected due to it being one of the original MCs that Guang-Xing Li et al. (2015) applied the method to. Table 1 provides key physical information for the MCs and technical details of the observational data.

Table 1: Basic Parameters and Observational Data for Perseus and Orion A

	<b>Perseus</b>	<b>Orion A</b>
Data source	COMPLETE Survey	Bell Laboratories
Instrument	FCRAO Radio Telescope (14 m)	7m Telescope
Beam FWHM	46 arcsec	60 arcsec
Spectral Resolution	0.067 km/s	0.27 km/s
Studied subregions	B1, B3, NGC 1333, IC348, etc.	M42, L1640, NGC 1918, etc.
Distance	250 pc	400 pc
Mass	$10^4 M_{\odot}$	$10^5 M_{\odot}$

### 4. RESULTS AND DISCUSSION

To identify GCRs, the Dendrogram method (Rosolowsky et al. 2008) was applied. This algorithm is well-suited for a hierarchical contour-based region segmentation. It enables us to isolate gravitationally coherent clumps in the G-Virial map. Figure 2 shows a panel of the  $^{13}\text{CO}$  maps with the dendrogram-derived regions highlighted.

#### 4.1. G-VIRIAL

The first result is shown in Figure 3 (left). The graph reveals the amount of mass enclosed within a contour of a given threshold of gravitational boundedness. A clear

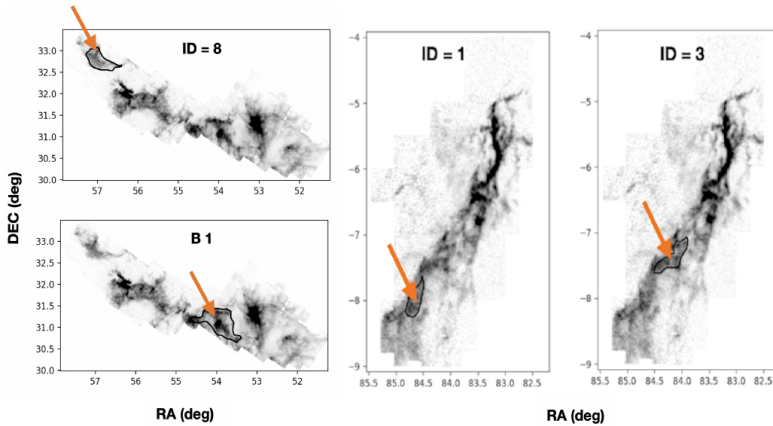


Figure 2: GCRs in the MCs Perseus (left) and Orion A (right), obtained by applying the dendrogram method to the maps of gravitational boundedness. The 2D projections of these regions are outlined with contours on the integrated  $^{13}\text{CO}(1-0)$  map. Arrows indicate the contour boundaries of the dendrogram objects.

trend emerges: for smaller values of gravitational boundedness, the contours enclose increasingly larger amounts of mass. This result is entirely expected, as greater mass should naturally imply a more pronounced role of kinetic energy that resists gravity and upholds the structure. In other words, Larson’s relations begin to appear here, even if not explicitly demonstrated. We also find that Orion A is characterized with higher values of boundedness than Perseus due to its cluster forming subregions.

The next result (Figure 3, right) concerns the profiles of gravitational boundedness. The G-Virial parameters radial gradient reflects increasing gravitational significance toward the centers of GCRs. Once again, the results are as expected gravitational boundedness decreases with increasing size. This is again an indication of adherence to Larson’s relations. Here there are a few interesting lines of thought that would be valuable to explore in future studies. For different curves, it seems possible for one to define asymptotes, which can be interpreted as the maximum size of the gravitationally coherent region. Some curves show a distinct plateau, indicating a regime of constant gravitational boundedness, followed by the beginning of a decline. The start of this decline might be interpreted as a cut-off radius - the point where the surrounding medium begins to have a significant effect. Naturally, these are speculations and will require further verification.

#### 4. 2. LARSON-TYPE RELATIONS

A crucial aspect of MC structure analysis lies in investigating mass-radius and velocity dispersion-radius scaling - Larson’s empirical relations. In Figure 4 we explicitly verify whether the identified regions adhere to these relations. We have plotted Larsons relations as formulated by Larson himself and by Kauffmann, who suggested an adjustment to the power-law index for more massive objects.

It is clear that the identified regions follow Larsons relations, as expected from general physical considerations. The differences result from the differing methods



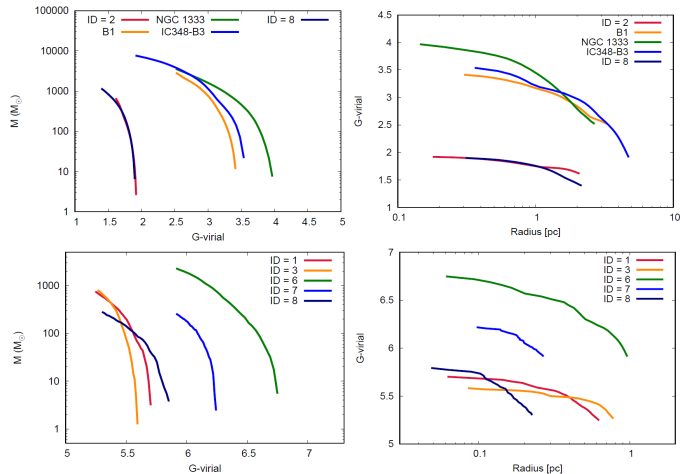


Figure 3: Amount of mass enclosed within a contour with the corresponding threshold value of the gravitational boundedness (left) and profile of the gravitational boundedness (right) in Perseus (top panel) and Orion A (bottom panel).

used to define the regions. In our case, we are examining GCRs that consider only the role of gravity.

## 5. SUMMARY

This study of Perseus and Orion A confirms that the G-Virial method effectively maps GCRs and complements traditional virial parameter calculations. The G-Virial method successfully circumvents the need for geometric assumptions and gives us the ability to coherently study the role of gravity in MCs on a global scale.

Our analysis reveals that: (1) for all GCRs the gravitational boundedness increases towards the center; (2) GCRs associated with star clusters are characterized with higher values of gravitational boundedness; (3) GCRs in both clouds obey the Larson relations; (4) Orion A is characterized with higher values of boundedness than Perseus.

Future work could extend this analysis to a broader range of MCs across the galaxy and a broader range of characteristics.

## Acknowledgements

We acknowledge the support by the Deutsche Forschungsgemeinschaft (DFG) under grant number KL 1358/20-3 and additional funding from the Ministry of Education and Science of the Republic of Bulgaria, National RI Roadmap Project DO1-326/4.12.2023.

## References

- Bally, J., Stark, A. A., Wilson, R. W., & Henkel, C. 1987, *The Astrophysical Journal Supplement*, **65**, 13, doi: 10.1086/191217
- Beaumont, C. N., Offner, S. S. R., Shetty, R., Glover, S. C. O., & Goodman, A. A. 2013, *The Astrophysical Journal*, **777**, 173, doi: 10.1088/0004-637X/777/2/173
- Bertoldi, F., & McKee, C. F. (1992). *The Astrophysical Journal*, **395**, 140, doi: 10.1086/171638

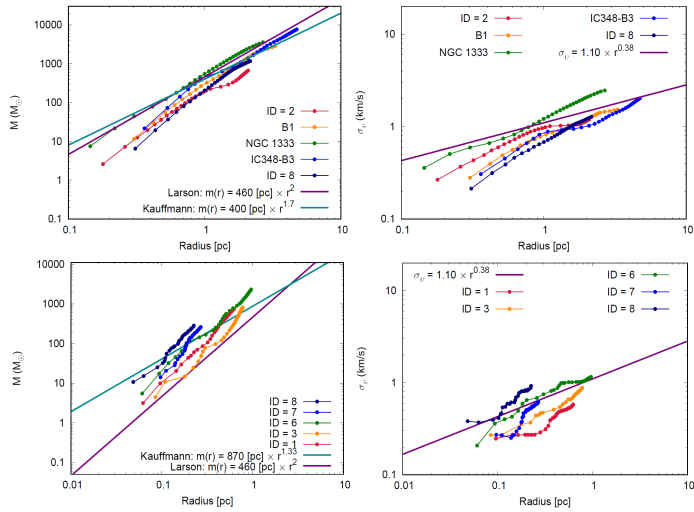


Figure 4: Mass-size relation (left) for the GCRs identified in Perseus (top) and Orion A (bottom). Larson’s (1981) and Kauffmann et al. (2010b) scaling relations are added. Velocity dispersion-size relation (right).

- Guang-Xing Li, Wyrowski, F., Menten, K., and Megeath, T. (2015). *Astronomy & Astrophysics*, **578**, A97, doi: 10.1051/0004-6361/201424030
- Heyer, M., Krawczyk, C., Duval, J., & Jackson, J. M. 2009, *The Astrophysical Journal*, **699**, 1092, doi: 10.1088/0004-637X/699/2/1092
- Kauffmann, J., Pillai, T., Shetty, R., Myers, P. C., & Goodman, A. A. (2010b). *The Astrophysical Journal*, **716**, 433, doi:10.1088/0004-637X/716/1/433
- Kauffmann, J., Pillai, T., & Goldsmith, P. F. 2013, *The Astrophysical Journal*, **779**, 185, doi: 10.1088/0004-637X/779/2/185
- Menshchikov, A., Andr, P., Didelon, P., et al. 2010, *Astronomy & Astrophysics*, **518**, L103, doi: 10.1051/0004-6361/201218797
- Ridge, N. A., Di Francesco, J., Kirk, H., et al. 2006, *Astronomical Journal*, **131**, 2921, doi: 10.1086/503704
- Rosolowsky, E.W., Pineda, J. E., Kauffmann, J., & Goodman, A. A. (2008). *The Astrophysical Journal*, **679**, 1338, doi: 10.1086/587685
- Schneider, N., & Elmegreen, B. G. (1979). *Astrophysical Journal Supplement*, **41**, 87, doi: 10.1086/190609

## MAGNETIC FIELD GROWTH IN GALACTIC DISCS OF VARIOUS THICKNESS

E. MIKHAILOV<sup>1,2</sup> , T. KHASAEVA<sup>2,3</sup>  and M. FROLOVA<sup>2</sup> 

<sup>1</sup>*P.N.Lebedev Physical Institute, Leninskiy prospect 53, 119991 Moscow, Russia*  
*E-mail: e.mikhajlov@lebedev.ru*

<sup>2</sup>*M.V.Lomonosov Moscow State University, Leninskie gori 1, 119991 Moscow, Russia*

<sup>3</sup>*Institute for Earthquake Prediction and Mathematical  
Geophysics, Profsoyuznaya street, 117997 Moscow, Russia*

**Abstract.** A large number of galaxies have regular magnetic fields of several microgauss. Their evolution is described using the dynamo mechanism. It is based on helicity of the turbulent motions in the interstellar medium and differential rotation of the object. The process is described by mean field dynamo equation which is quite difficult to solve both analytically and numerically. So different models taking into account geometrical shape of the object are used. One of the most popular approaches is connected with thin disc approximation which replaces the  $z$ -derivatives by algebraic expressions. However, as for discs with large half-thickness it does not give proper results. So we consider the thick disc model which can be useful for the objects with quite large half-thickness. Here we give the estimates of the magnetic field growth rate and check them numerically. It has been shown that for thick disc it is much more difficult to obtain the growing field. One of the most interesting questions (which has not been studied before) is connected with phase diagrams for the magnetic field. We have found a stable point and describe the typical phase trajectories leading to it

### 1. INTRODUCTION

A wide range of galaxies have large-scale magnetic fields of several microgauss (Beck et al 1996). First observational evidence was connected with studies of the cosmic rays: trajectories of the charged particles change under the influence of the magnetic fields. Fermi in his pioneer work has made estimates that are quite close to the values which are used now (Fermi 1949). Another important method is connected with studies of the synchrotron emission spectra which changes because of the magnetic field in the interstellar medium (Ginzburg 1959). However, today most of the observational studies of the galactic magnetic fields are done using Faraday rotation measurements (Manchester 1972). The polarized radiowaves pass through magnetized medium and the polarization plane rotates using the large-scale magnetic field as an axis. As for our Galaxy, usually pulsars are used as a source of the polarized radiowaves. Now there are more than 1000 objects that allow us to study the field structure in detail (Andreasyan et al. 2020).

Theoretically, the magnetic field generation is based on the dynamo mechanism (Beck 1996; Arshakian 2009). It is connected with helicity of the turbulent motions (which is also called alpha-effect) and differential rotation. They are described

by mean field dynamo equation (Krause & Raedler 1980). It is connected with a three-dimensional vector problem, that is quite difficult. Analytical methods are very complicated and numerical approaches are connected with quite large computational resources. So, for different astrophysical objects the specific models are used. They take into account their symmetry and reduce the equations to quasi-two-dimensional systems.

As for galaxies, the thin disc model (Moss 1995) is widely used. It assumes specific simple vertical structure of the magnetic field, that allows to change the corresponding second derivatives by the algebraic expressions. So, we assume the equations for two components of the magnetic field which depend on one (rarely two) spatial coordinates. The thin disc model is widely used in studying galactic magnetism and gives an opportunity to find the field structure for a wide range of concrete objects. It is interesting to say that this model is also used while studying magnetic fields of accretion discs.

However, there are a large number of galaxies where the half-thickness of the disc and its radius are quite comparable. Especially it is connected with the outer parts of the galaxy, where the disc can be thicker than 1 kpc (Mikhailov et al 2014). So, the thin disc model seems to be unapplicable. It is necessary to take different assumptions. In this paper we present a specific approach which considers the magnetic field as a sum of toroidal component (it is found in implicit form) and poloidal field that is calculated as a curl of the azimuthal part of the vector potential (Deinzer et al 1993; Mikhailov & Pushkarev 2021; Mikhailov & Pashentseva 2022). We take a system of equations for the field components which depend on distance from the rotation axis and distance from the equatorial plane (so-called rz-model). The typical time dependences of the field are described.

## 2. MEAN FIELD EQUATION

If we average the magnetic field in typical turbulent cells (as for galaxies, they have typical lengthscales of 50 – 100kpc, we shall obtain the Steenbeck – Krause – Raedler equation (Krause & Raedler 1980):

$$\frac{\partial \mathbf{B}}{\partial t} = \text{curl}(\alpha \mathbf{B}) + \text{curl}(\mathbf{V} \times \mathbf{B}) + \nu \Delta \mathbf{B};$$

where  $\mathbf{V}$  is the large-scale velocity (usually connected with galaxy rotation),  $\alpha$  is the helicity of the turbulent motions. As for the galaxies, we usually can say that  $\mathbf{V} = r\Omega \mathbf{e}_\varphi$ . For the alpha-effect we can take  $\alpha = \frac{\Omega l^2 z}{h^2}$ , where  $l$  is the typical turbulence lengthscale and  $h$  is the half-thickness of the disc (Arshakian et al 2009).

The magnetic field cannot grow infinitely, so we should use so-called equipartition value defined as  $B^* = 2v\sqrt{\pi\rho}$ . The alpha-effect should be calculated using by the nonlinear formula  $\alpha \sim (1 - \frac{B^2}{B^{*2}})$ . This leads to nonlinear saturation and simple attractors for the magnetic field (Arshakian et al 2009).

### 3. THIN DISC MODEL

If we take thin disc model, we can neglect the  $z$ -component of the field. Its vertical derivative can be obtained using solenoidality condition. As for the main part of the magnetic field, we can take the approximate law  $\mathbf{B}(r, z, t) = \mathbf{B}(r, 0, t) \cos\left(\frac{\pi z}{2h}\right)$ . So in the equipartition plane the second vertical derivatives of the field can be  $\frac{\partial^2 \mathbf{B}}{\partial z^2} = -\frac{\pi^2 \mathbf{B}}{4h^2}$ .

The equations in cylindrical coordinates and dimensionless units can be written as:

$$\begin{aligned} \frac{\partial B_r}{\partial t} &= -R_\alpha B_\varphi (1 - B_r^2 - B_\varphi^2) - \frac{\pi^2}{4} B_r + \lambda^2 \left( \frac{\partial^2 B_r}{\partial r^2} + \frac{1}{r} \frac{\partial B_r}{\partial r} - \frac{B_r}{r^2} \right); \\ \frac{\partial B_\varphi}{\partial t} &= R_\omega B_r - \frac{\pi^2}{4} B_\varphi + \lambda^2 \left( \frac{\partial^2 B_\varphi}{\partial r^2} + \frac{1}{r} \frac{\partial B_\varphi}{\partial r} - \frac{B_\varphi}{r^2} \right); \end{aligned}$$

where  $R_\alpha$  is connected with alpha-effect,  $R_\omega$  shows differential rotation and  $\lambda$  – turbulent diffusivity.

It can be obtained that the magnetic field evolution is described by the dynamo number which is constructed as  $D = R_\alpha R_\omega$ . The field can grow for cases  $D > D_{cr}$ , where  $D_{cr}$  is the critical dynamo number. Using eigenvalue formulation of the problem (Mikhailov 2020), it can be obtained that  $D_{cr} \approx 6.7$ . The magnetic field growth rate can be obtained as  $\gamma = -\frac{\pi^2}{4} + \sqrt{R_\alpha R_\omega}$ .

The numerical solution for the magnetic field evolution for different  $D$  is shown on figure 1. It can be seen, that the magnetic field for small  $D = 6$  really decays, and for larger  $D$  it grows exponentially. It can also be seen that for smaller  $D = 12$  the growth rate is smaller than for larger  $D = 18$ .

### 4. THICK DISC MODEL

As for the magnetic fields in thick discs (Mikhailov & Pushkarev 2021; Mikhailov & Pashentseva 2022), or for the peripheral parts, we should take another assumptions. The field can be presented in the following form:

$$\mathbf{B} = \text{curl}(A\mathbf{e}_\varphi) + B\mathbf{e}_\varphi.$$

The equations for the magnetic field will be:

$$\begin{aligned} \frac{\partial A}{\partial t} &= R_\alpha z B (1 - B^2) + \lambda^2 \left( \frac{\partial^2 A}{\partial r^2} + \frac{1}{r} \frac{\partial A}{\partial r} - \frac{A}{r^2} \right); \\ \frac{\partial B}{\partial t} &= R_\omega \frac{\partial A}{\partial z} + \lambda^2 \left( \frac{\partial^2 B}{\partial r^2} + \frac{1}{r} \frac{\partial B}{\partial r} - \frac{B}{r^2} \right). \end{aligned}$$

The magnetic field growth rate can be obtained using eigenvalue formulation (Mikhailov & Pashentseva 2023) as

$$\gamma = -\frac{\pi^2}{4} + \frac{3}{4} \sqrt{R_\alpha R_\omega}.$$

So, the field can grow if  $\gamma > 0$ , and if  $D > D_{cr}$ , where  $D_{cr} \approx 13$ .

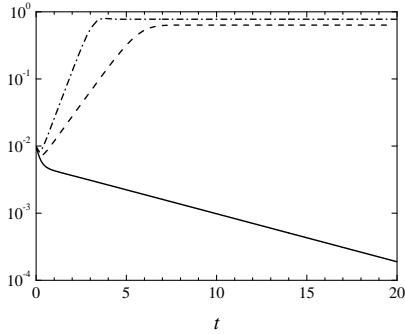


Figure 1: Evolution of the magnetic field in thin disc model. Solid line shows  $D = 6$ , dashed line –  $D = 12$ , dot-dashed line –  $D = 18$ .

The field evolution for this case is shown on figure 2. We can see, that for  $D = 12$  the magnetic field decays, contrary to the thin disc model. We can also see that the magnetic field growth rate here is smaller (Mikhailov & Pushkarev 2021).

It is also interesting to study the evolution of  $\frac{\partial A}{\partial z}$ . This value characterizes the radial magnetic field. It is presented on figure 3. We can see, that for cases  $D = 6$  and  $D = 12$  the field decays, and for  $D = 18$  it grows. Also it is worth to mention that the radial field is much smaller than the azimuthal one.

It is also interesting to study phase diagram of the system. The nonlinearity describes simple attractor with a stable point. Using different initial conditions (figure 4) we have found the typical stable solution for  $D = 20$ , corresponding to  $\frac{\partial A}{\partial z} = 0.24$ ,  $B = 1.01$ .

## 5. CONCLUSION

We have studied the magnetic field evolution using different approaches. First of all, we have studied it using the thin disc model. After that, the thick disc model have been studied. It is interesting that for the thick disc it is much more difficult to generate the field. Also we have studied the evolution of the  $\frac{\partial A}{\partial z}$ , which characterizes the radial magnetic field. The phase trajectories on the plane  $(\frac{\partial A}{\partial z}, B)$  have been studied, too. We have found the typical stable points for this case.

## Acknowledgements

The work was performed using the equipment of the Center for Collective Use of Supercomputing Resources of Lomonosov Moscow State University.

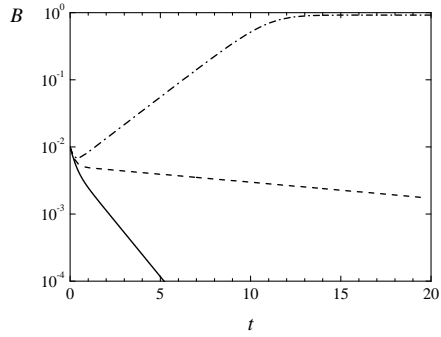


Figure 2: Evolution of derivative of vector potential component  $\frac{\partial A}{\partial z}$  in thick disc model. Solid line shows  $D = 6$ , dashed line –  $D = 12$ , dot-dashed line –  $D = 18$ .

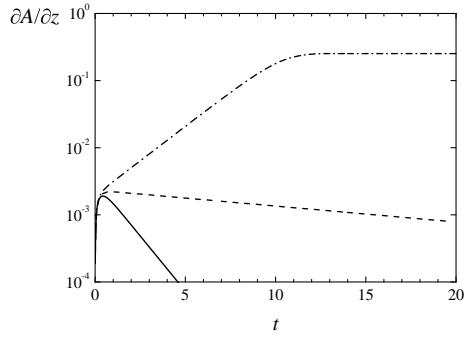


Figure 3: Evolution of derivative of azimuthal magnetic field  $B$  in thick disc model. Solid line shows  $D = 6$ , dashed line –  $D = 12$ , dot-dashed line –  $D = 18$ .

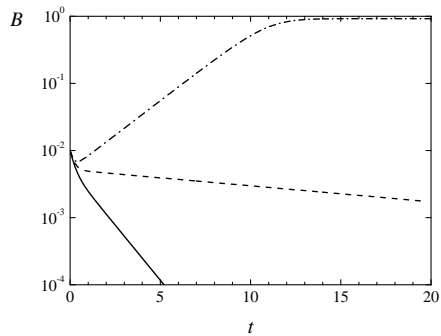


Figure 4: Phase diagram for thick disc model for  $D = 20$ . Different curves correspond to different initial conditions

**References**

- Beck, R., Brandenburg, A., Moss D., Shukurov, A., Sokoloff, D.: 1996, *Ann.Rev.Astron.Astrophys.*, **34**, 155, doi: 10.1146/annurev.astro.34.1.155
- Fermi, E.: 1949, *Phys. Rev.*, **75**, 1169, doi: 10.1103/PhysRev.75.1169
- Ginzburg V.: 1959, *Symposium International Astronomical Union*, **9**, 589.
- Manchester, R.: 1972, *The Astrophysical Journal*, **172**, 43, doi: 10.1086/151326
- Andreasyan, R.R., Mikhailov, E.A., Andreasyan, H.R.: 2020, *Astronomy Reports*, **62**, 189, doi:10.1134/S1063772920030014
- Arshakian, T., Beck, R., Krause, M., Sokoloff, D.: 2014, *Astronomy and Astrophysics*, **494**, 21, doi: 10.1051/0004-6361/200810964
- Krause, F., Raedler, K.-H. Mean-field electrodynamics and dynamo theory. Berlin, 1980.
- Moss, D. *Monthly Notices of the Royal Astronomical Society*, **275**, 191, doi: 10.1093/mnras/275.1.191
- Mikhailov, E., Kasparova, A., Moss, D., Beck, R., Sokoloff, D., Zasov, A. 2014: *Astronomy and Astrophysics*, **568**, A66. DOI:10.1051/0004-6361/201323341
- Deinzer, W., Grosser, H., Schmitt, D. 1993, *Astronomy and Astrophysics*, **273**, 405.
- Mikhailov, E., Pashentseva, M.: 2022, *Moscow University Physics Bulletin*, **77**, 741, doi:10.3103/S0027134922050101
- Mikhailov, E., Pushkarev, V.: 2021, *Research in Astronomy and Astrophysics*, **21**, 056, doi: 10.1088/1674-4527/21/3/056
- Mikhailov, E.: 2020, *Magnetohydrodynamics*, **56**, 403, doi: 10.22364/mhd.56.4.5
- Mikhailov, E., Pashentseva, M.: 2023, *Mathematics*, **11**, 3106, doi: 10.3390/math11143106



## ACCRETION MECHANISMS AND SUPERHUMPS OF THE NOVA-LIKE SYSTEM V592 CAS

D. BONEVA<sup>1</sup> and K. YANKOVA<sup>1</sup>

<sup>1</sup>*Space Research and Technology Institute, Bulgarian Academy of Sciences,  
Acad. Georgi Bonchev Str., bl. 1, 1113, Sofia, Bulgaria  
E-mail: danvasan@space.bas.bg*

**Abstract.** Accretion discs are complex energetic systems ruled by various dynamical physical processes. We consider different mechanisms that are responsible for the accretion dynamics in Nova-like stars. In this work, we focus our study onto their relation with the superhumps activity of Cataclysmic variable binaries, particularly in the Nova-like system V592 Cas. Based on the observational data obtained from both the National Astronomical Observatory (NAO) Rozhen and the American Association of Variable Star Observers (AAVSO), an appearance of superhumps in this object are detected. They are mostly visible in U band, with amplitude variations of  $\approx 0.2 - 0.3$  mag. The possible active mass-transfer mechanisms between the binary's components are suggested and discussed.

### 1. INTRODUCTION

Cataclysmic variable stars (CVs) are binary systems with a white dwarf primary star, accreting matter from a main-sequence secondary via Roche lobe overflow (Warner 1995). Nova-like (NL) stars are subclass of Cataclysmic variable binaries that do not produce outbursts. They have high-mass accretion rate and the emission in UV band in these systems is coming from the disc (from Godon 2017, la Dous 1991).

One interesting Nova like (NL) system is V592 Cas, discovered by Greenstein et al. (1970). The orbital period of the system is  $\approx 2.76$  h (Taylor et al. 1998, Witherick et al. 2003). The distance to the object is measured in the range: from 360 pc (see Taylor) to  $466 \pm 4$  pc (GAIA). The estimated accretion rate of V592 Cas is varied from  $9 \times 10^{-9} M_{\odot} y^{-1}$  to  $1 \times 10^{-8} M_{\odot} y^{-1}$  (Taylor et al. 1998, Hoard et al. 2009). Its blue color and spectral characteristics identified it as a disk-accreting Nova-like cataclysmic variable (CV). The presence of a wind is also detected by its spectrum (Witherick et al. 2003, Prinja et al. 2004). V592 Cas shows a behavior of an orbital modulation in the velocity extended UV lines profiles, typical for some cataclysmic variables. Observational effects that appeared as short-period, low-magnitude brightness variations are usually recognized as humps and/or superhumps (Isogai et al. 2016, Kato et al. 2000). They are typical for the Cataclysmic variable stars (CVs). The past observational data of V592 Cas show evidences that the star exhibits superhumps with all necessary conditions (Patterson 1998). The humps are observed with a periodicity  $P_h$  similar to the binary orbital period, usually in the quiescence low state. Superhumps' periodicity  $P_{sh}$  is a few percent longer than the binary period and they can be observed during the high state of the objects (Warner 1995).

In this work, we present observational data that show superhumps activity of V592 Cas. We discuss on the currently active mass-transfer mechanisms between the binary components. This could be relevant to the type of accretion, wind or disc is dominant for the studied object.

## 2. OBSERVATIONAL RESULTS

We use observational data both from AAVSO and 2m telescope of the National Astronomical Observatory (NAO) Rozhen, Bulgaria. Data from AAVSO are for the observational period of time: 20060921 to 20081119, in V band. During this time, an activity with several superhumps is clearly detected (Figure 1). We select a better distinguished superhump among them and it is on the night of JD 2454750.40 – 2454750.50 (20081010 – 20081011 UTC date). The maximum amplitude of the brightness variation is  $\approx 0.12 - 0.14$  mag in a frame of 3 hours. The magnitude is in the range 12.5612.42, in the V band.



Figure 1: Light curve of V592 Cas in V band. Observational time: 20081010 – 20081011. Superhump is seen during this period (marked with red arrows). AAVSO data.

The 2m telescope with two channel focal reductor FoReRo2 and two identical CCD cameras Andor iKON-L was used for observations in B and U bands. The obtained data are for two different dates. On the night of JD 2459615 (20220204 UTC date) the brightness of the object decreases with 0.5 magnitudes in a time-frame of one orbital period. Quasi-periodic oscillations are also observed within this time, with average amplitude variations in brightness  $\approx 0.3$  mag. They have very short periodicity, in a range of 5 – 10 minutes (Figure 2a).

On the night of JD 2459852 (20220929 UTC date), observations in the U band are in a frame of one orbital period of the star. A trend of a rising and decreasing brightness with an average amplitude of 0.3 mag during this time is seen. We measure its period and it is  $\approx 3.2 \pm 0.002$  hours, which is slightly longer than the orbital period. This brightness variation is identified more like superhump (Figure 2b). Within this superhump period, we deciphered short-period quasi-periodic variations in brightness again, with amplitudes of 0.15 – 0.3 mag. We suppose they look much more like

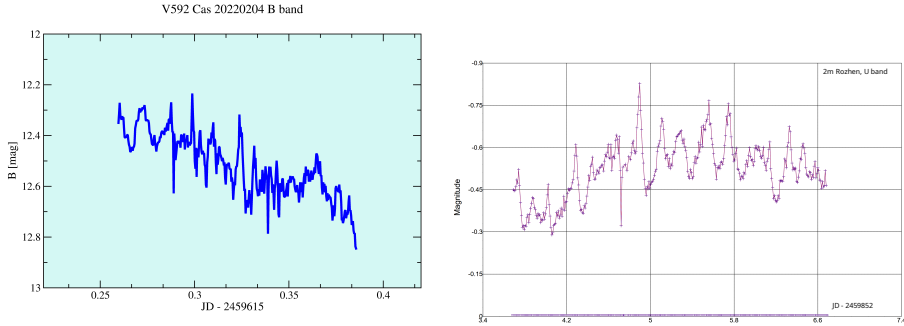


Figure 2: Light curve of V592 Cas in B band (2a-left) and U band (2b-right). Observational data are for different periods, obtained with the 2m telescope, NAO Rozhen. The magnitude in the U band is presented as amplitude variations.

flickering activity.

### 3. ACTIVE MASS-TRANSFER MECHANISMS AND EFFICIENCY

Further, to give a characteristic of an active mass-transfer mechanism, it is important to know an accretion efficiency values. It gives the measurement of how efficiently the mass energy of the accreted material is converted into radiation. We calculate average accretion efficiency values for V592 Cas, by using the expression of (Kolb 2010). Our results (current work and (Boneva & Yankova 2023)) confirm that V592 Cas is dominantly active in a disc than in a spherical accretion. The values both of the disc accretion rate ( $\dot{M}_d$ ) and the disc accretion efficiency  $\eta$ , are higher than those in the case with a spherical-like accretion, ( $\dot{M}_{\text{sph}}$ ) and efficiency  $\xi$  (see Table 1).

Table 1: Mean values of the accretion efficiency and accretion rate, calculated for the two modes' types.

Object/Mode	$\xi \times 10^{-4}$	$\eta \times 10^{-4}$	$\dot{M}_d M_{\odot} y^{-1}$	$\dot{M}_{\text{sph}} M_{\odot} y^{-1}$
V592 Cas	$0.50 \pm 0.02$	$2.05 \pm 0.11$	$1.3 \times 10^{-8}$ <sup>[1]</sup>	$5 \times 10^{-10}$ <sup>[2]</sup>

<sup>1</sup>Kafka et al. 2009 <sup>2</sup>Ringwald & Naylor 1998

We see that the observed precessing accretion disc around the primary component (Long 2003) could also affect on the values of the disc's accretion efficiency. The efficiency of V592 Cas is relatively low, but it increases through the modes, at higher accretion activity, during the time of a decreasing distance between the accretor and the accretion disc. In this binary, the stream from the secondary is most possibly transferring through the Lagrange point L1. A pseudo-spherical inflow is also possible to contact the outer parts of the accretion disc. Both type of inflows into the disc are affected by the two components' approach, which could cause a reaction in the spot or hot line contact area. Then, this reaction can be seen as a source of the superhumps.

#### 4. SUMMARY

We presented observational results of NL star V592 Cas from both sources: AAVSO for the period of time  $\approx 2$  years in the V band; our own, obtained from the 2m telescope of the NAO Rozhen, Bulgaria, for two nights in the U and B bands. We have detected a manifestation of superhumps in the U and V bands in different nights. We found indications of flickering during one night in B, and also in the U band that was appeared within one superhump's period. Flickering indicates the presence of activity in the disc. This activity generates an energy excess that contributes to the appearance of the hot accretion zone, which on the other hand could be responsible for the humps and superhumps appearance. The calculated dereddened colors of the star present it rather as a bluer object ( $B - V = -0.18$ ;  $U - B = -0.99$  (Taylor 1998)), but mostly expressed its activity in the U band. The roughly estimated negative value of the color index ( $U - B < 0$ ) during our observations is an indication of a hotter radiation zone in the accretion disc. These heating parts of the disc could be one reason for the humps and superhumps productions. We give our estimations of the accretion efficiency of V592 Cas and discussed on the possible dominated accretion mode around the primary component of the object.

#### Acknowledgements

The authors thank the AAVSO (American Association of Variable Star Observers) for providing the data of Light Curve Generator, contributed by observers worldwide and used in this research.

#### References

- Boneva D., Yankova Kr., 2023, *Publ. Astron. Soc. Rudjer Bošković*, **25**, 17
- Godon, P., Sion, E. M., Balman, Ş. and Blair, W. P., 2017, *The Astrophysical Journal*, **846**(1), 52, doi: 10.3847/1538-4357/aa7f71
- Greenstein, J. L., Sargent, A. I., Haug, U. 1970, *Astronomy & Astrophysics*, **7**, 1
- Hoard, D. W., Kafka, S., Wachter, S., et al.: 2009, *The Astrophysical Journal*, **693**, 236, doi: 10.1088/0004-637X/693/1/236
- Isogai, K., 2016, *Publ. Astron. Soc. Japan*, **68**, 4, 64, doi: 10.1093/pasj/psw063
- Kafka, S., Hoard, D. W., Honeycutt, R. K., Deliyannis, C. P., 2009, *Astronomical Journal*, **137**, 1, 197, doi: 10.1088/0004-6256/137/1/197
- Kato, T., Nogami, D., Baba, H., et al., 2000, *Monthly Notices of the Royal Astronomical Society*, **315**, 140, doi: 10.1046/j.1365-8711.2000.03440.x
- Kolb, U. 2010, *Extreme Environment Astrophysics*, Cambridge University Press, ISBN: 9780521187855
- la Dous, C. 1991, *Astronomy & Astrophysics*, **252**, 100.
- Long, K., 2003, *FUSE Proposal ID D11*, 2003fuse.prop.D114L.
- Patterson, J., 1998, *Publications of the Astronomical Society of the Pacific*, **110**(752), p.1132, doi: 10.1086/316233
- Prinja, R. K., Knigge, C., Whiterick, D. K., Long, K. S., Brammer, G. 2004, *Monthly Notices of the Royal Astronomical Society*, **355**, 137, doi: 10.1111/j.1365-2966.2004.08301.x
- Ringwald, F. A., Naylor, T., 1998, *Astronomical Journal*, **115**, 286, doi: 10.1086/300192
- Taylor, C. J., Thorstensen, J. R., Patterson, J., et al. 1998, *Publications of the Astronomical Society of the Pacific*, **110**, 1148, doi: 10.1086/316235
- Warner, B. 1995, *Cataclysmic Variable Stars* (Cambridge: Cambridge Univ. Press), doi: 10.1017/CBO9780511586491
- Whiterick, D. K., Prinja, R. K., Howell, S. B., Wagner, R. M., 2003, *Monthly Notices of the Royal Astronomical Society*, **346**, 861, W03, doi: 10.1111/j.1365-2966.2003.07130.x

## PHOTOMETRIC PERIODS OF M31 LBV AF AND IDENTIFIED VIA STRUCTURE EMINENCE FUNCTION METHOD

TS. GEORGIEV<sup>1</sup>, A. VALCHEVA<sup>2</sup> and P. NEDIALKOV<sup>2</sup>

<sup>1</sup>*Institute of Astronomy and National Astronomical Observatory, Bulgarian Academy of Sciences, 72 Tsarigradsko Chaussee Blvd., 1784 Sofia, Bulgaria*  
*E-mail: tsgeorg@astro.bas.bg*

<sup>2</sup>*Department of Astronomy, Faculty of Physics, Sofia University, 5 James Bourchier Blvd., 1164 Sofia, Bulgaria*

**Abstract.** We use *B*-band historical light curve of AF And in the time interval 1918-1990 to search for photometric periods applying Structure eminence function (SEF) method and its derivative the Periodograph function (PGF). Periods of  $3.90 \pm 0.10$  yr and  $4.55 \pm 0.10$  yr are found. SEF is the dependence of the structure amplitude on the structure time length and extracts and uses profiles of these structures. The positions of the SEF maxima mark eminent periods and quasi periods.

### 1. INTRODUCTION

Various methods exist for deriving periods in time series or light curves (LCs). The periodogram methods CLEAN (Roberts, 1987) and Lomb-Scargle (Lomb, 1976; Scargle, 1982), hereafter C&LS, are widely used in Astronomy.

Our Structure Eminence Function (SEF) method identifies and characterizes repetitive structures (patterns) responsible for the periodicity. SEF represents the average amplitude of the structure as a function of the time length of the structure ( $E(t)$ , Eq.1, Figs.(c)). The peak positions in the SEF mark significant periods and quasi-periods. After SEF, we use Periodograph Function (PGF), which enhances the visibility of the SEF peaks ( $G(t)$ , Eq.2, Figs.(d)).

The SEF method poses higher time resolution than the C&LS methods, with an improvement of up to 2 times. This advantage likely arises from its ability to operate with concrete profiles (shapes) of structures. Additionally, the structure profile may provide useful insights on the nature of the periodicity. Four variations of the SEF method can be distinguished according to the used preparatory procedures: resampling with a constant time step versus no resampling, as well as with local or global detrending. The SEF method was tested on various time series and its results were compared with the results of other periodogram analyses (Georgiev 2023, hereafter G23). Clearly prominent photometric period of 5.7 yr was found in the LCs of the LBV  $\eta$  Carinae (Georgiev et al. 2024, hereafter G+24).

In this study, an interpolated resampling with a step of 0.05 yr is performed for deriving a suitable input LCs (Figs.(a)). The resampling omits many sharp local LC peaks, but it (i) ensures uniform use of all parts of the LC and (ii) traces better the SEF humps. Detrending - the removal of large scale trend from the input LC - is

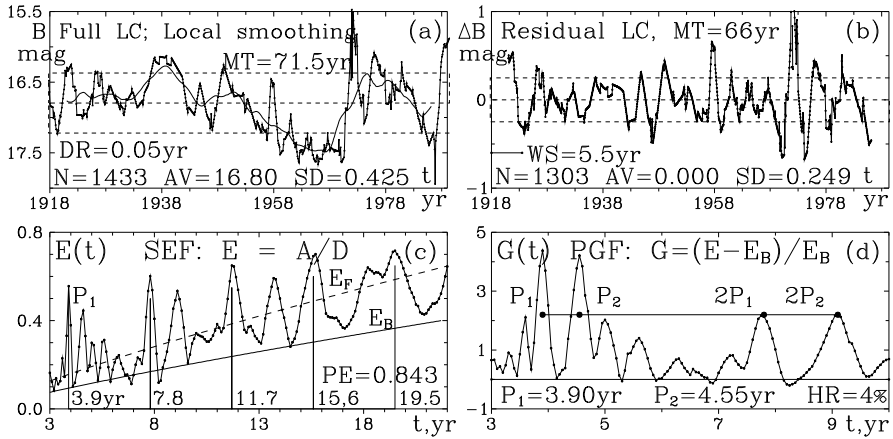


Figure 1: SEF (c) and PGF (d) build after resampling and local detrending of the 'Full LC' of AF And. See the text.

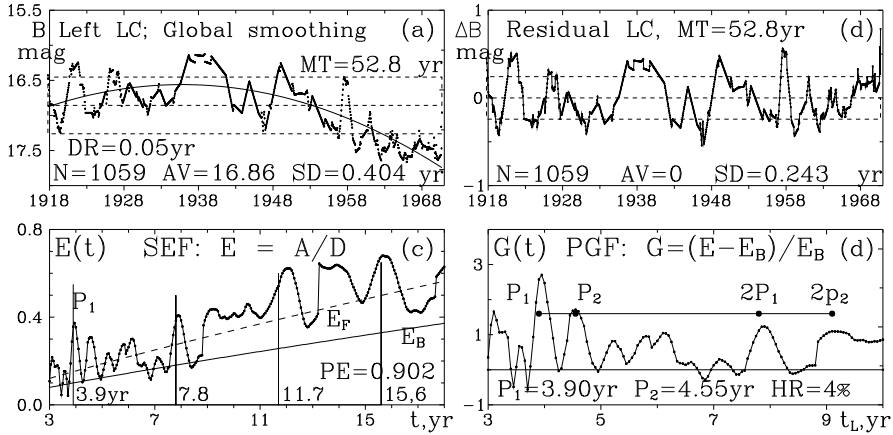


Figure 2: SEF (c) and PGF (d) build after resampling and global detrending of the 'Left part' of the LC of AF And. See the text.

obligatory when SEF method is applied. For this purpose, a smoothed version of the input LC is extracted, resulting in the residual LC (RLC).

The RLC (Figs. (b)) is a flat version of the input LC which is used for the SEF building. The RLC is also suitable as input for C&LS methods (G+24). Local smoothing through moving average is performed and shown in Fig.1a. The window size (WS) is 5.5 yr or 110 resampled data points (dp). This WS ensures the optimal prominence of the SEF/PGF maxima at about 4 yr. Global smoothing is performed through a second-degree polynomial fit of the input light curve, as shown in Fig. 2a.

## 2. AMPLITUDE AND NOISE OF THE STRUCTURE. SEF AND PGF

Let's consider RLC  $(t_i, z_i)$ ,  $i = 1 \dots N$  dp with constant data step  $\delta t$ , zero average value (AV) and relevant standard deviation (SD). Suppose this RLC contains significant

repetitive structure with a size of  $l$  dp or a time length  $T_L = L \times \delta t$ . Our code identifies the length  $L$  of the basic period after checking numerous LC segments with lengths  $L = L_1 \dots L_2$  as follows.

For every  $L$ , we pull up the first  $L$  RLC values,  $z_i, i = 1 \dots L$ , and put them into an initially empty set with cell numbers  $j = 1 \dots L$ . Then, we add there the next  $L$  dp,  $z_i, i = L + 1 \dots L + L$ , from the RLC. Later, we add the next  $L$  dp, etc. The (integer) number of possible adds is  $K = N/L$ . In the end, every  $j$ -th cell, containing  $K$  adds, has relevant AV  $a_j$  and SD  $d_j$ . So, the structure with length  $L$  dp is described by a signal profile  $a_j$  and a noise profile  $d_j$ . Finally, we derive the average amplitude  $A_L = \langle |a_j| \rangle_L$  and average noise  $D_L = \langle d_j \rangle_L$ . Note that  $A_L$  gathers absolute values  $|a_j|$ , i.e.  $A_L$  is one-side average amplitude of the structure. Applying SEF method, we extract numerous RLS segments with lengths  $L = L_1 \dots L_2$ , characterizing each of them by  $A_L$  and  $D_L$ . In this study, we specify  $L_1 = 20$  dp. For at least  $K = 3$  additions (for statistically significant AV and SD), the code derives and uses  $L_2 = N/3$ .

Every significant repetitive structure of the RLC produces local maximum in the amplitude function  $A$  and local minimum of the noise function  $D$ . Therefore, we have to define the dimensionless SEF (Figs.(c)) as follows:

$$E_L = A_L/D_L; \quad E(t) = A(t)/D(t). \quad (1)$$

The position of the leftmost local SEF maximum marks the basic period  $P$ . The periods  $2P, 3P$ , etc. cause additional default maxima.

The SEF fits,  $E_F$ , shown in Figs.(c) (dashed curves), are power functions. In log-log scale, they are straight lines. The SEF maxima become more prominent when the SEF background is removed. Therefore, the background line, which bounds 90% of the SEF points from below, is derived by shifting the SEF line downward. After transforming it back into linear scale, the SEF background line becomes a power function  $E_B$  with a power exponent (PE) similar to that of the  $E_F$  (Figs. (c), solid curves). As a result, we define the dimensionless PGF using the SEF values  $E$  and the corresponding SEF background values  $E_B$  (see Figs.(d)), as follows:

$$G_L = (EE_B)/E_B; \quad G(t) = (E(t)E(t)_B)/E(t)_B. \quad (2)$$

In the PGF, the SEF maxima are more prominent and the time resolution of the SEF method can be estimated better (Figs.(d)).

### 3. DERIVING PHOTOMETRIC PERIODS OF AF AND

We analyzed the historical  $B$ -band LC of the M31 LBV AF And in the time interval 1918-1990, compiled by Gantchev et al. (2017). The original 'Full LC' (Fig.1a) contains 393 dp in the monitoring time (MT) of 71.5 yr. The section of this LC prior to the eruptions in 1971-1973, referred to as the 'Left LC' (Fig.2a), contains 280 dp in the MT of 52.8 yr (1918-1970).

After resampling with a step of 0.05 yr, the input LCs for the 'Full LC' and the 'Left LC' contain  $N = 1433$  dp and  $N = 1059$  dp, respectively. The 'Full LC' is detrended using a moving average applied to the resampled LC with a WS of 5.5 yr (110 dp). The 'Left LC' is detrended by fitting a 2nd-degree polynomial to the resampled LC (Figs.(a),(b)).

Figures (a) show the input (resampled) LCs and their smoothed versions. Figures (b) show the corresponding RLCs (the differences between the smoothed and input LC). Horizontal lines show AV level and  $AV \pm SD$  levels. In Fig. 1b, due to the local smoothing, the RLC edges with lengths  $5.5/2 = 2.25$  yr (55 dp) each, are lost. Note that we use RLC in magnitude differences  $\Delta B = (B_{smooth} - B_{resampled})$  and the positive values  $\Delta B$  correspond to increased brightness.

Figures (c) show the SEFs (Eq. 1) derived from the RLCs shown in Figs.(b). For  $K = 3$  segment additions, the maximal checked segment lengths are  $66/3 = 22$  yr or  $52.8/3 = 17.7$  yr), respectively. Here,  $E_F$  and  $E_B$  are the fits of the SEF and SEF background, as power functions. Further,  $E_B$  is used for deriving of PGF (see Figs. (d) and Sect. 2). PE is the power exponent. The leftmost SEF maximum marks the basic period,  $P_1 = 3.90$  yr. Its default larger counterparts,  $2P_1, 3P_1$ , etc, cause other maxima. Shorter counterparts, e.g.  $P_1/2$  (see G23), are not detected here. However, a second period,  $P_2 = 4.5$  yr, is also clearly observable.

Figures (d) show the initial parts of the PGFs (Eq. 2). The peaks of the periods  $P_1$  and  $P_2$ , as well as  $2P_1$  and  $2P_2$  are clearly pronounced. The relative hump resolution (HR) of the SEF method, the half width at the half of the maximum, at about  $P = 4$  yr, is about 4% or 0.16 yr. However, the positions of the hump peaks may be located with an accuracy of at least  $\pm 0.1$  yr. We assume 0.1 yr to be the SD of our period estimation.

#### 4. SUMMARY

We analyzed the 20th century 'Full LC' and 'Left LC' of the historical LC of AF And, resampled with step of 0.05 yr. We apply universal local detrend of the 'Full LC' and a global detrend of the 'Left LC'. In both cases, we found two well prominent periods:  $P_1 = 3.90 \pm 0.10$  yr and  $P_2 = 4.55 \pm 0.10$  yr.

In addition, applying a local detrend of the 'Left LC' (not shown here), we found the same periods. Applying the same analysis after resampling with step of 0.1 yr (not shown here), we found periods of 3.9 yr and 4.6 yr.

We can speculate that one of these periods may corresponds to probable orbital period, similarly to the period of 4.7 yr in the case of  $\eta$  Carinae (see G+24) and the other one is of uncertain origin.

#### Acknowledgements

This study is financed by the European Union – NextGenerationEU, through the National Recovery and Resilience Plan of the Republic of Bulgaria, project SUMMIT BG-RRP-2.004-0008-C01. We also acknowledge partial support by Bulgarian National Roadmap for Research Infrastructure Project D01-326/04.12.2023 of the Ministry of Education and Science of the Republic of Bulgaria.

#### References

- Gantchev, G., Nedialkov, P.: 2019, *IAU Symposium 339*, 87, doi: 10.1017/S1743921318002284  
 Georgiev, Ts.: 2023, *Bulg. Astron. J.* **38**, 120 [G23], bibcode 2023BlgAJ..38..120G  
 Georgiev, Ts., Valcheva, A., Nedialkov, P., Stefanov, S., Moyseev, M.: 2024, *Bulg. Astron. J.*, submitted, [G+24]  
 Lomb, N. R.: 1976, *Astrophys.Sp.Sci.*, **39**, 447, doi 10.1007/BF00648343  
 Roberts, D. H., Lehar J., Dreher J. W.: 1987, *Astron. J.*, **93**, 968, doi 10.1086/114383  
 Scargle J. D.: 1982, *Astrophys. J.* **263**, 835, doi 10.1086/160554



## THE PATH OF MILUTIN MILANKOVIĆ'S BOOK MANUSCRIPT "MATHEMATICAL THEORY OF THERMAL PHENOMENA CAUSED BY SOLAR RADIATION"

N. JANC 

*independent researcher, Baltimore, MD, USA*  
*E-mail: natalijanc@earthlink.net*

**Abstract.** While working on the correspondence of Milutin Milanković (Dalj, 1879 – Belgrade, 1958) at the Serbian Academy of Sciences and Arts (SASA) in Belgrade, I came across a letter sent by Milanković to the Royal Hungarian Academy of Sciences in Budapest. In it, Milanković thanks the Academy for allowing him to spend his years of internment during the First World War in its library and enabling him to engage in scientific work. In those years, the text of his book “*Mathematical theory of thermal phenomena caused by solar radiation*” was written, and as a sign of gratitude he sent them its original typescript, which he wrote at the time under the title “*Mathematische Grundlagen der kosmischen Strahlungslehre*”. The letter is dated April 2, 1941. Given that Belgrade was bombed just a few days later, on April 6, 1941, I was interested in whether the manuscript reached the Hungarian Academy. To my inquiry, they replied that they had received it and that it was in the archive.

The path of the manuscript did not go as Milutin Milanković planned. After the First World War, it was desirable that the book be printed in French. Given that Milanković did not speak French well enough, the translation from German to French was entrusted to Ivan Djaja (Le Havre, 1884 – Belgrade, 1957) and Mihailo Petrović Alas (Belgrade, 1868 – Belgrade, 1943). Milanković duly copied his original manuscript in German and handed it over to Djaja and Petrović. After completing their translation, Milanković also copied the translation. Both manuscripts are in SASA. The book was published in Paris in 1920 under the title “*Théorie mathématique des phénomènes thermiques produits par la radiation solaire*”. The results published in this book have attracted the attention of many scientists. Wladimir Köppen and Alfred Wegener invited Milutin Milanković to collaborate in their book “*The climates of the geological past*”.

On April 20, 2017, in the Library and Information Centre of the Hungarian Academy of Sciences a memorial plaque in memory of Milutin Milanković was unveiled.

### 1. INTRODUCTION

During the First World War, although Milutin Milanković was in captivity, he was allowed to continue his scientific work in the library of the Hungarian Academy of Sciences in Budapest (Milanković, 1952). Starting in 1912, Milanković dealt with climate change based on mathematical calculations with the aim of calculating the temperature at different points on Earth (Szarka, Soon, Cionco, 2021).

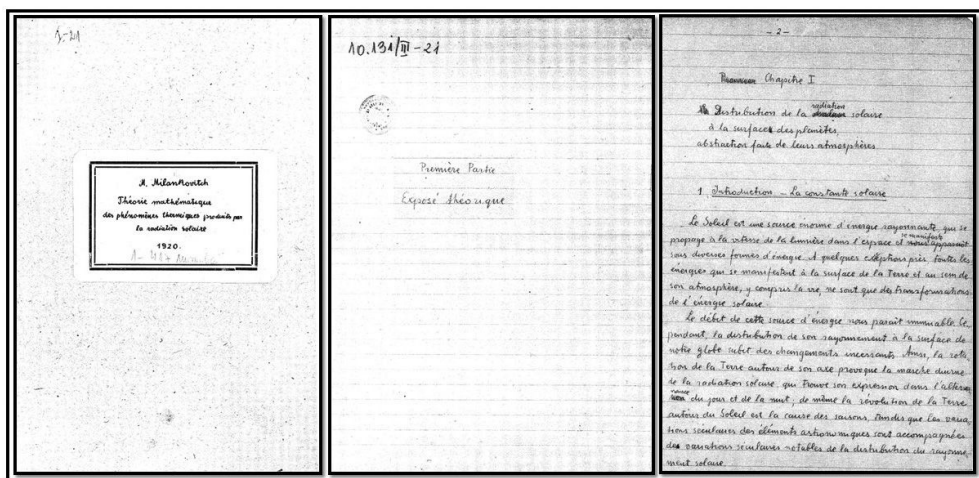


Figure 1: The manuscript of the book “Théorie mathématique des phénomènes thermiques produits par la radiation Solaire,” in French (SASA Archive – 10.131/III-21).

## 2. TRACE OF THE BOOK’S MANUSCRIPT

Milanković continued to work on the study of climate change during his entire stay in Budapest during the First World War. The manuscript that was created at the time was in German with the title “Mathematische Grundlagen der kosmischen Strahlungslehre” (“Mathematical foundations of the theory of cosmic radiation”) on 334 pages.

Milanković finished the work in the middle of 1917 and it was handed over to the publisher B. G. Teubner in Leipzig, the largest publishing company for works with a mathematical content (Milanković, 1952). Milanković’s work was ready for printing at the beginning of 1918, but the company ran out of paper (Milanković, 1952). However, since after the First World War it was recommended not to publish works in German, the book was translated into French (Trifunović, 2007). The translation from German to French was done in collaboration by Ivan Djaja<sup>1</sup> and Mihailo Petrović - Alas<sup>2</sup> (Trifunović, 2007). The manuscript in French is kept in the Serbian Academy of Sciences and Arts (Fig. 1).

The work was published in 1920 under the title “Théorie mathématique des phénomènes thermiques produits par la radiation solaire” (“Mathematical theory of thermal phenomena caused by solar radiation”) and was a crucial forerunner in the field of (paleo)climatology (Fig. 2). It was this book that launched Milanković into the scientific world in the field of (paleo)climatology, which enabled Milanković to meet, contact and collaborate with many scientists, primarily Wladimir Köppen and Alfred Wegener (Janc et al., 2018).

Milanković wanted to bequeath the original manuscript in German (Fig. 2) to the

<sup>1</sup>Ivan Djaja (Le Havre, 1884 – Belgrade, 1957) was a Serbian biologist and physiologist, professor and member of the Serbian Academy of Sciences. French was his mother tongue, so he was entrusted with the translation of Milanković’s monograph.

<sup>2</sup>Mihailo Petrović - Alas (Belgrade, 1868 – Belgrade, 1943) was a well-known professor of mathematics at Belgrade University and a member of the Serbian Royal Academy.

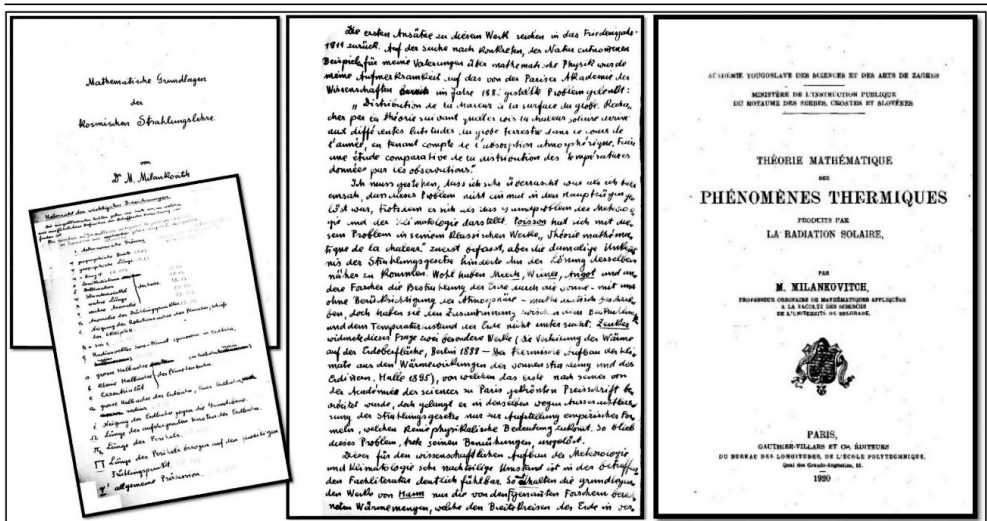


Figure 2: Title page of the manuscript “Mathematische Grundlagen der kosmischen Strahlungslehre” (“Mathematical Foundations of the Theory of Cosmic Radiation”), first page of the manuscript and list of mathematical symbols (copies obtained courtesy of the Hungarian Academy of Sciences on 15 December 2023), (left). The title page, *théorie mathématique des phénomènes thermiques produits par la radiation solaire* (Mathematical theory of thermal phenomena caused by solar radiation), M. Milankovitch, 1920. (right).

Hungarian Academy of Sciences, and sent it with a cover letter written on April 2, 1941 (Fig. 3), just a few days before the bombing of Belgrade, which began at dawn on April 6, 1941. The concept of the cover letter is kept in Archives of the Serbian Academy of Sciences and Arts. Fortunately, the manuscript reached the Hungarian Academy of Sciences undamaged, where it is kept in their archives.<sup>3</sup>

Milutin Milanković to the Hungarian Academy of Sciences, (SASA Archive, 10.131/10).

2-IV-1941

*To the Hungarian Academy of Sciences, Budapest*

*The accompanying manuscript, which was later published in a French translation under the title “Théorie mathématique des phénomènes thermiques produits par la radiation solaire”, Paris 1920, was written by myself in 1915–1917. in the reading room of this Academy thanks to the hospitality of the “Royal Hungarian Academy of Sciences”. I allow myself to present this manuscript, which was the starting point and on which all my further works in this field were built, as a token of my deepest gratitude to the Hungarian Academy of Sciences.*

*In memory to the stay and scientific work of Milutin Milanković in the Hungarian Academy of Sciences, a memorial plaque was installed, which was ceremonially unveiled on April 20, 2017 (Fig. 3).*

The text on the memorial plaque reads: “Serbian geophysicist and astronomer

<sup>3</sup>Information obtained from the Hungarian Academy of Sciences, (author’s note).

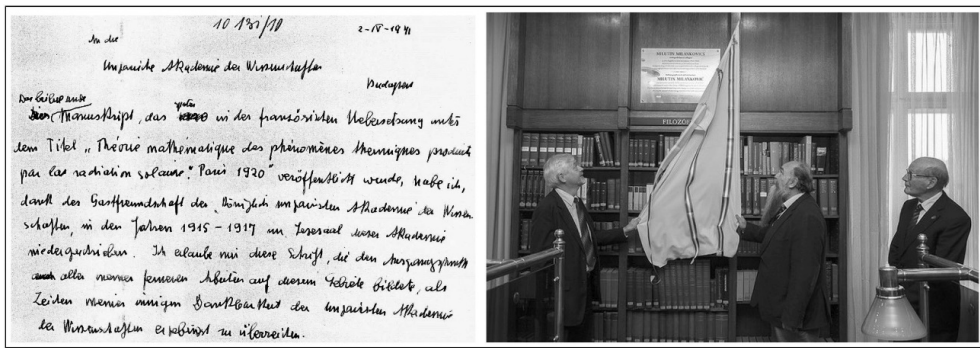


Figure 3: Facsimile of Milutin Milanković’s letter to the Hungarian Academy of Sciences, (SASA Archive 10.131/10), (left). Unveiling the memorial plaque to Milutin Milanković in the Library of the Hungarian Academy of Sciences where he was doing his research work during his WWI internment period (1914-1918). Aföld Napja - 2017 - Earth Day, MTA CSFK, MTA KIK (Photos by Dóra Velican-Patrus, Courtesy of the Library and Information Center of the Hungarian Academy of Sciences.) (right).

Milutin Milanković was allowed to spend his internment during the First World War (1914-1918) working on research in the Library of the Hungarian Academy of Sciences. The theory of the connection between long-term climate changes and astronomical factors that affect the amount of solar energy that the Earth receives is established here. Aföld Napja - 2017 - Earth Day, MTA CSFK, MTA KIK”.

### Acknowledgements

Thanks to the Library and Information Center of the Hungarian Academy of Sciences for the courtesy of providing information about the time Milanković was working in Budapest and all the photos of their wonderful library.



The Serbian Academy of Sciences and Arts has made available the Manuscripts of the Works of Milutin Milanković, for which the authors are grateful.

The author thank Mirko Janc, PhD (mathematics) for the precious help in translating several resources from the German language.

### References

- Janc N., Protić-Benišek V., Benišek V., Gavrilov M. B., Popović L. Č., Marković S. B.: 2018, Academicians Milutin Milanković and Vojislav Mišković: Correspondence about Alfred Wegener and Wladimir Köppen, *Astronomical and Astrophysical Transactions (AApTr): Journal of the Eurasian Astronomical Society*, **30**, Issue 4, 505–510
- Milanković M.: 1952, Uspomene, doživljaji i saznanja iz godina 1909. do 1944. Posebna izdanja, Knjiga CXC, Odeljenje prirodno-matematičkih nauka, Knjiga 6, (Reminiscences, Experiences and Knowledge 1909 to 1944, *Serbian Academy of Sciences, Special Editiona, Book CXC, Department of Natural and Mathematical Sciences, Book 6*, Beograd, p. 229, (In Serbian, cyrillic script)
- Laszlo Szarka, Willie W.-H. Soon, Rodolfo G. Cionco: 2021, How the astronomical aspects of climate science were settled? On the Milankovitch and Bacsak anniversaries, with lessons for today, *Advances in Space Research*, **67**, 700–707, doi: 10.1016/j.asr.2020.09.020
- Trifunović D.: 2007, Iz prepiske Milutina Milankovića, *Beosing*, Beograd, 320

## INTRA-NIGHT VARIABILITY OF 1722+119

M. D. JOVANOVIĆ  and G. DAMLJANOVIĆ 

*Astronomical Observatory, Volgina 7, 11060 Belgrade, Serbia*

*E-mail: miljana@aob.rs*

**Abstract.** Blazars (subclass of active galactic nuclei) eject relativistic jets near the observer's line of sight. Their flux is highly variable in the whole electromagnetic spectrum. Variability time-scales can be divided into three classes: intra-night variability, short-term variability, and long-term variability. The one subclass of blazars is BL Lac. These are blazars with rapid and large-amplitude flux variability. Source 1722+119 is BL Lacertae. The observations have been performed from July 2013 using telescopes located at the Astronomical station Vidojevica of Astronomical Observatory of Belgrade, Serbia. During more than ten years of flux monitoring of source 1722+119 amplitude brightness change by about 2 magnitudes in V and R bands. We monitored this source for about 3 hours per night on several nights to investigate the intra-night variability, and the results are presented here.

### 1. INTRODUCTION

Blazar 1722+119 is one of the 47 candidate sources for the link between International Celestial Reference Frame and Gaia Celestial Reference Frame (Bourda et al. 2011). Blazars are subclass of active galactic nuclei (AGN) which eject relativistic jets near the observers line of sight. Their flux is highly variable in the whole electromagnetic spectrum, and show variability on diverse time-scales. Variability time-scales can be divided into three classes: intra-night variability (from a few minutes to a less than a day), short-term variability (from a few days to a few months), and long-term variability (from a few months to several years); see Gupta (2014). The source 1722+119 is BL Lacertae. BL Lacertae are blazars which are characterized by rapid and large-amplitude flux variability.

### 2. METHODS AND RESULTS

We performed the optical photometric observations of 47 candidate sources, since July 2013. Observations were performed in *V* and *R* bands. 1722+119 is the most variable source. The brightness changed by about 2 magnitudes in both bands. We investigated intra-night variability of the source. Intra-night observations were performed using telescopes located at the Astronomical station Vidojevica (ASV) of Astronomical Observatory of Belgrade, Serbia ( $\lambda=21^\circ 5' E$ ,  $\varphi=43^\circ 1' N$ ). Telescope with the mirror diameter of 1.4 m (ASV 1.4 m) was equipped with Andor iKon-L, and 60 cm telescope (ASV 60 cm) with ProLine PL23042 CCD camera. CCD cameras specifications (name, CCD resolution, pixel size, pixel scale, field of view) are: Andor iKon-L CCD,  $2048 \times 2048$ ,  $13.5 \times 13.5 \mu m$ , 0.244 arcsec/pix,  $8.3 \times 8.3$  arcmin (for ASV 1.4 m), and ProLine PL23042,  $2048 \times 2064$ ,  $15.0 \times 15.0$ , 0.512,  $17.5 \times 17.6$  (for ASV 60 cm).

The brightness of the source was calculated using differential photometry with two comparison stars A, and B. The details about photometry (finding chart, and

selection of the stars) are presented in paper Jovanović *et al.* 2023. During the four nights, the intra-night brightness of the source 1722+119 did not change significantly. The average  $V$  magnitude was  $16.153 \pm 0.011$  mag, and  $R$  was  $15.725 \pm 0.019$  mag. The intra-night data were tested using Abbe’s criterion, and F – test.

## 2. 1. ABBE’S CRITERION

Abbe’s criterion is often used for checking the absence of systematic changes in a series of measurements. The statistics were calculated for differences of the magnitude of source (S) and stars A, and B ( $q_A$  and  $q_B$ ). The hypothesis about stochastic independence of the sample units is accepted under  $q_{A,B} > q_c$ , otherwise the elements of the sample cannot be accepted as random and independent. The  $q$  statistic was calculated:

$$q = \frac{1}{2} \left( \sum_{i=1}^{n-1} (x_{i+1} - x_i)^2 \right) / \left( \sum_{i=1}^n (x_i - \bar{x})^2 \right), \quad (1)$$

Statistics  $q_A$  and  $q_B$  were calculated:  $q_A : x = S - A$ ,  $q_B : x = S - B$ . The critical value is defined as  $q_c = 1 + u_\alpha / \sqrt{n + 0.5(1 + u_\alpha^2)}$ , where  $u_\alpha$  is the quantile of normal distribution for the significance level  $\alpha$ .

## 2. 2. F-TEST

F-test examines variances of two data sets X and Y to test if they are equal to each other. The test hypothesis was  $H_0 : VarX = VarY$ , and alternative  $H : VarX > VarY$ . We calculated statistics  $F_A : X = S - A$ ,  $F_B : X = S - B$ , and  $F_{A/B} = F_A/F_B$ ;  $Y = A - B$ , where  $S$ ,  $A$ , and  $B$ , are magnitude of source, comparison star A, and B.

If Abbe’s statistics ( $q_{A,B}$ ) are less than critical, and F-test statistics  $F_{A,B}$  are greater than the critical value, for significance level 0.001, and  $N$  number of data, we consider that the source is variable (V). For the opposite ( $q_{A,B} > q_c$ , and  $F_{A,B} < F_c$ ) source is nonvariable (NV). In other cases we consider that the source is possibly variable (PV). The statistical results are presented in Table 1: date of observation (with telescope which was used), band, number of data ( $N$ ), Abbe’s and F-test statistics, and variability. The night with the highest number of observations is March 29<sup>th</sup> 2020 (32 points in  $V$ , and 33 points in  $R$  bands). The light curves of  $V$  and  $R$  bands of March 29<sup>th</sup> 2020 are presented in Fig 1. With green diamonds is presented the light curve of  $V$  band, and with red squares the light curve of  $R$  band.

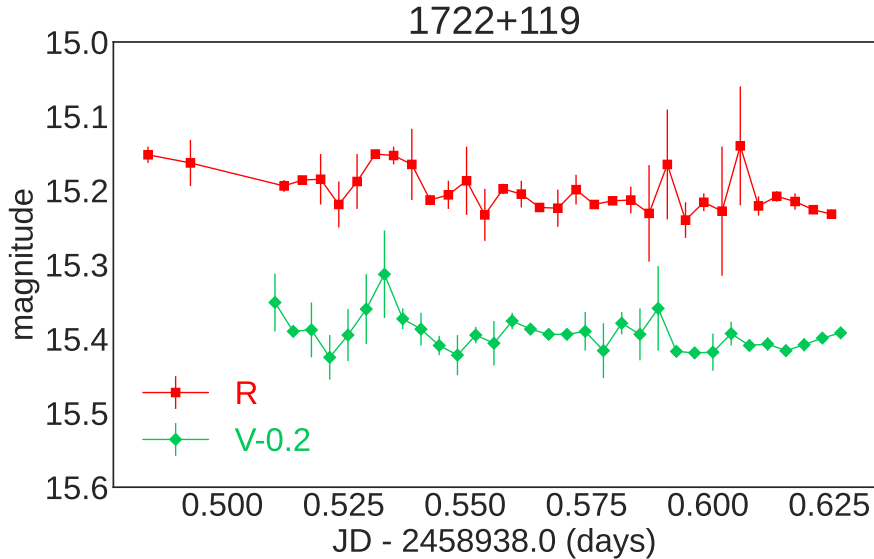
## 3. SUMMARY

We have observed 47 candidate sources for the link between ICRF and Gaia CRF, since July 2013. These sources are active galactic nuclei (AGN). The one of the most variable AGN are blazars (with detected intra-night, short-term, and long-term variability). The observational results were obtained with ASV telescopes, in  $V$  and  $R$  bands. For 12 sources the brightness variability was published in Jovanović *et al.* (2023). The most variable source is BL Lacertae 1722+119, with a change in brightness of almost 2 magnitudes, in both bands; during 2013–2019. In June 2015 during three hours of monitoring, the object did not show the variability in  $V$  band,

Table 1: Statistical results.

Date	Band	$N$	Abbe	F-test	Variable
Telescope			$q_A, q_B, q_c$	$F_{A/B}, F_A, F_B, F_c$	
02.09.2019.	$V$	11	0.53, 1.08, 0.26	1.10, 3.15, 2.88, 8.75	–
ASV 1.4 m	$R$	11	0.51, 0.39, 0.26	1.10, 1.56, 1.41, 8.75	–
29.03.2020.	$V$	32	0.50, 0.70, 0.49	1.34, 5.14, 6.90, 3.15	PV
ASV 60 cm	$R$	33	0.27, 0.32, 0.50	1.19, 19.24, 16.18, 3.09	$V$
27.07.2020.	$V$	14	0.44, 0.70, 0.31	1.01, 4.57, 4.53, 6.41	NV
ASV 1.4 m	$R$	14	0.62, 1.01, 0.31	1.11, 1.41, 1.26, 6.41	NV
09.04.2021.	$V$	9	1.18, 1.35, 0.22	1.51, 2.84, 1.89, 12.05	–
ASV 60 cm	$R$	10	0.81, 0.69, 0.24	1.13, 10.54, 9.33, 10.11	–

Notes. In the Variable column,  $V$  represents variable,  $NV$  nonvariable, and  $PV$  possibly variable source.


 Figure 1:  $V$  (green diamonds) and  $R$  (red squares) bands light curves of 1722+119 (March 29<sup>th</sup> 2020).

it showed possible variability in  $R$  band, and a strong redder-when-brighter trend of the optical spectrum (Kalita, Gupta & Gu (2021)).

Here we presented the intra-night variability of the source during 4 nights: September 2<sup>nd</sup> 2019 (2.5 h), March 29<sup>th</sup> 2020 (3.5 h), July 27<sup>th</sup> 2020 (4 h), and April 9<sup>th</sup> 2021 (1 h). The brightness of the source was determined using differential photometry with 2 comparison stars, and 5 control stars. In  $V$  band the brightness reached about 16.2 mag, in  $R$  15.7 mag, and did not change significantly during the mentioned 4 nights.

We tested the data for each night separately with Abbe's criterion and F – test. During the night of July 27<sup>th</sup> 2020 tests show that the source was nonvariable in both bands. During March 29<sup>th</sup> 2020 the source was variable in  $R$  band. In  $V$  band source was variable only with F – test. For September 2<sup>nd</sup> 2019 and April 9<sup>th</sup> 2021 were obtained only a small number of data (less than 12). We cannot conclude anything based on the test results. In order to better examine the activity of the source, we will continue with observations of this and the other sources.

### Acknowledgements

This research was supported by the Ministry of Science, Technological Development and Innovation of the Republic of Serbia (contract No. 451-03-66/2024-03/200002). GD acknowledges the support through the project F-187 of the Serbian Academy of Sciences and Arts. We acknowledge the financial support by the European Commission through project BELISSIMA (BELgrade Initiative for Space Science, Instrumentation and Modelling in Astrophysics, call FP7-REGPOT-2010-5, contract No. 256772) which was used to procure the "Milanković" 1.40 m telescope with support from the Ministry of Education, Science and Technological Development of the Republic of Serbia, and the observing and financial grant support from the Institute of Astronomy and Rozhen NAO BAS through the bilateral joint research projects: GAIA astrometry and fast variable astronomical objects (20232025; head - G. Damjanović), and Astrometry and photometry of visual double and multiple stars (20232025; head - O. Vince).

### References

- Bourda, G., Collioud, A., Charlot, P., Porcas, R., Garrington, S.: 2011, *Astronomy & Astrophysics*, **526**, 102, doi: 10.1051/0004-6361/201014249.
- Gupta, A. C.: 2014, *Journal of Astrophysics & Astronomy*, **35**, 307, doi: 10.1007/s12036-014-9219-7.
- Jovanović, M., Damjanović, G., Taris, F., et al.: 2023, *Monthly Notices of the Royal Astronomical Society*, **522**, 767-791, doi: 10.1093/mnras/stad904.
- Kalita N., Gupta A. C., Gu M., 2021, *The Astrophysical Journal Supplement*, **257**, 41, doi: 10.3847/1538-4365/ac1e9c.



## MULTI-INSTRUMENT OBSERVATION OF A FILAMENT ERUPTION AND ASSOCIATED CME DEFLECTION

K. KOLEVA<sup>1</sup>, M. DECHEV<sup>2</sup>  and P. DUCHLEV<sup>1</sup>

<sup>1</sup>*Space Research and Technology Institute, Bulgarian Academy of Sciences, Bulgaria  
E-mail: kkoleva@space.bas.bg*

<sup>2</sup>*Institute of Astronomy with NAO, Bulgarian Academy of Sciences, Bulgaria*

**Abstract.** We present the results from the investigation of a filament eruption, occurring in the southern solar hemisphere on October 18, 2017. The event was observed in the field-of-view of Atmospheric Imaging Assembly (AIA) onboard the Solar Dynamics Observatory (SDO) and STEREO A observatory and was associated with a halo CME. The CME displayed a strong non-radial motion towards the pole. The eruption started behind the limb, from a circular filament, close to the disk center.

We studied the eruption kinematic, using data from EUVI STEREO A. Additionally, the latitudinal offset of the CME with respect to the erupting filament in the LASCO field-of-view was examined.

### 1. INTRODUCTION

One of the most studied phenomena in solar physics is the eruption of solar prominence or filament, if seen on the disk. They are frequently associated with coronal mass ejections (CMEs). The erupted material can be observed as a bright core of CMEs (Munro et. al (1979); Schmieder et. al (2013); Seki et. al (2021) , and references cited therein). During the CME propagation in the interplanetary space a deflection from the radial direction can be observed in some cases (for example: Zuccarello et. al (2012); Koleva et. al (2024). To comprehend the geoeffectiveness of solar eruptions, it can be essential to investigate the deflection of filament eruption and CMEs.

In this work we present the study of a filament eruption that occurred in the southern solar hemisphere on October 18, 2017. The event was associated with a halo coronal mass ejection and was observed from two space observatories. Here we focused on the associated CME and its offset from the radial propagation. The used data and observations from two points of view are introduced in Section 2. Section 3 provides our results and the short summary is given in Section 4.

### 2. DATA AND OBSERVATIONS

The prominence eruption (PE) occurred at the southern solar hemisphere between 03:36 UT and 06:02 UT on October 18, 2017 in the AIA/SDO field-of-view (FOV). The eruption was associated with a halo CME, observed by SoHO/LASCO coronagraph. The CME displayed a strong non-radial motion towards the pole. The source region of the eruption was located behind the limb and was registered by STEREO A observatory.

For the current study we used data from the following sources:

**1. Solar Dynamics Observatory (SDO):** We used data from Atmospheric Imaging Assembly (AIA: Lemen *et al.* 2012) on board the Solar Dynamics Observatory (SDO: Pesnell *et al.* 2012) in 304 Å channel.

**2. Large Angle Spectroscopic Coronagraph (LASCO):** To study the associated CME and its non-radial motion, images obtained by the Large Angle and Spectrometric Coronagraph (LASCO) (Brueckner *et al.* 1995) onboard the Solar and Heliospheric Observatory (SOHO; Domingo *et al.* 1995) were also analyzed. LASCO has two working coronagraphs, namely, C2 and C3 that observe the Sun in white light from 2.5 to 30  $R_{\odot}$ .

To determine the CME position angle (PA) we also used the CME Catalog available online at the Coordinated Data Analysis Workshop (CDAW) Data Center (Yashiro *et al.* 2004; Gopalswamy *et al.* 2009) and the measuring tool therein.

**3. Solar Terrestrial Relations Observatory Ahead (STEREO A):** The filament eruption behind the limb was analyzed by observations in the 304 Å channel of the Extreme Ultraviolet Imager (EUVI) onboard STEREO Ahead (A) spacecraft (STEREO A: Kaiser *et al.* 2008).

### 3. RESULTS

Two distinct perspectives were used to examine the observed eruption and related CME. The results from our analysis are presented as follows:

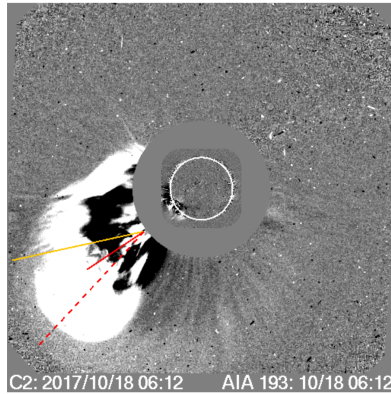


Figure 1: SOHO/LASCO/C2 and AIA/SDO 193 Å composite image at 06:12 UT. The initial PE direction is indicated by a yellow line. The CME PA at 05:48 UT and 06:12 UT are shown by red and dashed red lines, respectively.

#### 3. 1. SDO FOV

The eruption started in AIA FOV at 03:36 UT at PA of  $108^{\circ}$  and was associated with a halo CME. The CME first appearance at the LASCO/C2 field of view was at 05:48 UT and had a linear speed of 1576 km/s. The initial PA of the PE is taken from the Catalog of Prominence Eruptions compiled from SDOs Atmospheric Imaging Assembly in the 304 Å passband (Yashiro *et al.* 2020).

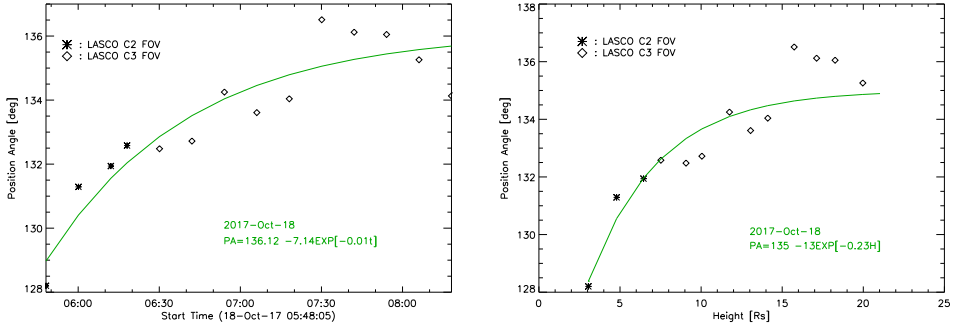


Figure 2: *left*: Variation of the position angle of CME nose as a function of time. Stars and diamonds represent measurements, respectively from C2, and C3 coronagraphs of SOHO/LASCO. *right*: CME PA at various heliocentric distances.

During the next 2 hr and 36 min, the CME nose and the prominence underwent a significant poleward deflection to PA of about  $137^\circ$ . Figure 1 shows the latitudinal offsets between the initial PE direction (indicated by a yellow line) and the CME PA at two different time. The PA offset between the initial PE location and the CME nose was  $29^\circ$  to the pole.

In Figure 2 the variation of the position angle of CME core and nose as a function of time (*left*) and heliocentric distances (*right*) are presented. The measurements were made in the FOV of LASCO/C2 and LASCO/C3 coronagraphs. The solid lines are the fit to data points. It is evident from the figure that non-radial motion gradually decreased and stopped at about  $10 R_\odot$ .

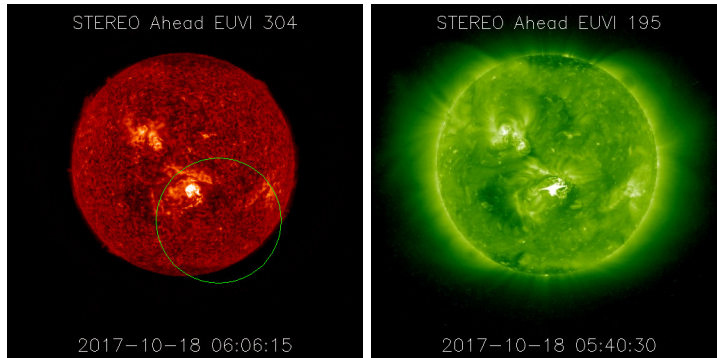


Figure 3: Images from EUVI A in the  $304 \text{ \AA}$  channel (*left*) and  $195 \text{ \AA}$  channel (*right*), showing the filament eruption and the flare. The green circle marks the filament eruption.

### 3. 2. STEREO A FOV

The source region of the eruption was located behind the limb and was well observed by STEREO A observatory. At the time of observation the separation angle of the STEREO A spacecraft with Earth was  $125.617^\circ$ .

In quiet state the filament behind the limb represented a circular filament and was linked to the solar flare (Figure 3).

In Figure 4 two snapshots of eruption evolution as observed in  $304 \text{ \AA}$  channel from EUVI instrument onboard the STEREO A observatory are presented.

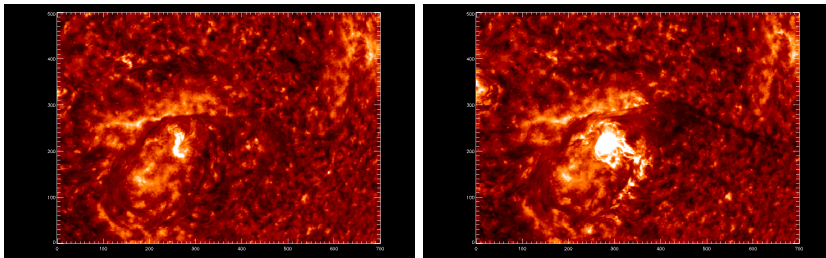


Figure 4: Eruption evolution as observed in EUVI A in the  $304 \text{ \AA}$  channel at 05:23 UT (*left*) and 06:11 UT (*right*).

## 4. SUMMARY

We analyzed the filament eruption, occurring in the southern solar hemisphere on October 18, 2017. The event was observed by the Solar Dynamics Observatory and STEREO A observatory and was associated with a halo CME and solar flare. The CME displayed a strong non-radial motion towards the pole.

We focused mainly on the latitudinal offset between the prominence location and CME propagation. PA offset between the initial PE location and the CME nose was  $29^\circ$  to the pole. The deflection stopped at about  $10 R_\odot$ .

### Acknowledgements

Financial support from the Bulgarian Academy of Sciences (Bilateral grant agreement between BAS and Astronomical Observatory, Belgrade) is gratefully acknowledged.

### References

- Brueckner, G. E., et al.: 1995, *Sol. Phys.*, **162**, 357, doi: 10.1007/BF00733434  
 Domingo, V., Fleck, B., & Poland, A. I.: 1995, *Sol. Phys.*, **162**, 1, doi: 10.1007/BF00733425  
 Gopalswamy, N., Yashiro, S., Michalek, G., et al.: 2009, *EM&P*, **104**, 295, doi: 10.1007/s11038-008-9282-7  
 Kaiser, M.L., Kucera, T.A., Davila, J.M., et. al.: 2008, *Space Sci. Rev.*, **136**, 5, doi: 10.1007/s11214-007-9277-0  
 Koleva, Kostadinka; Gopalswamy, Nat; Devi, Pooja, et al.: 2024, *ApJ*, **966**, 22, doi: 10.3847/1538-4357/ad2df3  
 Lemen, J. R., et al.: 2012, *Sol. Phys.*, **275**, 17, doi: 10.1007/s11207-011-9776-8  
 Munro, R. H., Gosling, J. T., Hildner, E., et. al.: 1979, *Sol. Phys.*, **61**, 201, doi: 10.1007/BF0155456  
 Pesnell, W. D., Thompson, B. J., & Chamberlin, P. C.: 2012, *Sol. Phys.*, **275**, 3, doi: 10.1007/s11207-011-9841-3

- Seki, Daikichi; Otsuji, Kenichi; Ishii, Takako T. et. al.: 2021, *EP&S*, **73**, 58, doi: 10.1186/s40623-021-01378-4
- Schmieder, B., Démoulin, P., Aulanier, G.: 2013, *AdSpR*, **51**, 1967, doi: 10.1016/j.asr.2012.12.026
- Yashiro, S., Gopalswamy, N., Michalek, G., et al.: 2004, *JGRA*, **109**, A07105, doi: 10.1029/2003JA010282
- Yashiro, S., Gopalswamy, N., Akiyama, S., & Mäkelä, P. A.: 2020, *JASTP*, **205**, 105324, doi: 10.1016/j.jastp.2020.105324
- Zuccarello, F. P., Bemporad, A., Jacobs, C., et. al.: 2012, *ApJ*, **744**, 66, doi: 10.1088/0004-637X/744/1/66



## X-RAY HARDNESS RATIO AND MID-INFRARED PARAMETERS FOR AGNS

M. D. LAKIĆEVIĆ<sup>1</sup> , J. KOVAČEVIĆ-DOJČINOVIĆ<sup>1</sup>  and L. Č. POPOVIĆ<sup>1,2</sup> 

<sup>1</sup>*Astronomical Observatory, Volgina 7, 11060 Belgrade, Serbia*  
*E-mail: mlakicevic@aob.rs*

<sup>2</sup>*Department of Astronomy, Faculty of Mathematics,*  
*Studentski trg 16, 11000 Belgrade, Serbia*

**Abstract.** We use the resulting parameters of the two different model decompositions of mid-infrared (MIR) spectra of 1) active and star-forming galaxies and 2) active galactic nuclei (AGN). These resulting parameters are the AGN, polycyclic aromatic hydrocarbons – PAH, H II and stellar contribution components, silicate contribution, etc. It is found that some of these parameters correlate with X-ray hardness ratios (especially *HR1*). This reveals the insight in the X-ray energy bands that influence the MIR parameters and it can point to the AGN sources that are more obscured. These correlations indicate the high attenuation of soft X-ray radiation by the dust.

### 1. INTRODUCTION

Studying correlations between X-ray and mid-infrared (MIR) spectral parameters for active galactic nuclei (AGNs) is crucial for our understanding of a wide range of astrophysical phenomena, from the physics and properties of individual objects to the broader cosmological context. X-rays are emitted from the hot, inner regions close to the black hole; soft X-rays (<10eV) are often associated with thermal processes, such as thermal bremsstrahlung emission from hot plasma or blackbody radiation from accretion disks around compact objects like black holes or neutron stars. The hardness ratios (HRs) are often used as a tool for classifying different types of AGNs, and as indicators for the attenuation: higher absorption tends to attenuate soft X-rays more strongly than hard X-rays, resulting in a harder spectrum. MIR emission often originates from the dusty torus, or from the host galaxy. MIR parameters are often used to estimate the star formation, nuclear activity, or the amount of AGN obscuration (Hernán-Caballero & Hatziminaoglou 2011, here H11). In this work we will compare silicate features as well as AGN contribution to MIR spectra obtained on the two different methods with X-ray HRs.

### 2. DATA AND METHODS

X-ray survey (4XMM-DR13 – from the catalogue Webb et al. 2020<sup>1</sup>) contains data for 550.124 unique sources, in following bands: Flux1: 0.2–0.5keV band, Flux2: 0.5–1.0keV, Flux3: 1.0–2.0keV, Flux4: 2–4.5keV, Flux5: 4.5–12keV, Flux8: 0.2–12keV and Flux9: 0.5–4.5keV. From these fluxes, they calculate HRs ratios using formula

<sup>1</sup>[http://xmmssc.irap.omp.eu/Catalogue/4XMM-DR13/4XMM\\_DR13.html](http://xmmssc.irap.omp.eu/Catalogue/4XMM-DR13/4XMM_DR13.html)

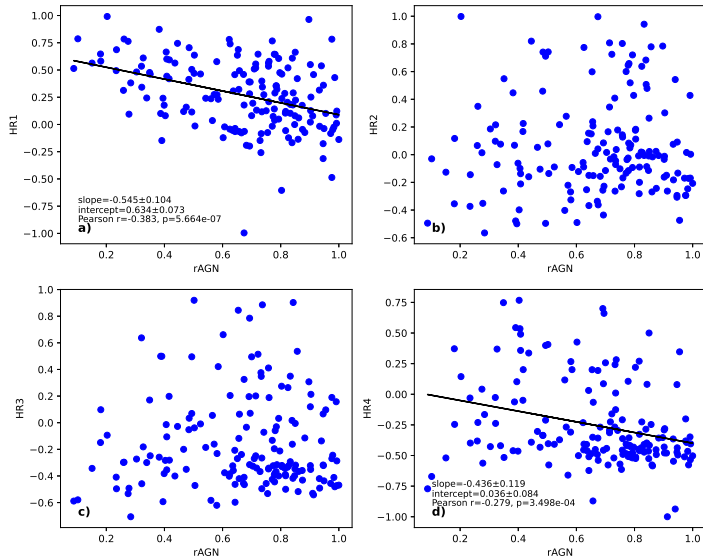


Figure 1: Dependence of AGN fraction in MIR spectra of the four hardness ratios (first dataset, from H11).

$HR_{1,2} = (F_2 - F_1) / (F_2 + F_1)$ , where adopted  $HR1 = HR_{1,2}$ ,  $HR2 = HR_{2,3}$ ,  $HR3 = HR_{3,4}$  and  $HR4 = HR_{4,5}$ .

We used the results of the two different decomposition analysis of MIR AGN *Spitzer IRS* spectra from the works of H11 and Hernán-Caballero et al. 2015 – here H15. The H11 dataset contains measurements of the strength of the silicates in emission/absorption (*Sil*), and decomposition of spectra to HII, Photodissociation Regions (PDRs) and AGN contributions, rAGN, rHII and rPDR for 739 star-forming and active galaxies. rPDR is measurement of PAHs in galaxies. *Sil* is well correlated with optical depth. The H15 dataset contains spectral decomposition of 118 spectra of local AGNs. Similarly as in the first decomposition, the results are measurements of *Sil*, rAGN, rPAH and rSTR (AGN, PAHs and stellar contributions).

The objects from the two MIR datasets (H11 and H15) were crossmatched with X-ray data and 176 sources are obtained for the first, and 98 objects for the second crossmatch, respectively.

### 3. RESULTS

As we can see in the Fig. 1, for H11 dataset: rAGN depends significantly on the *HR1*, although there is slight dependence on *HR4*, too. Likewise, we found the significant dependence of the *Sil* on the *HR1*, *HR3* and *HR4* (Fig. 2). Similar is for H15 dataset: rAGN depends on the *HR1*, while the correlations with other HRs are missing (Fig. 3). Here, *Sil* depends on the *HR1* and *HR4* (Fig. 4). In both samples *HR1* is mostly correlated with *Sil* and with rAGN parameter.



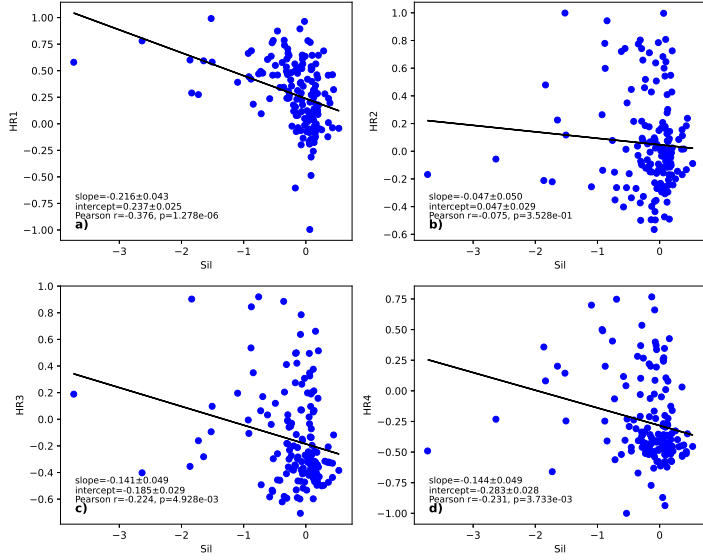


Figure 2: Dependence of silicate feature in MIR spectra of the four hardness ratios (first dataset, from H11).

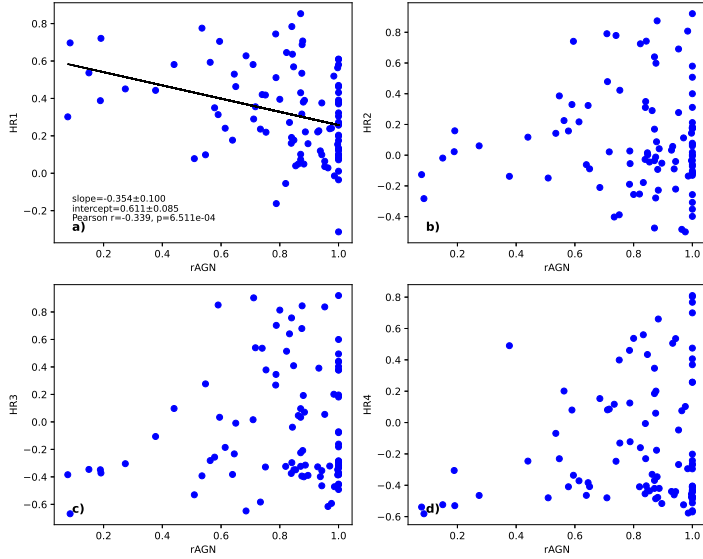


Figure 3: Dependence of AGN fraction in MIR spectra of the four hardness ratios (second dataset, from H15).

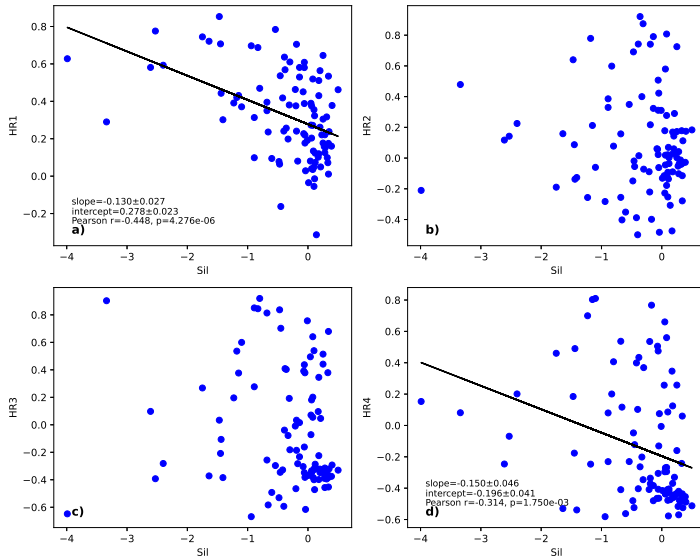


Figure 4: Dependence of silicate feature in MIR spectra of the four hardness ratios (second dataset, from H15).

#### 4. SUMMARY

We explored the correlations of HRs with *Sil* and rAGN for the two different datasets. *HR1* is always correlated with both of those parameters, while *HR3* and *HR4* are sometimes correlated with *Sil* and/or rAGN. Therefore, *HR1* is the most connected with MIR spectroscopic parameters. The trend between rAGN and *HR1* can be explained by the dust attenuation: higher absorption tends to attenuate soft X-rays more strongly than hard X-rays, therefore objects with low AGN contribution have a harder spectra (larger *HR1*). *Sil*-*HR* trend that we noticed is the consequence of known fAGN-*Sil* relation (H15).

#### Acknowledgements

This work is supported by the Ministry of Science, Technological Development and Innovations of R. Serbia, through project of Astronomical Observatory Belgrade (contract 451-03-47/2023-01/200002). This research has made use of data obtained from the 4XMM XMM-Newton serendipitous source catalogue compiled by the XMM-Newton Survey Science Centre consortium. Part of the analysis presented in this work was done with *TOPCAT*<sup>2</sup>, developed by M. Taylor.

#### References

- Hernán-Caballero, A. & Hatziminaoglou E. 2011, *Monthly Notices of the Royal Astronomical Society*, **414**, 500, doi: 10.1111/j.1365-2966.2011.18413.x
- Hernán-Caballero, A., Alonso-Herrero A., Hatziminaoglou E. et al. 2015, *The Astrophysical Journal*, **803**, 109, doi: 10.1088/0004-637X/803/2/109
- Webb, N. A., Coriat, M., Traulsen, I. et al. 2020, *Astronomy & Astrophysics*, **641**, 136, doi: 10.1051/0004-6361/201937353

<sup>2</sup><http://www.star.bris.ac.uk/mbt/topcat/>

## THE NEW 60-CM TELESCOPE OF THE SHUMEN UNIVERSITY ASTRONOMICAL CENTER

D. MARCHEV<sup>1</sup>, B. BORISOV<sup>1</sup>, S. IBRYAMOV<sup>1</sup>, T. ATANASOVA<sup>1</sup>,

G. YORDANOVA<sup>2</sup>, N. PAVLOVA<sup>2</sup> and A. GEORGIEV<sup>1</sup>

<sup>1</sup>*Department of Physics and Astronomy, University of  
Shumen, 115 Universitetska, 9700 Shumen, Bulgaria*

*E-mail: d.marchev@shu.bg*

<sup>2</sup>*Faculty of Mathematics and Computer Science, University  
of Shumen, 115 Universitetska, 9700, Shumen, Bulgaria*

**Abstract.** We present the 60-cm Ritchey-Chretien telescope of the Shumen University Astronomical Center (Fig.1) and its equipment allowing remote-controlled observations. We found that the unit is appropriate for observations of different types of stars up to 17 mag with precision better than 0.02 mag for short exposures. The fainter stars would require exposures in the order of several minutes. We determine the transformation equations for transfer to standard Sloan  $g'$ ,  $r'$ ,  $i'$  photometric system and standard set of UBVRI filters with response curves close to those listed in Bessell (1990).

We briefly describe the telescope assembly process and calibration procedures. The telescope will mainly be used for photometric observations of variable stars and finally, we present the first observational results gathered with the new instrument.

### 1. INTRODUCTION

The Astronomical Observatory of Shumen University (AOShU) is the newest one in Bulgaria Kjurkchieva (2017). There are two telescopes for professional astronomical observations, 40-cm and 60-cm. The first light of the 40-cm telescope was taken in late 2017 Kjurkchieva et. al. (2020), and the first light of the new 60-cm telescope was made in mid-2023. This paper presents information about the equipment of the 60-cm telescope, the realization of remote control and the first results based on observations by this unit.

### 2. THE 60-cm TELESCOPE AND ITS EQUIPMENT

The 60-cm Ritchey-Chretien ASA RC600 (Fig. 1) is located in the 4-m Scope-Dome. The ASA DDM200 equatorial mount is fixed on a custom pole specially designed for the latitude of the observatory. The diameter of the telescope's main mirror is 60 cm. Its focal length is 4200 mm with a relative aperture of f/7. The main detector is an SBIG Aluma AC4040 a large format Scientific CMOS camera, featuring a 16.8 megapixel sensor ( $4096 \times 4096$  pixels) with 9 micron pixels.

The presence of a focal reducer (x0.64) makes the field of view  $47 \times 47$  arcmin and the corresponding resolution is 0.69 arcsec/pixel. The telescope is equipped with an AFW-10-50SQ filter wheel with squared 50-mm Sloan filters  $g'$ ,  $r'$ ,  $i'$ , narrow-band filters  $H\alpha$  and also with a standard set of UBVRI filters with response curves



Figure 1: 60-cm Ritchey-Chretien telescope of the Shumen University

close to those listed in Bessell (1990). The remote control of the telescopes gives a possibility for more effective usage of the observational time and saving of human time, efforts and financial resources Iliev (2014). Remote-controlled small telescopes have provided the huge ground-based wide-field surveys: ASAS (Pojmanski 1997), ROTSE (Akerlof 2005), Super-WASP (Pollacco et al. 2006), CRTS (Drake et al. 2014), etc. They are able to discover variable stars, exoplanets, transient and other interesting celestial objects, as well as to carry out follow-up observations of most of them. The ASA-provided software, as well as the purchased TheSky 10Pro and MaXimDL 7.0, provide remote viewing of the telescope, dome, camera and filter unit.

### 3. OBSERVATIONS

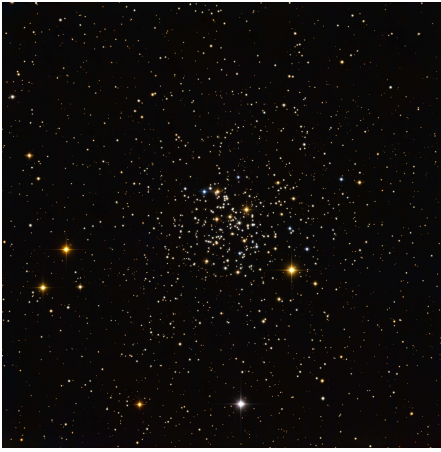
One of the first observations was of the open cluster M67 (Fig.2a) in order to determine the transformation coefficients of the system. The transformation coefficients are determined by the following formulas.

$$B_{var(transf)} = b_{var} - b_{comp} + T_{b-bv} * T_{bv} * [(b_{var} - v_{var}) - (b_{comp} - v_{comp})] + B_{comp} \quad (1)$$

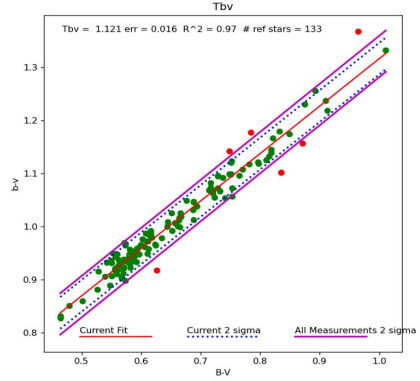
$$V_{var(transf)} = v_{var} - v_{comp} + T_{v-bv} * T_{bv} * [(b_{var} - v_{var}) - (b_{comp} - v_{comp})] + V_{comp} \quad (2)$$

$$R_{var(transf)} = r_{var} - r_{comp} + T_{r-vr} * T_{vr} * [(v_{var} - r_{var}) - (v_{comp} - r_{comp})] + R_{comp} \quad (3)$$

$$I_{var(transf)} = i_{var} - i_{comp} + T_{i-vi} * T_{vi} * [(v_{var} - i_{var}) - (v_{comp} - i_{comp})] + I_{comp} \quad (4)$$



(a) The open cluster M67 photographed with the 60-cm telescope on 03.03.2024 (BVRI-filters).



(b) The graph for determining one of the coefficients ( $T_{bv}$ )

Figure 2: About the transformation coefficients

Standard software of the AAVSO was used. Figure 2b illustrates the method for determining the coefficients. The obtained coefficients are shown in Table 1.

The symbiotic star T CrB has been observed in the last three months and it is expected to explode soon. Figure 3 shows the latest BVRI photometry of the star from 03.09.2024.

Table 1: Transformation coefficients with a set of BVRI filters.

Name	Value	Error
$T_{bv}$	1.121	0.016
$T_b - b_v$	0.091	0.013
$T_{br}$	1.136	0.012
$T_b - b_r$	0.063	0.009
$T_b - b_i$	0.060	0.007
$T_{bi}$	1.097	0.012
$T_v - b_v$	-0.035	0.011
$T_{vr}$	1.156	0.015
$T_v - v_r$	-0.066	0.021
$T_r - v_r$	-0.194	0.021
$T_{ri}$	0.984	0.028
$T_r - r_i$	-0.282	0.021
$T_i - r_i$	-0.250	0.037
$T_{vi}$	1.048	0.016
$T_v - v_i$	-0.051	0.012
$T_i - v_i$	-0.081	0.017
$T_r - v_i$	-0.113	0.011

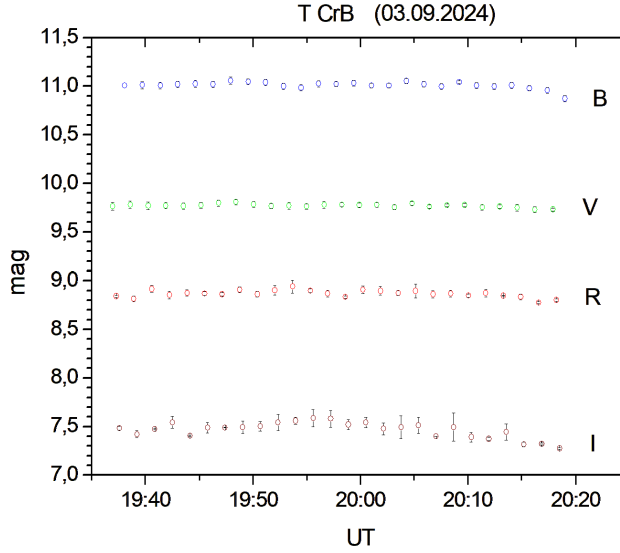


Figure 3: BVRI photometry of the T CrB from 03.09.2024

#### 4. SUMMARY

The system allows accurate photometry of stars down to magnitude 17. The large field (near a degree) is very convenient for variable star photometry. Precise aiming and good mount guidance allow for long exposures. These features of the system expand the range of tasks that can be worked on.



#### Acknowledgements

The research was supported partly by projects RACIO funded by the Ministry of Education and Science of Bulgaria (support for the Bulgarian National Roadmap for Research Infrastructure), as well as by project RD-08-137/2024 of Shumen University. We express our gratitude to V. Popov for the processing and presentation of images in true colors obtained with the presented telescope, as well as to M. Minev for help in determining the photometric error.

#### References

- Bessell, M.S.: 1990, *PASP*, **102**, 1181, doi: 10.1086/132749  
 Iliev, I.: 2014, *CoSka*, **43**, 169  
 Kjurkchieva, D.: 2017, *Astronomical Calendare 2018*, p.87, ISSN 0861-1270  
 Kjurkchieva, D., Marchev, D., Borisov, B., Ibryamov, S., Dimitrov, D., Popov, V., Milev, Al., Petrov, N.: 2020, *Bulgarian Astronomical Journal*, **32**,113

## MULTI-BAND INTRA-NIGHT VARIABILITY OF THE BLAZAR CTA 102 DURING ITS 2016 DECEMBER OUTBURST

B. M. MIHOV  and L. S. SLAVCHEVA-MIHOVA 

*Institute of Astronomy and NAO, Bulgarian Academy of  
Sciences, 72 Tsarigradsko Chaussee Blvd. 1784 Sofia, Bulgaria  
E-mail: bmihov@astro.bas.bg*

**Abstract.** During 2016 December the blazar CTA 102 underwent an unprecedented outburst thus becoming the brightest blazar observed up to date. We present some results from the intra-night monitoring of the blazar in the *BVRI* bands in three consecutive nights during the outburst.

### 1. INTRODUCTION

The blazar class of active galactic nuclei involves BL Lacertae objects and flat-spectrum radio-quasars. Violent variability across the electromagnetic spectrum is among their main characteristics. In particular, variability time scales could provide valuable information about the emitting region parameters.

The flat-spectrum radio-quasar CTA 102 ( $z = 1.032 \pm 0.003$ ) underwent an unprecedented outburst in 2016 December reaching an *R* band magnitude of  $10.82 \pm 0.04$  thus becoming the brightest blazar up to date. The outburst was monitored by the GASP–WEBT collaboration, and the results were published in Raiteri et al. (2017).

We perform temporal analysis of the multi-band intra-night variations of CTA 102 during the outburst with the aim to derive some physical parameters of the emitting regions.

### 2. OBSERVATIONS AND PHOTOMETRY

We monitored CTA 102 in the *BVRI* bands on 2016 December 3<sup>rd</sup> to 5<sup>th</sup> for about 4 hours per night using the 50/70 cm Schmidt telescope of the Rozhen NAO, Bulgaria, and the FLI PL18603 CCD camera (Kostov 2010).

The aperture photometry of the blazar, a control star (a field star of compatible brightness), and a couple of GASP–WEBT suggested reference stars was performed by means of DAOPHOT. The aperture radii were set to 2 or 3 times the FWHM. The light curves (LCs) for the nights of monitoring are shown in Figure 1. Some characteristics of the obtained intra-night data sets are listed in Table 1.

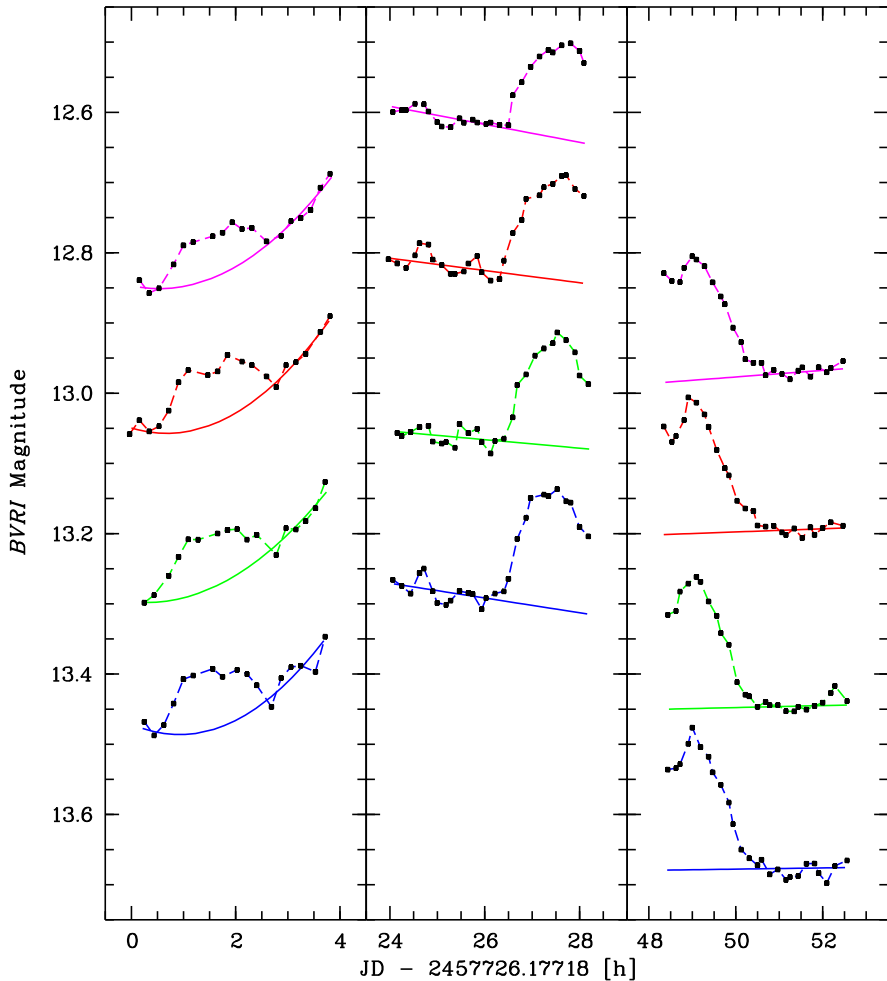


Figure 1: Light curves of CTA 102 in  $BVRI$  bands (ordered from bottom to top, respectively) for the nights of monitoring. The  $VRI$  band LCs are shifted down by 0.40, 0.59, and 0.94 mag, respectively, for a better display. The error bars are not shown, their sizes are comparable with the symbol sizes. The solid lines depict the fits to the smooth variability component for each band and night.

### 3. RESULTS AND DISCUSSION

The object showed brightness variations in the range 0.1–0.2 mag over all three nights. During the first night, the variability pattern revealed two components – we observed low-amplitude flares, best separated in the  $R$  band, superimposed onto a smooth trend with a time scale longer than the monitoring duration. In spite of their low amplitude, we shall consider the flares real since they can be traced in all bands.

The second night started with a weakly decreasing trend with some fluctuations superimposed. Over the second part of the night a flaring event was observed (i.e. there was a two-component variability pattern again). The close inspection of the



Table 1: Characteristics of the intra-night data sets.

Date in 2016	Band	Monitoring Duration [h]	Time Sampling [min]	Wtd Mean Magnitude [mag]	Wtd RMS Scatter [mag]	Variability Amplitude [%]	Fractional Variability
Dec 3	<i>B</i>	3.47	12.1	13.417	0.036	14.000	0.033
	<i>V</i>	3.47	12.1	12.815	0.038	17.186	0.030
	<i>R</i>	3.79	12.1	12.396	0.044	16.780	0.032
	<i>I</i>	3.68	12.1	11.840	0.041	17.000	0.026
Dec 4	<i>B</i>	4.08	9.4	13.242	0.060	17.027	0.065
	<i>V</i>	4.07	9.4	12.620	0.056	17.188	0.059
	<i>R</i>	4.07	9.4	12.187	0.052	14.972	0.057
	<i>I</i>	4.07	9.4	11.637	0.044	11.892	0.052
Dec 5	<i>B</i>	4.09	9.4	13.613	0.075	22.096	0.071
	<i>V</i>	4.10	9.4	12.980	0.072	19.132	0.068
	<i>R</i>	4.09	9.4	12.538	0.071	19.976	0.068
	<i>I</i>	4.09	9.4	11.965	0.066	17.490	0.065

*Note.* The fractional variability is computed for the deboosted LCs (see Section 3).

event revealed a very close superposition of two flares.

During the third night, we observed a flare followed by an almost constant flux level. At the beginning a flux fluctuation was detected, which pointed to preceding variations.

Generally, the intra-night variability pattern reveals two components – a smoothly varying component<sup>1</sup>, characterized by a time scale longer than the monitoring duration<sup>2</sup> and a flaring component consisting of one or more flaring events, each characterized by a time scale shorter than the monitoring duration.

In order to get more accurate flare parameters, one needs to remove the smooth component, that is, to do a detrending (see Agarwal et al. 2023 for detailed discussion and examples). For each night, we fitted a first or second degree polynomial to the LC data points, which we assume to belong to the smooth, low-frequency component. For a given night, the degree of polynomial and the fitting interval(s) are one and the same for all bands. The fits are shown in Figure 1. They are used to detrend the corresponding LCs under the assumption that the smooth component is of geometric origin, that is, we actually did a deboosting. Before that, the dereddened<sup>3</sup> LCs and polynomials were transformed to fluxes using the zero-points of Bessell et al. (1998). After the deboosting, the flux variations are characterized by a single, but unknown value of the Doppler factor (Figure 2).

We built  $(m_B - m_I)$  against  $m_R$  colour-magnitude diagrams for all nights of monitoring. For the first night, we found no significant chromatism (a linear Pearson correlation coefficient  $r = -0.408$  and a probability to get such a coefficient by chance  $p = 0.104$ ). For the third night, we got a significant bluer-when-brighter (BWB) chromatism ( $r = 0.747$  and  $p = 0.00001$ ).

<sup>1</sup>Actually, this component represents inter-night (or night-to-night) blazar variability.

<sup>2</sup>We assume that in general, the monitoring lasts over the whole night.

<sup>3</sup>Galactic extinctions are taken from NED:  $\{A_B, A_V, A_R, A_I\} = \{0.261, 0.198, 0.156, 0.108\}$  mag.

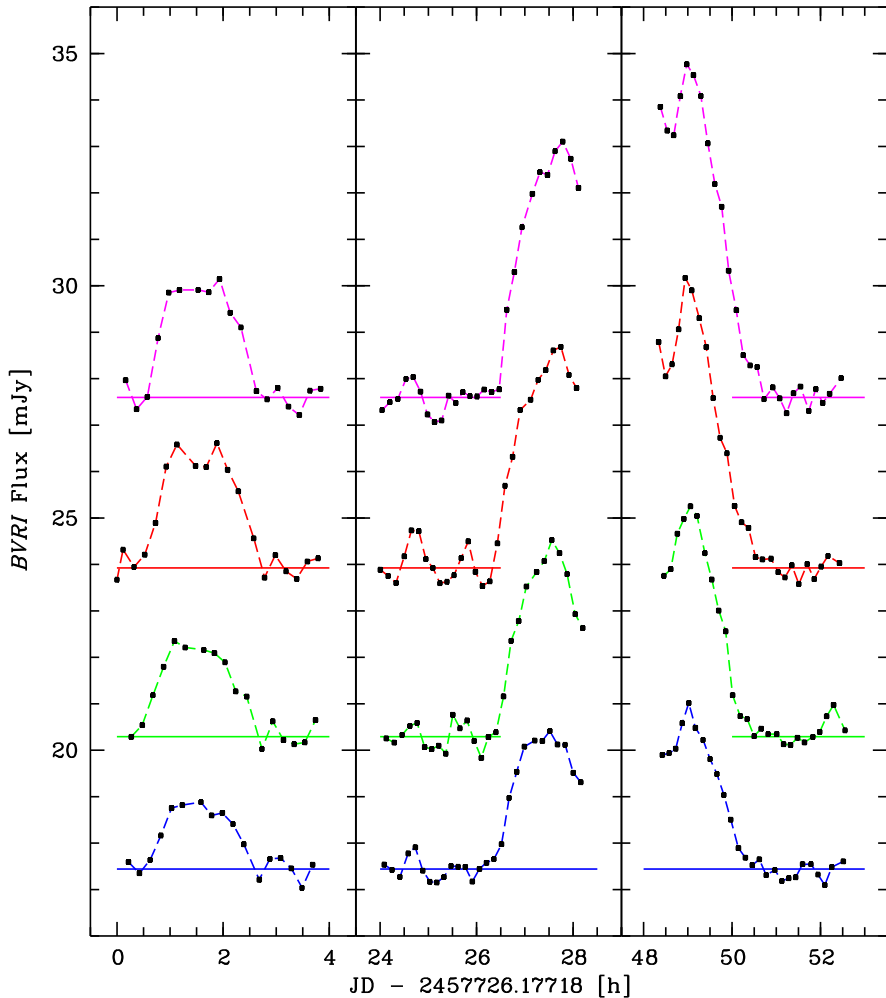


Figure 2: Deboosted *BVRI* band LCs (from bottom to top, respectively). Horizontal lines mark the baseline flux level. The *VRI* band LCs are shifted down by 6, 8, and 13 mJy, respectively, for a better display.

The second night is most intriguing – in addition to the significant BWB chromatism ( $r = 0.598$  and  $p = 0.001$ ), we detected a clockwise spectral hysteresis loop (the BWB and redder-when-fainter trends form a crude ellipse, Figure 3). This is an indication of evolution of the electron energy distribution owing to acceleration and cooling processes.

Let us assume that the flares observed on December 4<sup>th</sup> are produced by a shock hitting small inhomogeneities/turbulent cells within the jet. This leads to acceleration of electrons at the shock front followed by their cooling in the post-shock region via synchrotron and inverse Compton radiation. The electrons lose half of their energy

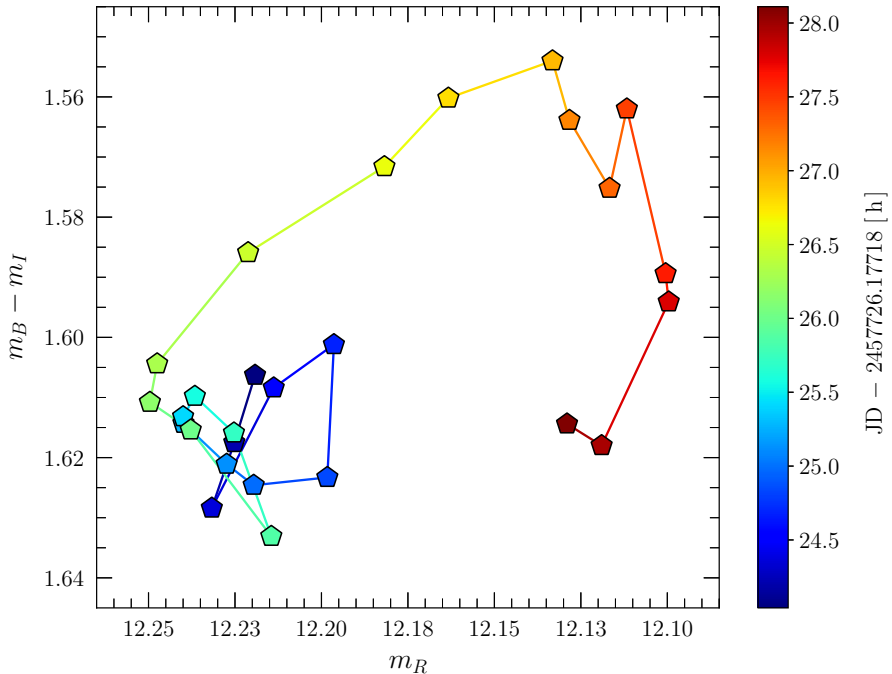


Figure 3: Colour-magnitude diagram for December 4<sup>th</sup>. A clockwise spectral hysteresis loop can be traced. The different colours denote the different observing times as indicated on the right.

within the cooling time,  $t_{\text{cool}}(\nu)$ :

$$t_{\text{cool}}(\nu) \simeq \frac{4.73 \times 10^4}{1+q} \mathcal{B}^{-3/2} \nu_{15}^{-1/2} \left( \frac{\delta}{1+z} \right)^{-1/2} \quad [\text{s}], \quad (1)$$

where  $\nu_{15}$  is the observed photon frequency (in units of  $10^{15}$  Hz,  $\nu = 10^{15} \nu_{15}$  Hz),  $\mathcal{B}$  is the co-moving magnetic field strength (in units of Gauss),  $\delta$  is the Doppler factor, and  $q$  is the Compton dominance parameter. The latter is the ratio of the co-moving energy densities of the radiation and magnetic fields,  $q = U'_{\text{rad}}/U'_{\mathcal{B}}$ . In the framework of this scenario, the clockwise spectral hysteresis arises when the synchrotron cooling time dominates over the acceleration and light-crossing times (Kirk et al. 1999). In addition, time lags between the flux variations in different bands should be expected – the electron Lorentz factor evolves as  $\dot{\gamma}_e \propto -\gamma_e^2$  and, therefore, the most energetic electrons are cooled first followed by the less energetic ones, thereby resulting in the so called soft time lag.

A detailed analysis of the CTA 102 variability will be presented elsewhere.

### Acknowledgements









This research was partially supported by the Bulgarian Ministry of Education and Science under Agreement D01-326/04.12.2023. This research has made use of the NASA/IPAC Extragalactic Database (NED), which is funded by the National Aero-

navitics and Space Administration and operated by the California Institute of Technology.

### References

- Agarwal, A., Mihov, B., et al.: 2023, *The Astrophysical Journal Suppl. Series*, **265**, id.51, doi: 10.3847/1538-4365/acbcbd
- Bessell, M. S., Castelli, F., Plez, B.: 1998, *Astronomy and Astrophysics*, **333**, 231
- Kirk, J. G., Rieger, F. M., Mastichiadis, A.: 1999, *ASP Conference Series*, **159**, 325
- Kostov, A.: 2010, *Proc. of Gaia Follow-up Network for Solar System Objects Workshop* (online at <https://gaiafunso.imcce.fr/workshop/GFSSO-Proceedings-2010.pdf>), 137
- Raiteri, C. M., Villata, M., Acosta-Pulido, J. A., et al.: 2017, *Nature*, **552**, 374, doi: 10.1038/nature24623

## URBAN OBSERVATORY OF BELGRADE (UrbObsBel)

R. PAVLOVIĆ<sup>1</sup> , Z. CVETKOVIĆ<sup>1</sup> , Z. SIMIĆ<sup>2</sup> , G. DAMLJANOVIĆ<sup>2</sup> ,  
S. SAMUROVIĆ<sup>2</sup> , B. ROVČANIN<sup>3</sup> , D. LUKIĆ<sup>1</sup>  and D. BJELAJAC<sup>4</sup> 

<sup>1</sup>*Institute of Physics Belgrade, Pregrevica 118, Belgrade, Serbia*  
*E-mail: rpavlovic@aob.rs*

<sup>2</sup>*Astronomical Observatory, Volgina 7, 11060 Belgrade, Serbia*

<sup>3</sup>*Faculty of Medicine, University of Belgrade, Dr Subotica 8, Belgrade, Serbia*

<sup>4</sup>*Department of Geography, Tourism and Hotel Management University of Novi Sad, Serbia*

**Abstract.** We present the 3-year project of the Urban Observatory of Belgrade, funded by the Science Fund of the Republic of Serbia, a new observing station within the Astronomical Observatory of Belgrade, Serbia. One of the main goals of the project is to measure and study one of the least understood forms of pollution on Earth, light pollution. We also plan to perform observations which will provide information on the distribution of energy consumption, which has a major impact on the environment and ecosystems. Our measurements will be made in Belgrade and also from the Vidojevica Astronomical Station near Prokuplje run by the Astronomical Observatory of Belgrade, one of the few remaining dark areas in Serbia. The results of the project are planned to be used by the Municipality of Zvezdara and the City of Belgrade because these measurements will provide elements for making decisions in the direction of creating a better environment that will improve the health of the population of Belgrade and its surroundings.

### 1. INTRODUCTION

The main goal of the 3-year UrbObsBel (Urban Observatory of Belgrade) project is further improvement and regional integration of the research capacity of the Astronomical Observatory of Belgrade (AOB) through construction of the new facility aimed at urban observations. These observations will provide valuable information on energy usage distribution that have a high impact on the environment and ecosystems. The study addresses an interesting cross-disciplinary topic that connects urbanization, ecology, industry and astronomy. This new infrastructure will be based on several observational instruments which will cover spectral range from visible ( $\sim 400\text{nm}$ ) to infrared ( $\sim 13\mu\text{m}$ ). As one of the premier research institutions in the Western Balkans countries and the South Eastern Europe regions, the AOB is expected to play the key role in the processes of integration of the researchers gathered around space, astronomical, and astrophysical research into the wider European context, as envisioned in the European Research Area concept where the UrbObsBel project will be useful in that respect. The UrbObsBel project started in January 2024.



Figure 1: The project team: left to right, Dr. Dajana Bjelajac, Dr. Dragan Lukić, Dr. Zorica Cvetković, Dr. Srdjan Samurović, Dr. Rade Pavlović, Dr. Branislav Rovčanin and Dr. Zoran Simić. Missing Dr. Goran Damljanović.

## 2. PROJECT TEAM

The project team, see Figure 1, is well-equipped to successfully carry out all tasks of the UrbObsBel project. Each team member possesses the qualifications necessary to achieve the project's scientific objectives. The entire team will actively contribute to every phase of the project, including the design and construction of the Urban Observatory, data collection and analysis, and the dissemination of results. This collaborative approach ensures a comprehensive and cohesive effort toward achieving the project's goals.

The Principal Investigator, Dr. Srdjan Samurović, will manage the formal aspects of the UrbObsBel project, including procurement procedures, import logistics, and report writing, with support from the coordinators of other work packages (WPs). In addition, Dr. Samurović will handle the installation and maintenance of the project server, ensuring seamless operation. He will also supervise and collaborate across all WPs, actively participating in their activities to ensure alignment and smooth execution of project tasks.

Dr. Zorica Cvetković, coordinator of WP2, and Dr. Rade Pavlović, coordinator of WP3, bring extensive expertise in instrumentation and software, making them ideal for handling the technical aspects of the UrbObsBel project. Dr. Cvetković

will oversee the specifications, procurement, installation, and mounting of the necessary hardware and instruments. Dr. Pavlović will manage software installation, maintenance, and data management processes. Additionally, both coordinators will oversee auxiliary observations at the Astronomical Station Vidojevica, operated by the Astronomical Observatory of Belgrade, to ensure seamless support for the projects observational needs.

Dr. Goran Damljanović, the leader of WP4, will apply his expertise to the acquisition and analysis of imagery for the UrbObsBel project.

Dr. Zoran Simić will focus on analyzing observational data and managing data integrity and organization.

Dr. Dragan Lukić has a strong background in experimental atomic, molecular, and optical physics, as well as experience in experimental astrophysics, making him a key contributor to the projects technical and analytical tasks.

Dr. Branislav Rovčanin will participate in observational activities, contribute to data analysis, and assess the impact of light pollution on public health using the data collected.

Dr. Dajana Bjelajac, the leader of WP5, will coordinate dissemination of the results and outreach, leveraging her expertise in light pollution to manage the use and operation of the detector suite acquired for the UrbObsBel project.

This multidisciplinary team brings together diverse expertise to advance the UrbObsBel projects goals effectively.

### 3. CONCEPT AND METHODOLOGY

The proliferation of artificial light at night (ALAN) has introduced a complex form of environmental disruption commonly referred to as light pollution (LP). With electric lighting becoming widespread in the 19th century, artificial light has increasingly impacted ecosystems and human health worldwide. Recent studies, such as the one by Sanchez de Miguel et al. (2022), which utilized data from cameras mounted on the International Space Station from 2012 to 2020, reveal the growing extent of ALAN across the globe.

Light pollution, a subset of environmental pollution, shares this category with other forms like air pollution, noise pollution, and water pollution, among others. LP has both natural and artificial sources, though the latter, generated by human activities, is rising at a troubling rate of 3–6% annually. Although light pollution may seem less immediately harmful compared to other types of pollution, its ecological and physiological impacts are substantial and far-reaching, affecting humans, plants, animals, and microorganisms alike.

Research has shown that nearly two-thirds of the worlds population lives in areas where nighttime light levels exceed natural thresholds. This level of exposure to artificial brightness disrupts not only natural ecosystems but also human health. For example, Falchi et al. (2016) highlighted the cultural and sensory deprivation caused by LP, showing that one-third of the global population cannot view the Milky Way due to excessive artificial lighting. This widespread impact on night-sky visibility underscores the need to understand and mitigate LPs growth and effects comprehensively.

LP poses a substantial threat beyond its impact on astronomy, as it disrupts ecosystems and leads to significant energy wastage. Urban areas, especially large

cities, experience the highest levels of LP, making it critical to map LP sources and identify cases where mitigation efforts could be effective. Initiatives like those by the International Dark-Sky Association aim to create comprehensive global LP maps. This process often involves measuring the brightness of standard stars using Johnson filters and small telescopes equipped with CCD cameras. By determining extinction coefficients in starless areas, researchers can infer overall sky brightness, an approach that also engages the public through educational outreach.

While the study of LP has traditionally received limited attention, the development of specialized photometric instruments has sparked renewed interest among professional astronomers. For instance, Sky Quality Meters (SQMs) provide single-band measurements of night sky brightness (NSB) when pointed at the zenith, offering valuable data for assessing LP's impact on observational conditions. Additionally, digital single-lens reflex (DSLR) cameras equipped with fisheye lenses offer spatially resolved NSB data over a broad, 180-degree field of view and capture light in three spectral channels, giving a more comprehensive view of LP distribution.

In recent years, technological advancements have expanded the range of instruments used to study LP and its environmental effects. Broadband infrared devices and hyperspectral imagers, in particular, have become valuable tools for more detailed LP analysis. These innovations, along with the existing devices, form the foundation of our proposed Urban Observatory, which will enable a more systematic approach to monitoring LP and assessing its multifaceted impacts on both urban and natural environments.

LP problem is especially serious in urban environments. According to the United Nations, today, 55% of the world's population lives in urban areas, and this proportion is expected to increase to 68% by 2050. Therefore, the need to address the problems of ALAN and LP is obvious.

Serbia has many light polluted areas but also the regions with a clear sky (see <https://www.lightpollutionmap.info>). One of the remaining dark spots is the Vidojevica mountain where Astronomical Station run by the Astronomical Observatory of Belgrade is situated. The participants of UrbObsBel played an important role in its construction. The SQM zenith sky brightness there is  $\sim 21.69$  mag/arcsec<sup>2</sup>. We plan to mount some auxiliary instruments there. Belgrade, the capital of Serbia, with 1.7 million inhabitants, is the brightest spot in Serbia with the SQM zenith sky brightness of  $\sim 17.73$  mag/arcsec<sup>2</sup> in its downtown area.

You can see more about the purchased instruments, the data usage, and the first obtained result in this volume in our paper "The UrbObsBel Project: Instruments and Detectors" (Pavlovic et al., 2025).

### Acknowledgements

This research was supported by the Science Fund of the Republic of Serbia, no. 6775, Urban Observatory of Belgrade - UrbObsBel and by the Ministry of Science, Technological Development and Innovations of the Republic of Serbia through the Project contract No. 451-03-66/2024-03/200002.



## References

- Falchi, F., Cinzano, P., Duriscoe, D., Kyba, C.C.M., Elvidge, C.D., Baugh, K., Portnov, B.A., Rybnikova, N.A. & Furgoni, R.: 2016, *Science Advances*, **2**, no. 6, e1600377-e1600377, doi: 10.1126/sciadv.1600377
- Pavlović, R., Cvetković, Z., Bjelajac, D., Damljanović, G., Lukić, D., Rovčanin, B., Samurović, S. & Simić, Z.: 2025, *Publ. Astr. Obs. Belgrade*, **107**, 129, doi: 10.69646/14sbac22p
- Sanchez de Miguel, A., Bennie, J., Rosenfeld, E., Dzurjak, S. & Gaston, K.G.: 2022, *Science Advances*, **8**, Issue 37, eabl6891, doi: 10.1126/sciadv.abl6891



## The UrbObsBel PROJECT: INSTRUMENTS AND DETECTORS

R. PAVLOVIĆ<sup>1</sup> , Z. CVETKOVIĆ<sup>1</sup> , D. BJELAJAC<sup>2</sup> , G. DAMLJANOVIĆ<sup>3</sup> ,  
D. LUKIĆ<sup>1</sup> , B. ROVČANIN<sup>4</sup> , S. SAMUROVIĆ<sup>3</sup>  and Z. SIMIĆ<sup>3</sup> 

<sup>1</sup>*Institute of Physics Belgrade, Pregrevica 118, Belgrade, Serbia*

*E-mail: rpavlovic@aob.rs*

<sup>2</sup>*Department of Geography, Tourism and Hotel Management University of Novi Sad, Serbia*

<sup>3</sup>*Astronomical Observatory, Volgina 7, 11060 Belgrade, Serbia*

<sup>4</sup>*Faculty of Medicine, University of Belgrade, Dr Subotica 8, Belgrade, Serbia*

**Abstract.** Urban Observatory of Belgrade (UrbObsBel) is a project hosted by Astronomical Observatory of Belgrade. Our main aim is to study, applying well-tested astronomical techniques, light pollution and dynamical processes of the Serbian capital, Belgrade. Our observations will provide valuable information on energy usage distribution that has a high impact on the environment and ecosystems. We have already mounted and we are also planning to mount several observational instruments covering spectral range from visible (400 nm) to infrared (13 micron), and use both broadband and hyperspectral imaging systems in our synoptic study. Apart from study of the urban dynamics we intend to use several instruments aimed at the study of sky brightness and various sources of sky pollution such as street lights. This would be achieved mounting identical instruments at Astronomical Observatory of Belgrade (AOB) and at our Astronomical Station at Vidojevica (ASV). Until now we have acquired the following equipment: Web and file server, TESS-W photometer, Unihedron Sky Quality Meter, Hyperspectral Imaging (HSI) devices, FLIR and AllSky Cameras.

### 1. INTRODUCTION

The main task of Urban Observatory of Belgrade (UrbObsBel) project was to mount a suite of imaging systems at the roof of the Tower at Astronomical Observatory of Belgrade (AOB) which is the highest point in the urban part of Serbias capital, Belgrade. Using this excellent position, we plan to measure as many observables as possible relevant for modern urban life and analyze them. Such a synoptic view of the city will provide the possibility to observe the city on various temporal scales, ranging from minutes to months and years. Our location provides a possibility to observe not only the urban zone (center of Belgrade), but also its surroundings, the forests and the river Danube, see Figure 1. You can find much more about the UrbObsBel project in the article Pavlović et al. (2025) or on the website <https://urbobsbel.aob.rs>. The UrbObsBel project started in January 2024 and will last for 3 years.

### 2. INSTRUMENTS AND DETECTORS

The UrbObsBel project began with the procurement of essential instruments for monitoring and studying light pollution (LP) in Belgrade. The instruments are:

- FLIR A700 cameras for thermal imaging,

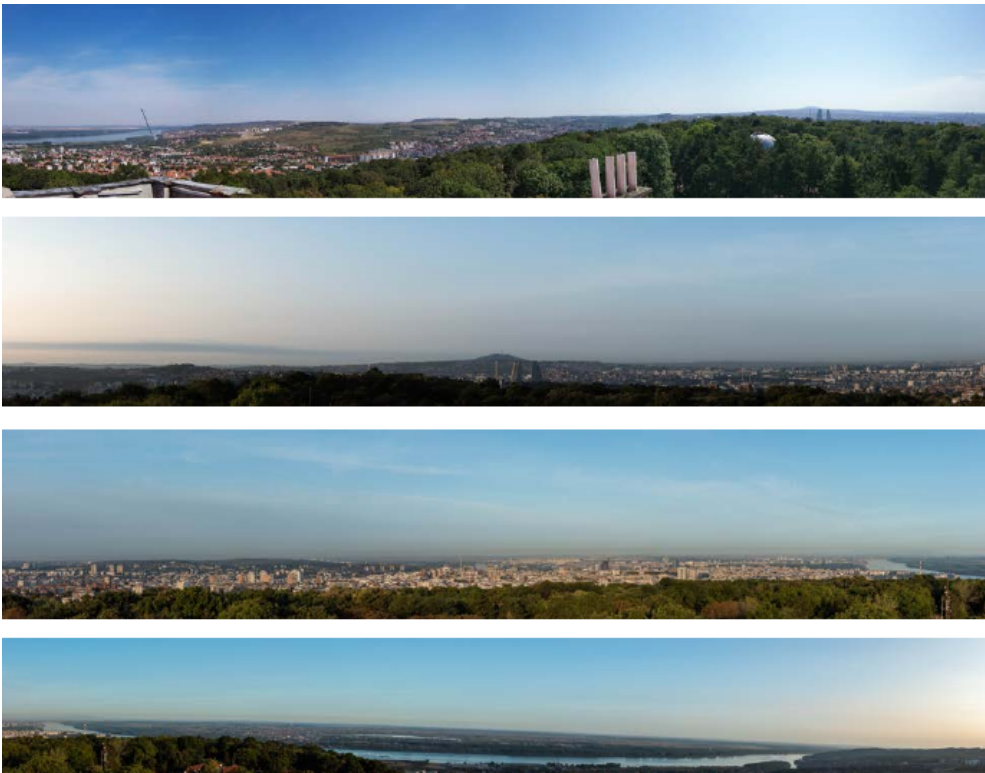


Figure 1: Panoramic view of Belgrade as seen from the top of the AOB Tower. From top to bottom: East, South, West, North. In the panel centered on the South the mountain Avala (elevation 511 m, located 16 km of downtown Belgrade) with the Tower overlooking Belgrade is visible and, in the panels, centered on the East, West and North one can see the river Danube.

- All-sky Camera for comprehensive sky monitoring,
- Sky Quality Meters (SQM) to measure night sky brightness,
- TESS-W Photometers (Telescope Encoder and Sky Sensor with WiFi) for sky condition monitoring,
- VNIR Hyperspectral Imaging Sensors (HSIs) to capture visible and near-infrared spectral data,
- Digital single-lens reflex (DSLR) camera with a fisheye lens and camera mount for panoramic imaging.

These instruments will be housed in a specially constructed, weather-resistant cover, allowing them to operate year-round and provide robust data on LP and environmental dynamics in Belgrades urban setting. Remote sensing will be integral to this approach. Additionally, one SQM and one TESS-W photometer were installed at the Astronomical Station Vidojevica for LP-free sky comparisons.



Figure 2: FLIR camera A700 (left) and All Sky camera Alcor OMEA 3C (right).

To support data storage and analysis, we acquired a dedicated data management server. The new server was located within our ready-to-use server cage at the Astronomical Observatory. Observational data will be archived in the FITS format, widely used in astronomy, and data cubes will be made publicly available upon acquisition.

Data analysis will employ techniques such as image processing, machine learning, computer vision, and specialized astronomical analysis, including Principal Component Analysis (PCA) as demonstrated by Dobler et al. (2021). Satellite data, including SENTINEL<sup>1</sup>, GOES<sup>2</sup>, and AQUA<sup>3</sup>, will complement the projects ground-based observations, offering a broad perspective on LP and environmental dynamics across various scales.

Teledyne **FLIR A700**<sup>4</sup> infrared camera (Figure 2, left) offer researchers and engineers a streamlined solution for accurate temperature measurement. It has IR resolution  $640 \times 480$  pixels, detector pitch  $12 \mu\text{m}$ , spectral range from  $7.5$  to  $14.0 \mu\text{m}$  and temperature sensitivity of  $\pm 2^\circ$ . We will also utilize two FLIR broadband infrared cameras simultaneously, positioning one toward the urban area and the other toward the surrounding areas of Belgrade, which are primarily covered with trees and grass. This setup will allow us to investigate the influences of factors such as weather, public holidays, major events, and construction sites within the spectral range of cameras.

**All Sky Camera** Alcor OMEA 3C<sup>5</sup> (Figure 2, right) is intended to monitor the entire sky in day and night conditions in a continuous manner. It is possible to assess, in real time, the night sky quality and record fast phenomena such as meteors and fireballs or slower ones such as artificial satellites, rockets, noctilucent clouds, airglow. This camera has a detector resolution of  $3100 \times 2100$  pixels,  $180^\circ \times 180^\circ$  field of view and pixel scale of  $5.4$  arcmin/pixel. For addressing the important issue of clouds, we plan to also use the wide-angle all-sky cameras (one is already installed at Vidojevica) and the latest machine learning algorithms (e.g., Mommert 2020) for estimates of the cloud coverage at any given time. It was shown that cloud coverage not only “dramatically amplifies the sky luminance” in urban areas (Kyba et al. 2011), but might also highly affect rural areas as well (Jechow et al. 2019).

<sup>1</sup><https://www.sentinel-hub.com>

<sup>2</sup><https://web.archive.org/web/20050905030322/http://www.oso.noaa.gov/goes/index.htm>

<sup>3</sup><https://aqua.nasa.gov/>

<sup>4</sup><https://www.flir.eu>

<sup>5</sup>[https://www.alcor-system.com/new/AllSky/Omea\\_camera.html](https://www.alcor-system.com/new/AllSky/Omea_camera.html)



Figure 3: Sky Quality Meters (top left), TESS-W Photometers (bottom left) and both instruments mounted at Astronomical Station Vidojevica (right).

We will use the **SQM and TESS-W photometers** (Figure 3) both in Belgrade and at the Astronomical Station Vidojevica for measuring the sky brightness, serving as a proxy for LP. The TESS-W is a newer instrument which is more extended to the red range and is able to estimate the cloud coverage at the same time together with the sky brightness. It sends the measurements to the STARS4ALL infrastructure thus placing both our observing stations in a broader context.

We built two **visible and near-infrared (VNIR) hyperspectral imaging (HSI)** (Figure 4) sensors as instructed by Salazar-Vasquez & Mendez-Vasquez (2020). Two such instruments (at only 2% of the cost of the commercially available HSIs) will also be directed to the urban area of Belgrade and its surroundings and will enable



Figure 4: Visible and near-infrared (VNIR) hyperspectral imaging (HSI) sensors.

us to perform, again simultaneously, remote sensing from 400 nm to 1052 nm in up to 315 wavebands. Both instruments will allow us to follow both short and long term changes in the urban dynamics through, for example, studying urban lighting as a proxy for environmental impact and as a measure of urbanization dynamics (Dobler et al. 2021).

Finally, a **DSLR camera** is in the process of being procured.

### 3. DATA USAGE

The UrbObsBel project will generate observational data obtained using the aforementioned instruments. We will use these measurements together with the data coming from various satellites mentioned above. All the data that will be obtained by us will be stored on our server and will be publicly available. The costs of data curation and preservation will be covered by the AOB.

Data Repository (DR) is going to be set up in the second project year and will provide access to all our measurements. The data server is going to be set up at the AOB and used for the storage of the data acquired, with scrupulous measures to be taken regarding access and data security. Accessibility of the DR through an adequate interface on the website will be provided at the end of realization of UrbObsBel and for five years after projects' ending. Clearly organized data for easy parsing and adequate employment of the scientific foreground is the priority. We will integrate our database into internationally available databases. We will use our observations for detailed analysis and we will rely on the available approaches such as in Kyba et al. (2011), Babari et al. (2011), Jechow, et al. (2017, 2019).

### 4. VERY FIRST RESULT

To analyze changes in the sky brightness in the urban area (AOB) and in the rural part of Serbia (ASV) we used two TESS-W devices mounted in these two locations. The first measurements of the TESS-W device during several nights in September 2024 are shown in Figure 5. By analyzing the data, we get  $\text{mag}_{\text{AOB}} = 16.35$  for the brightness of the sky in Belgrade, while in Vidojevica it is  $\text{mag}_{\text{AOB}} = 21.16$ . Therefore, on ASV we can see fainter objects up to 4.5 mag than on AOB, and the reason is clear – light pollution.

### 5. INSTEAD OF A CONCLUSION

Gaining a deeper perspective on urban dynamics will enhance our understanding of light pollution (LP) and environmental pollution more broadly. Investigating artificial light at night (ALAN) is crucial for grasping the complexity of modern cities. As Sanchez de Miguel et al. (2022) noted, studying ALANs biological risks requires remotely sensed data on the spatial and temporal variation in the spectral composition of ALANA goal we aim to achieve with our planned observations.

To comprehensively understand urban behavior, it is essential to consider the three main factors shaping life in a large city like Belgrade: its people, natural environment, and infrastructure. We are excited to use advanced instruments to conduct Serbia's first in-depth analysis of these urban factors. With our exceptional vantage point on the roof of the Belgrade Observatory Tower, we are well-positioned to carry out

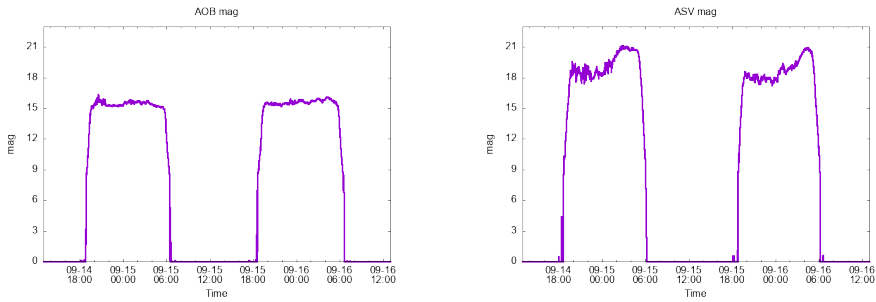


Figure 5: TESS-W measurements at Astronomical Observatory in Belgrade (left) and TESS-W measurements at Astronomical Station Vidojevica (right) during several nights in September 2024.

this pioneering study. We anticipate that our findings will offer valuable insights into urban dynamics and allow meaningful comparisons with similar studies across Europe and beyond.

### Acknowledgements





This research was supported by the Science Fund of the Republic of Serbia, no. 6775, Urban Observatory of Belgrade – UrbObsBel and by the Ministry of Science, Technological Development and Innovations of the Republic of Serbia through the Project contract No. 451-03-66/2024-03/200002.

### References

- Babari, R., Hautière, N., Dumont, É., Brémond, R. & Paparoditis, N.: 2011, *Atmospheric Environment*, **45**, Issue 30, 5316-5324, doi: 10.1016/j.atmosenv.2011.06.053
- Dobler, G., Bianco, F.B., Sharma, M.S., Karpf, A., Baur, J., Ghandehari, M., Wurtele, J.S. & Koonin, S.E.: 2021, *Remote Sensing*, **13**, 1426, doi: 10.3390/rs13081426
- Jechow, A., Kolláth, Z., Ribas, S.J., Spoelstra, H., Hölker, F. & Kyba, C.C.M.: 2017, *Scientific Reports*, **7**, id. 6741, doi:10.1038/s41598-017-06998-z
- Jechow, A., Hölker, F. & Kyba, C.C.M.: 2019, *Scientific Reports*, **9**, id. 1391, doi: 10.1038/s41598-018-37817-8
- Kyba, C.C.M., Ruhtz, T., Fisher, J. & Hölker, F.: 2011, *PLoS ONE*, **6**, Issue 3, e17307, 9, doi:10.1371/journal.pone.0017307
- Mommert, M.: 2020, *Astronomical Journal*, **159**, Issue 4, id.178, 8pp, doi: 10.3847/1538-3881/ab744f
- Pavlović, R., Cvetković, Z., Simić, Z., Damljanović, G., Samurović, S., Rovčanin, B., Lukić, D. & Bjelajac, D.: 2025, *Publ. Astr. Obs. Belgrade*, **107**, 123, doi: 10.69646/14sbac21p
- Salazar-Vazquez, J. & Mendez-Vazquez, A.: 2020, *HardwareX*, **7**, e00087, 21pp, doi: 10.1016/j.ohx.2019.e00087
- Sanchez de Miguel, A., Bennie, J., Rosenfeld, E., Dzurjak, S. & Gaston, K.G.: 2022, *Science Advances*, **8**, Issue 37, eabl6891, doi: 10.1126/sciadv.abl6891



## THE INFLUENCE OF THE COLLECTIVE EFFECTS IN PLASMA, BEHIND SIMPLE CUT-OFF

N. M. SAKAN<sup>1</sup> , Z. SIMIĆ<sup>2</sup> , V. A. SREĆKOVIĆ<sup>1</sup>  and M. DECHEV<sup>3</sup> 

<sup>1</sup>*University of Belgrade, Institute of Physics Belgrade, PO Box 57, 11001 Belgrade, Serbia*  
*E-mail: nsakan@ipb.ac.rs*

<sup>2</sup>*Astronomical Observatory, Volgina 7, 11060 Belgrade, Serbia*

<sup>3</sup>*Institute of Astronomy and National Astronomical Observatory, Bulgarian Academy of Sciences, 72, Tsarigradsko chaussee Blvd. Sofia, Bulgaria*

**Abstract.** The modeling of plasma behavior from mid up to strong non-ideality, e.g. plasma with a dominant Coulomb interaction is of interest. The micro field is strongly dependent on a form of used pseudo-potential. It is important to have in mind that the plasma behavior is considered as a variation to the main form of a potential. It was obvious from previous papers that the pseudo-potentials used in solid state physics, e.g. ab-initio ones, could be used successfully in describing of a dense plasma. Here we present the candidates potentials calculated with ab-initio method that should be analyzed in order to be used for describing a dense plasma. As a result, after studying of the potentials, it is expected to have a method of introducing a more complex atoms and ions in existing plasma model.

### 1. THEORETICAL REMARKS

In the dense plasma the inter-particle Coulomb interaction becomes dominant over the thermal kinetic energy (Fortov et al. 2006). In such conditions a coupled system of particles behaves partially like a crystal. The simplified version, for hydrogen case, of non-ideality parameter  $\Gamma$  is given by

$$\Gamma = \frac{E_p}{E_k} = \frac{e^2}{kT r_{WS}} \sim e^2 N_e^{1/3} \beta, \quad \beta = 1/kT, \quad r_{WS} = \left( \frac{3}{4\pi N_e} \right)^{1/3}. \quad (1)$$

The plasma interaction, cut-off Coulomb potential, was used successfully previously, see for example Dimitrijević, et al (2018), Srećković, et al. (2018), Mihajlov, et al. (2015), Ignjatović, et al. (2009). Although the expected plasma influence should be governed in the far field concerning a ionic core radius, it is expected to have a strong influence of the form of a ab-initio yielded pseudopotential. The area of interest in Hydrogen model is in range of  $0.1 \leq \Gamma \leq 1.5$ , while for other species the thorough investigation of model behavior is needed.

## 2. THE PSEUDO-POTENTIAL

The describing plasma depends of two parts, the atom/ion content, as well as plasma influence. While the plasma influence is described as a collective phenomena, the atom and ion influence is described with the help of pseudo-potential. The idea of describing a complex atom dense plasma as well as describing of complex atom mixtures plasma arises. The atom and ion influence should be described by the ionic core of the adequate complex atom and ion, while the plasma influence is described with the collective phenomena modeling.

Since the slow processes could be described as a pseudo-static ones, they could be included in a potential. The influence of ions could be described directly as a sort of crystalline structure. It processes a smallest inter-ionic distance so the emitter could feel a averaged potential of several layers of ions.

Besides mentioned approach, there are several ab-initio calculations that are potential candidates for generating a pseudo-potentials capable for being used in dense plasma modeling. Our choice was ATOM, the program originally written by Sverre Froyen at the University of California at Berkeley, and now maintained by Alberto Garcia.

It is expected that presented approach of pseudo static ionic content in plasma could also enable a inclusion of more complex atom and ion plasma models. A first step the comparison of exact model for Hydrogen with previously used Opium code generated one as well as ATOM generated should be carried out.

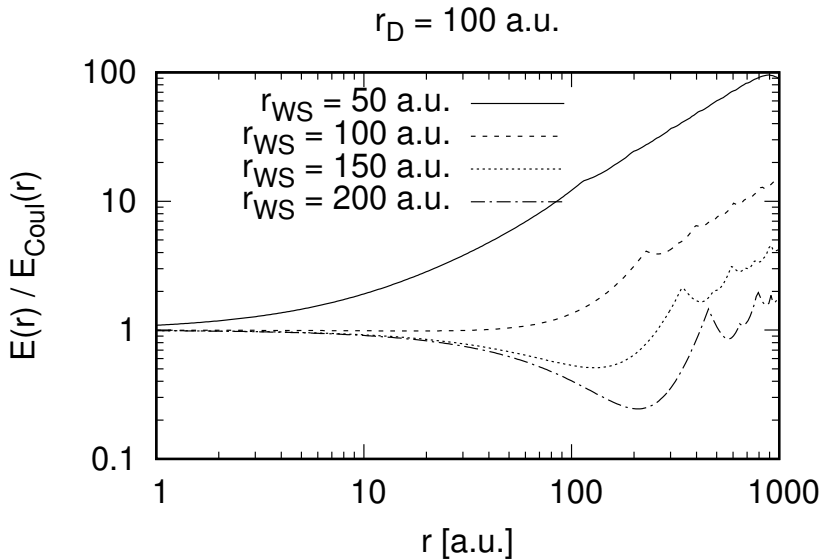


Figure 1: Dependence on ion density

### 3. RESULTS AND CONCLUSIONS

As a first step approach was to model the behavior of ionic collective phenomena as simple as possible and to have insight of influence of various processes.

The screening is modeled as a Debye one, although it is known that this kind of screening model does not describe a behavior of dense plasma completely, it posses a analytical form and could be easily included within analyzed model.

As a first model analysis a sensitivity on ion density is shown in Figure 1. Here it could be concluded that more dense ionic content is, faster it converges towards the constant value, e.g. it becomes a constant slope in the right part of a graph with larhe  $r$ . From this it could be concluded that the cut-off model describes well a plasma of high densities.

From Figure 2 it became obvious that if more intense screening is more separate ion influence is even in a case of plasma of high densities. The cut-off is not capable to adequately describe a plasma with high screening.

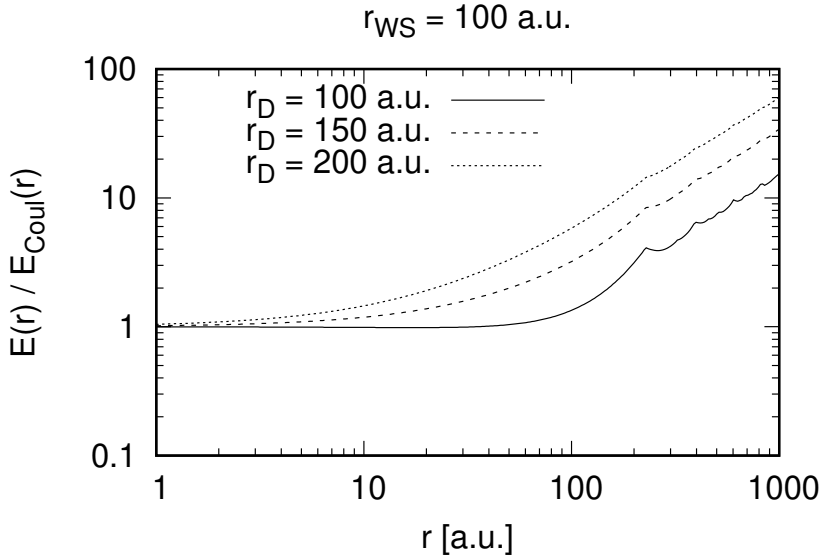


Figure 2: Dependence on screening length

From Figure 3 the influence on size of modeled pseudo crystal is shown. The behavior for single layer and 2 layer model is presented, the validity of describing is good up until a strongest local maximum in a area of  $r \gg r_c$ . The figure is more illustrative, since in every case of modelling it is necessary to have a prior investigation of adequate model size. The computing time depends strongly on number of layers.

The idea of inclusion of calculations of collective phenomena of ionic content is a inclusion of ionic processes directly in pseudo-potential. From the shown it could be deduced that this approach could lead to applicable results, capable of describing a plasma behavior more precisely than a cut-off model with the usage of non extensive computing power facilities, e.g. it could be available to model a desired plasma behavior on demand.

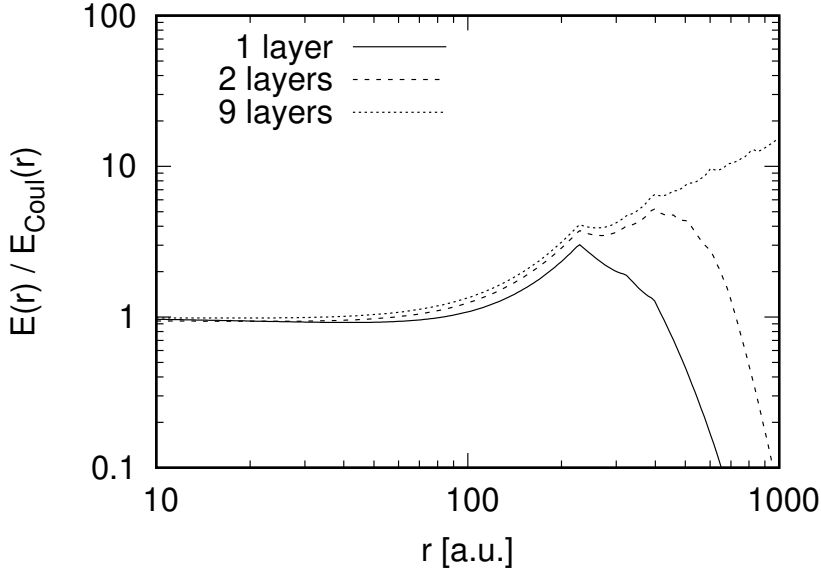


Figure 3: Dependence on number of layers

### Acknowledgements

This research was supported by the Ministry of Science, Technological Development and Innovation of the Republic of Serbia (MSTDIRS) through contract no. 451-03-66/2024-03/200002 made with Astronomical Observatory (Belgrade), 451-03-47/2023-01/200024 made with Institute of physics, NOVA2LIBS4fusion Grant no. 3108/2021 and with the financial support from the Bulgarian Academy of Sciences (Bilateral grant agreement between BAS and Astronomical Observatory, Belgrade), that is gratefully acknowledged.

### References

- Vitel Y.: 2004, *J. Quant. Spectrosc. Radiat. Transf.*, **83**, (3-4):387–405, doi: 10.1016/S0022-4073(02)00380-1
- Chabrier G., Saumon D., and Potekhin A. Y. : 2006, *J. Phys. A*, **39**(17):4411–4419, doi: 10.1088/0305-4470/39/17/S16
- Fortov V., Iakubov I., and Khrapak A.: 2006, *Physics of Strongly Coupled Plasma*, International Series of Monographs on Physics. OUP Oxford., ISBN: 9780199299805
- Dimitrijević M. S., Srećković V. A., Sakan N. M., Bezuglov N. N., and Klyucharev A. N.: 2018, *Geomagn. Aeron.*, **58**(8):1067–1072, doi:10.1134/S0016793218080054
- Srećković V. A., Sakan N., Šulić D., Jevremović D., Ignjatović Lj. M., and Dimitrijević M. S.: 2018, *Mon. Not. R. Astron. Soc.*, **475**(1):1131–1136, doi:10.1093/mnras/stx3237
- Mihajlov A. A., Srećković V. A., and Sakan N. M.: 2015, *J. Astrophys. Astron.*, **36**(4):635–642, doi:10.1007/s12036-015-9350-0
- Ignjatović Lj. M., Mihajlov A. A., Sakan N. M., Dimitrijević M. S., and Metropoulos A.: 2009, *Mon. Not. R. Astron. Soc.*, **396**(4):2201–2210, doi:10.1111/j.1365-2966.2009.14870.x
- Soler J. M., Artacho E., Gale J. D., Garcia A., Junquera J., Ordejon P., Sanchez-Portal D.: 2002, *Jour. Phys.: Condens. Matter*, **14**, 2745–2779, doi: 10.1088/0953-8984/14/11/302

## ZONES OF ACCRETION DISK ACTIVITY

K. YANKOVA

*Space Research and Technology Institute, Bulgarian Academy of Sciences,  
Acad. Georgi Bonchev Str., bl. 1, 1113, Sofia, Bulgaria  
E-mail: f7@space.bas*

**Abstract.** In this paper, we consider the accretion disk of a compact object. In the process of evolution, zones of activity are formed, which is developed into two types - internal and adjacent. We analyse the causes of occurrence and investigate the construction, location and characteristic features of each of them. We looking for the connections of the disc behaviour with energy exchange in these zones.

### 1. INTRODUCTION

In series of papers (Yankova, (2007-2015)), we created a new magneto-hydrodynamic model of accretion disc, based on a new specific advective hypothesis:

$$\frac{\partial(\rho v_i)}{\partial t} + \frac{\partial(\rho v_i v_j)}{\partial x_j} = \rho \left( \frac{\partial v_i}{\partial t} + v_j \frac{\partial v_i}{\partial x_j} \right) = \rho \frac{Dv_i}{Dt} \quad (1)$$

Here  $v$  is the flux velocity;  $\rho$  - mass density;  $x_i$  is spatial coordinates. The operator  $D/Dt$  defines the advective term as a stream with velocity. This means that there is a displacement of the mean stream with velocity in some direction, preserving its character. The solution as a whole is carried over to smaller radii (Yankova et al. 2014, Yankova 2015). Thus, the advective rings effectively maintain the cooling of the disc.

In the one-temperature, optical thick plasma of the advective Keplerian disc, the different instabilities create the irregular periodicities in variation of the substance features, which should not be neglect and can be used:

$$F_i = F_{i0} R \left( x = \frac{r}{r_0} \right) \exp[k_\varphi(x)\varphi + \omega(x)t] = F_{i0} f_i(x) \quad (2)$$

Functions  $F_i$  transformed the physical parameters of the flow, thereby setting the feedback of the instabilities characteristics with the magnitudes of the accreting plasma. Where  $f_i(x)$ - dimensionless functions of the physical parameters,  $R_0 = 10^n R_g$ , or  $R^*$ (the outer radius of the disc and star-accretor/Schwarzschild radii),  $F_{i0}$  are the values of the outer edge of the disc.

$K(x) = \frac{\text{warming}}{\text{cooling}}$  is the directly connection of the instabilities with the accreting flow.  $K$  is a dimensionless magnitude obtained in the modelling process, which is a measure of the disc ability to qualitative cooling (Iankova 2009).

---

## 2. THE ACTIVE ZONES

Based on our model, we locate the active areas of the disk and analyse the zones state/behaviour in a specific objects. In each of the zones, the activity is the result of the sudden change in the physical parameters in the stream, caused by the interaction of one of the components of the system (accretor magnetosphere, disk corona, etc.) with the disc structure. An energy excess is released in the flow, which generates long-term or short-term observational effects such as flickering, outbursts, non-thermal radiation, annihilation lines, etc.

### 2. 1. TYPES OF ACTIVE ZONES

We consider five active zones: *The real active zone (AZ)*: The real active zone is formed in the inner the disk, where the accretion rate increases by of up to about 15 percent due to the advection action. The active zone can be determined by indicators such as: - Outer radius of the corona, which we obtain from the condition  $v_a^2 \leq v_s^2$  (Iankova 2007), where  $v_s$  - sound velocity and  $v_a$  - Alfven velocity, respectively; - Temperature distribution in the disk; - Luminosity distribution in the disk; - Critical value of the local heating  $K > 1$ .

*External contact AZ*: The outer contact active zone is formed by the collision of the transfer inflow with the outer regions of the disk and is commonly known as a spot or hot line.

*Internal contact AZ*: In the destruction radius area of the disk, where the inner layer evaporates and the disk does not reach the star, is the inner contact active zone. In it the activity is caused by arcs collisions in the accretor magnetosphere and/or interaction whit the inner regions of the disk. We obtain the destruction radius of the disk from the condition  $\langle v_a \rangle^2 \leq (9/4) \langle v_\varphi \rangle^2$  (Iankova 2009), where  $v_\varphi$  is the angular velocity.

*Activity in the transfer stream*: Activity in the transfer stream is excited by the formation of a shock front upon variation in the plasma velocity due to orbital eccentricity or stellar wind acceleration, e.g.

*Activity in the disk corona or activity by the disk wind*: The surface boundaries of the disc are especially important because this is where the effects of the heating in the pad become apparent: The variability of the boundary distributions determines whether the disk will maintain a corona or generate wind. The activity in this area is brought in from the disc across the boundary.

### 2. 2. ZONAL CONNECTIONS

Some internal and adjacent zones are connected to each other by transferring activity or interaction between parameters: The activity in zone 5 (corona/or disk wind) has a migratory character, it arrives ready from the disk and especially from the real active zone-1. On the other hand, the processes in the disk do not contribute to the activity in the transfer stream, but this AZ-4 affects over the processes in zone 2 (spot or hot line).

### 2. 3. ZONES ENERGY BALANCE

*External contact AZ*: The disturbance in the heating distribution in the spot is about two-three orders  $K_{fl}$  (figs.1a, 1c). The heating K directly controls the pressure

(plasma and radiative) in the zone, so it together with the temperature will changes. The temperature jumps by about two orders of magnitude and  $p_g \uparrow$ , but with the spot increases the density  $\rho \downarrow$  decreases and  $p_g \downarrow$  falls. Then  $p_r \uparrow$  as  $T^4 \uparrow$  and radiative pressure will dominate. It pushes the spot to expand. So in the luminosity the activity is registered like flickering. So the activity is registered like flickering, in the luminosity.

*The real active zone and zone 5:* The main reason for the disk activity (zone 1) is the presence of advection: the rate of radial accretion increases, increased the released energy. Free energy is kept in the disk in the form of heat, which reduces the radial gradient of entropy towards the center. Negative entropy creates conditions to the energy absorbing by the instabilities and turning them into microstructures in the flow it stimulates feedbacks. So they close the advective cycle and thus keep the advection in the self-induction mode.

Simultaneously, the developing advection is the main reason for the export of activity from the disc to the peripheral component. Also, tool for determining the degree to transfer activity in the zone 5. The transfer is related with the Parker instabilities action that bring MRI into the corona together with buoyant field lines, (Yankova 2014). Boundary corona-disk is especially interesting because there mutability and mobility of boundary distributions of the sound and the magneto-sonic speeds is caused by the overall interaction between the parameters and non - linear effects in the disk. These two types of velocities are the most sensitive to the energy exchange and hence the action of the advection. They create multiple contours of increasing, which combined with fast growing magnetic field ensure the emergence of compacted regions genetically unrelated to the helices. These are precisely the advective rings that provide heating of the pad at the base of the corona/wind. Tightening of advective rings to the center in disk and negative entropy realize a new state. Then, the corona/wind is positioned over the inner regions of the disk.

The corona shows a non-thermal spectrum. And outbursts and flickering can be observed from RAZ-1, as a result of the interaction of different type's structures formed by the instabilities action in the flow.

*Internal contact AZ:* The activity caused by magnetic arcs collisions or interaction with the high speed plasma is typical coronal activity like a Sun's. Switching of opposite loops leads to the presence of annihilation lines in the object spectrum.

### 3. RESULTS

We have calculated how the internal active zones are located in the disk for three types of real sources:

#### 3. 1. RS OPH - SYMBIOTIC NOVA

RS Oph is a member of the recurrent novae group (Ilkiewicz et al. 2019, Merc et al. 2023). RS Ophiuchus is a binary system consisting of a red giant and a white dwarf. The masses of the two components are estimated as  $0.68 - 0.80M_{\odot}$  for the red giant (Brandi et al. 2009) and for the white dwarf it is  $1.2 - 1.4M_{\odot}$  (Mikolajewska and Shara 2017). The orbital period of the system found to be 453.6 days (Brandi et al. 2009), and white dwarf has an accretion disk.

The recurrent nova outbursts of RS Oph happen in approximately every 15-20 years, with a brightness variability of  $\approx 11$  to 6 magnitudes in the V band. Between out-

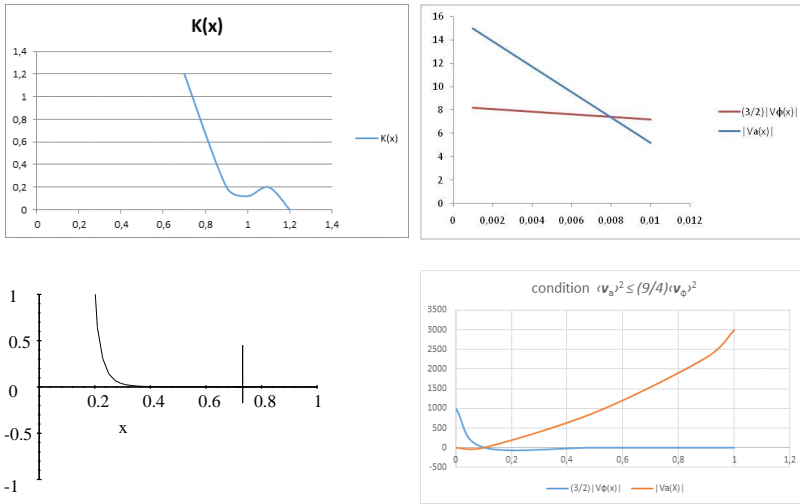


Figure 1: (1a) Distribution of the local heating of the RS Oph disk. (1b) Distribution of the condition  $v_a^2 \leq (9/4)v_\phi^2$  of the RS Oph disk (upper panels). (1c) Distribution of the local heating of the Cyg X-1 disk. (1d) Distribution of the condition  $v_a^2 \leq (9/4)v_\phi^2$  of the Cyg X-1 disk (lower panels).

bursts, the system has a stellar magnitude of  $12.5^m$ . The novae outbursts could be the result of thermonuclear processes on the white dwarf's surface (Starrfield 2008) or by accretion disk instabilities as in the dwarf-nova-like objects (King and Pringle 2009, Alexander et al. 2011).

We found out that the inner active zones in the RS Oph disc are distributed as follows:  $(AZ - 3) < R_{dstr} \sim 0.007R_0$ ;  $(AZ - 1) \sim (0.008; 0.5)R_0$  (as we showed in Yankova 2023);  $(AZ - 2) \sim (0.9; 1.2)R_0$ . We show that the perturbation in  $K(x)$  develops in the region  $(0.9; 1.2)R_0$  (see Fig.1a), it is an indicator to localization the external contact AZ. We obtain  $R_{dstr}$  in interval  $(0.007; 0.01)R_0$ , (see Fig.1b).

### 3. 2. CYG X-1 MICROQUASAR

Cyg X-1 represents TDS - a spectroscopic binary of a supergiant  $\sim 20M_\odot$  of  $9^m$ , spectral class  $9.7Iab$ , and a compact object  $\sim 10 - 15M_\odot$  (Ninkov et al. 1987, Orosz et al. 2011), with orbital period of  $\approx 5.6$  days. Variations in the optical range with the same period are observed, related to the mass transfer between the system components and the formed accretion disk. The observations also show a variable circular polarization. It requires a magnetic field source. The characteristic size of the field coincides with the ergo-sphere.

Cyg X-1 is highly variable in the X-ray spectrum, with periods ranging from millisec-



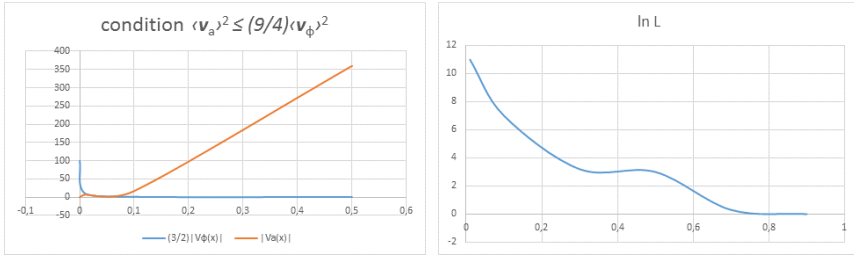


Figure 2: (2a) Distribution of the condition  $v_a^2 \leq (9/4)v_\phi^2$  of the SgrA\* disk. (2b) Distribution of the Luminosity of the SgrA\* disk.

onds to years. The X-ray luminosity is of the order of  $\approx 2 - 8 \times 10^{27} \text{ ergs}^{-1}$ , from (soft X-ray  $\sim 2 - 20$  keV) to (hard X-ray  $\sim 40 - 450$  keV), low-energy X-ray (1.3-12 keV) and high-energy X-ray (20-200 keV)(Nayakshin and Dove 1998, Zhang et al. 1997). In spectrum registers the  $K_\alpha$  line of iron; reflection of EMR from the inner regions to the outer regions of the disc is observed; and  $\gamma$ -radiation is captured, which are associated with the behavior of the AGN microquasar.

We found out that the inner active zones in the Cyg X-1 disc are distributed as follows:  $(AZ - 3) < R_{dstr} < 0.1R_0$  (see Fig.1c);  $(AZ - 1) \sim (0.1; 0.4)R_0$  (as we showed in Yankova 2023);  $(AZ - 2) \sim (0.7; 0.75)R_0$  (see Fig.1d).

### 3. 3. SGR A\* DORMANT GALACTIC CORE

The Milky Way is a weakly active galaxy with  $L \approx 1.5 \times 10^{39}$  erg/s in the range 2-200 keV (Revnivtsev et al. 2004) and magnetic field  $\sim 3.5 \times 10^{-6}G$ . Its center is located in the constellation Sagittarius. The emission from the region is diverse in nature, but specifically the soft -rays and X-rays (soft and hard X-rays) come from the non-thermal synchrotron radio source SgrA\*, which is associated with a compact object and matches within  $\pm 0.1$  with the dynamical center of the Galaxy. In its spectrum,  $\gamma$ -emission of Brom is registered, which is associated with minispirals (the accretion disk spirals), the  $K_\alpha$ -lines of various highly ionized elements from the outer edge of the disk and the annihilation line 511 keV (Cesare 2011) from the interior of the disk, as well as emission at 10 keV and from his envelope (? corona).

We found out that the inner active zones in the SgrA\* disc are distributed as follows:  $(AZ - 3) < R_{dstr} \sim 0.03R_0$  (see Fig.2a);  $(AZ - 1) \sim (0,05; 0,6)R_0$ (see Fig.2a, 2b). For obvious reasons, the object does not have zone 2.

We showed that the condition for the outer radius of the corona  $v_a^2 \leq v_s^2$ , is drawn outwards as it approaches to the equatorial plane, but outwards and the thickness of the disc decreases. This gives grounds for asserting that the corona covers the entire disc and flows into the torus at  $\sim 60 R_g$ , Yankova 2014. We obtain that the luminosity decreases smoothly and drops sharply at  $0.6R_0$  (see Fig.a1), which is a convenient indicator of the beginning of active zone-1.

From the condition  $v_a^2 \leq (9/4)v_\phi^2$  we find that disk in the core does not destroy in the corona. It evaporates  $\sim 3R_g$ , but the reasons are of a completely different nature - the angular velocity of the flow  $\Omega$  is already relativistic. In fig.a2 one can see how the velocities overlap in some interval. The reason is the relativistic entrainment near SMBH.

---

#### 4. SUMMARY

In this paper, we considered some processes in the accretion disk of a compact object, which lead to simultaneous or sequential activation of areas of the disc or its surroundings. We presented the possible types of disk activity zones that arise in the process of evolution in different types of compact objects. We have calculated how the internal active zones are located in the disk for three types of real sources: RS Oph - symbiotic nova; Cyg X-1 microquasar; Sgr A\* - dormant galactic core.

We discussed the activating mechanisms and energy balance in each zone. And we found that RAZ-1 is concentrated in the inner disc areas due to the advective shift. This affects the zone-5 due to the connection between the two zones and it also forms over the inner regions of the disk. Such evolutionary mobility could also manifest in AZ-2 in case of increased activity in AZ-4.

#### References

- Alexander, R. D., Wynn, G. A., King, A. R., and Pringle, J. E.: 2011, *Monthly Notices of the Royal Astronomical Society*, **418**, 2576, doi: 10.1111/j.1365-2966.2011.19647.x
- Brandi, E., Quiroga, C., Mikolajewska, J., Ferrer, O. E., and Garca, L. G.: 2009, *Astron.Astrophys.*, **497**, 815, doi: 10.1051/0004-6361/200811417
- Cesare G. De: 2011, *Astron.Astrophys.*, **531**, A56, doi: 10.1051/0004-6361/201116516
- Iankova Kr.: 2007, *Bulg. J. Phys.*, **34**, 326
- Iankova Kr.D.: 2009, *Publ. Astron. Soc. "RudjerBokovi"*, **9**, 327
- Ilkiewicz, K., Mikolajewska, J., Miszalski, B., et al.: 2019, *Astron.Astrophys.*, **624**, A133, doi:10.1051/0004-6361/201834165
- King, A. R. and Pringle, J. E.: 2009, *Monthly Notices of the Royal Astronomical Society*, **397**, L51, doi: 10.1111/j.1745-3933.2009.00682.x
- Merc, J., Glis, R., Velez, P., et al.: 2023, *Monthly Notices of the Royal Astronomical Society*, **523**, 163, doi:10.1093/mnras/stad1434
- Mikolajewska, J. and Shara, M. M.: 2017, *The Astrophysical Journal*, **847**, 99, doi: 10.3847/1538-4357/aa87b6
- Nayakshin, S., Dove, J. B.: 1998, *arXiv e-prints*, <https://arxiv.org/pdf/astro-ph/9811059>, doi: 10.48550/arXiv.astro-ph/9811059
- Ninkov, Z., Walker, G. A. H., Yang, S.: 1987, *The Astrophysical Journal*, **321**, 425, doi: 10.1086/165641
- Orosz J. A., McClintock J. E., Aufdenberg J. P., Remillard R. A., Reid M. J., Narayan R., Gou L.: 2011, *arXiv e-prints*, arXiv:1106.3689, doi: 10.48550/arXiv.1106.3689
- Revnivtsev M.G., Churazov E.M., Sazonov S.Yu., Sunyaev R.A., Lutovinov A.A., Gilfanov M.R., Vikhlinin A.A., Shtykovsky P.E., Pavlinsky M.N.:2004, *Astron.Astrophys.*, **425**, L49-L52, doi: 10.1051/0004-6361:200400064
- Starrfield, S.: 2008, *PASPCS*, **401**, 4
- Yankova, K.; Filipov, L.; Boneva, B.; Gotchev, D.: 2014, *Bulg. Astron. J.*, **21**, 74
- Yankova Kr.: 2014, MHD of accretion-disk flows, (monograph in Bulgarian)
- Yankova Kr.: 2015, *Bulg. Astron. J.*, **22**, 83
- Yankova, K.: 2023, *Publ. Astron. Soc. Rudjer Bokovi*, **25**, 179
- Zhang S. N. et al.: 1997 *The Astrophysical Journal*, **477**, L95

**IN MEMORY OF EVGENI SEMKOV – THE TEACHER, THE  
INSPIRER, THE ASTRONOMER, AND SIMPLY THE FRIEND**

Corresponding Member Evgeni Semkov was born in Sofia on January 7, 1960. He completed his secondary education at the 21st High School “Hristo Botev” (Sofia) in 1978. During this time, his interest in astronomy began to grow, fueled by his passion for popular science books. He devoured most of the translated science fiction books available in Bulgaria. Though he couldn’t become an astronaut, astronomy captivated him deeply. In 1980, he enrolled in the Faculty of Physics at Sofia University “St. Kliment Ohridski”, where in 1985, under the guidance of Assoc. Prof. Dr. Milcho Tsvetkov, defended his thesis and graduated with a master’s degree in physics, specializing in astronomy.

He began his professional journey in astronomy as a methodologist at the Sofia City Astronomical Observatory (1985–1987). This experience left a lasting impact on his development. After the closure of the City Observatory and the discontinuation of astronomy clubs in Sofia, he consistently advocated for their revival. *“Unfortunately, Sofia still lacks astronomy clubs to this day”*, Corresponding Member Semkov would say. *“There is no planetarium here, unlike other cities in Bulgaria. We cannot compare to Smolyan, Dimitrovgrad, Varna...”*. In 1987, Assoc. Prof. Dr. Milcho Tsvetkov invited him to join the Independent Astronomy Section at the National Astronomical Observatory (NAO) of the Bulgarian Academy of Sciences (BAS), where he defended his PhD thesis in 1995 on “Study of Non-Stationary and Eruptive Stars in the Regions of the Diffuse Nebula NGC 7129 and the Open Star Cluster  $\alpha$  Per”. Corresponding Member Semkov advanced through all stages of a Bulgarian astronomer’s career: from operator of the 2-meter telescope at NAO Rozhen (1990–1994), physicist at the Institute of Astronomy, BAS (1995–1997), research associate (1997–2000), senior research associate (2000–2006), associate professor (2006–2015), to full professor (2015–2024). In May 2023, he defended his doctoral thesis on “Pre-Main Sequence Stars” and was elected Corresponding Member of BAS in September 2024. He served as Scientific Secretary of the Institute of Astronomy with NAO–BAS (2008–2016), Acting Director (2016–2018), and then Director for two terms (2018 until his passing on December 29, 2024). He was also a member of the General Assembly of BAS and its committees.

Corresponding Member Semkov was one of Bulgaria’s most accomplished and active astronomers in recent years. His research focused on observational astronomy (photometric and spectral variability of stars) and astrophysics (star-forming regions of pre-main sequence stars, young variable stars, and symbiotic stars), as well as accreting supermassive black holes (active galactic nuclei, quasars, blazars). He authored 205 scientific publications and received over 1,700 citations (excluding self-citations). He was awarded the BAS Jubilee Certificate for outstanding scientific

achievements on its 145th anniversary, nominated for the “Successful Leader of International Projects” category in the Pythagoras Awards (2017), and received the “Established Scholar in Natural and Engineering Sciences” award in the 2024 Pythagoras Awards. He specialized abroad and collaborated with observatories and institutes in Armenia, Greece, India, Italy, Japan, the USA, France, Germany, Croatia, and others. Domestically, he worked closely with leading astronomers, including Assoc. Prof. Dr. Milcho Tsvetkov, Assoc. Prof. Dr. Katya Tsvetkova, Prof. Tsvetan Georgiev, and Assoc. Prof. Dr. Sunay Ibryamov. Under his leadership, the Institute of Astronomy with NAO secured international projects (including ESA and EU Horizon funding) and coordinated two national scientific infrastructure initiatives: RACIO (Regional Astronomical Center for Research and Education) and LOFAR-BG. He spearheaded the design and construction of a new 1.5-meter optical telescope at NAO Rozhen – “the contribution of our generation of Bulgarian astronomers to the future”. He was a member of the International Astronomical Union, the European Astronomical Union, and the Union of Astronomers in Bulgaria.

Beyond his scientific and administrative work, Corresponding Member Semkov dedicated significant effort to mentoring young colleagues. He supervised four successful PhD students and often remarked, “*While training them, I never stopped learning from them*”. His youthful spirit was nurtured by his passion for athletics. He was an ardent supporter of Levski Sofia’s athletics club, where he competed, completing 14 full marathons with a personal best of 2 hours and 52 minutes.

With the passing of Corresponding Member Evgeni Semkov, the Bulgarian astronomical community has lost one of its brightest minds – a teacher, an inspirer, and a true friend.

**We bow to his luminous memory!**

Collegium of Astronomers from Bulgaria

## AUTHORS' INDEX

- Arsenov N. 43  
Atanasova T. 113  
Bachev R. 5, 57  
Bjelajac D. 123, 129  
Boeva S. 13, 57  
Bogdán Á. 43  
Boneva D. 87  
Borisov B. 113  
Borka D. 51  
Borka Jovanović V. 51  
Christova M.D. 21, 63  
Cvetković Z. 13, 123, 129  
Damljanović G. 57, 99, 123, 129  
Dechev M. 29, 103, 135  
Dimitrijević M.S. 21, 63  
Donkov S. 69  
Duchlev P. 103  
Fogasy J. 43  
Frey S. 43  
Frolova M. 81  
Gabányi K. É. 43  
Georgiev A. 113  
Georgiev Ts. 91  
Ibryamov S. 113  
Janc N. 95  
Jovanović M.D. 57, 99  
Jovanović P. 51  
Khasaeva T. 81  
Koleva K. 103  
Kovačević-Dojčinović J. 109  
Kovács A. 43  
Lakićević M. 109  
Latev G. 13  
Lukić D. 123, 129  
Marchev D. 113  
Marinkova L. 69  
Mihaylov H. 75  
Mihov B. 117  
Mikhailov E. 81  
Mishev A. 37  
Miteva R. 13, 29  
Nedialkov P. 91  
Pavlova N. 113  
Pavlović R. 123, 129  
Perger K. 43  
Petrov N. 37  
Popović L.Č. 109  
Rovčanin B. 123, 129  
Sahal-Bréchet S. 63  
Sakan N.M. 135  
Samurović S. 123, 129  
Samwel S.W. 29  
Shirov G. 37  
Simić Z. 123, 129, 135  
Slavcheva-Mihova L. 43, 117  
Srećković V.A. 135  
Stanchev O. 75  
Stojanović M. 57  
Tsvetkov Ts. 37  
Valcheva A. 91  
Veltchev T.V. 69, 75  
Yankova K. 87, 139  
Yordanova G. 113  
Yotov V. 37



CIP - Каталогизација у публикацији Народна библиотека Србије, Београд

520/524(082)

**SERBIAN-Bulgarian Astronomical Conference (14 ; 2024 ; Vrnjačka Banja)**

Proceedings of the XIV Serbian-Bulgarian Astronomical Conference, Vrnjačka Banja, Serbia, September 23–27, 2024 / [organizers Astronomical Observatory, Belgrade, Serbia [and] Institute of Astronomy with National Astronomical Observatory, Bulgarian Academy of Sciences, Sofia, Bulgaria] ; [co-organizer University of Belgrade, Faculty of Mathematics and Department of Astronomy] ; eds. Milan S. Dimitrijević ... [et al.]. - Belgrade : Astronomical Observatory Belgrade, 2025 (Mionica: Vesna Vasić-Pavlović PR). - 148 str.: ilustr. ; 25 cm. - (Публикације Астрономске опсерваторије у Београду; св. 107 = Publications of the Astronomical Observatory of Belgrade ; no. 107)

Tiraž 100. - Napomene i bibliografske reference uz tekst. - Bibliografija uz svaki rad. - Registar.

ISBN 978-86-82296-15-7

а) Астрономија -- Зборници б) Астрофизика -- Зборници

COBISS.SR-ID 162961673

